LIBRARY
Michigan State
University

This is to certify that the

dissertation entitled

Internal Conversion Vs. Photochemistry in Pentammine and Bis(2,2'Bipyridine), (4-Acylpyridine) Ruthenium (II) Complexes. Photodisproportionation of Pentacarbonyl (4-Acylpyridine) Tungsten(0) Complexes in the Absence of an Entering Ligand.

presented by

Nicholas Leventis

has been accepted towards fulfillment
of the requirements for

Ph.D. degree in Chemistry

Major professor

Date 10/18/85

MSU is an Affirmative Action/Equal Opportunity Institution O-12771

MSU
LIBRARIES

RETURNING MATERIALS:
Place in book drop to remove this checkout from your record. FINES will be charged if book is returned after the date stamped below.

INTERNAL CONVERSION VS. PHOTOCHEMISTRY IN PENTAAMMINE AND BIS(2,2'BIPYRIDINE), (4-ACYLPYRIDINE) RUTHENIUM(II) COMPLEXES.

PHOTODISPROPORTIONATION OF PENTACARBONYL (4-ACYLPYRIDINE) TUNGSTEN(0) COMPLEXES IN THE ABSENCE OF AN ENTERING LIGAND.

By

Nicholas Leventis

AN ABSTRACT OF
A DISSERTATION

Submitted to

Michigan State University

in partial fulfillment of the requirements

for the degree of

DOCTOR OF PHILOSOPHY

Department of Chemistry

1985

ABSTRACT

INTERNAL CONVERSION VS. PHOTOCHEMISTRY IN PENTAAMMINE AND BIS(2,2'BIPYRIDINE), (4-ACYLPYRIDINE) RUTHENIUM(II) COMPLEXES.

PHOTODISPROPORTIONATION OF PENTACARBONYL (4-ACYLPYRIDINE) TUNGSTEN(0) COMPLEXES IN THE ABSENCE OF AN ENTERING LIGAND.

By

Nicholas Leventis

This dissertation primarily concerns the estimation of the rate of the Internal Conversion of an upper Internal Ligand excited state to lower excited states in inorganic complexes.

As representative examples, various Ruthenium pentaammine and bis(2,2'bipyridine) complexes were chosen. The rate of the Internal Conversion of the Internal Ligand $n\pi^*$ excited state of coordinated pyridyl ketones was estimated by varying the reactivity of the pyridyl ketones towards the Norrish Type II Internal Ligand photochemical cleavage, so that for sufficiently low reactivity of the coordinated pyridyl ketones, the Internal Conversion competes with the Type II cleavage. It was found that the rate of the Internal conversion of the $n\pi^*$ Internal Ligand excited state in $[Ru(NH_3)_5(4\text{-pyridyl ketone})]^{2+}$ is $\leq 4.0\ 10^7\ sec^{-1}$, and in $cis\text{-}[Ru(bipy)_2(4\text{-pyridyl ketone})_2]^{2+}$ is $2.9\ 10^8\ sec^{-1}$; (bipy = 2,2'bipyridine). The higher rate of the Internal Conversion in the bis(2,2'bipyridine) complexes was

explained in terms of poor orbital overlap between the n orbital localized on the pyridyl ketone oxygen and the non-bonding d orbitals of Ruthenium on one hand, but, on the other hand, favorable orbital orientation and overlap between the n orbital of the pyridyl ketone oxygen and the 2,2'bipyridine π system.

Efforts to transfer the same approach for the Internal Conversion rate estimation in Pentacarbonyl (4-pyridyl ketone) Tungsten(0) complexes failed, due to a fast photochemical reaction of these complexes, to yield $W(CO)_6$ and cis-$W(CO)_4$(4-pyridyl ketone)$_2$. This reaction has been overlooked in the chemical literature so research was concentrated on the elucidation of the mechanism by which this reaction takes place. It was found that, in the absence of any 4-pyridyl ketone in the irradiated solution (solvent: benzene or methylcyclohexane), two mechanisms seem to proceed simultaneously both at short or long irradiation wavelengths (490 or 410 nm, respectively): an associative one, presumably from the MLCT lowest excited state, and a dissociative one from the higher LF state which leads primarily to 4-pyridyl ketone photodissociation. The $W(CO)_5$ intermediate attacks a ground state molecule from which it abstracts a CO molecule to give $W(CO)_6$ and a $W(CO)_4$(4-pyridyl ketone) intermediate that eventually finds a 4-pyridyl ketone molecule in the solution to give cis-$W(CO)_4$(4-pyridyl ketone)$_2$. The presence of 4-pyridyl ketone in the irradiated solution quenches the tetracarbonyl

product formation more efficiently at longer irradiation wavelengths (λ_{irr}>400 nm) than at shorter irradiation wavelengths (λ_{irr} 400 nm). At higher energy irradiations (~400 nm), loss of CO becomes competitive with 4-pyridyl ketone loss, and another mechanism through the direct formation and trapping of a $W(CO)_4$(4-pyridyl ketone) intermediate becomes important; the main reaction path, though, remains the one through loss of 4-pyridyl ketone.

To my parents, Spyro and Efrosini Leventis

ACKNOWLEDGMENTS

First and foremost, I want to thank Professor Peter J. Wagner for his encouragement, support and understanding throughout the years of "hard work". I believe that his honesty and words of wisdom made me not only a better chemist but a better human being as well.

I want to thank the past and the present members of Wagner's group for their friendship. Here, I want to mention Young C. Chung, a very special friend from Dr. Leroi's group; our long talks, either philosophical, political or scientific, were always enjoyable.

I want to acknowledge my parents. Words cannot express my thanks to them. My cousin, Nicholas T. Leventis: who set the standards in the family which I tried to push further. My friend, John E. Spatharas: the only real friend I have left in Greece.

Finally, I would like to thank the Chemistry Department of Michigan State University for financial support, research assistantships and the use of its facilities. Thanks also to the NSF for research assistantships administered by Dr. Wagner and to Ethyl Corporation and Yates Memorial for Summer Fellowships administered by the Chemistry Department of Michigan State University.

TABLE OF CONTENTS

	Page
LIST OF TABLES	IX
LIST OF FIGURES	XVII
INTRODUCTION	1
ELECTRONIC TRANSITION AND PHOTOCHEMISTRY IN TRANSITION METAL COMPLEXES	1
PHOTOCHEMISTRY OF RUTHENIUM(II) COMPLEXES	5
RESONANCE RAMAN SPECTROSCOPY OF TRANSITION METAL COMPLEXES	10
PHOTOCHEMISTRY OF TUNGSTEN CARBONYLS	11
KINETICS	16
RESEARCH GOALS	22
RESULTS	24
PHOTOREDUCTION OF KETONES BY TETRAHYDROFURAN	24
RUTHENIUM COMPLEXES	33
Ruthenium Pentaammine Complexes	33
Ruthenium 2,2'bipyridine and 1,10-phenanthroline Complexes	35
Ruthenium Porphyrines	37
Spectroscopic Studies	38
Raman Studies	50
Intramolecular Photoreduction	54

Page

Photoproduct Identification 55

Quantum Yield Studies 60

Quenching Studies 65

Ruthenium 2,2'bipyridine and Ruthenium-Osmium 2,2'bipyrimidine bridged complexes. . . 75

Compound Preparation and identification - Spectroscopic Studies 75

Raman Studies 81

Photochemistry of Tungsten Carbonyls 82

Compound Preparation and Identification . . 82

Ligands 82

Pentacarbonyl Tungsten(0) Complexes 83

Spectroscopic Studies. 86

Photochemical Studies. 86

Photoproduct Identification, Mass Balance, and Cross-coupling Experiments . . 86

Comparison of the Photobehavior of $W(CO)_5(4VP)$ with Other Pentacarbonyl Complexes of Tungsten-Stability of the Photoproduced Tetracarbonyl Complexes. 97

Quantum Yield Studies 102

Quenching Studies 106

A Energy Transfer Quenching 106

A1 Reaction Quenching 106

A2 Emission Quenching. 106

B Chemical Quenching. 115

B1 Reaction Quenching. 115

B2 Emission Quenching. 117

Page

Intermediate Trapping Experiments 117

DISCUSSION 127

PHOTOREDUCTION OF KETONES BY TETRAHYDROFURAN. . . 127

PYRIDYL KETONE PENTAAMMINE AND BIS(2,2'BIPYRIDINE) 128

RUTHENIUM(II) COMPLEXES 128

Absorption and Emission Studies. . . . . .

Raman Studies. 130

Photochemical Studies. 131

RUTHENIUM 2,2'BIPYRIDINE AND RUTHENIUM-OSMIUM 2,2'BIPYRIDINE BRIDGED COMPLEXES. 150

TUNGSTEN CARBONYLS. 150

Electronic Absorption and Emission Spectra . . 151

Photochemistry of $W(CO)_5(4VP)$. 152

SUMMARY 176

SUGGESTIONS FOR FURTHER STUDY 177

EXPERIMENTAL 180

INSTRUMENTATION 181

CHEMICALS 182

Solvents 182

Internal Standards 185

External Standards 185

Quenchers. 186

Actinometers 186

Ketones. 187

Pyridyl Ketone Hydrochloride Salts 193

Page

Nitrogen Coordinating Ligands. 194

Photoreduction Products. 195

Type II Products 196

Ruthenium Complexes. 196

Pentaammine Pyridine Ruthenium(II) Tetrafluoroborate and the Pyridine Substituted Derivatives 197

Diaquo cis-bis(2,2'bipyridine) Ruthenium(II) Dichloride. 201

Aqueous cis-bis(1,10-phenanthroline) Ruthenium(II) Dichloride. 202

Synthesis of Monocarbonyl Tetraphenylporphyrinato Ruthenium(II) . . . 211

Synthesis of bis(4-phenyl-1-(4-pyridyl)butanone) Tetraphenyl Porphyronato Ruthenium(II). 212

Synthesis of bis(4-phenyl-1-(4-pyridyl)butanone) octaethylporphyrinato Ruthenium(II) 213

Synthesis of Carbonyl Pyrazino Tetraphenylporphyrinato Ruthenium(II) . . . 215

Synthesis of Carbonyl (Carbonyl Pyrazino Tetraphenylporphyrinato Ruthenium(II)) Tetraphenylporphyrinato Ruthenium(II) . . . 215

Osmium Complexes 217

Aqueous cis-bis(2,2'bipyridine)Osmium(II) Chloride. 217

Aqueous bis(1,10-phenanthroline)Osmium(II) chloride. 218

Ruthenium-Osmium 2,2'bipyridine Bridged, Mixed Ligand Binuclear Complexes. 218

Tungsten Complexes 221

Pentacarbonyl (4-substituted-pyridine) Tungsten(0) Complexes 221

Page

Photoproduct Isolation and Identification . 226

cis-Tetracarbonyl bis(1-(4-pyridyl)pentanone) Tungsten(0). 226

Hexacarbonyl Tungsten(0). 227

METHODS AND TECHNIQUES. 228

Preparation of Samples 228

Photochemical Glassware 228

Irradiation Tubes 228

Stock Solutions and Photolysis Solutions. . 229

Degassing Procedures. 229

Irradiation Procedures. 229

Analysis of Samples. 230

Identification of Photoproducts 230

Gas Chromatography Procedures 232

High-pressure Liquid Chromatography Procedures. 233

Actinometry and Quantum Yield Determination. . 233

Valerophenone Actinometry 236

Uranyl Oxalate Actinometry. 237

Potassium Reineckate Actinometry. 238

Absorption Spectra 242

Emission Spectra 242

LIST OF REFERENCES 243

APPENDIX 252

LIST OF TABLES

		Page
Table 1.	Entering group concentration effects on photosubstitution of $W(CO)_5(pip)$ in benzene at 25°C.	14
Table 2.	Quantum Yields for Photoreactions of $W(CO)_5L$ Complexes.	15
Table 3.	Results from the Intermolecular photoreduction of pyridyl ketones by THF.	32
Table 4.	UV-Visible Absorption Spectral Data for some Pyridyl ketones and their Ruthenium Complexes.	40
Table 5.	Emission Data for Some Ligands and Their Ruthenium Complexes.	48
Table 6.	Mass Balance Experiment for styrene and 4AP been produced in the Type II cleavage of cis-$[Ru(bipy)_2(4PhBP)_2](BF_4)_2$.	57
Table 7.	UV-Visible absorption data of $[Ru(NH_3)_5(4PhBP)](BF_4)_2$, cis-$[Ru(bipy)_2(4PhBP)_2](BF_4)_2$, $[Ru(NH_3)_5(4EsterBP)](BF_4)_2$ and cis-$[Ru(bipy)_2(4EsterBP)_2](BF_4)_2$ upon irradiation at 313 nm.	49
Table 8.	Quantum Yields and $k_q\tau$ values for 4PhBP, 4EsterBP, 4PhBP.HCl, 4EsterBP.HCl and the corresponding Ruthenium Complexes.	61
Table 9.	Results from Stern-Volmer quenching of butyrophenone by Ruthenium(II) complexes.	75

Page

Table 10. UV-Visible Absorption data of mononuclear and binuclear 2,2'bipyrimidine complexes 78

Table 11. Emission data of mononuclear and binuclear 2,2'bipyrimidine Complexes . . . 80

Table 12. Carbonyl Compounds of Tungsten(0) and the Abbreviations Used 84

Table 13. Absorption and Emission Data for the Tungsten Carbonyls 87

Table 14. Mass balance experiments for Pentacarbonyl 4-valerylpyridine Tungsten(0) Photolysis 96

Table 15. Cross-Coupling Experiments for $W(CO)_5(4VP)$ and $W(CO)_5(4BP)$ Irradiated Together 97

Table 16. Formation Quantum Yield Data for cis-$W(CO)_4(4VP)_2$ from $W(CO)_5(4VP)$. 102

Table 17. Photoproduct and Emission Quenching from $W(CO)_5(4VP)$ 109

Table 18. cis-$W(CO)_4(4VP)_2$ formation Stern-Volmer Quenching by 4VP for $\lambda_{irr} > 400$ and $\lambda_{irr} > 475$ nm 115

Table 19. Effect of Added Butyrylpyridine on Photoproduct Formation with Visible Irradiation of $W(CO)_5(4VP)$ 122

Table 20. Relative Reactivities of Various Phenyl Ketones, Pyridyl Ketones and the Corresponding Pyridyl Ketone Hydrochloride Salts. 132

Table 21. Rate Constants for Quenching of Triplet BP by Various Ruthenium Complexes in Acetonitrile 135

Table 22. Pyridyl Proton Chemical Shifts in Free Pyridyl Ketone Ligands, Their Hydrochloride Salts and Their Ruthenium Complexes. 136

Page

Table 23. Type II Fragmentation Quantum Yields for the Hydrochloride Salts, Pentaammine, 2,2'Bipyridine and Porphyrine Ruthenium(II) Complexes of the Pyridyl Ketones. 138

Table 24. Lifetime Data for Ruthenium Complexes. . . 139

Table 25. Comparison of the Quantum Yields of Type II Products of Various Pentaammine Ruthenium Complexes. 140

Table 26. Rates of H-abstraction and Rates of Internal Conversion of Ruthenium Complexes. 144

Table 27. Response Factors for Various Compounds . . 235

Table 28. Mass Balance Experiment for the Photoreduction of Acetophenone by THF in acetonitrile. 253

Table 29. Double Reciprocal for DTHF vs. $[THF]^{-1}$ in the Photoreduction of acetophenone by THF 254

Table 30. Double Reciprocal for $THFCH_3CN$ vs. $[THF]^{-1}$ in the Photoreduction of Acetophenone by THF. 256

Table 31. Double Reciprocal for DTHF vs. $[THF]^{-1}$ in the Photoreduction of 4-acetylpyridine by THF. 257

Table 32. Double Reciprocal for $THFCH_3CN$ vs. $[THF]^{-1}$ in the Photoreduction of 4-acetylpyridine by THF. 258

Table 33. Double Reciprocal for DTHF vs. $[THF]^{-1}$ in the Photoreduction of Benzophenone by THF 259

Table 34. Double Reciprocal for $THFCH_3CN$ vs. $[THF]^{-1}$ in the Photoreduction of Benzophenone by THF. 260

Table 35. Double Reciprocal for DTHF vs $[THF]^{-1}$ in the Photoreduction of 4-benzoylpyridine by THF 261

Page

Table 36. Double Reciprocal for $THFCH_3CN$ vs. $[THF]^{-1}$ in the Photoreduction of 4-benzoylpyridine by THF 262

Table 37. Stern Volmer Data for 4-phenyl-1-(4-pyridyl) butanone. 263

Table 38. Stern Volmer data for 4-Phenyl-1-(4-pyridyl)butanone hydrochloride 264

Table 39. Concentration Dependence of the Quantum Yield of the Type II cleavage of 4-Phenyl-1-(4-pyridyl)butanone 265

Table 40. Concentration Dependence of the Quantum Yield of the Type II reaction of 4-Phenyl-1-(4-pyridyl)butanone hydrochloride. 266

Table 41. Independent Quantum Yield Determination for the Type II Cleavage of Pentaammine 4-Phenyl-1-(4-pyridyl)butanone Ruthenium(II) Tetrafluoroborate. 267

Table 42. Quantum Yield and Stern Volmer data for Penaammine 4-Phenyl-1-(4-pyridyl)butanone Ruthenium(II) Tetrafluoroborate. 268

Table 43. Quantum Yield and Stern Volmer Data for cis-bis(2,2'bipyridine) bis(4-Phenyl-1-(4-pyridyl)butanone) Ruthenium(II) Tetrafluoroborate. 269

Table 44. Concentration Dependence of the Quantum Yield of the Type II Cleavage of Pentaammine 4-Phenyl-1-(4-pyridyl)butanone Ruthenium(II) Tetrafluoroborate. 270

Table 45. Concentration Dependence of the Quantum Yield of the Type II cleavage of cis-bis(2,2'bipyridine)-bis(4-Phenyl-1-(4-pyridyl)butanone) Ruthenium(II) Tetrafluoroborate. 271

Page

Table 46. Stern-Volmer data for the cis-bis(2,2'bipyridine)- bis(4-Phenyl-1-(4-pyridyl)butanone) Ruthenium(II) Tetrafluoroborate Using Complex Concentration 0.010 M. 272

Table 47. Mass Balance Styrene and 4-acetylpyridine Produced from the Type II Cleavage of cis-bis(2,2'bipyridine)-bis(4-Phenyl-1-(4-pyridyl)butanone) Ruthenium(II) Tetrafluoroborate. 273

Table 48. Quantum Yield and Stern-Volmer Data for the Type II Cleavage of n-butyl-4-[(4-pyridyl)carbonyl]butyrate. 274

Table 49. Independent Quantum Yield Determination for the Type II Cleavage of the n-butyl-4-[(4-pyridyl)carbonyl]butyrate. . . 275

Table 50. Quantum Yield and Stern-Volmer Data for the Type II Cleavage of n-butyl-4-[(4-pyridyl)carbonyl]butyrate Hydrochloride. 276

Table 51. Quantum Yield and Stern-Volmer Data for the Type II Cleavage of Pentaammine n-butyl-4-[(4-pyridyl)carbonyl]butyrate Ruthenium(II) Tetrafluoroborate. 277

Table 52. Independent Quantum Yield Determination for the Type II Cleavage of Pentaammine n-butyl-4-[(4-pyridyl)carbonyl]butyrate Ruthenium(II) Tetrafluoroborate. 278

Table 53. Stern-Volmer Data for the Type II Cleavage of Cis-Bis (2,2'bipyridine) bis(n-butyl-4-[(4-pyridyl)carbonyl]-butyrate) Ruthenium(II) Tetrafluoro-borate 279

Table 54. Determination and Concentration Dependence of the Quantum Yield of cis-bis(2,2'bipyridine)-bis(n-butyl-4-[(4-pyridyl)carbonyl]butyrate) Ruthenium(II) Tetrafluoroborate. 280

Page

Table 55. Stern-Volmer Data for the Quenching of Butyrophenone by Pentaammine 4-acetylpyridine Ruthenium(II) Tetrafluoroborate. 281

Table 56. Stern-Volmer Data for the Quenching of Butyrophenone by cis-bis (2,2'bipyridine)bis(4-acetylpyridine) Ruthenium(II) Tetrafluoroborate. 282

Table 57. Stern-Volmer Data for the Quenching of Butyrophenone by cis-bis(1,10-phenanthroline)bis(4-acetylpyridine) Ruthenium(II) Tetrafluoroborate. 283

Table 58. Determination and Concentration Dependence of the Quantum Yield of the Type II Cleavage of Ruthenium Tetraphenylporphyrinato bis(4-phenyl-1-(4-pyridyl) butanone). 284

Table 59. Determination of the Quantum Yield of the Type II Cleavage of Ruthenium Octaethylporphyrinato bis(4-phenyl-1-(4-pyridyl)butanone) 285

Table 60. Data for the Calculation of the Response Factors of Various Compounds vs. Benzene for the HPLC Analysis. 286

Table 61. Mass Balance Experiment for the Irradiation of Pentacarbonyl 1-(4-pyridyl)pentanone Tungsten(0). 288

Table 62. Comperative Mass Balance Experiment for the Irradiation of Pentacarbonyl 1-(4-pyridyl)pentanone Tungsten(0), Degassed Normally and Under Carbon Monoxide 289

Table 63. Quantum Yield Data for Pentacarbonyl 1-(4-pyridyl)pentanone Tungsten(0) Photolysis at 490 nm 290

Table 64. Quantum Yield Data for Pentacarbonyl 1-(4-pyridyl)pentanone Tungsten(0) Photolysis at 410 nm 291

Page

Table 65. Concentration Dependence of the Quantum Yield of $W(CO)_5(4VP)$ Photolysis at λ = 490 nm 292

Table 66. Concentration Dependence of the Quantum Yield of $W(CO)_5(4VP)$ Photolysis at λ = 410 nm 293

Table 67. Stern-Volmer Data for $W(CO)_5(4VP)$ irradiated at 490 nm 294

Table 68. Stern-Volmer Data for $W(CO)_5(4VP)$ Irradiated at 490 nm 295

Table 69. Stern-Volmer Data for the $W(CO)_5(4VP)$ Emission Quenching 296

Table 70. Stern-Volmer Quenching Data for the cis-$W(CO)_4(4VP)_2$ Formation from $W(CO)_5(4VP)$ at [complex] = 0.00508 M . . . 297

Table 71. Stern-Volmer Quenching Data for the Emission from $W(CO)_5(4VP)$ at [Complex] = 0.00508 M. 298

Table 72. Stern-Volmer Data for $W(CO)_5(4VP)$ Emission Quenching 299

Table 73. Stern-Volmer Data for $W(CO)_5(4VP)$ Irradiated at 410 nm 300

Table 74. Stern-Volmer Data for $W(CO)_5(4VP)$ Irradiated at 410 nm 301

Table 75. Stern-Volmer for $W(CO)_5(4VP)$ Irradiated at 410 nm. 302

Table 76. Chemical Quenching Stern-Volmer Data for $W(CO)_5(4VP)$ Irradiated at λ > 400 nm 303

Table 77. Chemical Quenching Stern-Volmer Data for $W(CO)_5(4VP)$ Irradiated at λ > 475 nm 304

Table 78. Stern-Volmer Data for $W(CO)_5(4VP)$ Emission Quenching by 4AP. 305

Page

Table 79. Stern-Volmer Data for $W(CO)_5(4VP)$ Emission Quenching by 4VP. 306

Table 80. Intermediate Trapping Data for $W(CO)_5(4VP)$ Irradiated at $\lambda > 400$ nm . . . 307

Table 81. Intermediate Trapping Data for $W(CO)_5(4VP)$ Irradiated at $\lambda > 475$ nm . . . 309

Table 82. Thermal and Photochemical Behavior of cis-$W(CO)_4(4VP)_2$ in the Absence and in the Presence of 4BP. 311

Table 83. Data for the Thermal Reaction of cis-$W(CO)_4(4VP)_2$ with 4BP. 312

LIST OF FIGURES

		Page
Figure 1	Simplified molecular orbital diagram of a d_6 pyridyl ketone complex. . . .	2
Figure 2	Double reciprocal plots for Φ_{DTHF}^{-1} and $\Phi_{THFCH3CN}^{-1}$ vs. $[THF]^{-1}$ in the photoreduction of acetophenone by THF in acetonitrile.	26
Figure 3	Double reciprocal plot for Φ_{DTHF}^{-1} vs. $[THF]^{-1}$ in the photoreduction of acetophenone by THF in benzene.	27
Figure 4	Double reciprocal plots for Φ_{DTHF}^{-1} and $\Phi_{THFCH3CN}^{-1}$ vs. $[THF]^{-1}$ in the photoreduction of benzophenone by THF in acetonitrile.	28
Figure 5	Double reciprocal plots for Φ_{DTHF}^{-1} and $\Phi_{THFCH3CN}^{-1}$ vs. $[THF]^{-1}$ in the photoreduction of 4-acetylpyridine by THF in acetonitrile.	29
Figure 6	Double reciprocal plots for Φ_{DTHF}^{-1} and $\Phi_{THFCH3CN}^{-1}$ vs. $[THF]^{-1}$ in the photoreduction of 4-benzoylpyridine by THF in CH_3CN.	30
Figure 7	Absorption spectra in acetonitrile of 4PhBP, 4PhBP.HCl, $[Ru(NH_3)_5(4PhBP)](BF_4)_2$ and cis-$[Ru(bipy)_2(4PhBP)_2](BF_4)_2$.	45
Figure 8	Absorption spectra in acetonitrile of 4EsterBP, 4EsterBP.HCl, $[Ru(NH_3)_5(4EsterBP)](BF_4)_2$ and cis-$[Ru(bipy)_2(4EsterBP)_2](BF_4)_2$.	46

		Page
Figure 9	Absorption spectra in CH_2Cl_2 of $RuTPP(4PhBP)_2$ and $RuOEP(4PhBP)_2$.	47
Figure 10	Emission spectra of 4PhBP, 4PhBP.HCl, cis-$[Ru(bipy)_2(4PhBP)_2](BF_4)_2$ and $[Ru(bipy)_3](BF_4)_2$.	51
Figure 11	Emission spectra of 4EsterBP, 4EsterBP.HCl, cis-$[Ru(bipy)_2(4EsterBP)_2](BF_4)_2$ and $[Ru(bipy)_3](BF_4)_2$.	52
Figure 12	Absorption and emission spectra of 2,2'bipyridine and 4,5-diazafluorene.	53
Figure 13	UV-Visible absorption spectra upon 313 nm irradiation of $[Ru(NH_3)_5(4EsterBP)](BF_4)_2$ and $[Ru(NH_3)_5(4PhBP)](BF_4)_2$ in acetonitrile.	58
Figure 14	Effect of ketone concentration on the Type II products quantum yield for 4PhBP and 4PhBP.HCl irradiated at 313 nm in acetonitrile.	62
Figure 15	Effect of concentration of Ruthenium complex on quantum yield for $[Ru(NH_3)_5(4PhBP)](BF_4)_2$, cis-$[Ru(bipy)_2(4PhBP)_2](BF_4)_2$ and cis-$[Ru(bipy)_2(4EsterBP)_2](BF_4)_2$	63
Figure 16	Effect of concentration of $RuTPP(4PhBP)_2$ on the quantum yield for the Type II cleavage of the ligand.	64
Figure 17	Stern-Volmer plots for 4PhBP and for 4PhBP.HCl in acetonitrile.	66
Figure 18	Stern-Volmer plots for 4EsterBP and 4EsterBP.HCl in acetonitrile.	67
Figure 19	Stern-Volmer plots for $[Ru(NH_3)_5(4PhBP)](BF_4)_2$ and for cis-$[Ru(bipy)_2(4PhBP)_2](BF_4)_2$ in acetonitrile.	68
Figure 20	Stern-Volmer plots for $[Ru(NH_3)_5(4EsterBP)](BF_4)_2$ and for cis-$[Ru(bipy)_2(4PhBP)_2](BF_4)_2$ in acetonitrile.	69

		Page
Figure 21	Stern-Volmer plot for butyrophenone quenched by $[Ru(NH_3)_5(4AP)](BF_4)_2$.	72
Figure 22	Stern-Volmer plot for butyrophenone quenched by cis-$[Ru(bipy)_2(4AP)_2](BF_4)_2$.	73
Figure 23	Stern-Volmer plot for butyrophenone quenched by cis-$[Ru(phen)_2(4AP)_2](BF_4)_2$.	74
Figure 24	Absorption and emission spectra of $W(CO)_5(4VP)$ in benzene and methylcyclohexane.	89
Figure 25	Absorption spectra of cis-$W(CO)_4(4VP)_2$ in benzene and methylcyclohexane.	91
Figure 26	Infrared spectrum of cis-$W(CO)_4(4VP)_2$ in a KBr pellet.	92
Figure 27	Carbon-13 nmr spectra of cis-$W(CO)_4(4VP)_2$ in C_6D_6.	93
Figure 28	Proton nmr of cis-$W(CO)_4(4VP)_2$ in C_6D_6 and $CDCl_3$.	94
Figure 29	Absorption spectra of $W(CO)_5(4VP)$ in methylcyclohexane upon irradiation with $\lambda>400$ nm.	99
Figure 30	Absorption spectra of $W(CO)_5(4VP)$ in benzene upon irradiation with $\lambda>400$ nm. Carbon monoxide saturated sample.	100
Figure 31	Absorption spectra of $W(CO)_5(4CNpy)$ in methylcyclohexane and in benzene upon irradiation with $\lambda>400$ nm.	101
Figure 32	Carbon-13 nmr spectra of $W(CO)_5(4Bzpy)$ before and after irradiation in benzene-d_6.	103
Figure 33	Carbon-13 nmr spectra of $W(CO)_5(4VP)$ before and after irradiation in benzene-d_6.	104

		Page
Figure 34	Carbon-13 nmr spectra of $W(CO)_5(4BP)$ before and after irradiation in benzene-d_6.	105
Figure 35	Effect of concentration of $W(CO)_5(4VP)$ on the cis-$W(CO)_4(4VP)_2$ formation quantum yield. Irradiation at 410 nm in benzene.	107
Figure 36	Effect of concentration of $W(CO)_5(4VP)$ on the cis-$W(CO)_4(4VP)_2$ formation quantum yield. Irradiation at 490 nm in benzene.	108
Figure 37	Stern-Volmer plots for $W(CO)_5(4VP)$ irradiated at 410 nm in benzene. Three different complex concentrations.	110
Figure 38	Stern-Volmer plot for $W(CO)_5(4VP)$ irradiated at 490 nm in benzene. Cis-$W(CO)_4(4VP)_2$ formation quenching by anthracene. [$W(CO)_5(4VP)$] = 0.0105 M.	111
Figure 39	Stern-Volmer plots for $W(CO)_5(4VP)$. [Complex] = 0.00508 M. Cis-$W(CO)_4(4VP)_2$ formation and emission quenching by anthracene in benzene.	112
Figure 40	Stern-Volmer plots for $W(CO)_5(4VP)$. [Complex] = 0.000897 M. Cis-$W(CO)_4(4VP)_2$ formation and emission quenching by anthracene in benzene.	113
Figure 41	Stern-Volmer for the emission quenching of $W(CO)_5(4VP)$ by anthracene in benzene. [Complex] = 0.0000829 M.	114
Figure 42	Stern-Volmer plots for cis-$W(CO)_4(4VP)_2$ formation from $W(CO)_5(4VP)$ in benzene, quenched by free ligand (4VP).	116
Figure 43	Stern-Volmer emission quenching plot of $W(CO)_5(4VP)$ by 4AP in benzene.	118

		Page
Figure 44	Stern-Volmer emission quenching plot of $W(CO)_5(4VP)$ by 4VP in benzene.	119
Figure 45	Thermal reaction kinetics of cis-$W(CO)_4(4VP)_2$ with 4BP in benzene.	120
Figure 46	Product distribution after irradiation of $W(CO)_5(4VP)$ in the presence of 4BP in benzene. $\lambda_{irr}>400$ nm.	123
Figure 47	Product distribution after irradiation of $W(CO)_5(4VP)$ in the presence of 4BP in benzene. $\lambda_{irr}>475$ nm.	124
Figure 48	Variation of the concentration of cis-$W(CO)_4(4BP)_2$ produced upon irradiation of $W(CO)_5(4VP)$ in benzene with $\lambda_{irr}>400$ nm, in the presence of 4BP.	125
Figure 49	Stern-Volmer plots for $W(CO)_5(4VP)$ in benzene. Total tetracarbonyl product cis-$W(CO)_4(4VP)_2$, cis-$W(CO)_4(4BP)_2$ and cis-$W(CO)_4(4VP)(4BP)$ formation quenching by free ligand (4BP).	126
Figure 50	Internal ligand $n\pi^*$ excited state of cis-$[Ru(bipy)_2(4\text{-pyridyl ketone})_2]^{2+}$ complex.	146
Figure 51	Jablonski diagram for the cis-$[Ru(bipy)_2(4\text{-pyridyl ketone})_2]^{2+}$ complex.	149
Figure 52	MLCT and LF transitions in $W(CO)_5(4VP)$.	164
Figure 53	Simulation of equation 61 for the Stern-Volmer quenching by 4VP of cis-$W(CO)_4(4VP)_2$ formation from $W(CO)_5(4VP)$ at various k_L/k_{CO} values. The experimental points shown have the same meaning as in Figure 42.	174

INTRODUCTION

Electronic Transitions and Photochemistry in Transition Metal Complexes.

The excited state behavior of transition metal complexes having at least one conjugated ligand (i.e., ligand with low lying antibonding orbitals) has been explained adequately by considering three types of electronic transitions: The Internal Ligand (IL), the Ligand Field (LF) and the Metal to Ligand or Ligand to Metal Charge Transfer (MLCT or LMCT) transitions. Figure 1 is a simplified molecular orbital diagram of a d_6 pyridyl ketone complex in a C_{4v} field which illustrates the three types of electronic transitions,[1] in the case where the MLCT transition is the lowest one.

The internal ligand (IL) transitions involve electronic redistribution localized on the ligand and reaction patterns must involve ligand structural changes, reactions with other substrates, etc. similar to those of the free ligands. This is a relatively unexplored area of transition metal photochemistry.

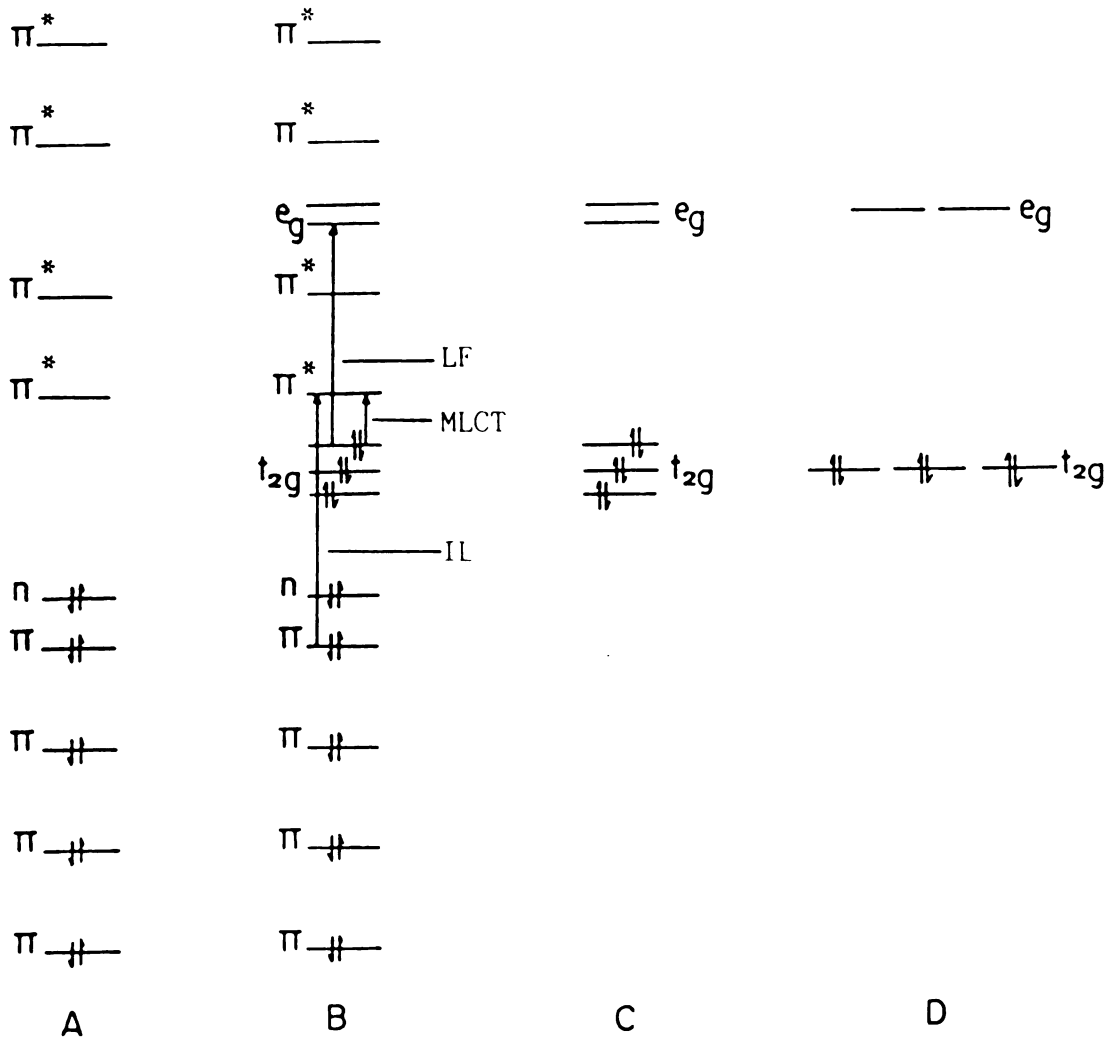

Figure 1. Simplified molecular orbital diagram of a d_6 pyridyl ketone complex: A. pyridyl ketone; B. orbitals resulting from the mixing of metal and antibonding ligand orbitals, π-back bonding is not considered; C. metal orbitals in the presence of a distorted octahedral field; D. crystal field approximation of d orbitals.

The ligand field (LF) or d-d transitions involve only d-orbitals of the metal and are localized mainly on it. These transitions are insensitive to solvent polarity or ligand substituents. The photochemistry originating from the LF excited states is dissociative in nature. In Figure 1 for example, electron transfer from the t_{2g} non-bonding orbitals to the e_g antibonding orbitals weakens the bonds between the metal and its ligands with resulting ligand dissociation.

Finally, the metal-to-ligand or ligand-to-metal charge transfer transitions (MLCT or LMCT, respectively) whose occurrence depends upon the origin of the excited electron have energies which depend both on the nature of the transition metal and on the nature of the ligands and are affected by the solvent polarity. These transitions do not involve any bond weakening so the corresponding excited states are not dissociative in nature (see below). A closer look reveals that these transitions leave an oxidized metal center and a reduced ligand, so it is not surprising that these transitions cause important red-ox reactions of the complexes. Wrighton, for example, reported[2] the reduction of 4-acetylpyridine (4AP) to 1-(4-pyridyl)ethanol in fac-$[Re(CO)_3(4AP)_2Cl]$ by MLCT excitation in the presence of triethylammine. Whitten[33], on the other hand, has opened the way to a water-splitting reaction using tris-(2,2'bipyridine) Ruthenium(II) complexes as sensitizers which participate in a red-ox reaction originating from the

MLCT excited state. Finally, the possibility of photodissociation from the MLCT excited states has been underlined first by Zink[3] who attributed the potential reactivity of the MLCT excited states to different ligand properties in the excited state compared to those in the ground state. More recently, Gray[4] explored the possibility the MLCT states favor an associative substitution pathway. No clear-cut proof has been presented though on MLCT excited states photodissociative properties.

Although d-d transitions are insensitive to solvent and to ligand substituents, MLCT transitions are greatly affected by those factors. In some cases, by varying the ligand substituents and/or the solvent, the excited state sequence can be tuned so that the lowest excited state is either the MLCT or the LF, with dramatic results on the photochemistry of the complexes.

In this work, emphasis has been given first to Internal Ligand reactions in pentaammine and polypyridyl complexes of Ruthenium as well as pentacarbonyl complexes of Tungsten, and second, to the excited state sequencing and characterization of the Ruthenium pentaammine and polypyridyl complexes. A brief account of the photochemistry of Ruthenium complexes is followed by a summary of the Resonance Raman spectroscopy by which the excited state sequencing of the Ruthenium complexes has been achieved. Next, an introduction to the photochemistry of Tungsten carbonyls follows. Finally, a description of the

excited state kinetics shows how kinetic parameters and mechanistic conclusions for transition metal complexes are extracted from experimental data. The Introduction concludes with the research goals.

Photochemistry of Ruthenium(II) Complexes.

Interest in the photochemistry of Ru(II) complexes has been considerable in recent years[5,6,7,8] and has been spurred by the discoveries that excited states of certain Ru(II) aromatic amine complexes can undergo either energy transfer[9] or electron transfer with the appropriate substrates.[10] There have been assigned four types of electronic transitions, i.e., charge transfer to solvent (CTTS) and Ligand Field (LF), in the case of $[Ru(NH_3)_6]^{2+}$,[11,12] as well as Metal to Ligand Charge Transfer (MLCT) and Internal Ligand (IL), in the cases of $[Ru(NH_3)_5(py\text{-}x)]^{2+}$ and cis-$[Ru(bipy)_2(py\text{-}x)_2]^{2+}$ (py-x = substituted pyridine). The latter two are more intense and obscure the other two transitions.[13] The presentation to follow starts with the photochemistry of the ammine complexes of Ruthenium in relation to the excited states involved and continues with the photochemistry of the polypyridyl complexes. Special emphasis is given always to the internal ligand reactions.

Aqueous solutions of $[Ru(NH_3)_6]^{2+}$ at pH=3 irradiated at $\lambda_{irr}>313$ nm, yield both oxidation (ΦRu(III)) = 0.03 $\pm$ 0.01) and aquation, i.e., photosubstitution (Φ_{aq} = 0.26 $\pm$ 0.01)

both w

a comm

result

light

oxida

seen,

state

absor

aquec

both

band

coord

state

cross

longe

dete

excha

latt

stat

orig

from

stat

than

elec

stat

[Ru(

both wavelength independent, attributed to the population of a common excited state, presumably LF in character, as the result of irradiation in this region.[14] For λ_{irr}<280 nm, light absorption is directly into the CTTS state, and oxidation is dominant. Residual photoaquation has also been seen, either as a result of interconversion from the CTTS states into the LF states or alternatively to direct absorption into LF bands obscured by more intense CT bands.

Photolysis of the pyridine complex $[Ru(NH_3)_5(py)]^{2+}$ in aqueous solution at wavelengths shorter than 334 nm gives both photoaquation and photooxidation. The major absorption band in this region is the IL $\pi \rightarrow \pi^*$ transition of the coordinated pyridine but the products are formed from other states, perhaps produced by internal conversion/intersystem crossing from the initially populated IL configuration. At longer irradiation wavelengths, no photooxidation is detected, only photoaquation and a low quantum yield ($\sim 10^{-4}$) exchange of pyridine hydrogens with solvent hydrogens. The latter reaction has been explained in terms of the MLCT state, while the ligand labilization has been proposed to originate from a LF state, populated by internal conversion from the initially formed MLCT state.[12,15,16] Since the LF states are much less affected by substituents on pyridine than are the MLCT states[12], choice of an appropriate electron-withdrawing group should give a lowest energy MLCT state. Complexes like $[Ru(NH_3)_5(4\text{-acetylpyridine})]^{2+}$ and $[Ru(NH_3)_5(\text{isonicotinamide})]^{2+}$, with $\lambda_{max(MLCT)}$ longer than

~460 nm, are significantly less reactive than $[Ru(NH_3)_5(py)]^{2+}$ when irradiated at their $\lambda_{max(CT)}$, with wavelength dependent Φ values as much as three orders of magnitude smaller. This pattern suggests that the crossover point between complexes with a lowest energy LF state and those with a lowest energy MLCT state comes when $\lambda_{max(MLCT)}$ is ~460 nm.

Finally, the only example of an Internal Ligand reaction for the Ruthenium Pentaammine system involves the Type II cleavage of 3- and 4-valerylpyridine coordinated to Ruthenium(II) according to equation (1).[17]

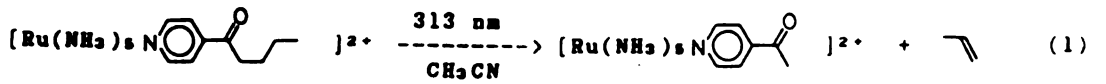

(1)

The quantum yields corrected for partial absorption of light by the ligand are unaffected by the coordination to the Ruthenium center. This permits an estimation of an upper limit to 10^8 sec^{-1} for the rate of the internal conversion of the $n\pi^*$ IL excited state to lower LF and MLCT states.[17]

Another large class of Ruthenium complexes includes the Ruthenium polypyridyl complexes, the chemistry of which started with the synthesis of $[Ru(bipy)_3]X_2.nH_2O$ by Burstall[18] (bipy = 2,2'bipyridine) in 1936, but it attracted little interest until 1959 when Paris and Brandt[19] discovered its visible-region luminescence at 77° K. After further research, a large amount of evidence accumulated

from luminescence lifetime studies of $[Ru(bipy)_3]^{2+}$ that strongly supported a $d\pi^*$[20,21,22,23,24] heavy-atom perturbed[25] spin forbidden process as the basis for the observed phenomenon. $[Ru(bipy)_3]^{2+}$, once thought to be photochemically inert, has been proven[26,27,28] to be photochemically active, giving products according to equation (2).

$$[Ru(bipy)_3]X_2 \xrightarrow{h\nu} [(bipy)_2RuX(bipy)]X \longrightarrow [(bipy)_2RuX_2] + bipy \quad (2)$$

For the salt $[Ru(bipy)_3](NCS)_2$, Φ in dichloromethane was measured as 0.068 at 25°C. The proposed mechanism[28] is: initial excitation leads to a charge-transfer state largely triplet in character. The CT state undergoes thermal activation to give a d-d excited state. The d-d state undergoes further thermal activation by loss of a pyridyl group to give a five coordinate intermediate, which captures a sixth ligand (either solvent or an anion held close to the activated metal center by ion-pairing) or chelate ring closure to return to $[Ru(bipy)_3]^{2+}$. The apparent photochemical stability of $[Ru(bipy)_3]^{2+}$ in water has been attributed to a consequence of the dominance of chelate ring closure and not of an inherently low photochemical reactivity. In related complexes, photochemical substitution in cis-$[Ru(bipy)_2(py)_2]^{2+}$ (py=pyridine) has been shown to be of synthetic value[29] and both photochemical

cis

obse

[Ru

enc

of

ison

wave

whic

cis-

wave

that

stat

inve

reac

irre

[Ru

octa

phot

atte

like

a t

stud

[Ru

[Ru

cis <----> trans isomerization and ClO_4^- oxidation have been observed for cis-$[Ru(bipy)_2(H_2O)_2]^{2+}$.[30]

Internal ligand photochemical reaction from cis-$[Ru(bipy)_2X_2](BF_4)_2$ complexes has been reported by Whitten and Zarnegar[31,32] when X=4-stilbazole. No photodissociation of these complexes was observed. Coordinated 4-stilbazole isomerizes in a wavelength dependent manner. Long wavelengths of irradiation produces MLCT excited states which behave like the radical anion of 4-stilbazole with cis- to trans- isomerization being more efficient. Short wavelengths yield a cis- to trans- ratio very similar to that of the free ligand.

Finally, the red-ox properties of the MLCT excited states of Ruthenium polypyridyl complexes have been investigated extensively with respect to the water splitting reaction. Whitten[33] demonstrated that visible wavelength irradiation of some samples of the complexes cis-$[Ru(bipy)_2(4,4'-(ROOC)_2bipy)]^{2+}$ (R=dihydrocholesterol and octadecyl) under special experimental conditions, causes photoinduced cleavage of H_2O into H_2 and O_2. Thus, attention was focused on other possible candidate complexes like bis(2,2'bipyridine) Ruthenium(II) complexes possessing a third, strong-field bidentate ligand for continuing studies in this area. Species like $[Ru(bipy)_2(phen)]^{2+}$,[34,35] $[Ru(bipy)_2(bipym)]^{2+}$ [36,37] and $[Ru(bipym)_3]^{2+}$ [36] (phen=1,10-phenanthroline, bipym=2,2'-

bipyrimidine) have been reported. Utilization of these and related complexes in the water splitting reaction revealed certain advantages over the classical $[Ru(bipy)_3]^{2+}$ complex (higher quantum yields for H_2 evolation, etc.).[38] Certain binuclear species like $[Ru(bipy)_2(bipym)Ru(bipy)_2]^{4+}$ have been reported[36,37] and they have been studied with respect to their red-ox and emission properties.[37] After one electron oxidation, an Intervalence-Transfer absorption band appears, the intensity of which allows an estimate for the extent of delocalization (α^2), which was found to be small, supporting the suggestion that electronic coupling between sites is weak.[39] Only very recently, binuclear complexes have been reported that they can carry the water splitting reaction with efficiencies claimed higher than those obtained with $[Ru(bipy)_3]^{2+}$.[40]

Resonance Raman Spectroscopy of Transition Metal Complexes.

Resonance enhanced Raman spectroscopy has proved to be a powerful tool in obtaining excitation profiles of transition metal complexes, thus elucidating which transitions are responsible for the broad and intense CT absorptions.[41] The innovation in the field came in 1979 when Woodruff reported[42,43] the Raman spectrum of the MLCT excited state of $[Ru(bipy)_3]^{2+}$. This spectrum is identical to the spectrum reported by Wrighton[44] four years later for fac-$[Re(CO)_3(bipy)Cl]$, and both are almost identical to the 2,2'bipyridine anion radical Raman spectrum.[43] The

implications of these results are overwhelming. It proves that the electron is localized on one bipy ligand in the MLCT excited state. The question rises: what makes the electron discriminate against the two bipy molecules and localize on the third one, despite the fact that the MLCT excited state of $[Ru(bipy)_3]^{2+}$ is long lived and, therefore, delocalization would have plenty of time to occur? On the other hand, $[Ru(bipy)_3]^{2+}$ in 1:1 (v/v) water/glycol mixtures, above and well below the glass-forming temperature, led to a disappearance of the discrete frequencies observed in liquid solutions and replacement by a broad scattering.[45] The latter fact has been taken as evidence that charge localization takes place rapidly in the solutions but is inhibited in rigid media.

Photochemistry of Tungsten Carbonyls.

The primary photochemical step for most metal carbonyls is the loss of a carbon monoxide molecule.[46]

The discovery of the photosensitivity of Group VI hexacarbonyls in 1961[47,48] opened the route for the preparation of many pentacarbonyl species by the photochemical substitution of CO by some donor (eg. pyridine, PPh_3, pentene).[49] Many early[50,51,52,53] and recent[54,55,56,57] reports concern the nature of the intermediates after photolysis of the parent hexacarbonyls in solution and in rigid glasses, employing either steady state or flash photolysis techniques. It seems that the

primary photoproduct is $W(CO)_5$ which coordinates weakly with a ground state molecule through the carbonyl oxygen as in $(CO)_5W\text{-}OC\text{-}W(CO)_5$.[55,56] Since this thesis concerns pyridyl complexes of Tungsten, an extensive review of the photochemistry of pentacarbonyl- and tetracarbonyl-(substituted pyridine) Tungsten(0) complexes is presented below.

Complexes of the general formula $W(CO)_5L$, where L is a nitrogen donor ligand, have interesting and interrelated spectroscopic and photochemical characteristics. They luminesce is both rigid glasses at 77°K[58,59,60] and in solution at 298°K,[63,69] the emission having been assigned to either a ^3E ---> $^1A_1$ ligand field (LF) transition or a W ---> L Charge Transfer (MLCT) transition. The electronic absorption spectra suggest that as L becomes more electron withdrawing, the MLCT state lowers in energy and, for some ligands (eg. 4-acetylpyridine: 4AP, 4-cyanopyridine: 4CNpy), it crosses below the LF state, thus becoming the lowest-lying state.[60]

The identity of the lowest excited state has been shown to be of primary importance when the complex photosubstitution reactivity is investigated. Complexes with W ----> L CT lowest excited state are less reactive towards photosubstitution compared to the complexes with LF lowest excited state,[60] in analogy to previous findings for $[Ru(NH_3)_5L]^{2+}$ complexes.[14,16]

In general, complexes of the type $W(CO)_5L$ are supposed to react according to Scheme 1. Adamson and Lees

Scheme 1.

$$W(CO)_5L \xrightarrow{h\nu} W(CO)_5 + L \quad (3a)$$

$$W(CO)_5L \xrightarrow{h\nu} C_{4v}\text{-}[W(CO)_4L] + CO \quad (3b)$$

$$W(CO)_5L \xrightarrow{h\nu} C_s\text{-}[W(CO)_4L] + CO \quad (3c)$$

reported,[61] based on room temperature flash photolysis data, that the primary photoproduct from $W(CO)_5(4AP)$ is the same obtained from $W(CO)_6$ and they assigned the structure $W(CO)_5S$ (S=Solvent). The C_s-$[W(CO)_4L]$ species seems also to exist based on IR data.[55] C_s-$[W(CO)_4(pyridine)]$ is formed and has been detected after short wavelengths of irradiation (229 and 254 nm) in an Ar matrix at 10°K. No experimental evidence has ever been collected for the C_{4v}-$[W(CO)_4L]$ species. Its existence has only been suggested; and since the only tetracarbonyl Tungsten(0) complexes ever isolated are of the cis- geometry, it has been proposed[62] that C_{4v}-geometry can rearrange to the C_s- one so that the final

product is always the cis-disubstituted tetracarbonyl product and not the trans. A very important point here is that all the experiments described in the literature concern irradiations of $W(CO)_5L$ in the presence of L or another entering group like 1-pentene or ethanol as an intermediate trapper. The photochemistry of $W(CO)_5L$ in the absence of an entering ligand has been assumed complicated[63] and never carefully studied. In order to verify the mechanism of Scheme 1 for CO substitution in $W(CO)_5L$ accounting for cis-$W(CO)_4L_2$ formation, Wrighton investigated the entering group concentration effects on photosubstitution in $W(CO)_5(pip)$[64] (pip=piperidine) and his results are displayed in Table 1.

Table 1. Entering group concentration effects on photosubstitution of $W(CO)_5(pip)$ in benzene at 25°C.

Entering group, (M)	Product	λ_{irr}, nm	Relative Q.Y.
piperidine, 0.025	cis-$W(CO)_4(pip)_2$	366	1.10
piperidine, 0.25	cis-$W(CO)_4(pip)_2$	366	1.00
piperidine, 1.00	cis-$W(CO)_4(pip)_2$	366	0.98
1-pentene, 0.025	$W(CO)_5$(1-pen)	436	0.94
1-pentene, 0.25	$W(CO)_5$(1-pen)	436	1.00
1-pentene, 1.00	$W(CO)_5$(1-pen)	436	1.09

Wrighton[64] considered that there is no entering group concentration effect on substitution quantum yields and he thought that this is consistent with a dissociative type of

mechanism for the photosubstitution of both CO and L in $W(CO)_5L$.

Internal ligand photochemical reaction, as in the case of cis-$[Ru(bipy)_2(4\text{-styrylpyridine})_2]^{2+}$,[31,32] has been observed in $W(CO)_5$(4-styrylpyridine) too.[65] According to Wrighton, this reaction is an example of a photoassisted reaction.[66] The photoreactions of $W(CO)_5$(pyridine) and $W(CO)_5$(4-styrylpyridine) in 3.66 M 1-pentene, isooctane solvent have been compared. The data demonstrate that photosubstitution of the pyridyl group can be attenuated by the provision of another chemical decay path: energy migration from the coordination sphere to the ligand followed by independent reaction of the ligand. The quantum yields for cis-trans isomerization of the 4-styrylpyridine seem to account for most of the loss in substitution yields. Equations (4), (5), (6) and (7) of Table 2 demonstrate the fact.

Table 2. Quantum Yields for Photoreactions of $W(CO)_5L$ Complexes[a]

			Φ_{436}	
$W(CO)_5$py	436 nm --------->	$W(CO)_5$(1-pent)	0.63	(4)[b]
$W(CO)_5$py	436 nm --------->	cis-$W(CO)_4(py)_2$	0.002	(5)[c]
$W(CO)_5$(t-4-stypy)	436 nm --------->	$W(CO)_5$(1-pent)	0.16	(6)[b]
$W(CO)_5$(t-4-stypy)	436 nm --------->	$W(CO)_5$(c-4-stypy)	0.49	(7)[b]

[a] py = pyridine, 1-pent = 1-pentene, 4-stypy = 4-styrylpyridine.

[b] Φ measured at room temperature in the presence of 3.66 M 1-pentene, isooctane solvent.

[c] Φ for formation of cis-$W(CO)_4(py)_2$ at room temperature in presence of 0.25 M pyridine in isooctane.

The cis-$W(CO)_4L_2$ complexes have been prepared utilizing equation 3b, as has been explained above, by photolyzing $W(CO)_5L$ in the presence of L.[64,67,68] When L is a substituted pyridine, the spectral data show that the W ---> py CT state moves smoothly to lower energy with more electron-withdrawing substituents on the pyridine, while the ligand field states are essentially insensitive to these changes.[67] The 298°K emission centered in the 550-700 nm region is sensitive to the nature of the pyridyl ligand substituents and emission quantum yields range from 1.0 x 10^{-4} to 56 x 10^{-4}.[68] The W ----> L CT state is virtually unreactive; eg. cis-$W(CO)_4$(4-formylpyridine)$_2$ undergoes photosubstitution with a 436 nm quantum yield of ~0.0007. Complexes having LF lowest excited state are very photosubstitution labile; eg. for L = 3,4-dimethylpyridine, 4-ethylpyridine, or pyridine the photosubstitution of L in cis-$W(CO)_4L_2$ occurs with a 436 nm irradiation quantum yield of ~0.4.[68]

Kinetics.

In order to elucidate the excited state processes in a certain photochemical reaction, it is necessary to make quantitative measurements of the Quantum Yields, excited state lifetimes, and rate constants of the different processes originating from the excited states.

A simple mechanistic scheme which can fit any unimolecular photochemical reaction originating from the triplet state is as follows:

Scheme 2.

$GS \xrightarrow{h\nu} {}^1ES^*$ creation of singlet excited state

${}^1ES^* \xrightarrow{\Phi_{(ISC)}} {}^3ES^*$ Intersystem Crossing of excited singlet to triplet state

${}^3ES^* \xrightarrow{k_r}$ intermediates

Intermediates $\xrightarrow{\alpha}$ Products; α: efficiency with which intermediates yield products

${}^3ES^* \xrightarrow{k_p} GS$ radiative decay to GS (phosphorescence)

${}^3ES^* \xrightarrow{k_d} GS$ radiationless decay to GS

${}^3ES^* + Q \xrightarrow{k_q} GS$ bimolecular deactivation process (quenching)

GS = Ground State

ES = Excited State

The quantum yield of a product is

$$\Phi_{(product)} = \Phi_{(ISC)} \times \alpha \times P_{(product)}; \qquad (8)$$

where $P_{(product)}$ is the probability that the triplet state yields the product versus any other process.

In the absence of an externally added quencher:

$$P_{(product)} = \frac{k_r}{k_r + k_p + k_d} \qquad (9)$$

In the presence of an externally added quencher Q:

$$P_{(product)} = \frac{k_r}{k_r + k_p + k_d + k_q[Q]} \qquad (10)$$

Therefore, the Quantum Yield in the absence of a quencher is:

$$\Phi^o = \Phi_{(ISC)} \times \alpha \times \frac{k_r}{k_r + k_p + k_d} \qquad (11)$$

In the presence of a quencher:

$$\Phi = \Phi_{(ISC)} \times \alpha \times \frac{k_r}{k_r + k_p + k_d + k_q[Q]} \qquad (12)$$

The Stern-Volmer equation[70] is obtained from (11) and (12):

$$\Phi^o/\Phi = 1 + k_q \tau [Q] \qquad (13)$$

τ is the lifetime of the excited state and is defined as

$$\tau = (k_r + k_p + k_d)^{-1} \qquad (14)$$

From equation (13), a plot of Φ^o/Φ versus [Q] gives a straight line with a slope $k_q \tau$. The value of k_q is known

for triplet quenchers in various solvents[71,72,73] and the value of τ is easily determined.

If the excited triplet state reacts intermolecularly with another substrate to give intermediates which decay either to GS or to products, Scheme 2 is modified to Scheme 3.

Scheme 3.

$$GS \xrightarrow{h\nu} {}^1ES^*$$

$${}^1ES^* \xrightarrow{\Phi(isc)} {}^3ES^*$$

$${}^3ES^* + S \xrightarrow{k_r} \text{Intermediates; S: Substrate reacting with the excited state}$$

$$\text{Intermediates} \xrightarrow{\alpha} \text{products; } \alpha\text{: efficiency with which intermediates yield products}$$

$$\text{Intermediates} \xrightarrow{1-\alpha} GS + S$$

$${}^3ES^* \xrightarrow{k_p + k_d} GS$$

$${}^3ES^* + Q \xrightarrow{k_q} GS + Q$$

The product Quantum Yield in the absence of a quencher is:

$$\Phi^o_{(product)} = \Phi_{(ISC)} \frac{\alpha\, k_r[S]}{k_r[S] + k_p + k_d} \qquad (15)$$

Eq. (15) and the product quantum yield in the presence of external quencher is:

$$\Phi_{(product)} = \Phi_{(ISC)} \frac{\alpha\, k_r[S]}{k_r[S] + k_p + k_d + k_q[Q]} \qquad (16)$$

Dividing (15) by (16), one obtains the Stern-Volmer equation:

$$\Phi^{o}/\Phi = 1 + k_q \tau[Q] \qquad (17)$$

where $$\tau = (k_r[S] + k_p + k_d)^{-1} \qquad (18)$$

Inversion of (15) gives a linear relationship (19) between Φ^{-1} and $[S]^{-1}$:

$$1/\Phi = (\Phi_{(ISC)}\ \alpha)^{-1} \times \left(1 + \frac{k_p + k_d}{k_r[S]}\right) \qquad (19)$$

Dividing the slope by the intercept of equation (19) gives $(k_p+k_d)/k_r$ which can be substituted into (18) along with the value of τ determined from Stern-Volmer quenching studies (17) to obtain the values for (k_p+k_d) and k_r.

When the irradiated substrate is a metal complex, the triplet excited state (^{3}ES*) can be LF, MLCT or IL. One can selectively populate an excited state by choosing the wavelength of irradiation.

Reaction of a ligand (like isomerization of stilbazole or Type II cleavage of 4-valerylpyridine) from an IL upper excited state fits to Scheme 2, where k_p and k_d have been substituted by k_{IC}: the rate constant for the internal conversion which includes any deactivation to lower excited states or any other intramolecular deactivation process.

Photodissociation, i.e., ligand loss from the LF excited state is another unimolecular process and fits also the Scheme 2, where we separate two cases. If LF is the lowest state, k_p and k_d have the meaning given in Scheme 2. Otherwise, they have to be replaced by k_{IC} as above.

Red-ox reactions originating from the MLCT excited state are bimolecular processes and, therefore, they have to be treated according to Scheme 3.

A final comment needed to be made is that if the lowest excited state emits, one is able to obtain an independent measurement of the lowest excited state lifetime by emission quenching. It is supposed that the Kasha's rule is obeyed and emission originates only from the lowest excited state. If the same lowest excited state yields also photochemistry or populates another state which gives photochemistry, the two lifetimes, i.e., the one obtained from photochemistry quenching and the one obtained from emission quenching, should be identical. It is implied that when photochemistry originates from an upper excited state, the two lifetimes have to be, in principle, different, unless the two excited states interconvert.

Research Goals.

The familiar Type II Intramolecular photoreduction[74] of pyridyl ketones coordinated to a Ruthenium(II) Pentaammine center has been used to estimate the rate of internal conversion from the IL upper excited state to lower excited states in coordination compounds.[17] The studies presented in this thesis are the continuation of this concept in two dimensions.

First, the reaction originating from the internal ligand excited state was slowed down so it would compete with internal conversion, allowing a better estimate for the rate of the internal conversion. In parallel, we investigated the possibility of intramolecular energy transfer from the reacting ligand to another ligand of lower triplet energy. For this purpose, we synthesized complexes like cis-$[Ru(bipy)_2X_2](BF_4)_2$ (X = pyridyl ketone able to give Type II reaction).

Second, we focused on Tungsten complexes like $W(CO)_5$(4-valerylpyridine) after the observation by Adamson and Lees in 1980[63] of room temperature emission. These complexes having MLCT lowest excited state are relatively substitution inert and, therefore, good candidates to test the generality of our approach for Internal Conversion rate estimation. The room temperature emission was a promising factor that, besides photochemistry, emission kinetics could be studied, too. These complexes failed to give the Internal Ligand

Type II reaction, giving instead ligand substitution products identical to those obtained with long wavelengths irradiation. Research in this direction led to elucidation of the photochemistry of Pentacarbonyl Substituted pyridine Tungsten(0) complexes in the absence of an entering ligand.

Finally, excited state resonance Raman spectroscopy was used in a collaborative project with Y. C. Chung in order to elucidate the generality of Woodruff's model for complexes like cis-$[Ru(bipy)_2L_2]^{2+}$ or $[Ru(bipy)_2(bipym)]^{2+}$ or $[Ru(bipy)_2(bipym)Ru(bipy)_2]^{4+}$. Clues are drawn about the origin of the MLCT excited state localization in Woodruff's model.

RESULTS

Photoreduction of Ketones by Tetrahydrofuran.

Following the reasoning that an Intermolecular photoreduction of a coordinated pyridyl ketone would be slow enough to compete with internal conversion, studies were started on the Photoreduction of acetophenone by THF in acetonitrile, benzene or neat THF in order to identify the coupling product of two 2-tetrahydrofuryl radicals (octahydro-2,2'bifuran). An additional peak with short retention time appears in the g.c. traces when the photoreduction takes place in acetonitrile. Preparative gas chromatography yielded enough product for a proton nmr spectra. Gc/ms does not give a molecular ion peak but, otherwise, is consistent with the assignment of 2-(2-tetrahydrofuryl)acetaldimine ($THFCH_3CN$) to this product. The rest of the products were identified either by gc/ms (octahydro-2,2'bifuran: DTHF and cross-coupling products) or by the comparison of the gc retention times with an authentic sample (pinacol). Spectral data for these products are given in the experimental section. A mass balance experiment (Table 28) accounted for only 80% of the acetophenone consumed. Scheme 4 shows the photochemical reaction of acetophenone with THF in acetonitrile.

Scheme 4.

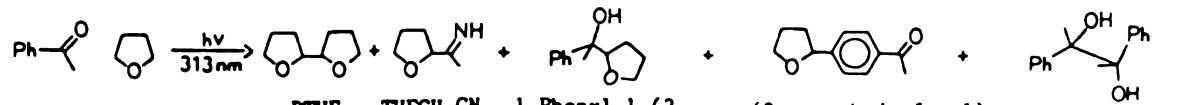

Benzophenone, 4-acetylpyridine and 4-benzoylpyridine were irradiated in acetonitrile only and were found to yield $THFCH_3CN$ in parallel to DTHF production. None of the products was isolated quantitatively.

The phenyl and pyridyl ketones studied were irradiated at 313 nm in acetonitrile (0.1 M) with varying concentration of THF (hydrogen donor). All runs were analyzed for DTHF and for $THFCH_3CN$. Plots of Φ^{-1} products vs. $[THF]^{-1}$ (Double reciprocals) for both products analyzed are shown on Figures 2-6. The intercept of these double reciprocal plots is equal to Φ_{max}^{-1}, i.e., the quantum yield for the photoreduction of the corresponding ketone at infinite hydrogen donor concentration while the slope over the intercept is equal to the k_d/k_r value of the triplet excited state of the ketone under study (k_r is the same as defined in Scheme 3 of the introduction; k_d includes both k_d and k_p constants of Scheme 3). Table 3 shows the intercepts as Φ_{max}^{-1} values as well as the k_d/k_r values for each ketone studied for both products analyzed, together with the number of points used from each figure to draw the best line.

Octahydro-2,2'bifuran usually gives a good linear correlation where 2-(2-tetrahydrofuryl)acetaldimine proved difficult to analyze; several points usually do not

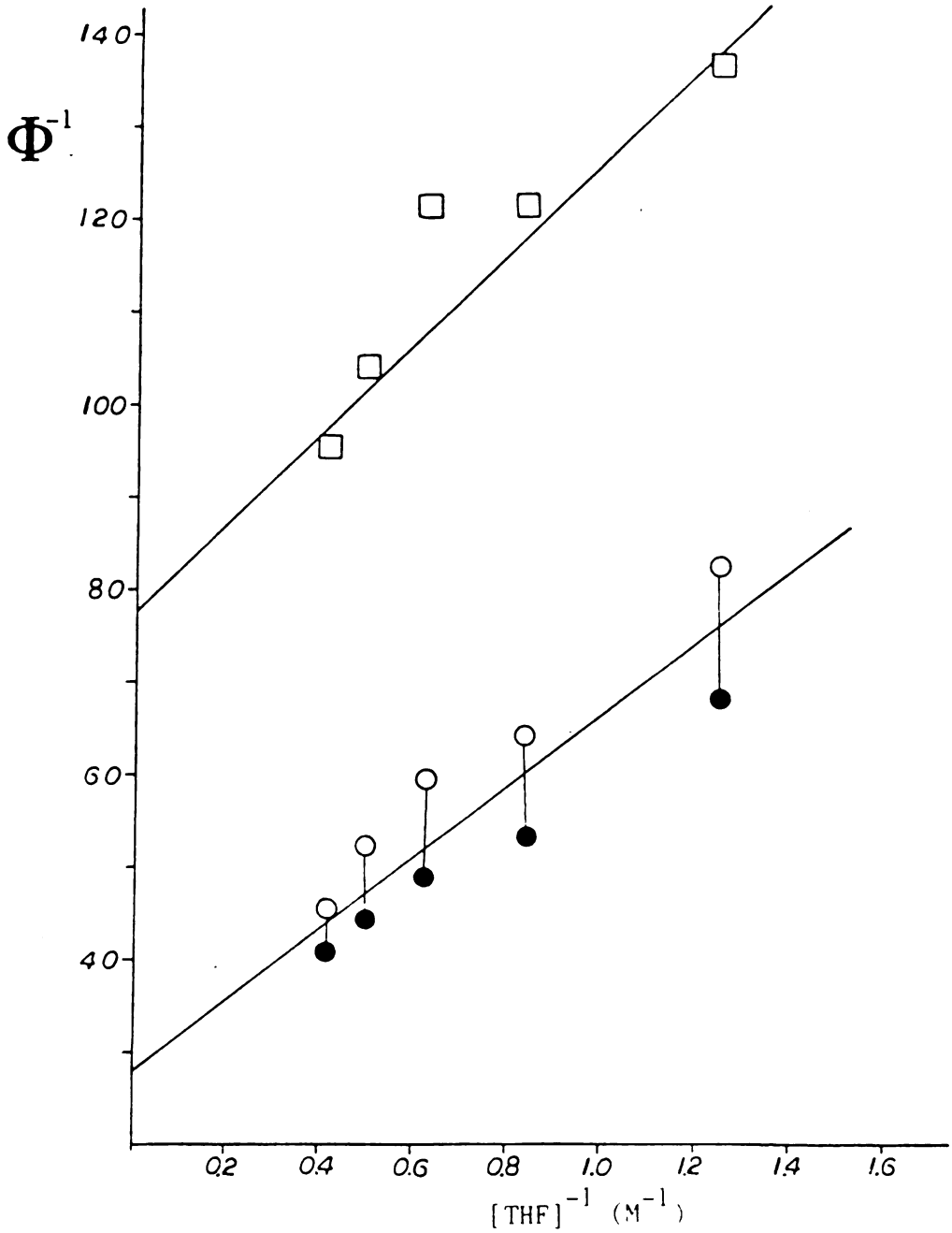

Figure 2. Double reciprocal plots for Φ^{-1}_{DTHF} (○) and $\Phi^{-1}_{THFCH_3CN}$ (□) vs. $[THF]^{-1}$ in the photoreduction of acetophenone by THF in acetonitrile.

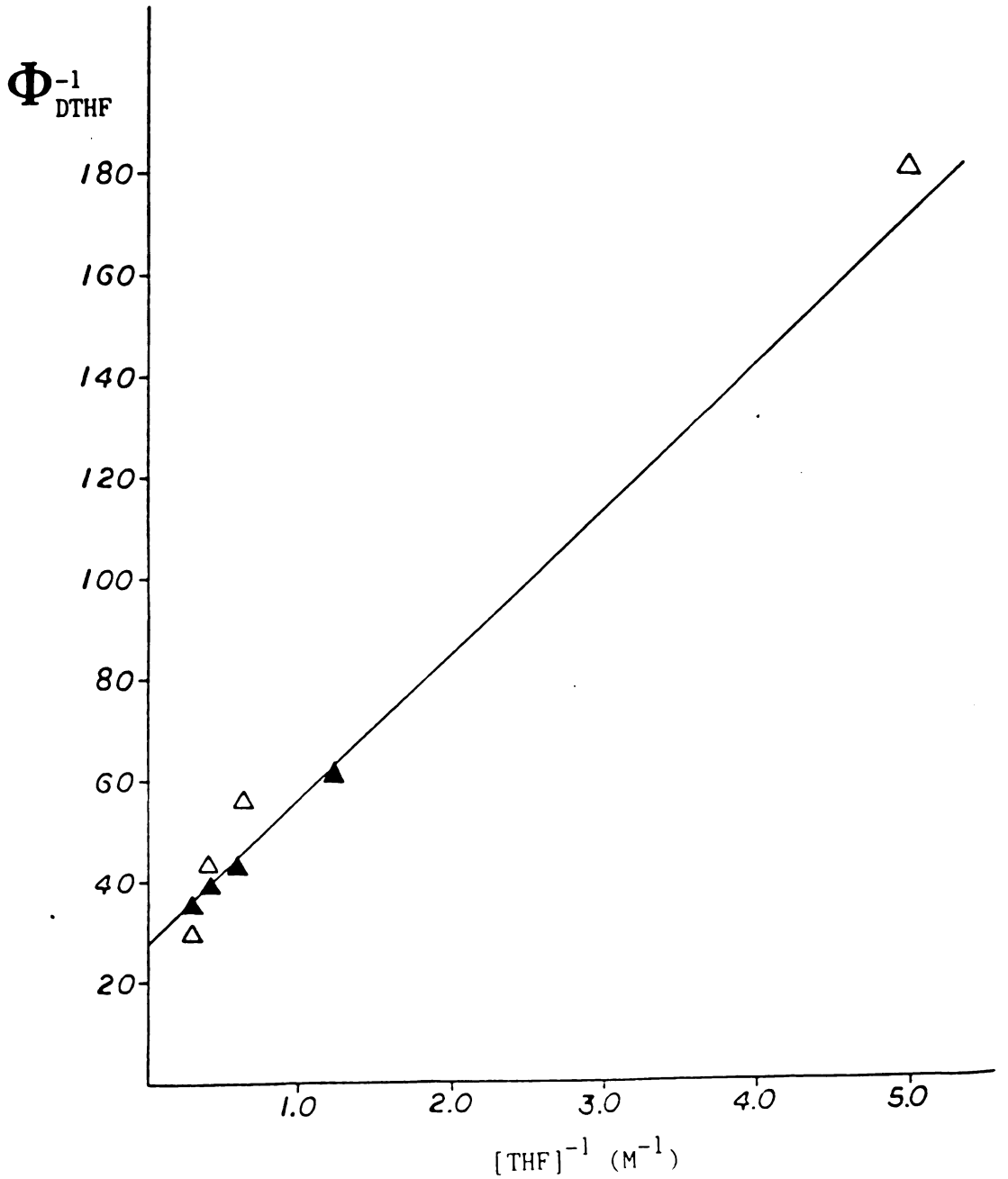

Figure 3. Double reciprocal plot for Φ^{-1}_{DTHF} (△) vs. $[THF]^{-1}$ in the photoreduction of acetophenone by THF in benzene.

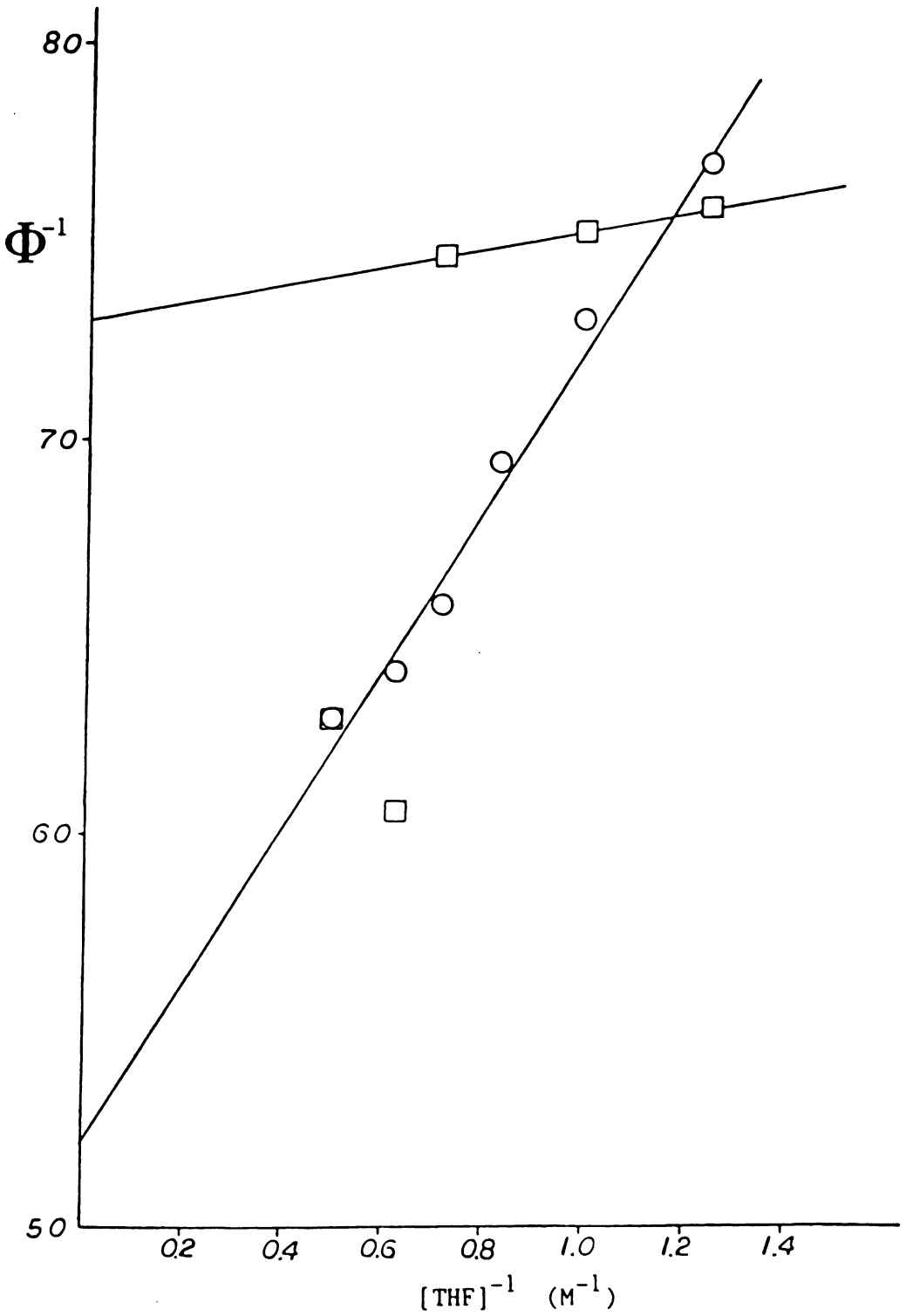

Figure 4. Double reciprocal plots for Φ^{-1}_{DTHF} (○) and $\Phi^{-1}_{THFCH_3CN}$ (□) vs. $[THF]^{-1}$ in the photoreduction of benzophenone by THF in acetonitrile.

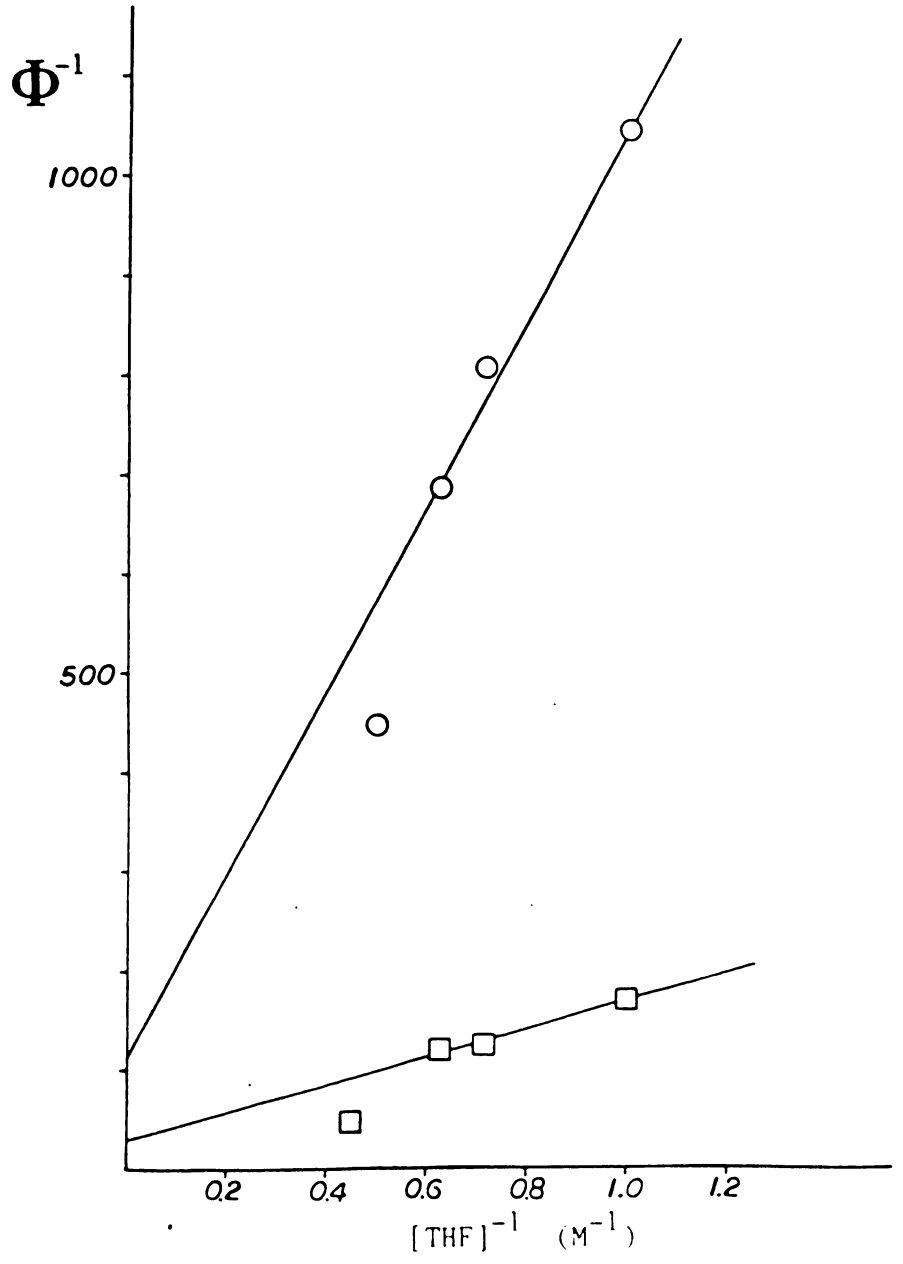

Figure 5. Double reciprocal plots for Φ^{-1}_{DTHF} (○) and $\Phi^{-1}_{THFCH_3CN}$ (□) vs. $[THF]^{-1}$ in the photoreduction of 4-acetylpyridine by THF in acetonitrile.

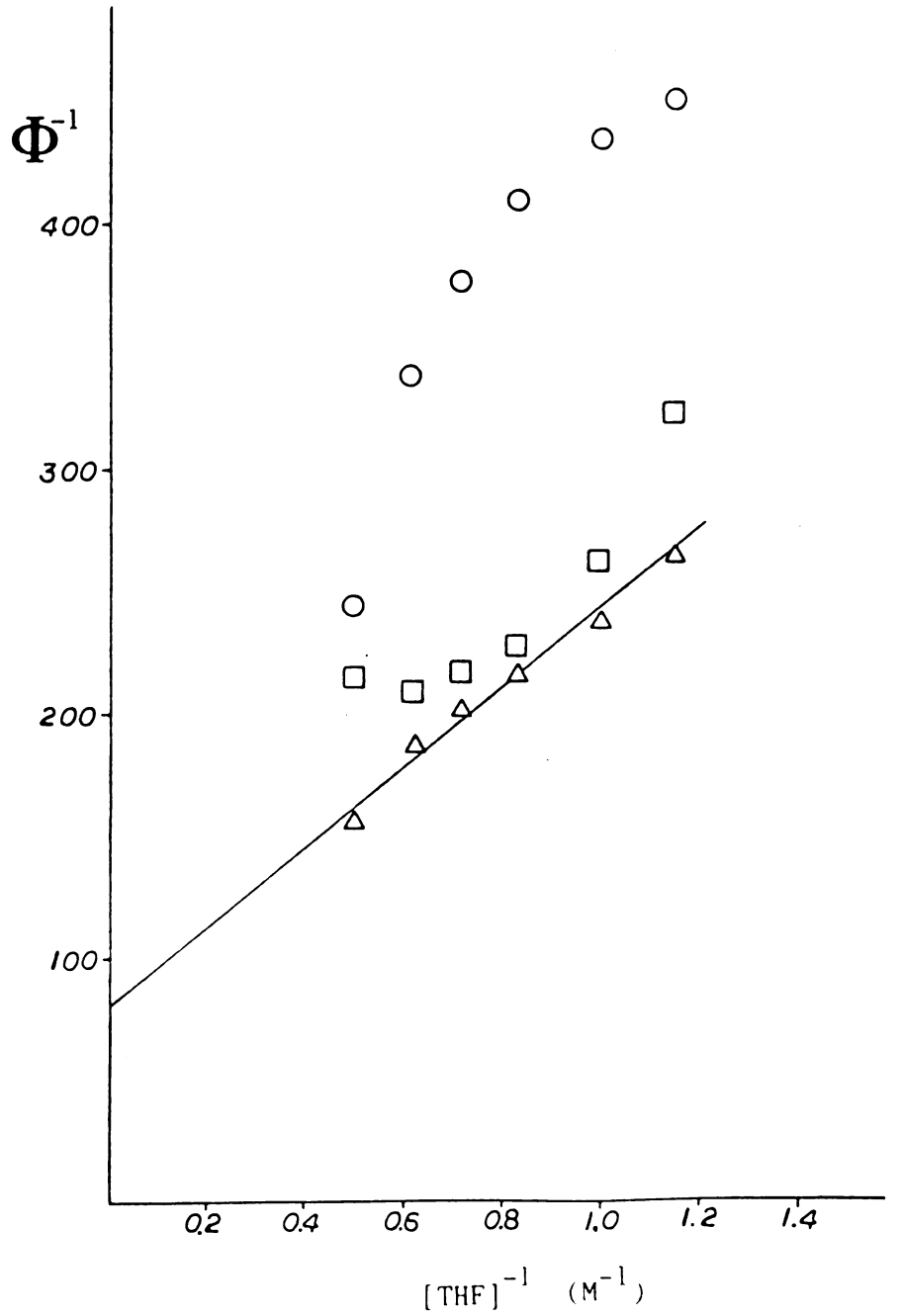

Figure 6. Double reciprocal plots for Φ^{-1}_{DTHF} (○) and $\Phi^{-1}_{THFCH_3CN}$ (□) vs. $[THF]^{-1}$ in the photoreduction of 4-benzoylpyridine by THF in acetonitrile. (△) correspond to the corrected Double reciprocal plot for DTHF (see text).

correlate well with the rest. In the case of benzophenone, only three out of six points correlate well with each other. The case of 4-benzoylpyridine needs a little more attention. Neither product gives a double-reciprocal plot with good linear correlation. Correcting the concentration of octahydro-2,2'bifuran by adding half the concentration of 2-(2-tetrahydrofuryl)acetaldimine, a double reciprocal plot (Figure 6) with excellent linear correlation was obtained. The concentration of $THFCH_3CN$ was divided in half assuming that this product has been produced by a mechanism involving THF radicals at the expense of octahydro-2,2'bifuran using, thus, the statistical correction factor 2. It is extremely interesting to note from Table 3 as well as from the Figures 2, 4, 5 and 6 that the quantum yields of 2-(2-tetrahydrofuryl)acetaldimine are always lower than the quantum yields of octahydro-2,2'bifuran in the cases of phenyl ketones, while exactly the opposite happens in the case of pyridyl ketones. It is also noteworthy that the quantum yields of 2-(2-tetrahydrofuryl)acetaldimine vary little by changing the ketone, compared to the quantum yields of octahydro-2,2'bifuran which can vary over one order of magnitube.

Finally, when it was attempted to transfer the reaction to complexed acylpyridines using the corresponding pantaammine 4-acylpyridine Ruthenium(II) tetrafluoroborate complexes in acetonitrile (solutions 0.02 M in complex, 2.0 M in THF), complete bleaching of the solutions was observed

Table 3. Results from the Intermolecular photoreduction of pyridyl ketones by THF.

ketone[a]	Product Analysed					
	DTHF[b]			$THFCH_3CN$[b]		
	Φ_{max}^{-1}	k_d/k_r	Number of points	Φ_{max}^{-1}	k_d/k_r	number of points
Acetophenone						
in CH_3CN	28.1 ± 2.5	1.37 ± 0.01	[d]	78.0	1.62	4
in benzene	27.9 ± 1.1	1.02 ± 0.03	[e]	--	--	-
Benzophenone						
in CH_3CN	52.2	0.38	6	73.0	0.031	3
4-Acetylpyridine						
in CH_3CN	126	7.31	3	29.9	4.63	3
4-Benzoylpyridine						
in CH_3CN	169	1.5	6	119	1.3	6
	96[c]	1.4	6[c]			

[a] [ketone] = 0.10 M

[b] DTHF = octahydro-2,2:bifuran. $THFCH_3CN$=2-(2-tetrahydrofuryl)acetaldimine

[c] Corrected DTHF quantum yields (see text).

[d] Averge of two runs; 5 and 6 points, respectively.

[e] Average of two runs; 4 points each.

even after a very short time of irradiation (about 0.5 hr.). Free ligand which was not present before irradiation was detected by g.c. analysis; after much longer irradiation times, octahydro-2,2'bifuran and 2-(2-tetrahydrofuryl)acetaldimine were detected, consistent with a free ligand reaction. The same reaction carried out in water using the same concentrations as in acetonitrile gave no free ligand and no photoreduction products even after prolonged irradiation (130 hrs.).

Ruthenium Complexes.

A full list of all the ligands used and their hydrochloride salts, their syntheses as well as their purification procedures, where applicable, are given in the experimental section.

Pyridyl ketones and their hydrochloride salts were kept in the dark at room temperature. No decomposition problem was encountered.

Ruthenium Pentaammine Complexes.

They were prepared by the procedure shown in Scheme 5.[15,75]

Scheme 5.

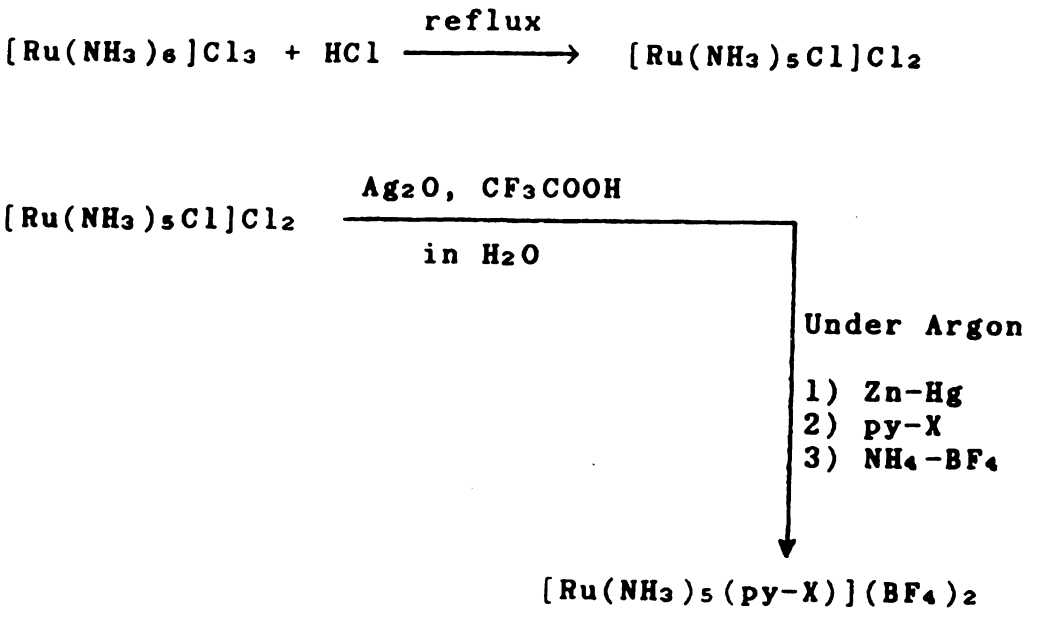

Reduction and complexation were accomplished in a continuous process as is described in detail in the Experimental Section. Pentaammine pyridyl complexes are sensitive to long exposure to the air so they were prepared under Argon. Complexation results in color change of the reduced Ru(II) (deep yellow) to deeper yellow for pyridine and 4-cyanopyridine or to deep purple for all the other complexes. The absorption spectrum (look under spectroscopic studies) is dominated by the strong MLCT transition in the visible

region with characteristic extinction co-efficients in the area of 10000 M^{-1} cm^{-1}. Further verification of the compound identity is given by the proton nmr spectra.[76] All complexes were isolated as the tetrafluoroborate salts. In the IR spectra of all the compounds, we see the strong absorption band of the tetrafluoroborate group in the region of 1200-900 cm^{-1}.[77] Free ligand present in the complexes was less then 0.01% by g.c.

Ruthenium 2,2'bipyridine and 1,10-Phenanthroline Complexes.

They were prepared by the procedure shown in Scheme 6.[78,79]

Scheme 6.

$K_3[RuCl_6] \xrightarrow[\text{pH ~ 1.1}\\ \text{2 biden}]{HCl/H_2O} [bidenH][Ru(biden)Cl_4]\cdot H_2O$

$[bidenH][Ru(biden)Cl_4]\cdot H_2O$ → 1) DMF/reflux; 2) MeOH/H_2O, reflux; 3) LiCl → $cis\text{-}[Ru(biden)_2Cl_2]\cdot nH_2O$

$cis\text{-}[Ru(biden)_2Cl_2]\cdot nH_2O$ → 1) H_2O/MeOH, py-X, reflux 6 hrs.; 2) NH_4BF_4 → $cis\text{-}[Ru(biden)_2(py\text{-}X)_2](BF_4)_2$

biden = bidentate ligand: 2,2'bipyridine, 1,10-Phenanthroline

n = 1 for biden = 1,10-Phenanthroline

n = 2 for biden = 2,2'bipyridine

Reflux in DMF brings the bidentate ligand operating as counter cation in the first complex into the first coordination sphere with simultaneous reduction of Ru(III) to Ru(II). Recrystallization from water/methanol 1:1 (v/v) follows which gives the deep brown solution of $[Ru(biden)_2Cl(H_2O)]^+$ which is precipitated as cis-$[Ru(biden)_2Cl_2].nH_2O$ by the addition of excess LiCl and removal of solvent. This retains one or two water molecules depending on the bidentate ligand (look at Scheme 6).[78,79] The two chlorine atoms can easily be removed from the first coordination sphere and the bis (pyridyl) complexes can be prepared. The relatively long reflux needed is probably due to the low solubility of the cis-$[Ru(biden)_2Cl_2].nH_2O$ complexes. All the bis(2,2'bipyridine)-bis(substituted pyridine) Ruthenium(II) complexes are orange-yellow in color and their visible absorption spectrum is dominated by the strong MLCT absorptions with extinction coefficients in the region of 10000-14000 M^{-1} cm^{-1}. Further verification of the complex identity is given as in the case of their pentaammine counterparts by the proton nmr spectra. $[Ru(bipy)_3](BF_4)_2$ gives a clean proton nmr spectrum of 2,2'bipyridine where one can distinguish each proton separately. The proton nmr of cis-$[Ru(bipy)_2(py\text{-}x)_2](BF_4)_2$, though, exhibits a complicated aromatic region similar to cis-$[Ru(bipy)_2Cl_2].2H_2O$. Diastereomeric placement of the two 2,2'bipyridines renders them magnetically unequivalent

with different chemical shifts. All complexes were isolated as the tetrafluoroborate salts. In the IR spectra of all the compounds, we see the BF_4^- absorption (1200-900 cm^{-1}).[77] Free ligand present in the complexes was less than 0.01% by g.c.

Ruthenium Porphyrines.

Ruthenium Porphyrines were synthesized by the procedure given in Scheme 7.[80,81,82]

Scheme 7.

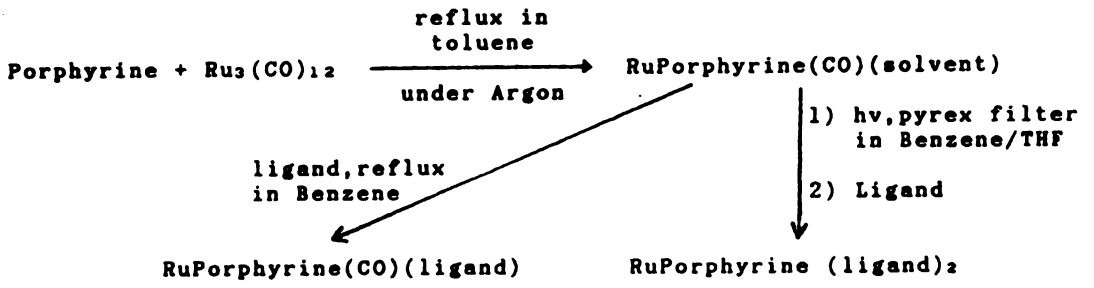

Porphyrine = Tetraphenyl Porphine or Octaethyl Porphine.

Solvent = THF in the case of Tetraphenylporphine and CH_3OH in the case of Octaethylporphine.

From the first step, RuPorphyrine(CO) is isolated where the sixth coordination position of Ruthenium is occupied by a solvent molecule such as THF originating from the purification procedure (column chromatography and recrystallization).[80] This weak ligand can easily be replaced by reflux of RuPorphyrine(CO)(THF) with the desired ligand in benzene. Bidentate ligands like pyrazine can form

di

of

ex

Ru

wh

re

ca

re

pr

Ru

ad

is

id

Sp

so

so

ab

al

We

ac

Co

fo

Co

Me

us

dimers when added in half stichiometric amount of monomers of the type RuPorphyrine(CO)(pyrazine) when added in large excess. To replace CO and prepare complexes of the type RuPorphyrine(ligand)$_2$, we modified the literature method by which RuPorphyrine(pyridine)$_2$ has been prepared.[80,82] CO is removed photochemically in the presence of pyridine. In our case, the pyridyl ketone ligands are photochemically reactive, so RuPorphyrine(CO)(solvent) was irradiated in the presence of THF so the highly reactive intermediate RuPorphyrine(THF)$_2$ is presumably formed and subsequently added to the free ligand. The desired RuPorphyrine(ligand)$_2$ is immediately formed. Decisive proof about the compound identity has been given by proton nmr and IR spectra.

Spectroscopic Studies.

Ruthenium Complexes are absorbed on the surface of old, scratched glass. Glassware treated in hot water-alconox solution 3-4 times, for 24 hrs. each time, becomes foggy and absorbs the complexes, in some cases leaving the solution almost colorless. The absorbed complex seems to be very well bound on the surface and washings with solvent are not adequate to remove it; it can be removed only with concentrated hydrochloric acid. In order to make solutions for quantitative measurements, including extinction coefficient determinations as well as quantum yield measurements and Stern-Volmer studies, it is necessary to use new glassware.

Table 4 displays the absorption maxima and the extinction coefficients for all the compounds studied, together with literature values when data are available. For the calculation of the molecular weight of the pentaammine and bis(2,2'bipyridine) Ruthenium Complexes used to measure the extinction coefficients, it was assumed no water of crystallization, even though in the IR spectra of all these complexes a broad strong absorption is always observed in the 3500-3000 cm^{-1} region, characteristic of the O-H stretching vibration. For the pantaammine complexes, this IR band is not conclusive about the existance of crystallization water since N-H vibrations are expected in the same region overlapping with O-H vibrations. Nevertheless, the error in the worst cases of low extinction coefficients and low complex molecular weight is less than 7%, assuming two water molecules are co-crystallizing with the complex. Figures 7, 8 and 9 display the absorption spectra of some pyridyl ketone ligands, their hydrochloride salts, and the corresponding Pentaammine, bis(2,2'bipyridine) and Porphyrine Ruthenium complexes.

Pentaammine complexes do not emit either at room temperature or at 77°K.[85a] In Table 5, emission maxima are listed in parallel with the triplet energies in kcal/mol for all the complexes which emit. When a vibrational structure is present in the emission spectrum, the triplet energy reported corresponds to the highest energy peak. Those compounds for which the only emission spectra given are in

Table 4. UV-Vis. Absorption Spectral Data for some Pyridyl ketones and their Ruthenium Complexes.

Compound	Solvent	λ_{max}, (ε $M^{-1}cm^{-1}$)		ε_{313} ($M^{-1}cm^{-1}$)
2,2'bipyridine (bipy)	acetonitrile	237	(10000)	
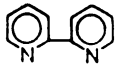		243.5	(9251)	
		280	(12899)	83
	water, basic solution [83]	233	($1.03\ 10^4$)	
		281	($1.30\ 10^4$)	
1,10-Phenanthroline (phen)	acetonitrile	230	(56872)	
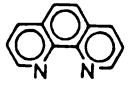		263	(32291)	837
	absolute EtOH[83]	229	($40.6\ 10^4$)	
		265	($2.76\ 10^4$)	
4,5-diazafluorene	acetonitrile	244	(5469)	
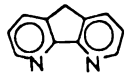		296.5	(14123)	
		302.5	(14688)	
		309	(21575)	6406
	MeOH [84]	249	($6.03\ 10^3$)	
		289	($1.20\ 10^4$)	
		302	($1.23\ 10^4$)	

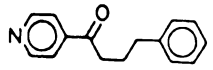	(4PhBP)	acetonitrile	280	(2078)	124
	(4PhBP.HCl)	acetonitrile	275	(1238)	104
		methylene chloride	274	(2734)	166
$[Ru(NH_3)_5(4PhBP)](BF_4)_2$		acetonitrile	268	(3860)	
			505	(10572)	432
$cis-[Ru(bipy)_2(4PhBP)_2](BF_4)_2$		acetonitrile	248	(21557)	
			254	(21972)	
			288	(52180)	
			359	(8997)	
			422	(12768)	
			443	(12353)	7682
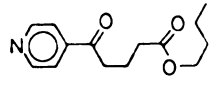	(4EsterBP)	acetonitrile	274.5	(1884)	112
	(4EsterBP.HCl)	acetonitrile	271	(2941)	82
$[Ru(NH_3)_5(4EsterBP)](BF_4)_2$		acetonitrile	266.5	(2989)	
			507	(8853)	433
$cis-[Ru(bipy)_2(4EsterBP)_2](BF_4)_2$		acetonitrile	293	(64077)	

		365	(10785)	
		403.5	(12072)	
		456	(13367)	7895
$[Ru(NH_3)_5(py)](BF_4)_2$	water	244	(3798)	
py =		407	(4900)	
	1.0 M $HClO_4$[76]	245	($4.62\ 10^3$)	
		407	($7.78\ 10^3$)	
$[Ru(NH_3)_5(4AP)](BF_4)_2$	acetonitrile	268.5	(3696)	
4AP = 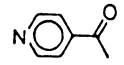		509	(11256)	336
	acetonitrile[85b]	266	(4035)	
		510	(11450)	260
$[Ru(NH_3)_5(MeINic)](BF_4)_2$	acetonitrile	264	(4044)	
		488.5	(11865)	319
MeINic = 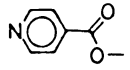	1.0 M $HClO_4$[76]	265	($3.77\ 10^3$)	
		495	($12.4\ 10^3$)	
cis-$[Ru(bipy)_2(py)_2](BF_4)_2$	water	243	(29700)	

		288	(67412)	
		338	(20364)	
		463	(14382)	
	acetonitrile[35]	41.2*	(24 10^3)	
		34.7*	(53 10^3)	
		29.8*	(12 10^3)	
		22.2*	(7.9 10^3)	
cis-[Ru(bipy)$_2$(4AP)$_2$](BF$_4$)$_2$	water	243.5	(20793)	
		288	(67005)	
		445	(14820)	
	acetonitrile	244	(18467)	
		286	(49957)	
		422.5	(11280)	7588
	methylene chloride	22.03**	(10^3)	
cis-[Ru(phen)$_2$(py)$_2$](BF$_4$)$_2$	water	224	(57916)	
		265	(75707)	
		316	(9337)	
		415	(11375)	
cis-[Ru(phen)$_2$(4AP)$_2$](BF$_4$)$_2$	water	222	(66608)	
		263	(70625)	

		411.5	(19341)	
	acetonitrile	221	(61195)	
		264	(66195)	
		409	(16375)	4813
$RuTPP(4PhBP)_2$	methylene chloride	283	(39909)	
		418.5	(144207)	
		507	(25000)	9756
$RuOEP(4PhBP)_2$	methylene chloride	285	(41095)	
		401.5	(85085)	
		498	(14558)	
		524.5	(30098)	
		619	(10545)	21810

* absorption maxima in kK.

** absorption maximum in cm^{-1}.

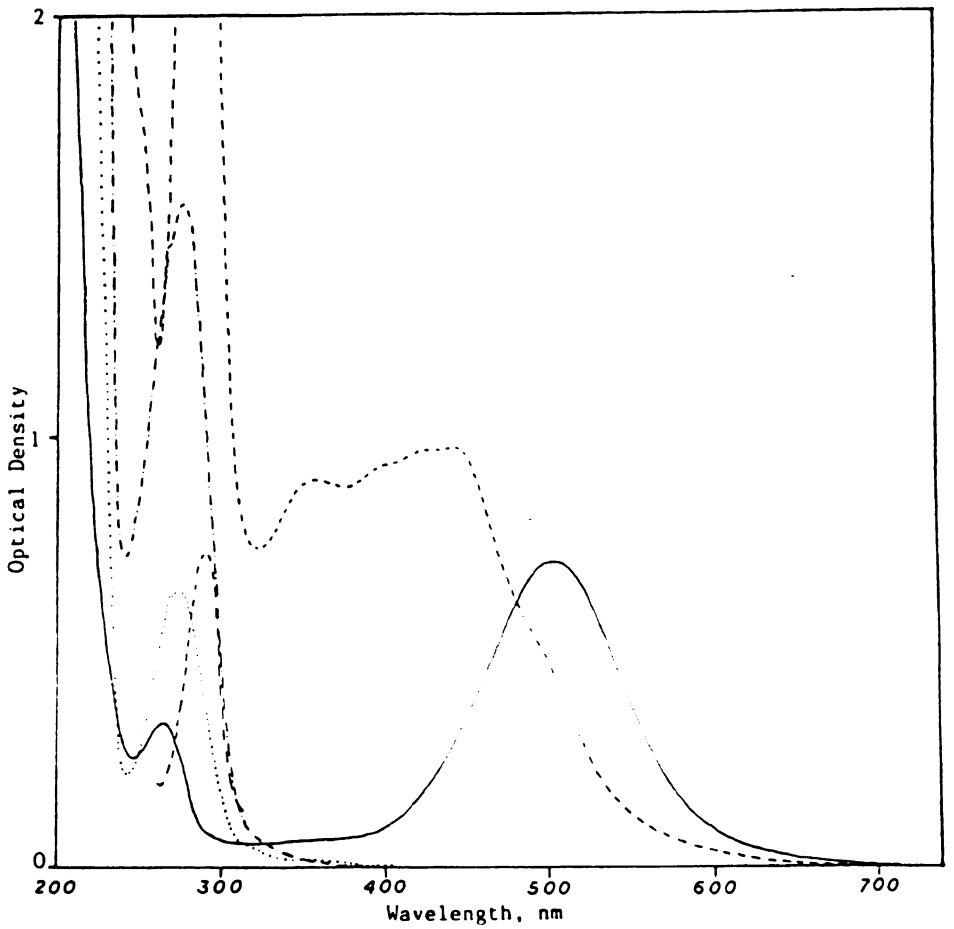

Figure 7. Absorption spectra in acetonitrile of 4PhBP (-·-·-) at 7.4 10^{-4} M, 4PhBP.HCl (·····) at 5.2 10^{-4} M, $[Ru(NH_3)_5(4PhBP)](BF_4)_2$ (——) at 6.8 10^{-5} M and cis-$[Ru(bipy)_2(4PhBP)_2](BF_4)_2$ (- - -) at 1.2 10^{-4} M.

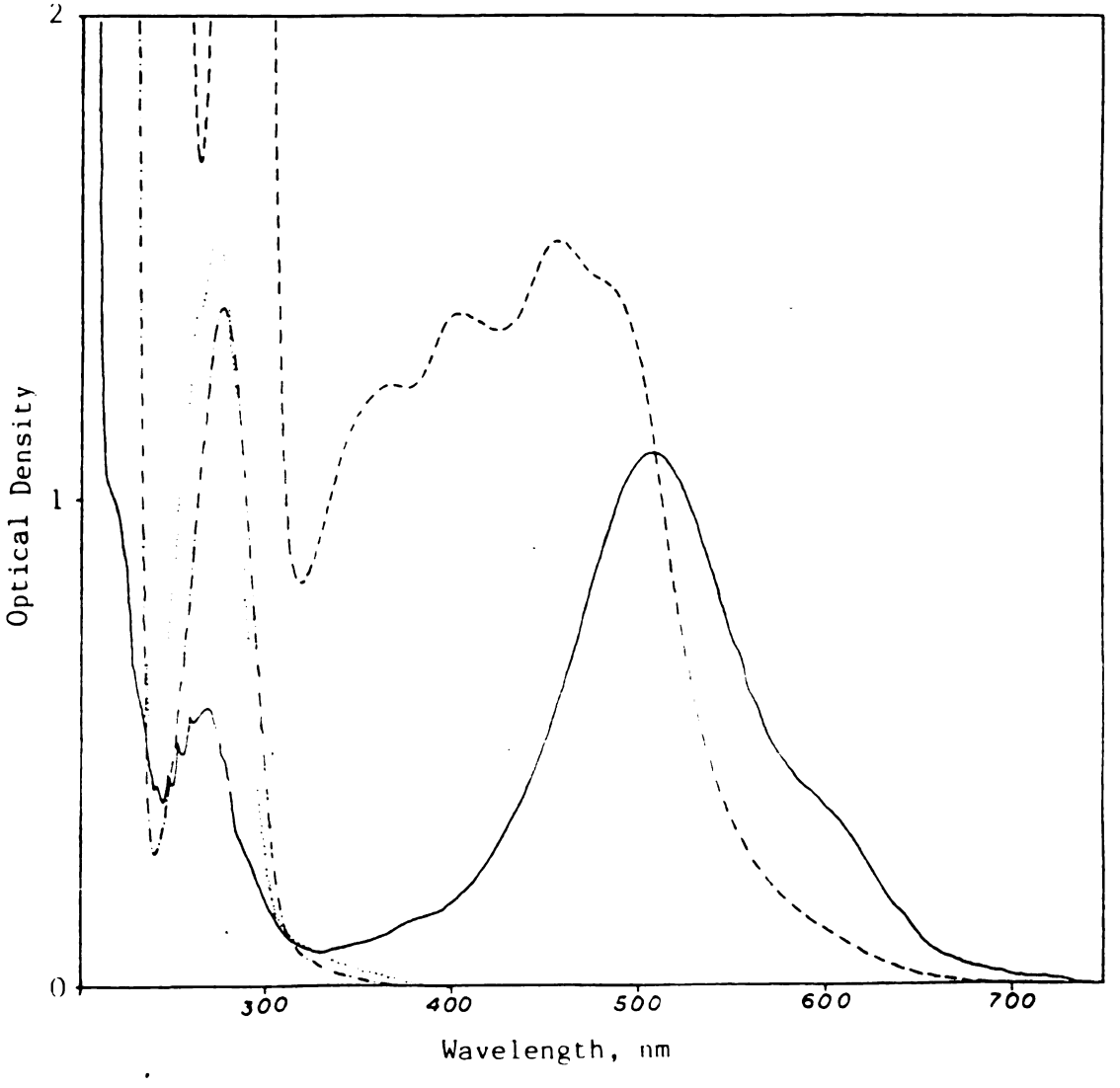

Figure 8. Absorption spectra in acetonitrile of 4EsterBP (-·-·-) at $7.8\ 10^{-4}$ M, 4EsterBP.HCl (·····) at $5.5\ 10^{-4}$ M, $[Ru(NH_3)_5(4EsterBP)](BF_4)_2$ (——) at $1.2\ 10^{-4}$ M and cis-$[Ru(bipy)_2(4EsterBP)_2](BF_4)_2$ (- - -) at $1.2\ 10^{-4}$ M.

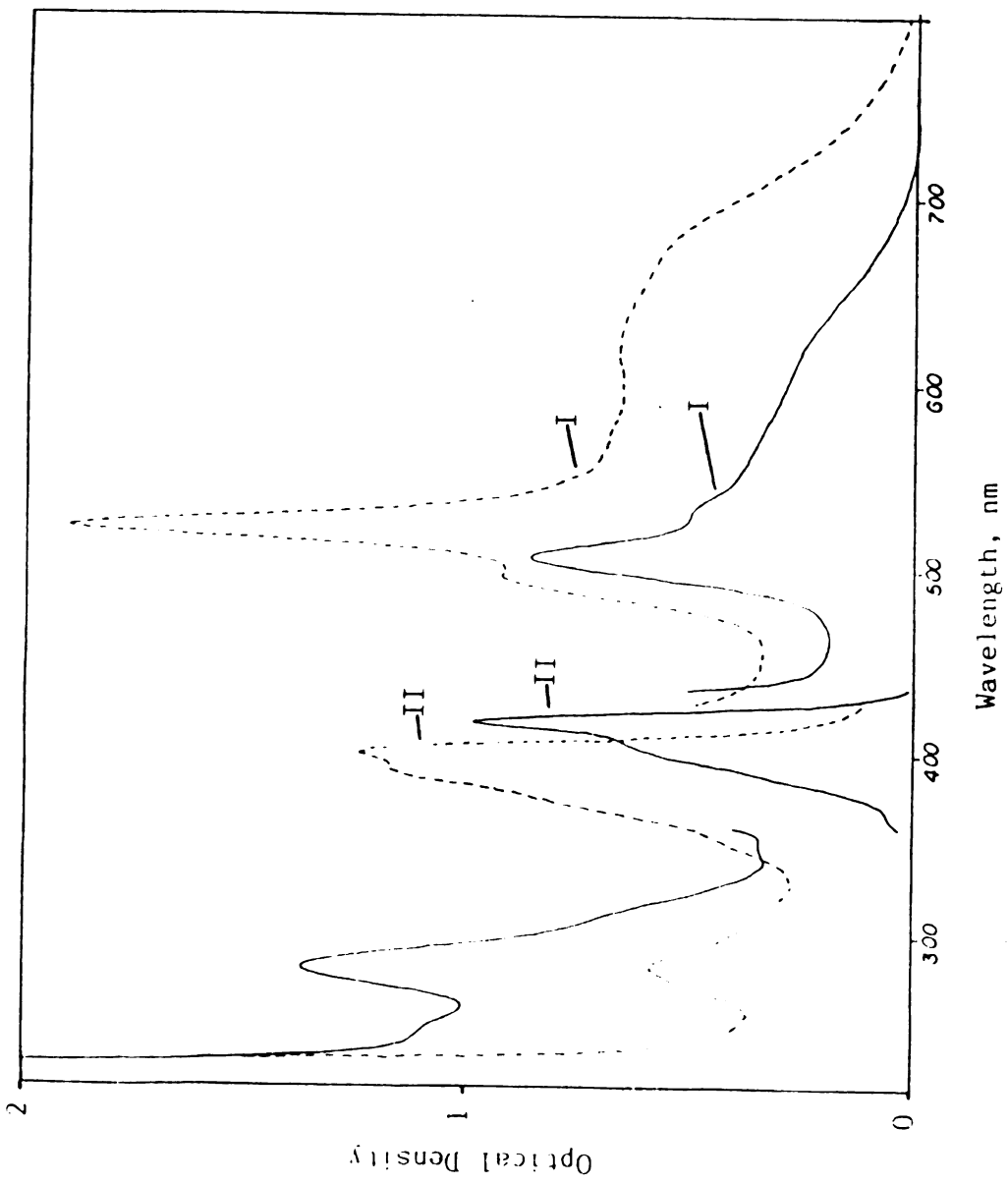

Figure 9. Absorption spectra in methylene chloride of RuTPP(4PhBP)$_2$ (——) at 3.4 10^{-5} M (I); (II): zero suppressed by 2. RuOEP(4PhBP)$_2$ (- - -) in methylene chloride at 6.0 10^{-5} M (I); (II) at 1.2 10^{-5} M.

Table 5: Emission data for some ligands and their Ruthenium Complexes.

Table 5. Emission data for some ligands and their Ruthenium Complexes.

Compound	Solvent	T, °K	excitation, nm	emission λ_{max}, nm	E_T, Kcal/mol
bipy	MeOH/EtOH	77	300	433 460 483	66.0
phen	MeOH/EtOH	77	300	459 494 528	62.3
4,5-Diazafluorene	MeOH/EtOH	77	300	436 452	65.6
4PhBP	MeOH/EtOH	77	300	406 433 460	70.4
4PhBP.HCl	MeOH/EtOH	77	300	409 433	69.9
4EsterBP	MeOH/EtOH	77	300	404 432 ~456	70.8
4EsterBP.HCl	MeOH/EtOH	77	300	403 430 ~454	70.9
cis-$[Ru(bipy)_2(4PhBP)_2](BF)_4)_2$	MeOH/EtOH	77	300	580 624	49.3
cis-$[Ru(bipy)_2(4Ester)_2](BF_4)_2$	MeOH/EtOH	77	300	582 ~631	49.1
	MeOH/EtOH	77	420	579 ~628	49.4

cis-[Ru(bipy)$_2$(py)$_2$](BF$_4$)$_2$	MeTHF	77	460	580 626	49.3
cis-[Ru(bipy)$_2$(py)$_2$](BF$_4$)$_2$	2-MeTHF	77	338	584 ~628	49.0
	MeOH/EtOH	77	410	587 ~636	48.7
cis-[Ru(bipy)$_2$(4AP)$_2$](BF$_4$)$_2$	MeOH/EtOH	77	410	579 622	49.4
cis-[Ru(phen)$_2$(py)$_2$](BF$_4$)$_2$	MeOH/EtOH	77	410	569 617	50.2
cis-[Ru(phen)$_2$(4AP)$_2$](BF$_4$)$_2$	MeOH/EtOH	77	410	567 612	50.4
[Ru(bipy)$_3$](BF$_4$)$_2$	MeOH/EtOH	77	300	584 ~630	49.0
	MeOH/EtOH	77	420	584 ~630	49.0
	water	R.T.	420	615	46.5
[Ru(bipy)$_2$(phen)](BF$_4$)$_2$	water	R.T.	440	609	46.7
[Ru(bipy)(phen)$_2$](BF$_4$)$_2$	water	R.T.	440	605	47.3
[Ru(phen)$_3$](BF$_4$)$_2$	water	R.T.	440	598	47.8

methanol/ethanol glass at 77°K do not emit at room temperature. Figures 10 and 11 display the emission spectra of some pyridyl ketone ligands, their hydrochloride salts and the corresponding Ruthenium complexes, used in intramolecular photoreduction studies for direct comparison. All emission spectra are uncorrected. Figure 12 displays the absorption and emission spectra of bis(2,2'bipyridine) and 4,5-diazafluorene; the implications and conclusions extracted from these spectra are discussed later in the Discussion Section.

Raman Studies.

Ground and lowest excited state (MLCT) resonance Raman spectra were recorded for almost all the Ruthenium complexes cited in Tables 4 and 5. Most of the Ruthenium complexes which contain 2,2'bipyridine give excited state resonance Raman spectra identical to the one obtained for $[Ru(bipy)_3]^{2+}$.[42,43] Cis-$[Ru(bipy)_2(py)_2]^{2+}$ gives a mixture of excited state spectrum (Raman scattering from cis-$[Ru(III)(bipy)(bipy^{-})(py)_2]^{2+}$) and ground state spectrum.[86] Cis-$[Ru(bipy)_2(4AP)_2]^{2+}$ exhibits only a ground state spectrum containing contributions of both 2,2'bipyridine and 4-acetylpyridine.

1,10-Phenanthroline complexes (without 2,2'bipyridine) do not give excited state spectra even in the case of $[Ru(phen)_3]^{2+}$, the MLCT excited state of which is known to

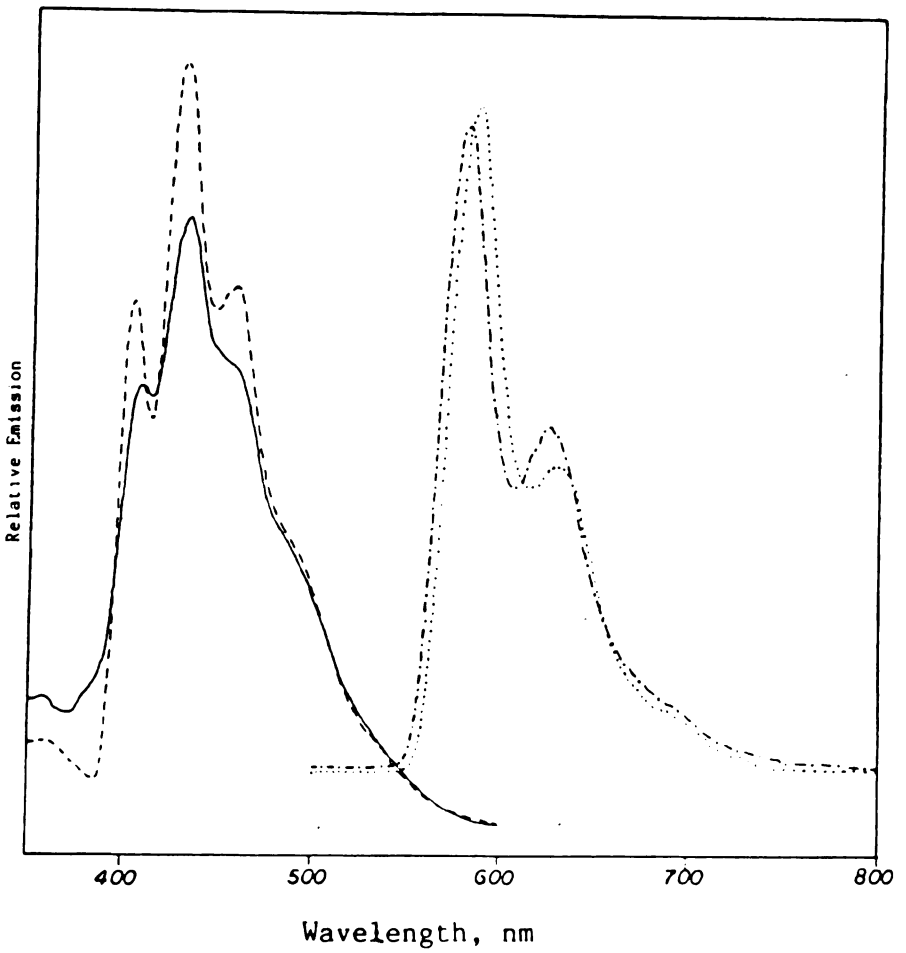

Figure 10. Emission spectra of 4PhBP (- - -), 4PhBP.HCl (———), cis-$[Ru(bipy)_2(4PhBP)_2](BF_4)_2$ (-·-·-), $[Ru(bipy)_3](BF_4)_2$ (·····), at 77 °K in 1:1 (v/v) ethanol/methanol glass. Concentrations between 10^{-5} and 10^{-4} M. Excitation at 300 nm.

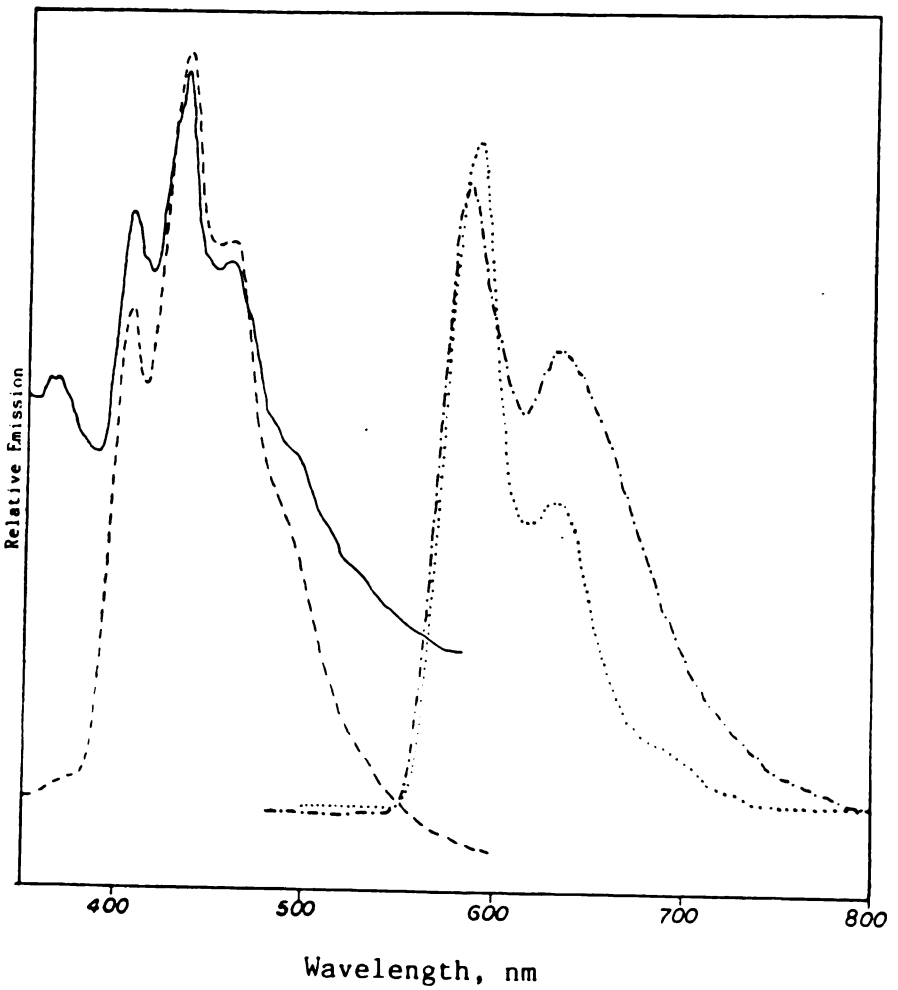

Figure 11. Emission spectra of 4EsterBP (- - -), 4EsterBP.HCl (———), cis-$[Ru(bipy)_2(4EsterBP)_2](BF_4)_2$ (-·-·-) and $[Ru(bipy)_3](BF_4)_2$ (·····) at 77 °K in 1:1 (v/v) ethanol/methanol glass. Concentrations between 10^{-5} and 10^{-4} M. Excitation at 300 nm.

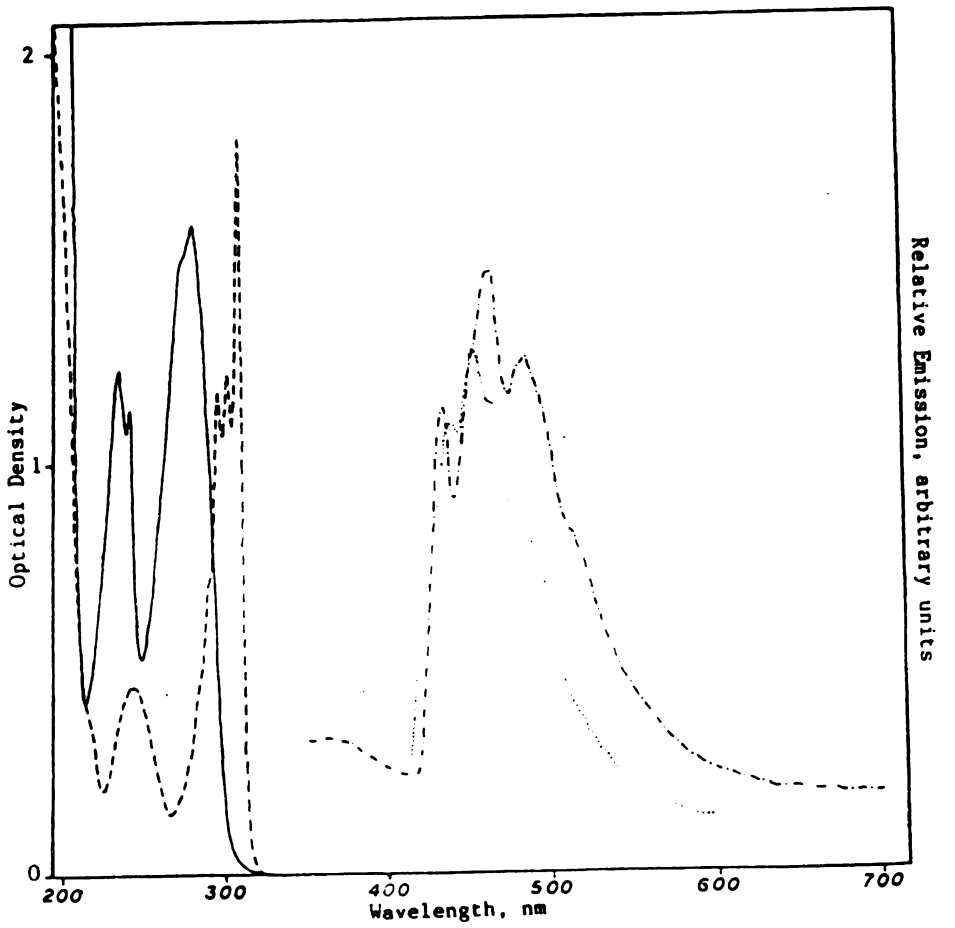

Figure 12. Absorption spectra in acetonitrile of bipy (——) at 1.2 10^{-4} M and 4,5-diazafluorene (- - -) at 8.3 10^{-5} M. Emission spectra of bipy (-·-·-) and 4,5-diazafluorene (·····) in 1:1 (v/v) ethanol/methanol glass at 77 °K. Concentrations in the range of 10^{-5} to 10^{-4} M. Excitation at 300 nm.

be long lived.[87] Instead, they give spectra identical to the ground state spectrum.

The Pentaammine 4-acetylpyridine Ruthenium(II) complex gives a spectrum[88] similar to the 4-acetylpyridine anion radical while the Pentaammine pyridine[88] or 4-cyanopyridine Ruthenium(II)[89] complexes exhibit scattering only from the ground state.

Conclusions drawn from the Raman data are given in the discussion section.

Intramolecular Photoreduction.

The Intramolecular Type II photoreduction of free pyridyl ketones, pyridyl ketone hydrochloride salts and of pyridyl ketones coordinated to a Ruthenium center were studied. The Ruthenium complexes studied were the pentaammine, the 2,2'bipyridine and the tetraphenyl- or octaethylporphyrine ones.

The intermolecular quenching effect of the $[Ru(NH_3)_5(4AP)](BF_4)_2$, cis-$[Ru(bipy)_2(4AP)_2](BF_4)_2$ and cis-$[Ru(phen)_2(4AP)_2](BF_4)_2$ complexes on the intramolecular photoreduction of butyrophenone was also studied. These results have been used, as shown in the discussion section, in order to make corrections on the coordinated ketone lifetimes, taking into account the bimolecular self-quenching effect of the Ruthenium complexes.

Photoproduct Identification.

The following five reactions were investigated with respect to the photochemical Type II fragmentation of the coordinated pyridyl ketone and compared with the photochemical data from the free pyridyl ketone ligand and its hydrochloride salt (see below).

$$[Ru(NH_3)_5(4PhBP)](BF_4)_2 \xrightarrow[CH_3CN]{313\ nm} [Ru(NH_3)_5(4AP)](BF_4)_2 + \quad (20)$$

$$cis\text{-}[Ru(bipy)_2(4PhBP)_2](BF_4)_2 \xrightarrow[CH_3CN]{313\ nm}$$

$$cis\text{-}[Ru(bipy)_2(4PhBP)(4AP)](BF_4)_2 + \quad (21)$$

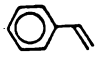

$$RuPorthyrin(4PhBP)_2 \xrightarrow[CH_2Cl_2]{313\ nm} RuPorphyrine(4PhBP)(4AP) + \quad (22)$$

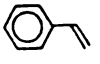

$$[Ru(NH_3)_5(4EsterBP)](BF_4)_2 \xrightarrow[CH_3CN]{313\ nm} [Ru(NH_3)_5(4AP)](BF_4)_2 + \quad (23)$$

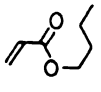

$$cis\text{-}[Ru(bipy)_2(4EsterBP)_2](BF_4)_2 \xrightarrow[CH_3CN]{313\ nm} cis\text{-}[Ru(bipy)_2(4EsterBP)(4AP)](BF_4)_2$$

$$cis\text{-}[Ru(bipy)_2(4EsterBP)(4AP)](BF_4)_2 + \quad (24)$$

All the irradiations were performed at 313 nm. All the starting complex concentrations were 0.02 M. Solvents are shown for each reaction separately. Irradiation times

varied widely. For a 5-10% conversion, reaction (20) needs 15-20 hrs.; reaction (21) needs 20-25 hrs.; reaction (22) needs 10 days; reaction (23) needs 30-35 hrs. and reaction (24) needs 7 days.

Styrene produced from (20), (21) and (22) becomes apparent by its characteristic odor and was identified from its gas chromatographic retention time, by comparing to an authentic sample.

N-butylacrylate produced from (23) and (24) was identified from its chromatographic retention time by comparison to an authentic sample as well as by gc/ms. A sample of cis-$[Ru(bipy)_2(4EsterBP)_2](BF_4)_2$ was analyzed before and after irradiation for n-butylacrylate. No gc peak corresponding to n-Butylacrylate was present before irradiation, while after irradiation a peak was present which gave the same mass fragmentation pattern given by a neat sample of n-butylacrylate.

All Ruthenium complexes were tested after irradiation for ligand dissociation and in no case was any pyridyl ketone ligand or photoproduced 4-acetylpyridine found in the bulk solution.

An experiment to measure the 4AP produced and compare it with the amount of styrene formed failed to give quantitative release of the coordinated photoproduced 4AP. According to Whitten, he was able to remove quantitatively the coordinated 4-stilbazole molecules from cis-$[Ru(bipy)_2(4\text{-stilbazole})_2](PF_6)_2$ by refluxing the complex in

n-butyronitrile in the presence of triphenyl phosphine for 24 hrs.[32] Efforts to repeat Whitten's experiment with cis-$[Ru(bipy)_2(4PhBP)_2](BF_4)_2$ gave the results displayed in Table 6. In the best case, it was possible to obtain only 35% as much 4AP as styrene.

Table 6. Mass Balance Experiment for styrene and 4AP been produced in the Type II cleavage of cis-$[Ru(bipy)_2(4PhBP)_2](BF_4)_2$.[a]

Reflux solvent	time,(hrs.)	[styrene],(M)	[4AP],(M)
acetonitrile	24	0.00168	0.000590
n-butyronitrile	24	0.00164	0.0000743

[a] [complex] = 0.02 M, $[PPh_3]$ = 0.2 M.

Finally, in agreement with previous observations,[85c] pentaammine complexes bleach while bis(2,2'bipyridine) complexes remain unaffected by prolonged irradiations. Figure 13 illustrates this phenomenon for the two pentaammine Ruthenium complexes studied. The bleaching (loss of optical density) becomes less effective as the amount of a quencher, like ethyl sorbate, increases. Table 7 summarizes the data from Figure 13. No products have been isolated.

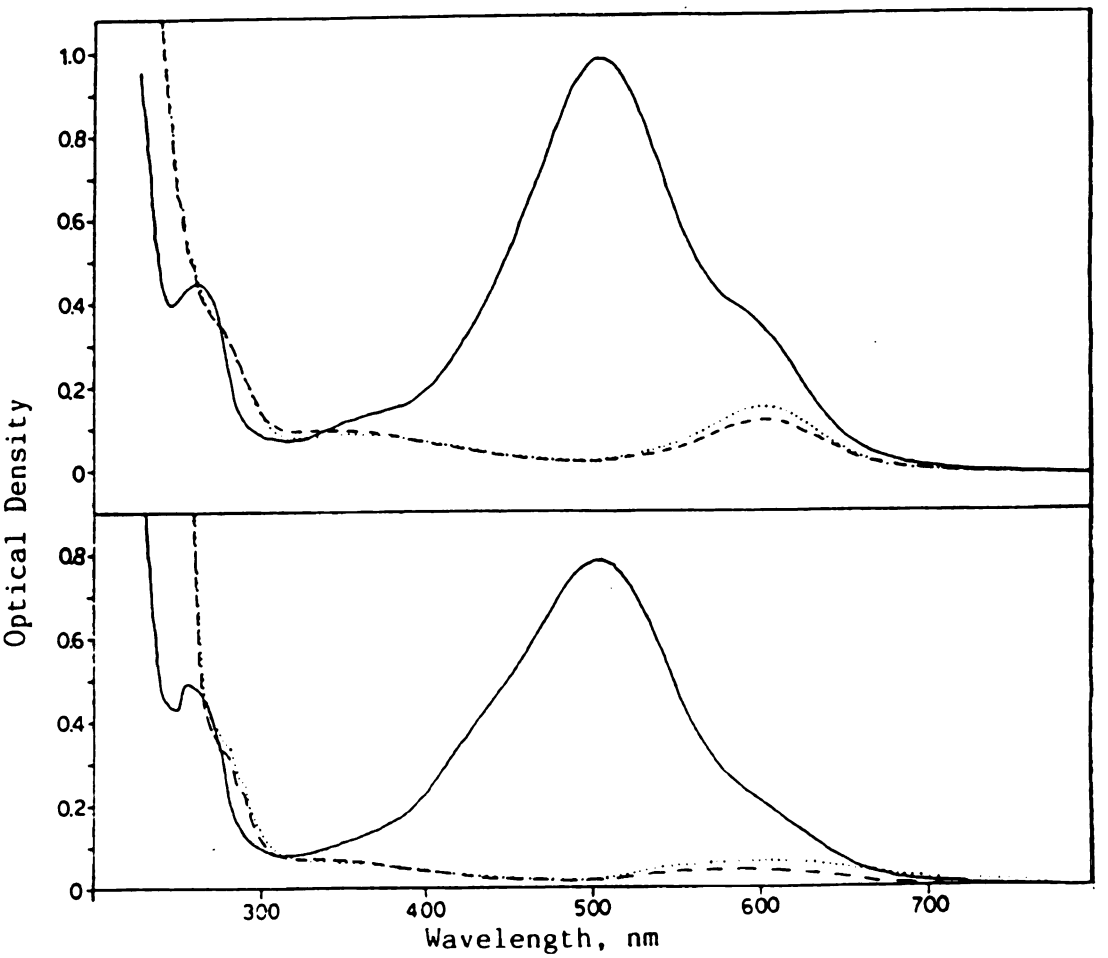

Figure 13. UV-Vis. absorption spectra upon 313 nm irradiation of $1.0\ 10^{-4}$ M $[Ru(NH_3)_5(4EsterBP)](BF_4)_2$ (top frame) and $7.5\ 10^{-5}$ M of $[Ru(NH_3)_5(4PhBP)](BF_4)_2$ (bottom frame) in acetonitrile. (·····): 2 hrs irradiation, 0.00920 einstein. (- - -): 6 hrs irradiation, 0.0287 einstein.

Table 7. UV-Vis absorption data of $[Ru(NH_3)_5(4PhBP)](BF_4)_2$, cis-$[Ru(bipy)_2(4PhBP)_2](BF_4)_2$, $[Ru(NH_3)_5(4EsterBP)](BF_4)_2$ and cis-$[Ru(bipy)_2(4EsterBP)_2](BF_4)_2$ upon irradiation at 313 nm.

Complex	Time of irr. (hrs.)	Amount of light (einstein)	λ_{max}, (A)	A_{313}
$[Ru(NH_3)_5(4PhBP)](BF_4)_2$[a]	0	0.0	(507) 0.790	0.082
	2	0.00920	(596) 0.056	0.086
	6	0.0287	(593) 0.047	0.084
cis-$[Ru(bipy)_2(4PhBP)](BF_4)_2$[b]	0	0.0	(422) 0.336	0.342
	6	0.0287	(422) 0.256	0.313
	12	0.0829	(422) 0.251	0.311
$[Ru(NH_3)_5(4EsterBP)](BF_4)_2$[c]	0	0.0	(507) 1.002	0.123
	2	0.00920	(601) 0.172	0.107
	6	0.0287	(603) 0.137	0.093
cis-$[Ru(bipy)_2(4EsterBP)](BF_4)_2$[d]	0	0.0	(456) 0.370	0.339
	6	0.0287	(456) 0.374	0.349
	12	0.0829	(456) 0.374	0.341

[a] $7.5\ 10^{-5}$ M in acetonitrile.

[b] $2.6\ 10^{-5}$ M in acetonitrile.

[c] $1.1\ 10^{-4}$ M in acetonitrile.

[d] $2.8\ 10^{-5}$ M in acetonitrile.

Quantum Yield Studies.

Quantum yields for photoproduct formation were obtained by irradiation of the appropriate samples at 313 nm in a "merry-go-round" apparatus at room temperature using Valerophenone actinometry. Photoproduct quantum yield from cis-$[Ru(bipy)_2(4EsterBP)_2](BF_4)_2$ and from RuPorphyrine$(4PhBP)_2$ were obtained using o-methylbutyrophenone and o-methylvalerophenone actinometry[90] due to long irradiations necessary to build measurable amounts of product. Table 8 displays the Quantum Yields measured and Figures 14, 15 and 16 demonstrate the effect of varying ketone (or complex) concentration on the Quantum Yields.

Free pyridyl ketone Quantum Yields according to previous observations[85d,91] increase linearly by increasing the ketone concentration while hydrochloride salt quantum yields seem to be insensitive to concentration variation.[85d] Quantum Yields of Type II cleavage from Ruthenium Pentaammine and 2,2'bipyridine complexes seem to be very strongly sensitive to complex concentration with a decrease in the quantum yield under conditions where all the light at 313 nm is absorbed by the complex (O.D.>2). This observation implies an intermolecular quenching effect, thus justifying the experiments of quenching of butyrophenone by Ruthenium Complexes described under "Quenching Studies" below.

Table 8. Quantum Yields and $k_q\tau$ values for 4PhBP, 4EsterBP, 4PhBP.HCl, 4EsterBP.HCl and the corresponding Ruthenium Complexes.[a]

Compound	$\Phi_{(II)}$	$k_q\tau$[d]
4PhBP	0.42[c]	9.74 ± 0.54[g]
4PhBP.HCl	0.093[c]	2.05[h]
$[Ru(NH_3)_5(4PhBP)](BF_4)_2$	0.014 ± 0.001	6.89 ± 0.98 (4.99 ± 0.01)[i]
cis-$[Ru(bipy)_2(4PhBP)_2](BF_4)_2$	0.0072 ± 0.0001	3.44 ± 0.30
4EsterBP[e]	0.41 ± 0.04	167 ± 12.5
4EsterBP.HCl[f]	0.096	31.5 ± 1.2
$[Ru(NH_3)_5(4EsterBP)](BF_4)_2$	0.0051 ± 0.0008	68.3 (52.6)[i]
cis-$[Ru(bipy)_2(4EsterBP)_2](BF_4)_2$	0.0017 ± 0.0001	23.6 ± 0.01
$RuTPP(4PhBP)_2$[b]	0.000203	
$RuOEP(4PhBP)_2$[b]	0.000220	

[a] All compounds 0.020 M in acetonitrile (unless otherwise noted) irradiated at 313 nm.

[b] Methylene chloride solvent.

[c] Estimated from Figure 14 for [4PhBP] = 0.020 M and for [4PhBP.HCl] = 0.020 M.

[d] Average of two runs.

[e] [4EsterBP] = 0.021 M.

[f] [4EsterBP.HCl] = 0.030 M.

[g] [4PhBP] = 0.040 M, 2 runs.

[h] [4PhBP.HCl] = 0.040 M, 1 run.

[i] For numbers in parentheses, see text: eq. 25.

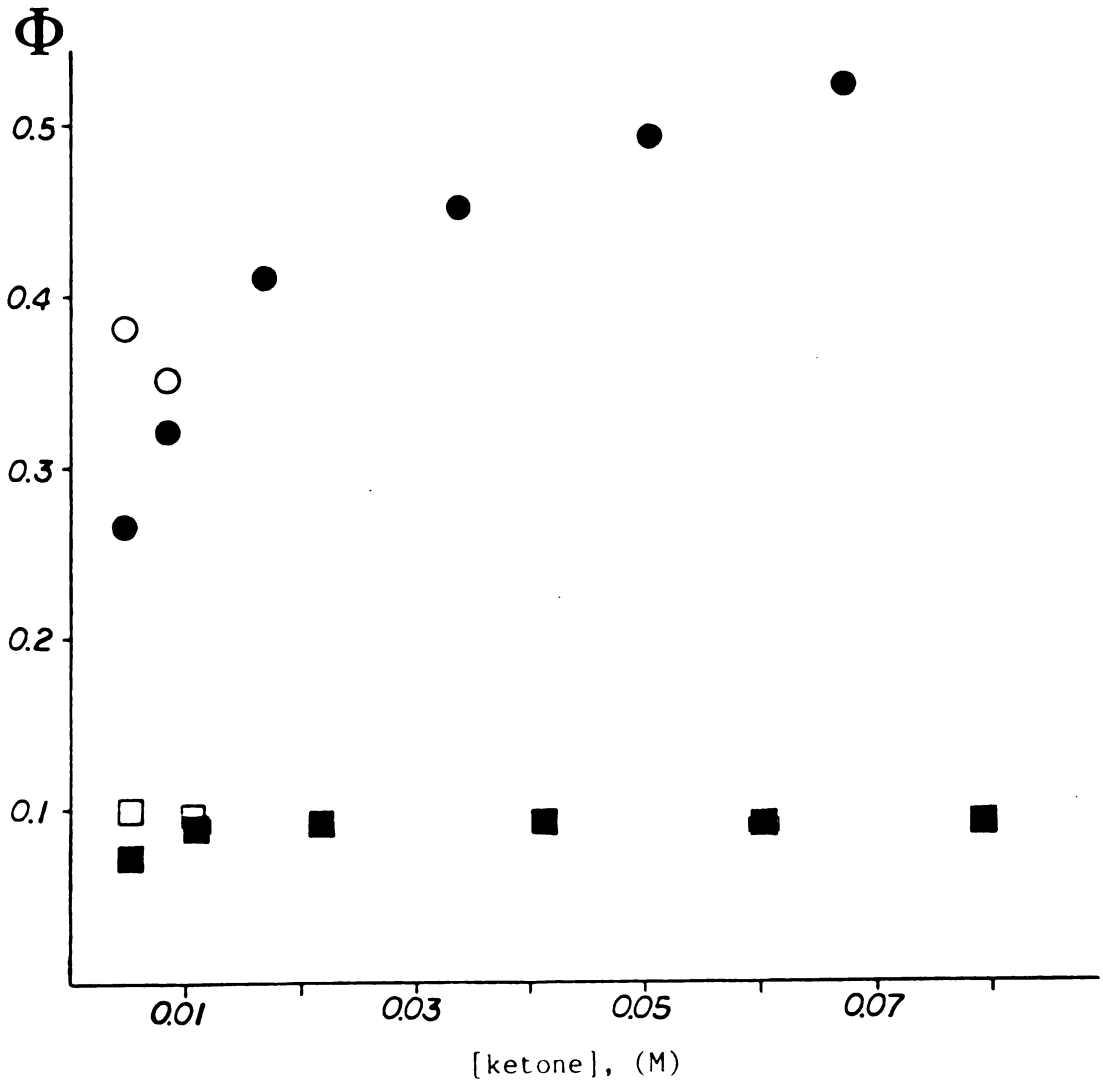

Figure 14. Effect of ketone concentration on the Type II products quantum yield. Ketones irradiated at 313 nm in acetonitrile. (●): 4PhBP; (■): 4PhBP.HCl. (○) and (□) correspond to quantum yields corrected for partial light absorption by the ketone.

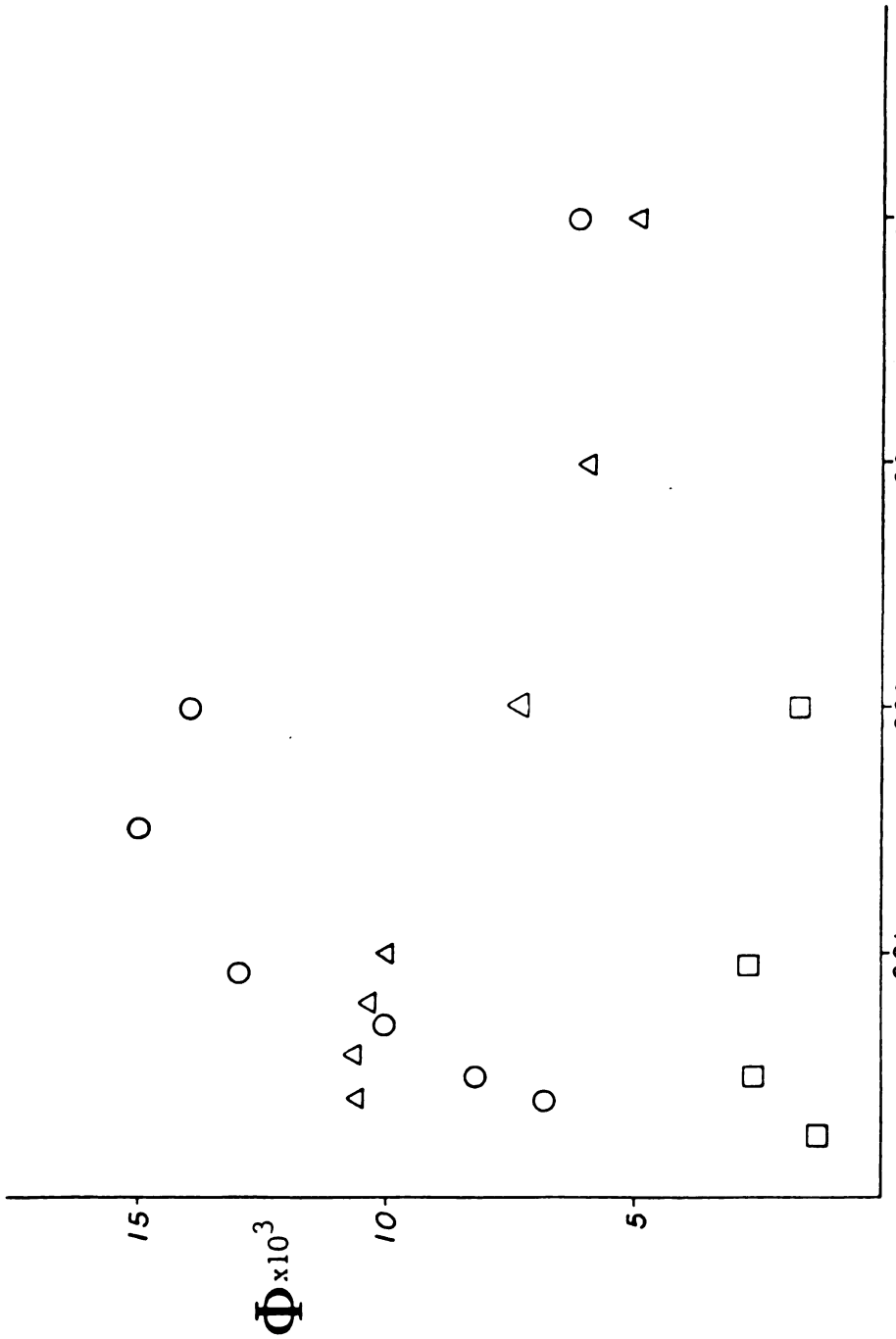

Figure 15. Effect of concentration of Ruthenium complex on quantum yield for $[Ru(NH_3)_5(4PhBP)](BF_4)_2$ (○), cis-$[Ru(bipy)_2(4PhBP)_2](BF_4)_2$ (△), and for cis-$[Ru(bipy)_2(4EsterBP)_2](BF_4)_2$ (□).

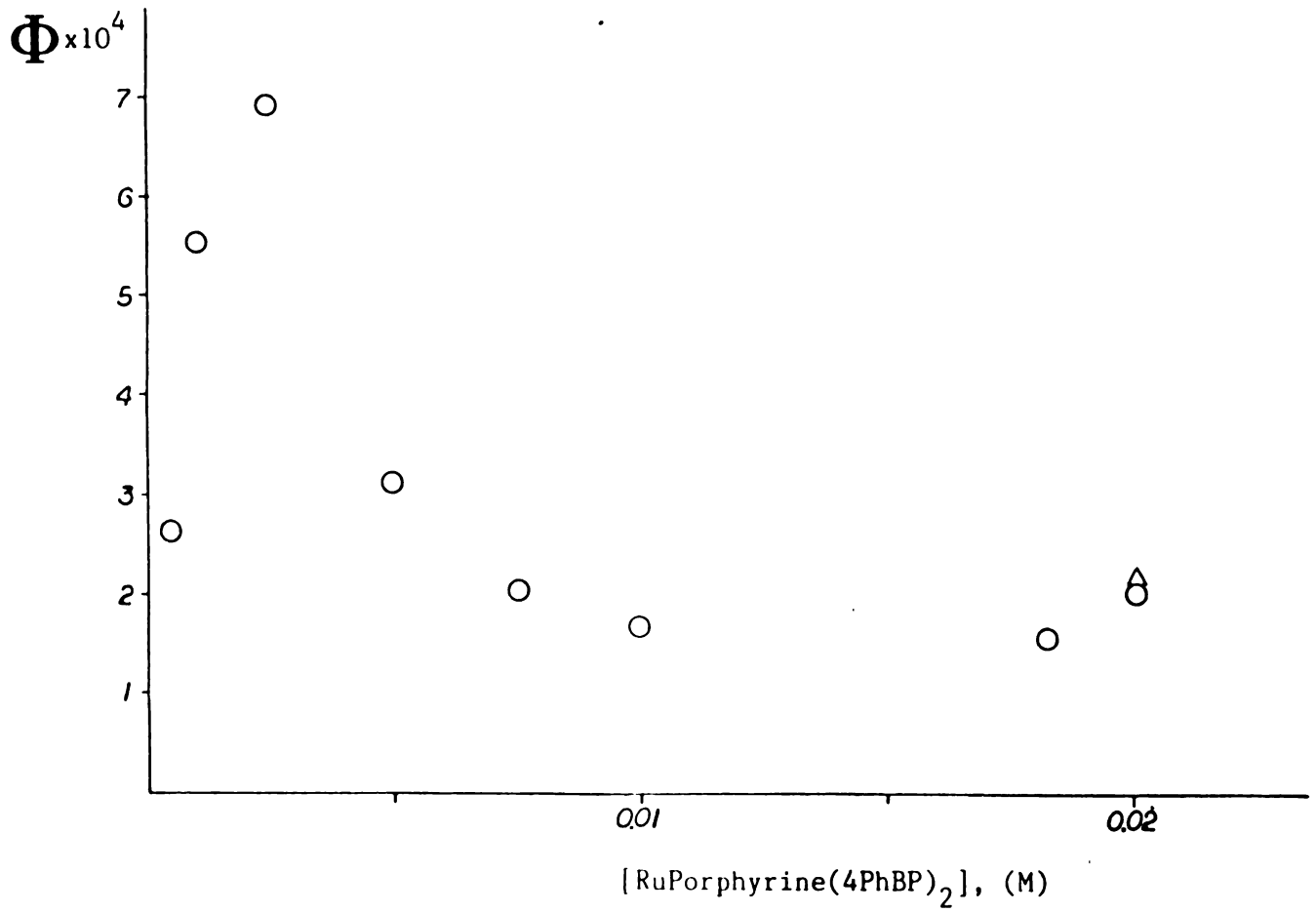

Figure 16. Effect of concentration of $RuTPP(4PhBP)_2$ on the quantum yield for the Type II cleavage of the ligand (○). (△) corresponds to the quantum yield of $RuOEP(4PhBP)_2$.

Quenching Studies.

Stern-Volmer quenching of the Type II cleavage was performed by the 313 nm irradiation of constant concentration (see Table 8) of the pyridyl ketones, pyridyl ketone hydrochloric salts, Pentaammine pyridyl ketone Ruthenium(II) complexes as well as of the cis-bis(2,2'bipyridine)-bis(pyridyl ketone) Ruthenium(II) complexes with varying concentrations of quencher as described in the experimental section. The Quencher used was ethyl sorbate which is a diene (classical triplet quencher) miscible with acetonitrile in any proportion. Conversions to products were usually kept below 10%, and the $k_q \tau$ values reported (Table 8) usually come from duplicate runs. Figures 17 and 18 compare the Stern-Volmer plots of the pyridyl ketones and the pyridyl ketone hydrochloride salts in the cases of 4PhBP and 4EsterBP, respectively. Figures 19 and 20 compare the Stern-Volmer plots for the Pentaammine pyridyl ketone and the cis-bis(2,2'bipyridine)-bis(pyridyl ketone) Ruthenium(II) complexes for the same two ketones. The Stern-Volmer plots of Pentaammine pyridyl ketone Ruthenium(II) complexes exhibit an unusual phenomenon: they have intercepts lower than unity, while the slopes are quite reproducible. The slope/intercept values vary widely; $k_q \tau$ values reported on Table 8 are the slope values only. The numbers in parentheses cited next to these values are the $k_q \tau$ values calculated through the modified

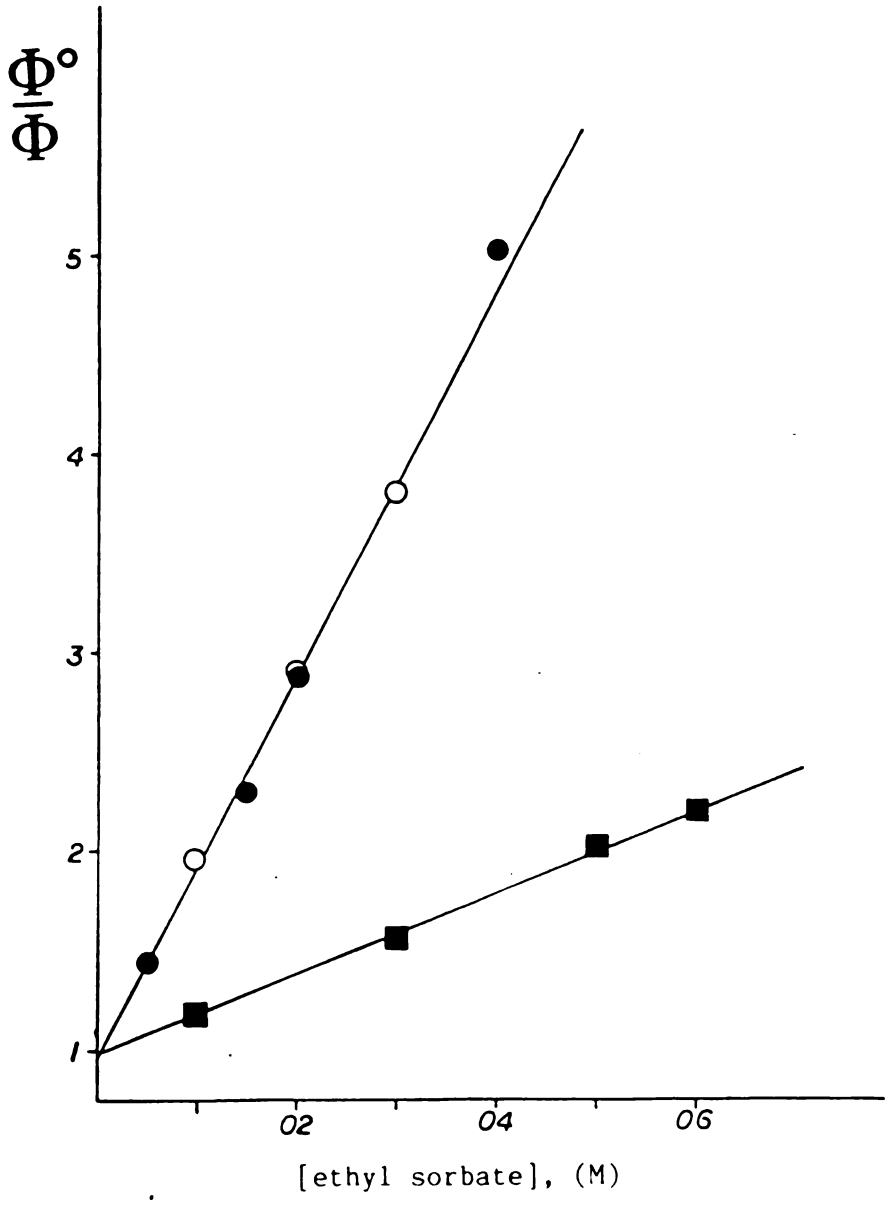

Figure 17. Stern Volmer plots for 4PhBP (○) and for 4PhBP.HCl (□) in acetonitrile.

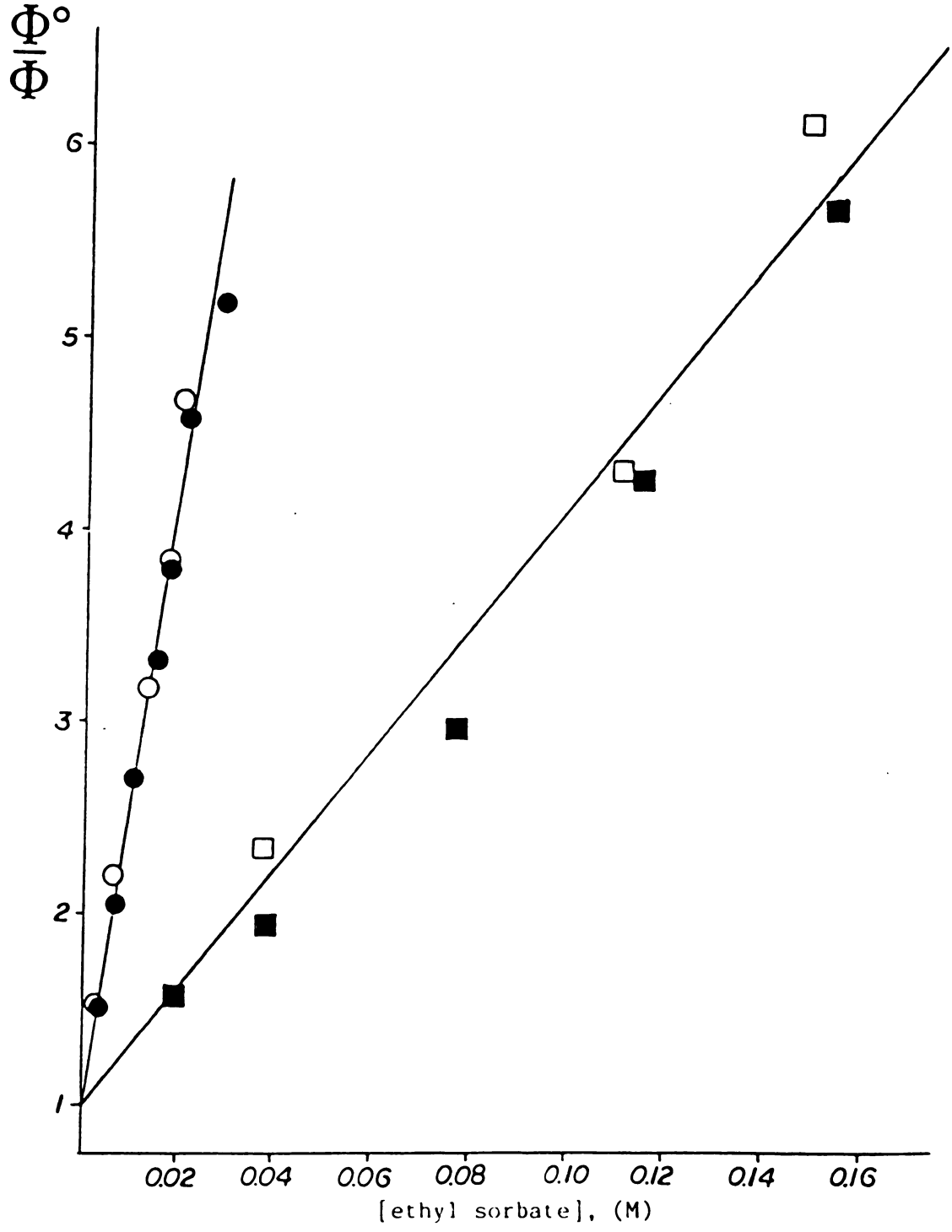

Figure 18. Stern Volmer plots for 4EsterBP (○) and 4EsterBP.HCl (□) in acetonitrile.

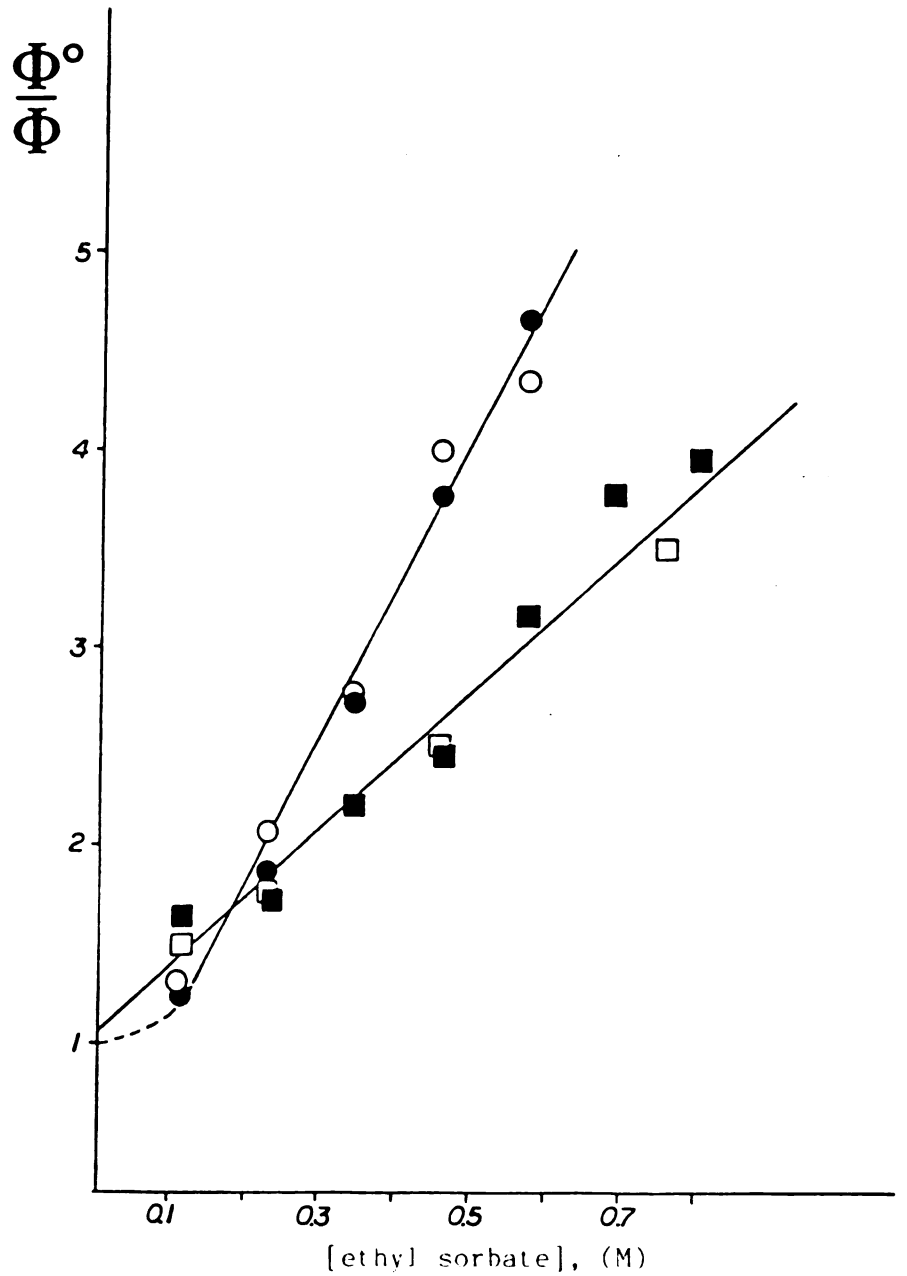

Figure 19. Stern Volmer plots for $[Ru(NH_3)_5(4PhBP)](BF_4)_2$ (○) and for cis-$[Ru(bipy)_2(4PhBP)_2](BF_4)_2$ (□) in acetonitrile.

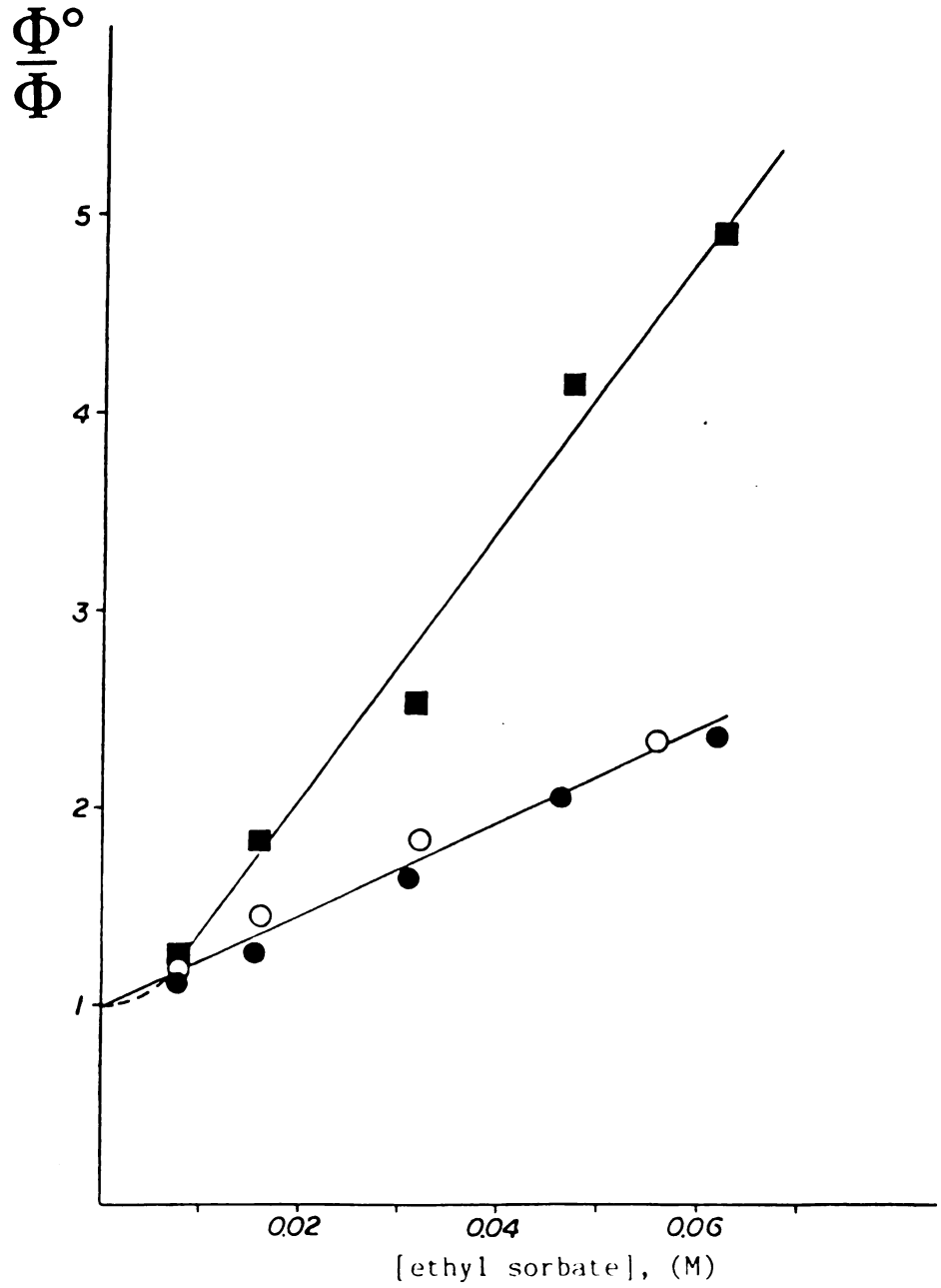

Figure 20. Stern Volmer plots for $[Ru(NH_3)_5(4EsterBP)](BF_4)_2$ (□) and for $cis\text{-}[Ru(bipy)_2(4EsterBP)_2](BF_4)_2$ (○) in acetonitrile.

Stern-Volmer relation (25) for each point of the Stern-Volmer plots (Figures 19 and 20) individually and averaging.

$$k_q \tau = \frac{1-\Phi^o/\Phi}{[Q]} \qquad (25)$$

Stern-Volmer quenching studies were also performed using as quenchers the $[Ru(NH_3)_5(4AP)](BF_4)_2$, cis-$[Ru(bipy)_2(4AP)_2](BF_4)_2$ and cis-$[Ru(phen)_2(4AP)_2](BF_4)_2$ complexes to quench the intramolecular Type II photoreduction of butyrophenone. The purpose of this experiment was double. First was to verify that there is an intermolecular triplet energy transfer from the pyridyl ketones to another complex molecule, thus explaining the decrease in the quantum yield of the intramolecular Type II cleavage of coordinated pyridyl ketones with increasing complex concentration. Secondly was to prove that the photoreduction from the Ruthenium complexes comes from complexed ligand only and that any free ligand, even though not detectable by g.c., is completely quenched by the relatively high concentration (0.02 M) of the Ruthenium complex. Butyrophenone concentration in all these experiments was high (0.5 M) in order to absorb most of the light at 313 nm while the concentrations of the Ruthenium complexes were kept low. It was found that Ruthenium complex concentrations up to 0.005 M were enough to quench 60-80% of the photoreduction. Quantum yields always were corrected for the fraction of the light absorbed by the

ketone. Details are given in the experimental section. Figures 21 and 22 display both the uncorrected and the corrected Stern-Volmer plots for the quenching of butyrophenone by $[Ru(NH_3)_5(4AP)](BF_4)_2$ and by cis-$[Ru(bipy)_2(4AP)_2](BF_4)_2$, respectively. As can be observed from Figure 22, the intercepts of the corrected Stern-Volmer plots in the case of cis-$[Ru(bipy)_2(4AP)_2](BF_4)_2$ quencher are consistently higher than unity.

Figure 23 displays the effect of cis-$[Ru(phen)_2 4AP_2](BF_4)_2$ on the butyrophenone photoreduction; it was though that 1,10-Phenanthroline, due to its extended conjugation relative to 2,2'bipyridine, can serve as a representative model to elucidate the ruthenium complexes' quenching trend, going from 2,2'bipyridine to Tetraphenylporphyrine and Octaethylporphyrine, comparing this way the quantum yield found for the Type II photoreduction of $RuTPP(4PhBP)_2$ and of $RuOEP(4PhBP)_2$ with the quantum yield found for $[Ru(bipy)_2 4PhBP_2](BF_4)_2$. $k_q\tau$ values calculated from the corrected curves for each complex are cited in Table 9.

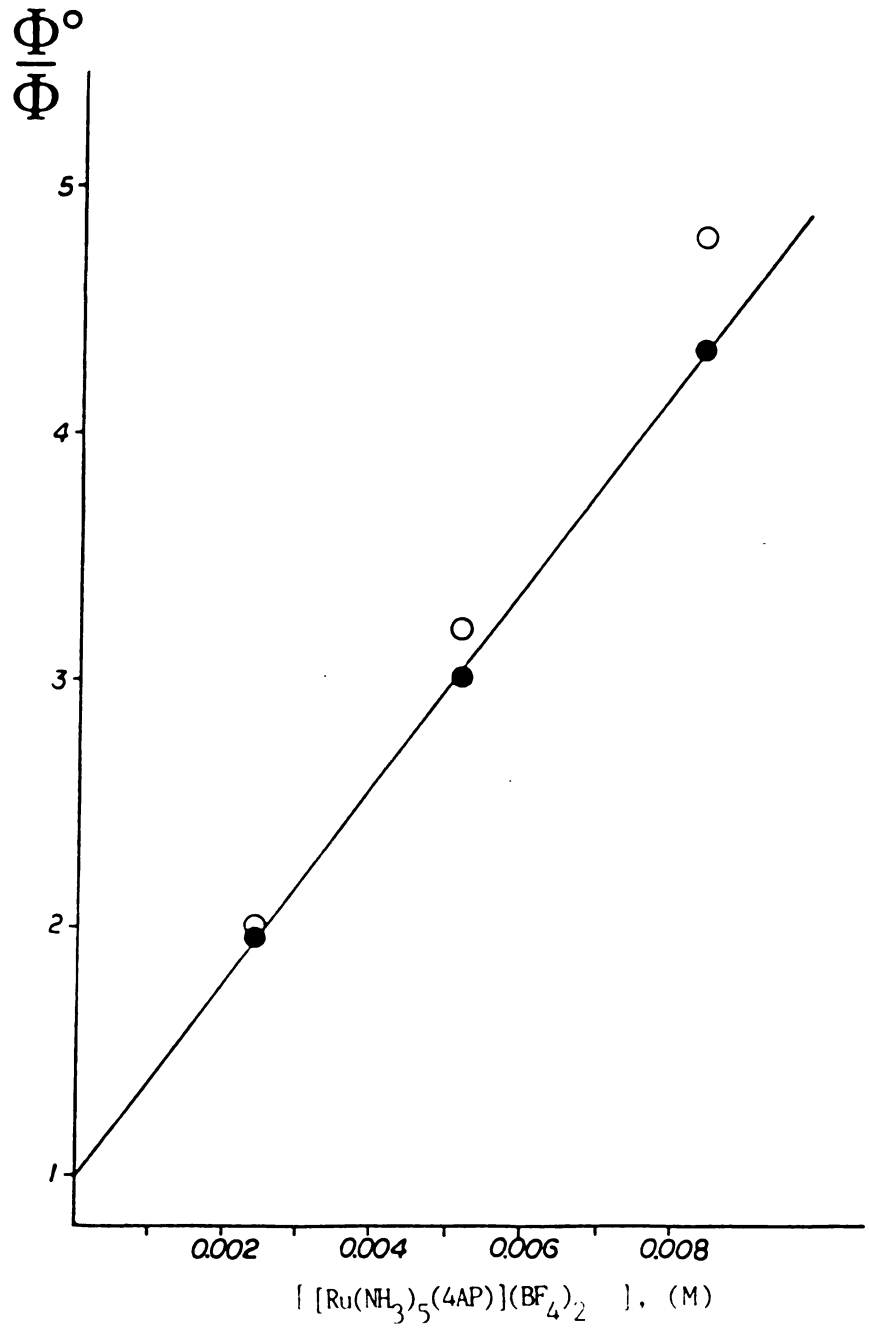

Figure 21. Stern Volmer plot for butyrophenone quenched by $[Ru(NH_3)_5(4AP)](BF_4)_2$. (○): uncorrected curve. (●): curve corrected for partial light absorption by the ketone.

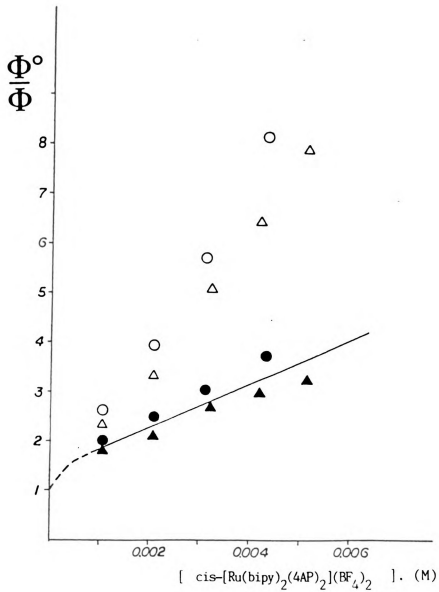

Figure 22. Stern Volmer plot for butyrophenone quenched by cis-cis-$[Ru(bipy)_2(4AP)_2](BF_4)_2$. Two runs. (○) and (△): uncorrected curves; (●) and (▲): curves corrected for partial light absorption by the ketone.

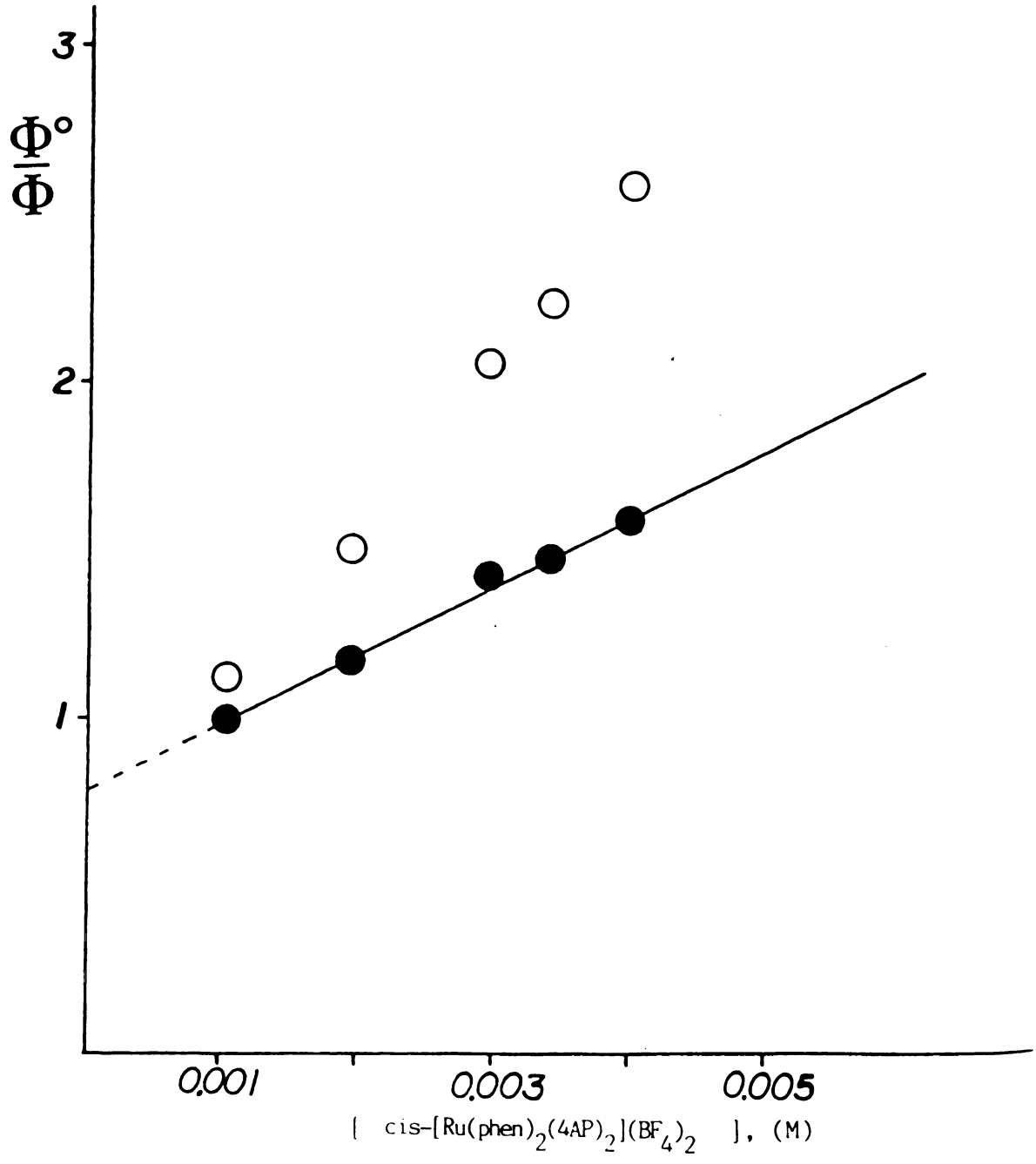

Figure 23. Stern Volmer plot for butyrophenone quenched by cis-$[Ru(phen)_2(4AP)_2](BF_4)_2$. (○): uncorrected curve; (●): curve corrected for partial light absorption by the ketone.

Table 9. Results from Stern-Volmer quenching of butyrophenone by Ruthenium(II) complexes.

Quencher	Intercept	slope($k_q \tau$)	slope/intercept
$[Ru(NH_3)_5(4AP)](BF_4)_2$	0.97	400	412
cis-$[Ru(bipy)_2(4AP)_2](BF_4)_2$	1.42	527	371
	1.40	365	261
cis-$[Ru(phen)_2(4AP)_2](BF_4)_2$	0.78	203	260

Ruthenium 2,2'bipyrimidine and Ruthenium-Osmium 2,2'bipyrimidine bridged Complexes.

Compound Preparation and Identification - Spectroscopic Studies.

Ruthenium(II) tris (2,2'bipyrimidine) Chloride was synthesized by the route shown on Scheme 8, a modification of the literature procedure.[36]

Scheme 8.

$$RuCl_3 \xrightarrow[2)\ bipym,\ EtOH/H_2O]{1)\ 3\ bipym,\ DMF} [Ru(bipym)_3]Cl_2$$

bipym = 2,2'bipyrimidine

$[Ru(bipy)_2(bipym)](BF_4)_2$ and $[Ru(phen)_2(bipym)](BF_4)_2$ were synthesized from cis-$[Ru(bipy)_2Cl_2].2H_2O$ or cis-$[Ru(phen)_2Cl_2].H_2O$ by refluxing these complexes in the presence of 5 molar excess of 2,2'bipyrimidine in 1:1 (v/v) water/methanol.

Osmium Complexes (cis-$[Os(bipy)_2Cl_2].H_2O$ and cis-$[Os(phen)_2Cl_2].H_2O$) were synthesized by the literature procedure according the Scheme 9.[92]

Scheme 9.

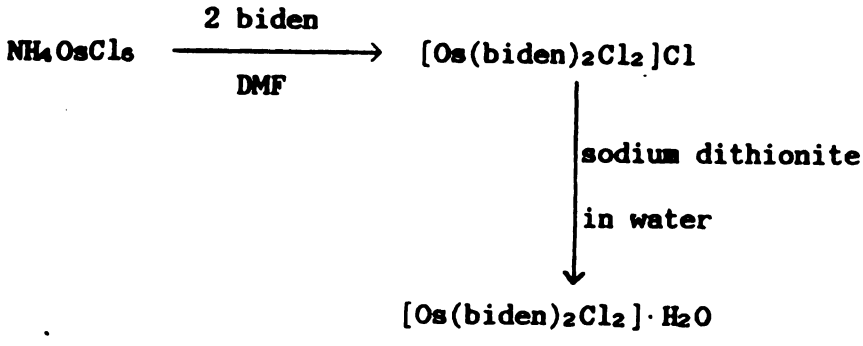

biden = bidentate ligand (2,2'bipyridine or 1,10-Phenanthroline).

Bimetallic complexes were synthesized according to Scheme 10.

Scheme 10.

$$[Ru(biden)_2(bipym)](BF_4)_2 + 1.5[Os(biden)_2Cl_2]\cdot H_2O \xrightarrow[2)\ NH_4BF_4]{1)\ \text{reflux in 1:1 (v/v) } H_2O/MeOH}$$

$$[Ru(biden)_2(bipym)Os(biden)_2](BF_4)_4$$

biden = bidentate ligand (2,2'bipyridine or 1,10-Phenanthroline).

bipym = 2,2'bipyrimidine.

Detailed synthetic procedures for all the complexes prepared are given in the Experimental Section.

The compounds were identified by their Infrared Absorption Spectra, showing all the characteristic absorptions of the coordinated ligands. Further verification of the compounds identity is given by the comparison of their UV-Vis. absorption spectra as well as their emission spectra with the ones cited in the literature. The absorption maxima usually match well with the literature reported ones, eventhough the extinction coefficients were found somewhat lower. Table 10 summarizes our results in comparison to the literature ones when data are available. Here again, as for the Ruthenium Complexes of the previous section of this chapter, we assume no water of crystallization in the calculation of the extinction

Table 10. UV-Vis. Absorption data of mononuclear and binuclear 2,2'bipyrimidine complexes.[a]

Compound	λ max, nm (ε $M^{-1}cm^{-1}$), this thesis	λ max, nm (ε $M^{-1}cm^{-1}$), literature
$[Ru(bipym)_3]Cl_2$	246 (38463) 331 (10398) sh 364 412 (5640) 452 (5434)	331 ($1.48\ 10^4$)[36] 412 ($0.76\ 10^4$) 452 ($0.74\ 10^4$)
$[Ru(bipy)_2(bipym)](BF_4)_2$	243.5 (28046) 283 (44754) 417 (9995)	sh 398 415 ($1.13\ 10^4$)[36,37] sh 475 420 ($1.05\ 10^4$)
$[Ru(phen)_2(bipym)](BF_4)_2$	222.5 (25043) 262 (36752) sh 290 392.5 (6205) sh 424	
$[Ru(bipy)_2(bipym)Ru(bipy)_2](BF_4)_4$	245 (34203) 278.5 (67137) 411 (21403) sh 560 609 (5444)	408 ($3.13\ 10^4$)[36,37,39] sh 560 606 ($0.76\ 10^4$) 408 ($2.98\ 10^4$) 592 ($0.79\ 10^4$)
$[Ru(bipy)_2(bipym)Os(bipy)_2](BF_4)_4$	243 (13788) sh 250 283.5 (23372) 417 (5665) sh's 396, 500, 560 623 (731)	244 ($5.5\ 10^4$)[39] sh 250 282 ($1.1\ 10^5$) 415 ($3.1\ 10^4$) sh's 396, 515, 560 617 ($1.0\ 10^4$)
$[Ru(bipy)_2(bipym)Os(phen)_2](BF_4)_4$	264 (18302) sh 280 410 (5951) sh 564 631 (1453)	

$[Ru(phen)_2(bipym)Os(bipy)_2](BF_4)_4$	261	(43248)
	sh 280	
	407	(12096)
	sh's 520, 560	
	629	(2799)
$[Ru(phen)_2(bipym)Os(phen)_2](BF_4)_4$	222	(102083)
	262	(126304)
	392	(22610)
	sh's 412, 560	
	623	(2280)
	766	(1259)

[a] Solvent water.

Table 11. Emission data of mononuclear and binuclear 2,2'bipyrimidine Complexes.

Compound	Solvent	T, °K	excitation λ, nm	emission λ, nm	E_T (kcal/mol)
$[Ru(bipym)_3]Cl_2$	water	RT	410	625	45.7
$[Ru(bipy)_2(bipym)](BF_4)_2$	MeOH/EtOH				
$[Ru(phen)_2(bipym)](BF_4)_2$	MeOH/EtOH	77	410	622	46.0
$[Ru(bipy)_2(bipym)Ru(bipy)_2](BF_4)_4$	MeOH/EtOH	77	410	635	45.0
$[Ru(bipy)_2(bipym)Os(bipy)_2](BF_4)_4$	MeOH/EtOH	77	410	632	45.2
$[Ru(bipy)_2(bipym)Os(phen)_2](BF_4)_4$	MeOH/EtOH	77	410	690	41.4
$[Ru(phen)_2(bipym)Os(bipy)_2](BF_4)_4$	MeOH/EtOH	77	410	626	45.7
$[Ru(phen)_2(bipym)Os(phen)_2](BF_4)_4$	MeOH/EtOH	77	410	626,684	45.7, 41.8

coefficients, eventhough the IR spectra suggest the existence of some water molcules. For some of the compounds cited in the literature, it has been proven that they retain a variable number of water molecules in their crystal structure. It is noteworthy that for some of the mixed ligand bimetallic complexes, the extinction coefficients found are substantially lower than expected for charge transfer transitions, a fact probably due to the purification procedure (Column Chromatography on a cation exchange Sephadex column eluting with NH_4BF_4 aqueous solution) combined with the small scale preparation which tend to give products containing substantial amounts of NH_4BF_4. Nevertheless, when literature data are available, it can be seen that the ratios of the extinction coefficients at the absorption maxima found in this work match well with the corresponding ratios from the literature, fact taken as further verification of the complex identity.

Finally, Table 11 displays the emission data of the complexes studied.

Raman Studies.

Ground and lower excited state (when applicable) Raman Spectra have been recorded by Y. C. Chung for all the compounds listed in this section.

Tris (2,2'bipyrimidine) Ruthenium(II) chloride shows clear evidence that its peculiar absorption spectrum is the

contribution from two distinct MLCT states, one being in resonance at the 442 nm cw excitation wavelength, the other being in resonance 364 nm cw excitation. Employment of pulsed excitation from the Nd-YAG laser at 440 nm and 354.7 nm reveals new peaks which have been attributed to scattering from the complex having one of the 2,2'bipyrimidine ligands in the MLCT state: $[Ru(III)(bipym)_2(bipym^{-})]^{2+}$. Differences again in the relative peak intensity and the appearance of two new peaks at 1255 and 1362 cm^{-1} to the red of the excitation line at 354.7 nm have been attributed to different upper electronic states being in resonance with the MLCT excited state of the $[Ru(bipym)_3]^{2+}$ when the two pulsed excitation wavelengths were employed.

Similar behavior has been demonstrated for most of the 2,2'bipyrimidine complexes under this section of this chapter. Complete experimental description and interpretation of the Raman spectra with respect to their significance in the resolution of the absorption and emission spectra can be found in Y. C. Chung, Ph.D. Thesis, Michigan State University, 1985.

Photochemistry of Tungsten Carbonyls.

Compound Preparation and Identification.

Ligands. The ligands used were either commercially available or synthesized (4-valerylpyridine, 4-butyrylpyridine and 4-acetylpyridine) by the Grignard

reaction using 4-cyanopyridine and n-butyl bromide, n-propyl bromide or methyl iodide, respectively. Verification of the product identity comes from the spectroscopic data for each compound, a detailed list of which can be found in the experimental section of this thesis. All complexes synthesized along with their abbreviations are listed in Table 12.

Pentacarbonyl Tungsten(0) Complexes. These complexes were synthesized from Hexacarbonyl Tungsten(0) according to the classical Strohmeier method. Scheme 11 shows the general synthetic route to prepare these complexes.[49,69]

Scheme 11.

$$W(CO)_6 \xrightarrow[THF,\ Ar]{h\nu,\ \text{pyrex filter}} W(CO)_5(THF) \xrightarrow{\text{Ligand}} W(CO)_5(\text{Ligand})$$

THF replaces one photochemically removed CO molecule and THF is subsequently, after the end of the irradiation, substituted by a better ligand, like the substituted pyridines used. THF has to be dry, otherwise, a white precipitate appears during the first minutes of irradiation, presumably $W(CO)_5(H_2O)$ and the reaction fails. The absence of the pyridyl ligand in the irradiation step is essential for two reasons. First, some pyridyl ketones are photochemically reactive and, second, this method, as has been reported,[69] leads to replacement of only one CO molecule and formation of Pentacarbonyl Tungsten(0)

Table 12. Carbonyl Compounds of Tungsten (0) and the Abbreviations Used.

Compound	Symbol
Pentacarbonyl (4-Acetylpyridine) Tungsten (0)	$W(CO)_5(4AP)$
Pentacarbonyl (methyl-isonicotinate) Tungsten (0)	$W(CO)_5(MeINic)$
Pentacarbonyl (4-Benzoylpyridine) Tungsten (0)	$W(CO)_5(4Bzpy)$
Pentacarbonyl (4-Cyanopyridine) Tungsten (0)	$W(CO)_5(4CNpy)$
Pentacarbonyl (4-Butyrylpyridine) Tungsten (0)	$W(CO)_5(4BP)$
Pentacarbonyl (4-Valerylpyridine) Tungsten (0)	$W(CO)_5(4VP)$
cis-Tetracarbonyl bis(4-Valerylpyridine) Tungsten (0)	$cis\text{-}W(CO)_4(4VP)_2$
Hexacarbonyl Tungsten (0)	$W(CO)_6$

complexes. Purification is achieved by column chromatography and, when possible, recrystallization.

All the complexes studied are yellow solids, except Pentacarbonyl [1-(4-pyridyl) pentanone] Tungsten(0) which is a deep orange oil. They all decompose at temperatures ranging between 70 and 130°C yielding brown-reddish oils. Only Pentacarbonyl (4-cyanopyridine) Tungsten(0) seems to be stable since it can be recovered after melting. Nevertheless, all these complexes give interpretable mass spectra, including the molecular ion peak; the rest of the spectrum is dominated by the ligand fragmentation pattern as well as peaks corresponding to the original complex losing successive CO molecules. Proton and Carbon-13 nmr spectra are also conclusive about the complex identity. Finally, visible light absorption spectra match precisely the spectra cited in the literature for those of the complexes having been synthesized before by other researchers.

Spectroscopic Studies.

Absorption and emission spectra were recorded in both benzene and methylcyclohexane for all the compounds studied. Table 13 lists the absorption and emission data. Figure 24 displays representative absorption and emission spectra for Pentacarbonyl [1-(4-pyridyl)pentanone] Tungsten(0). In agreement with previous observations for a solvent-sensitive, MLCT lowest excited state, all the complexes' absorption spectra show a solvent dependent long wavelength feature. In the less-polarizable methylcyclohexane, a separate peak is observed at the long wavelength side of the solvent insensitive peak at approximately 402 nm; the two merge as one moves to the more polarizable benzene.[60,69]

Emission was recorded in fluid solution at room temperature. Eventhough emission maxima tend to be insensitive to solvent polarity, the emission spectrum overall becomes broader in the less polar methylcyclohexane with a broad shoulder on the blue side of the maximum emission.

Photochemical Studies

Photoproduct Identification. Mass Balance and Cross-coupling Experiments.

Irradiation of four freeze-pump-thaw, degassed and hermetically sealed $W(CO)_5(4VP)$ solutions in both benzene and methylcyclohexane at 313 nm, 410 nm or 490 nm resulted in change of the solution color from orange-yellow to deep

Table 13. Absorption and Emission Data for the Tungsten Carbonyls.

Compound	Solvent	Absorption		Emission[a]	
		λ_{max}, nm (ε $M^{-1}cm^{-1}$)	ε_{313} ($M^{-1}cm^{-1}$)	λ_{max}, nm	E_T (kcal/mol)
W(CO)$_5$(4AP)	benzene	sh 332 402 (9210) sh 430	2308	625	45.7
	methylcyclohexane	sh 332 404 (8244) 441 (8109)		sh 540 622	
W(CO)$_5$(MeINic)	benzene	sh 332 402 (8483)	1983	---	---
	methylcyclohexane	sh 332 405 (9549) sh 430		---	---
W(CO)$_5$(4Bzpy)	benzene	sh 332 403 (9424) sh 430		624	45.8
	methylcyclohexane	sh 332 405 (8082) 435 (7106)		sh 540 622	46.0
W(CO)$_5$(4CNpy)	benzene	sh 330 404 (7364) sh 430		633	45.2
	methylcyclohexane	sh 330 403 (-) 453 (-)		sh 540 624	45.8
W(CO)$_5$(4BP)	benzene	sh 332 402 (8967) sh 430		623	45.9
	methylcyclohexane	sh 332		sh 540	

		405 (7305) 438 (7069)		621	46.0
$W(CO)_5(4VP)$	benzene	sh 332 402 (8534) sh 430	2220	623	45.9
	methylcyclohexane	sh 332 405 (8353) 437 (7664)	2206	sh 540 623	45.9

[a] Excitation at 402 nm, temperature = 298°K.

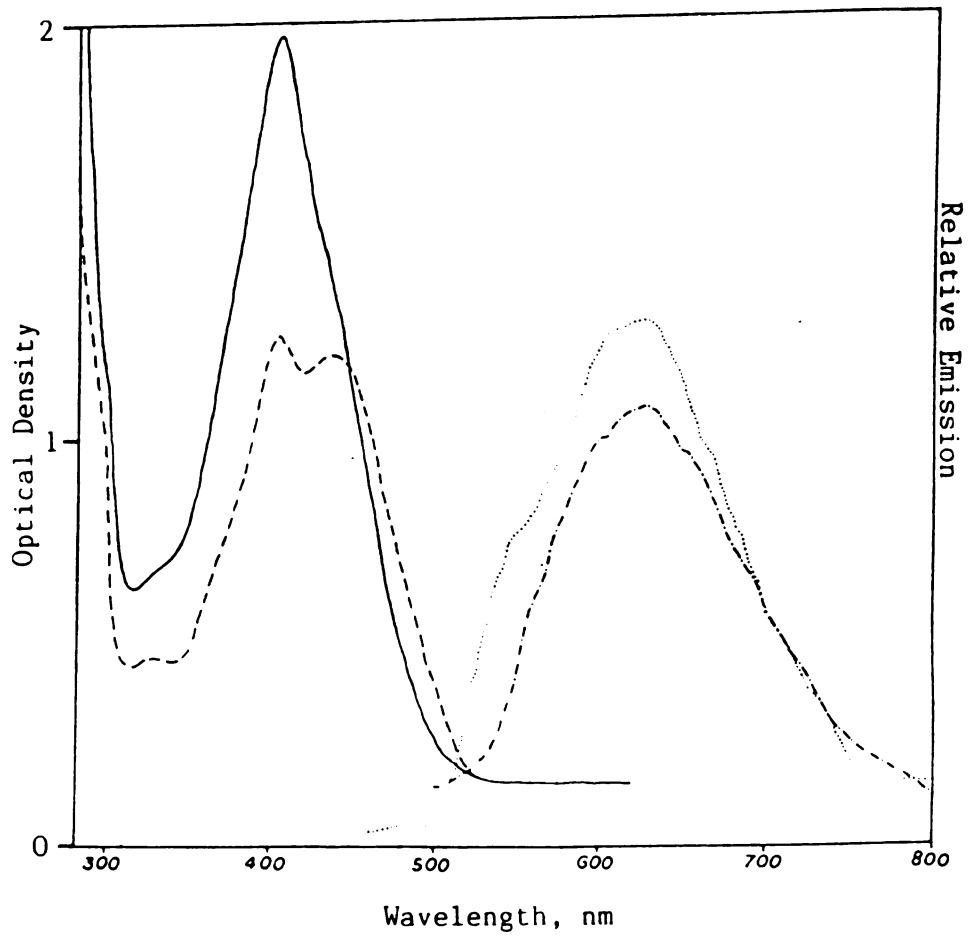

Figure 24. Absorption spectra of $W(CO)_5(4VP)$ in benzene at $2.3\ 10^{-4}$ M (———) and in methylcyclohexane at $1.4\ 10^{-4}$ M (- - -). Emission spectra of $W(CO)_5(4VP)$ in benzene (-·-·-) and in methylcyclohexane (·····). Concentrations between 10^{-5} and 10^{-4} M.

red. HPLC analysis gave two product peaks. The first product was initially identified as $W(CO)_6$ by comparing its HPLC retention time with an authentic sample. At longer conversions, upon longer irradiation, a white product precipitated out of solution. It was collected and identified as $W(CO)_6$ by mass spectrometry. Finally, a C-13 nmr spectrum of this product gives a peak at 191 ppm downfield from TMS, identical to the peak given by a neat sample of $W(CO)_6$.

The product responsible for the color change was isolated by column chromatography/recrystallization (for details, look at the experimental section) and identified as cis-Tetracarbonyl bis[1-(4-pyridyl)pentanone] Tungsten(0) (cis-$W(CO)_4(4VP)_2$). Figure 25 displays the absorption spectrum of the compound in both benzene and methylcyclohexane; these spectra are identical to the spectrum reported by Lees for cis-$W(CO)_4$(4-benzoylpyridine)$_2$.[68] Figure 26 displays the Infrared spectrum of this compound, consistent with the assignment of the cis-geometry.[94] The peak at 1695 cm^{-1} corresponds to the two equivalent ketone carbonyls of the ligands, while the strong peaks at 1990, 1880, 1855, and 1810 cm^{-1} correspond to the CO's coordinated to Tungsten. Figure 27 displays the proton decoupled Carbon-13 nmr spectrum; two peaks of equal intensity appear at 205 and 213 ppm. As has been reported[95], peripheral carbonyls coordinated to zero valent metal centers appear between 180 and 220 ppm, while bridging

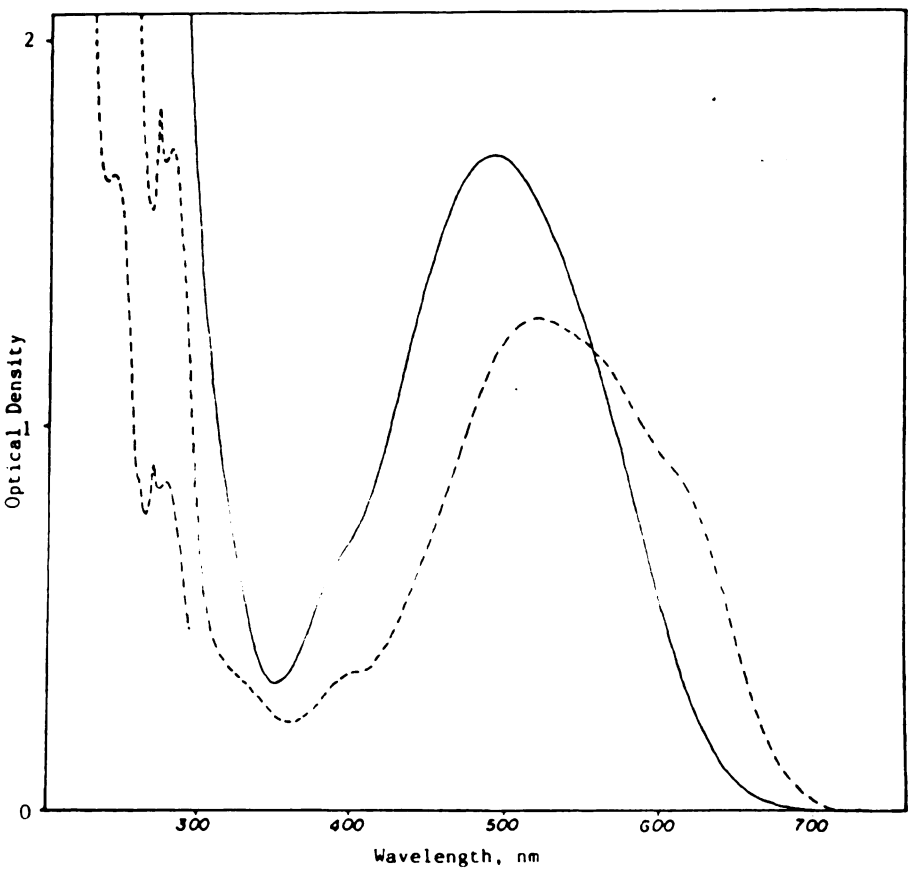

Figure 25. Absorption spectra of 1.9 10^{-4} M cis-$W(CO)_4(4VP)_2$ in benzene (———). (- - -): absorption spectra of cis-$W(CO)_4(4VP)_2$ in methylcyclohexane.

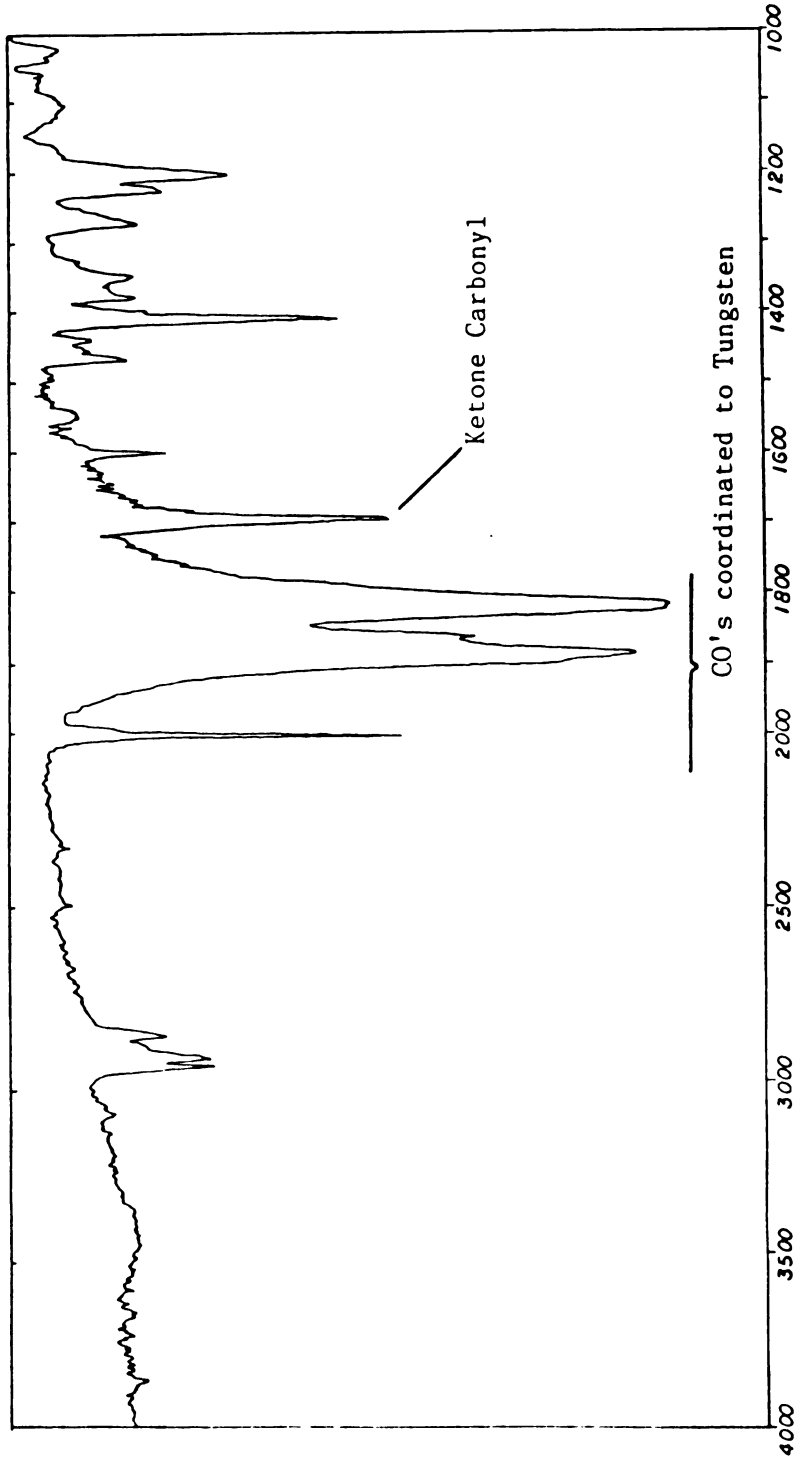

Figure 26. Infrared spectrum of cis-$W(CO)_4(4VP)_2$ in a KBr pellet.

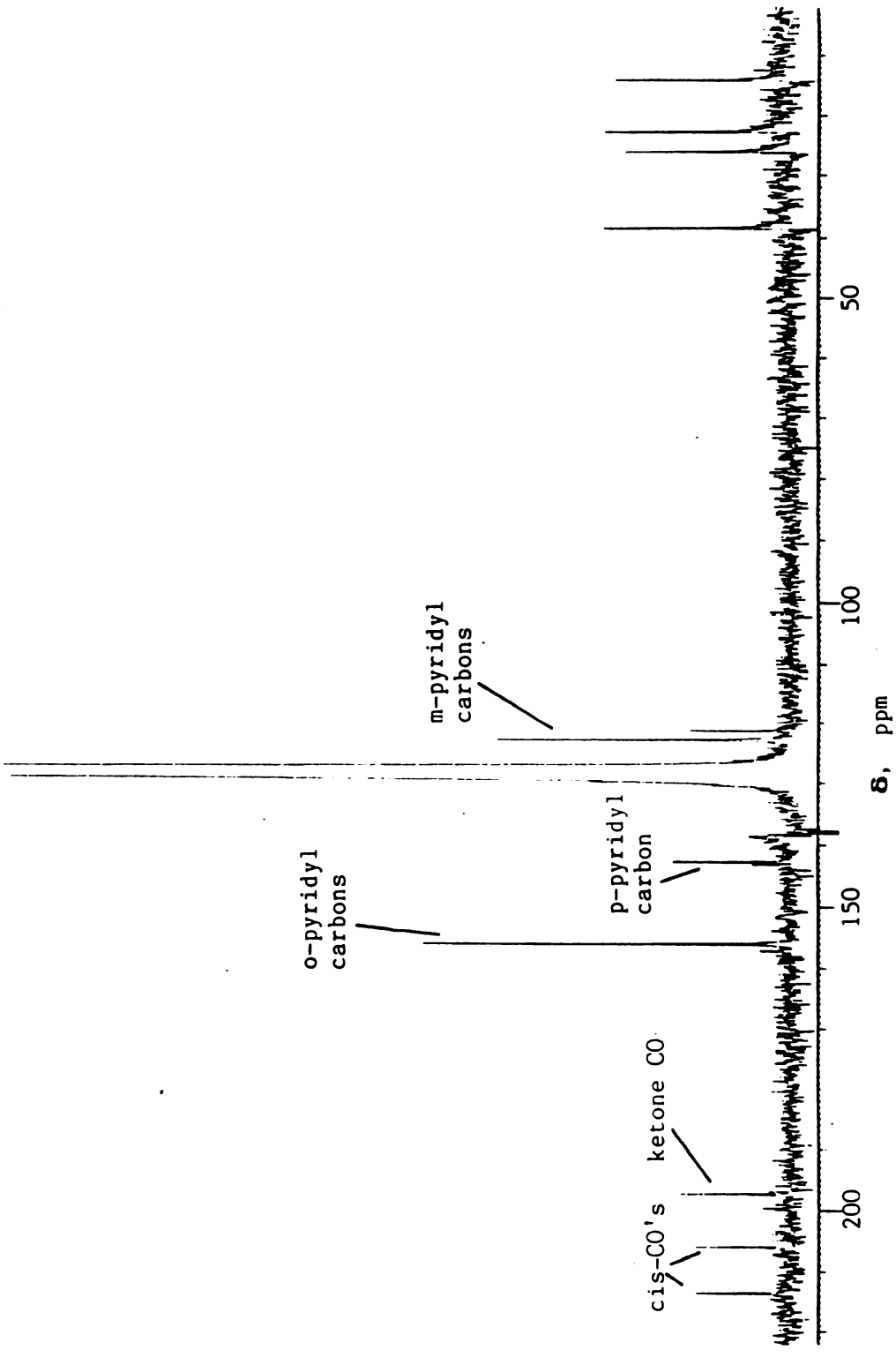

Figure 27. Carbon-13 nmr spectrum of cis-$W(CO)_4(4VP)_2$ in benzene-d_6 containing 1 % (w/v) $Cr(acac)_3$.

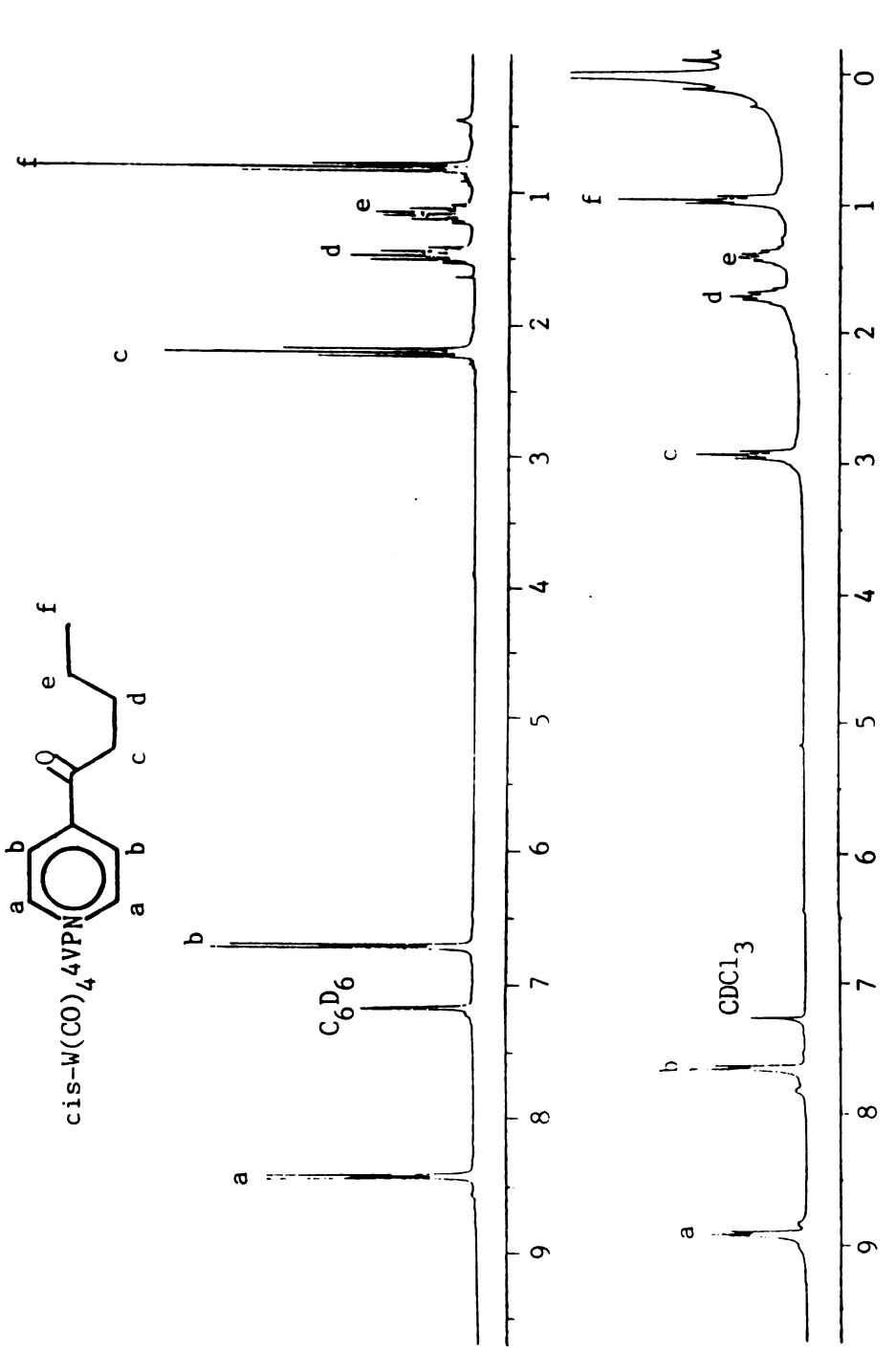

Figure 28. Proton nmr spectrum of cis-$W(CO)_4(4VP)_2$ in benzene-d_6 (top) and $CDCl_3$ (bottom).

carbonyls appear between 220 and 240 ppm. Thus, any kind of bridging is excluded. Trans-geometry is also excluded since all four carbonyls would be identical and, therefore, only one signal for the coordinated carbonyls would be observed in the C-13 nmr spectrum. Finally, Figure 28 provides further verification that the ligand is not involved in any internal ligand photochemical reaction, but it is transferred from the reactant ($W(CO)_5(4VP)$) to the product ($cis\text{-}W(CO)_4(4VP)_2$) intact.

Table 14 gives the mass balance data for irradiation ($\lambda_{irr}>400$ nm) of Pentacarbonyl [1-(4-pyridyl)pentanone]-Tungsten(0) in benzene in two cases, i.e., degassed normally with four freeze-pump-thaw cycles and under 2 atm. of carbon monoxide. In the latter case, the sample remains yellow and $W(CO)_6$ is formed as a white precipitate.

Parallel irradiation of an almost equimolar solution of $W(CO)_5(4VP)$ and $W(CO)_5(4BP)$ in benzene resulted in the formation of three products besides $W(CO)_6$ as analyzed by HPLC. Two of these correspond to the Tetracarbonyl products observed in the irradiation of each compound separately. The middle product, formed in a yield equal to the sum of the yields of the other two products, corresponds probably to $cis\text{-}W(CO)_4(4VP)(4BP)$. Table 15 summarizes these results.

Table 14. Mass balance experiments for Pentacarbonyl 4-valerylpyridine Tungsten(0) Photolysis.[a]

	[W(CO)$_5$(4VP)], (M)	[cis-(W(CO)$_4$(4VP)$_2$], (M)	[W(CO)$_6$], (M)	[4VP], (M)
Sample Degassed				
non irradiated sample	0.00958	---	---	---
after irradiation	0.00170	0.00352	0.00364	---
Sample Degassed				
non irradiated sample	0.0129	---	---	---
after irradiation	0.00849	0.00269	0.00258	---
Sample Degassed[b]				
non irradiated sample	0.0167	---	---	---
after irradiation	0.0112	0.000681	[c]	---
Sample Under 2 atm CO[b]				
non irradiated sample	0.0167	---	[c]	---
after irradiation	0.0114	0.0000452	[c]	0.00365

[a] $\lambda_{irr} > 400$ nm.

[b] irradiated in parallel.

[c] not measured.

Table 15. Cross-Coupling Experiments for $W(CO)_5(4VP)$ and $W(CO)_5(4BP)$ Irradiated Together.[a]

Area $W(CO)_5(4VP)$:	446173
Area $W(CO)_5(4BP)$:	656522
Area cis-$W(CO)_4(4VP)_2$:	19274
Area cis-$W(CO)_4(4VP)(4BP)$:	49735
Area cis-$W(CO)_4(4BP)_2$:	30617

[a] HPLC analysis, detector at 402 nm; $\lambda_{irr} > 400$ nm; results after irradiation.

The 1:2.5:1.5 ratio of the tetracarbonyl products represents statistical ratio since the two reactants were in 1:1.5 ratio initially.

Comparison of the Photobehavior of $W(CO)_5(4VP)$ with other Pentacarbonyl Complexes of Tungsten

Stability of the Photoproduced Tetracarbonyl Complexes.

Two methods were employed to verify that other complexes like $W(CO)_5L$, where L is a substituted pyridyl ligand, behave photochemically similarly to $W(CO)_5(4VP)$.

The first method is to compare the UV-Visille absorption changes of the complexes under visible light irradiation. The second method involves comparison with

each other of the C-13 nmr spectra of the complexes before and after irradiation.

Figure 29 displays the absorption changes of an Argon bubbled degassed $W(CO)_5(4VP)$ solution in methylcyclohexane upon visible light (λ_{irr}>400 nm) irradiation. An isosbestic point, probably due to cis-$W(CO)_4(4VP)_2$ appears at 525 nm only at the beginning of the reaction. The early loss of this isosbestic point is probably due to a photooxidation reaction of cis-$W(CO)_4(4VP)_2$. On the other hand, cis-$W(CO)_4(4VP)_2$ in a four freeze-pump-thaw cycle degassed and hermetically sealed nmr tube does not bleach upon long exposures to room light and does not lose any of the C-13 nmr signals.

$W(CO)_5(4VP)$ irradiated in 1:1 (v/v) benzene/methanol or in CO saturated benzene solution gives no long wavelength isosbestic points. Figure 30 displays this behavior in CO saturated benzene solution; a new isosbestic point appears at 318 nm with the simultaneous increase of the $W(CO)_6$ absorption maximum at 290 nm. Finally, Figure 31 exhibits the behavior of $W(CO)_5(4CNpy)$ in Argon degassed benzene and methylcyclohexane.

Certain of the compounds were dissolved in benzene containing 1-2.5% (w/v) Chromium trisacetylacetonate (shiftless relaxation reagent),[95,96] degassed and sealed in an nmr tube. Carbon-13 nmr spectra were recorded before and after irradiation of the tubes with visible light (λ_{irr}>400

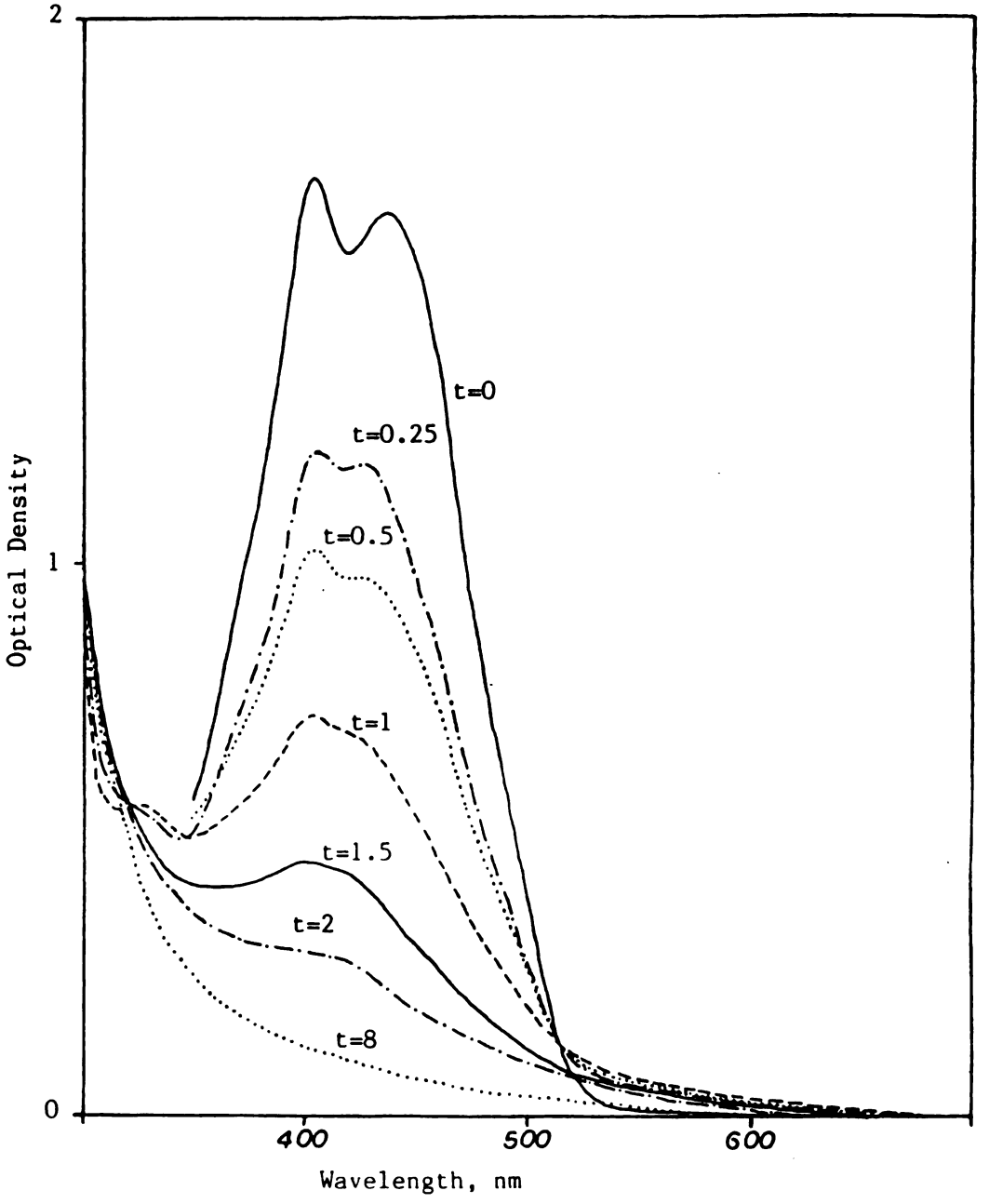

Figure 29. Absorption spectra of 2.0 10^{-4} M $W(CO)_5$4VP in methylcyclohexane upon irradiation with $\lambda > 400$ nm. Argon bubbled degassed sample. Time (t) in minutes.

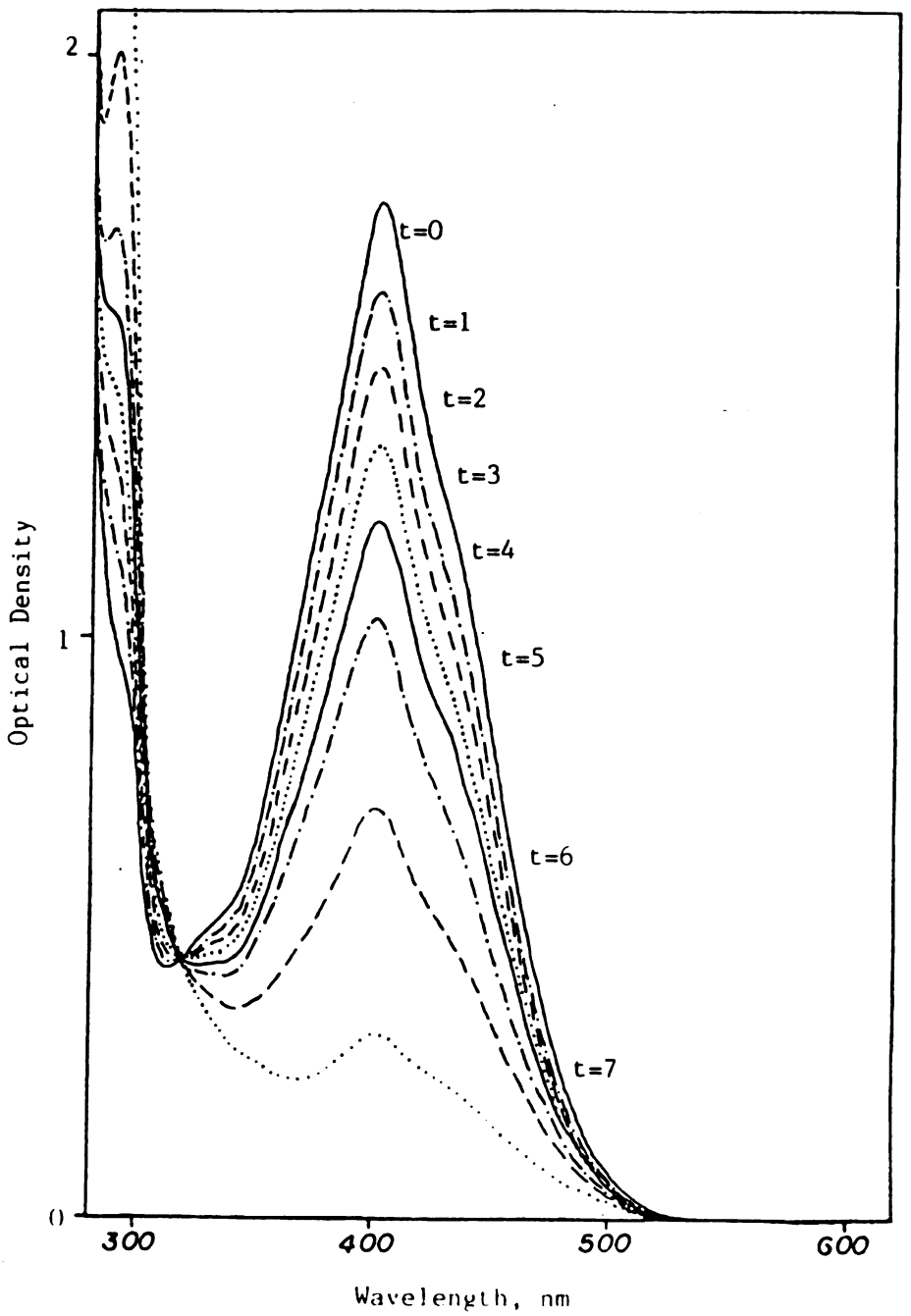

Figure 30. Absorption spectra of $2.1\ 10^{-4}$ M $W(CO)_5(4VP)$ in benzene upon irradiation with λ>400 nm. Carbon monoxide saturated sample. Time (t) in minutes.

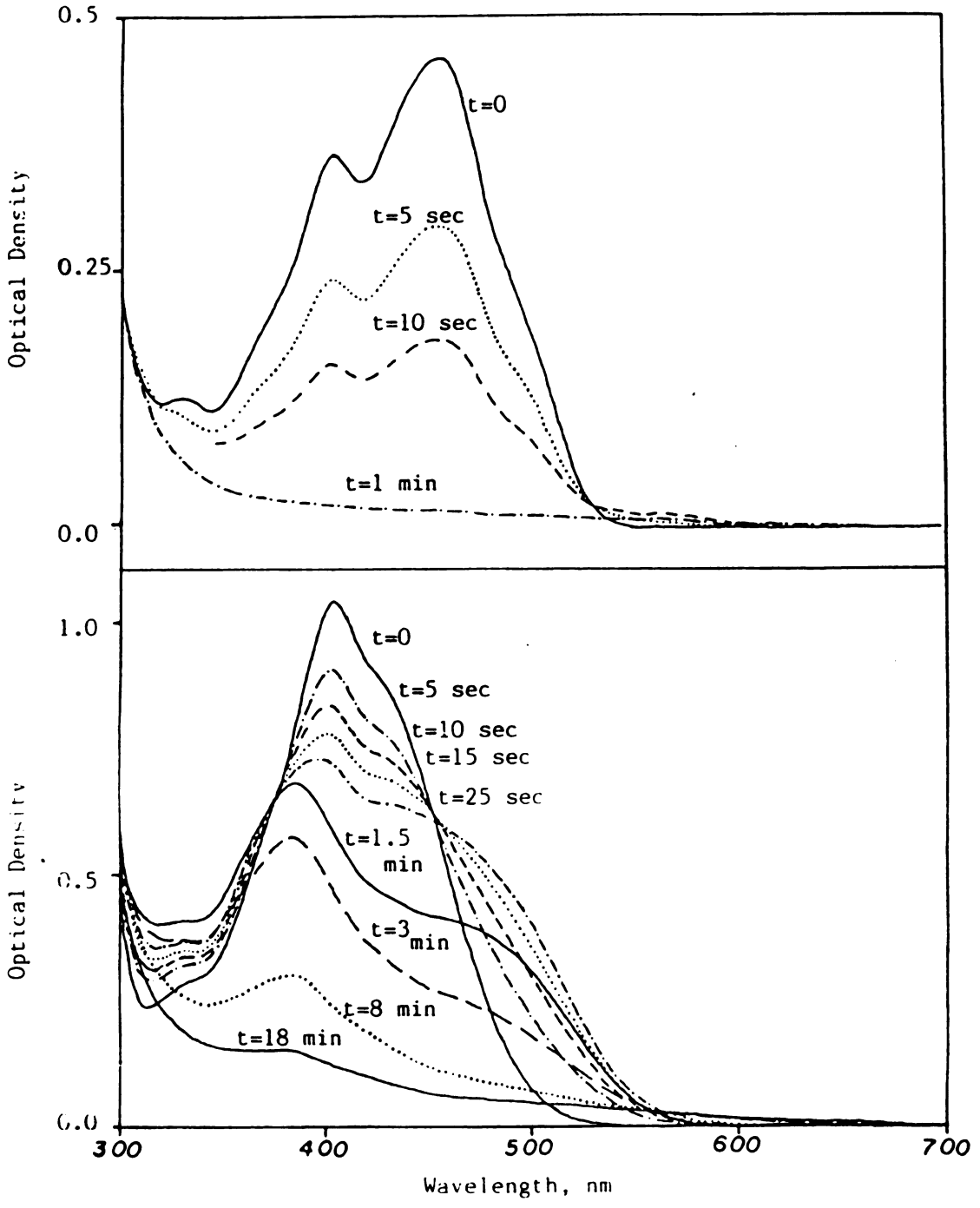

Figure 31. Absorption spectra of about $1.4\ 10^{-4}$ M $W(CO)_5(4CNpy)$ in methylcyclohexane (top frame) and $5.0\ 10^{-5}$ M in benzene (bottom frame) upon irradiation with λ>400 nm. Argon bubbled degassed samples.

nm). Figures 32, 33 and 34 display the results obtained. After irradiation, all the compounds studied show a peak at 191 ppm due to photogenerated $W(CO)_6$ along with the peaks at 205 ppm and 213 ppm due to cis-Tetracarbonyl bis(substituted pyridine) Tungsten(0) complexes.

Quantum Yield Studies.

Solutions of Pentacarbonyl [1-(4-pyridyl)pentanone] Tungsten(0) in benzene and methylcyclohexane (0.050 M) were irradiated at 410 nm and at 490 nm, and the quantum yields of cis-Tetracarbonyl bis[1-(4-pyridyl) pentanone] Tungsten(0) formation were measured by two methods: First by HPLC analysis and second by the product visible light absorption at 600 nm. Details about both methods are given in the experimental section.

Uranyl oxalate actinometry[97] was used for the 410 nm irradiation while Potassium Reineckate[98] actinometry was employed for the 490 nm irradiation. Results are summarized in Table 16.

Table 16. Formation Quantum Yield Data for cis-$W(CO)_4(4VP)_2$ from $W(CO)_5(4VP)$.

Solvent:	benzene[a]		methylcyclohexane[b]	
Irradiation wavelength (nm):	410	490	410	490
cis-$W(CO)_4(4VP)_2$:	0.0657	0.000658	0.0285	0.0000408

[a] $[W(CO)_5(4VP)]$ = 0.0504 M.

[b] $[W(CO)_5(4VP)]$ = 0.0501 M.

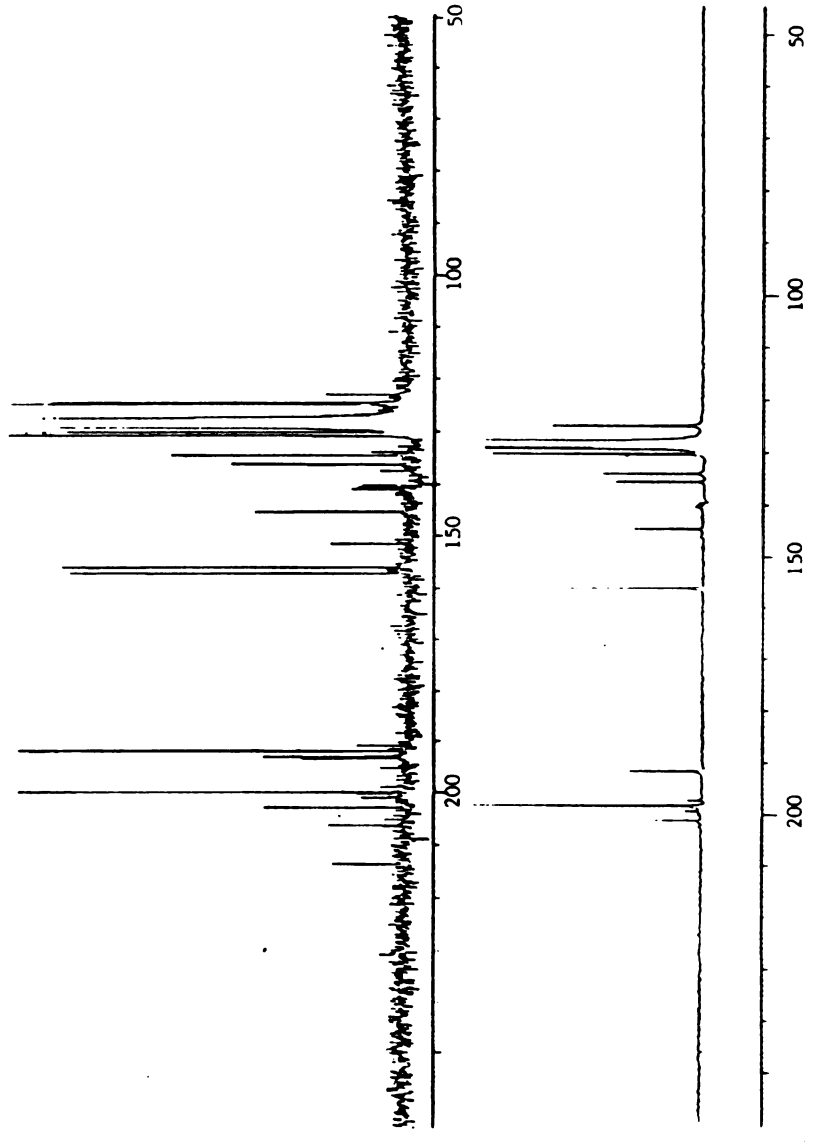

Figure 32. Carbon-13 nmr spectra of $W(CO)_5(4Bzpy)$. Bottom frame: before irradiation; top frame: after irradiation with $\lambda > 400$ nm. Solvent: benzene-d_6 containing 1% (w/v) $Cr(acac)_3$.

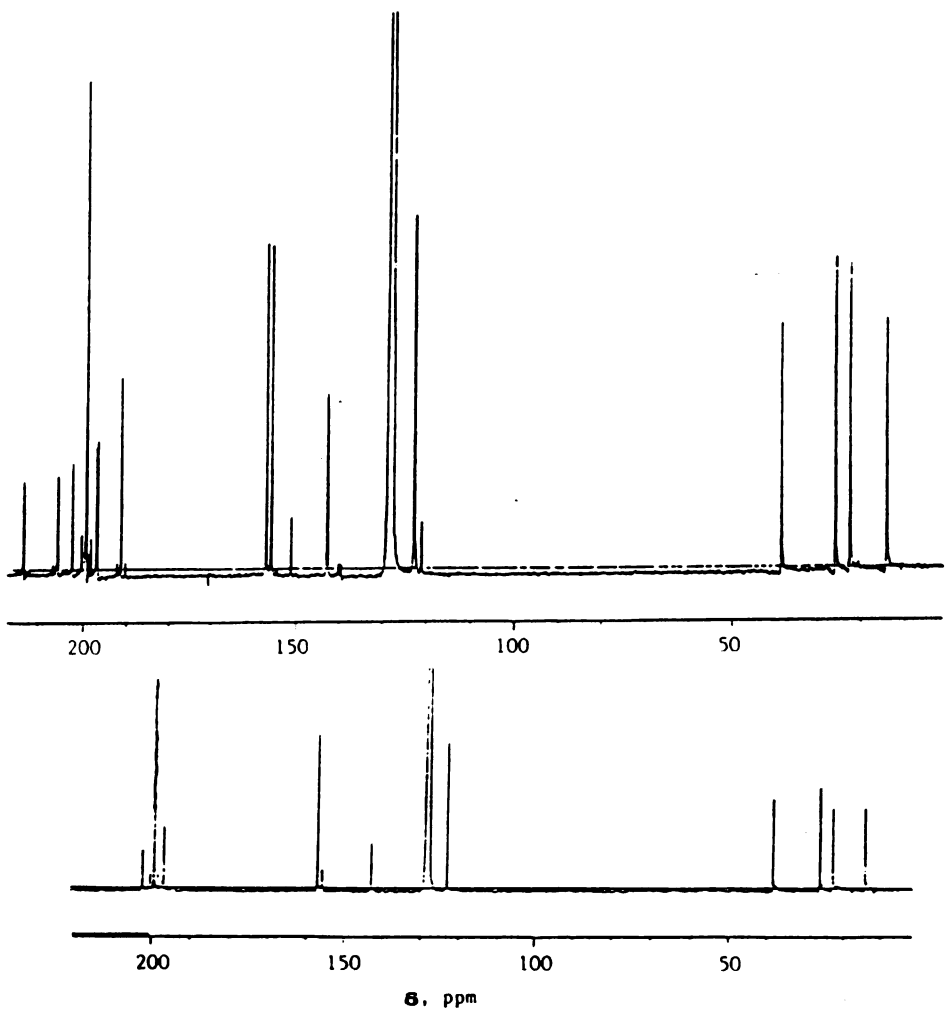

Figure 33. Carbon-13 nmr spectra of $W(CO)_5(4VP)$. Bottom frame: before irradiation; top frame: after irradiation with λ>400nm. Solvent: benzene-d_6 containing 1% (w/v) $Cr(acac)_3$.

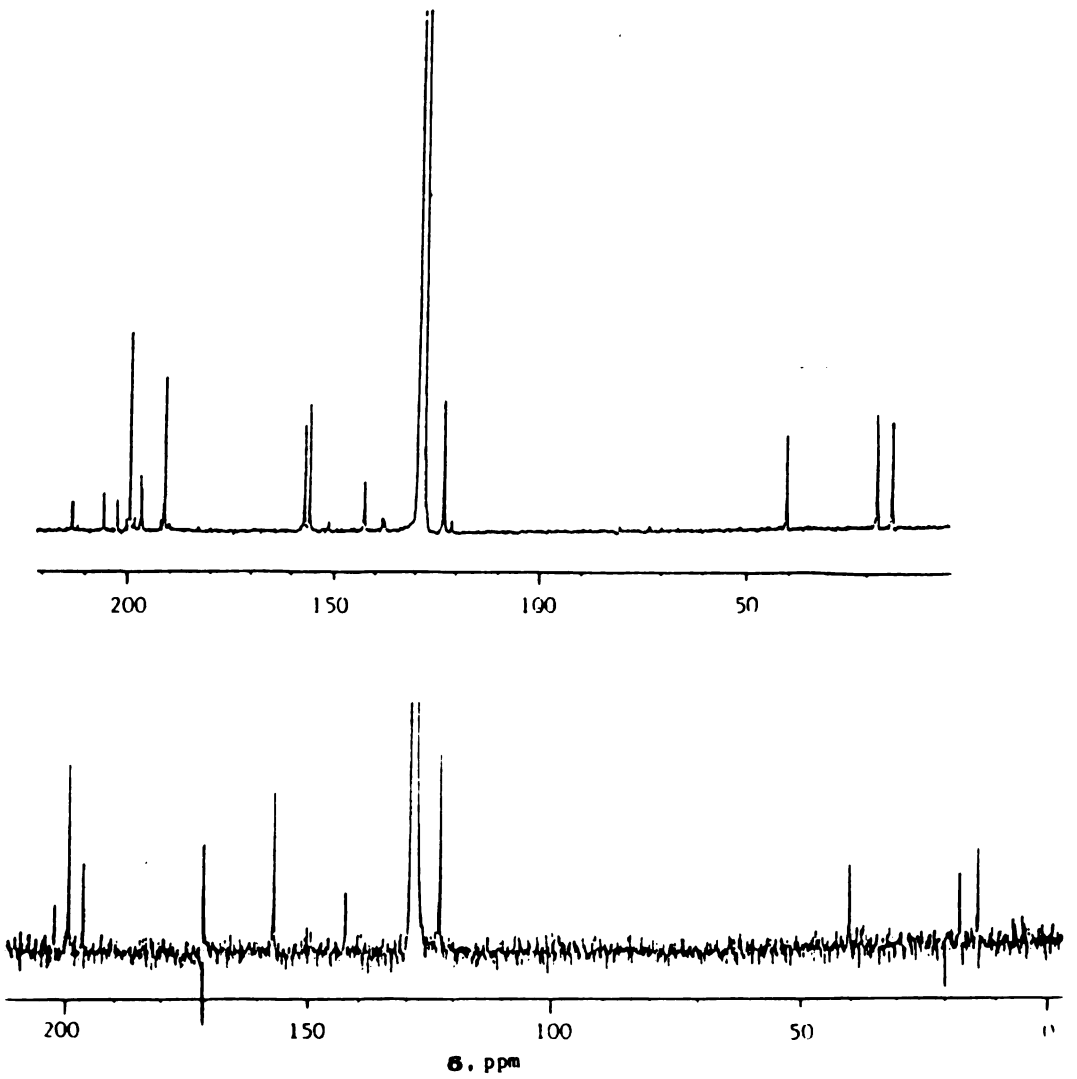

Figure 34. Carbon-13 nmr spectra of $W(CO)_5(4BP)$. Bottom frame: before irradiation; top frame: after irradiation with $\lambda > 400$ nm. Solvent: benzene-d_6 containing 1% (w/v) $Cr(acac)_3$.

Because cis-$W(CO)_4(4VP)_2$ is sparingly soluble in methylcyclohexane, its extinction coefficient at 600 nm has been measured only in benzene; therefore, in order to calculate the quantum yields in methylcyclohexane, methylcyclohexane had to be replaced by benzene after irradiation. The formation quantum yield depends on ground state concentration in benzene, as displayed in Figures 35 and 36.

Quenching Studies.

A Energy Transfer Quenching

A1 Reaction Quenching

$W(CO)_5(4VP)$ was irradiated at 410 and 490 nm in benzene in the presence of varying concentration of anthracene. The formation of cis-$W(CO)_4(4VP)_2$ was quenched as shown in Figures 37, 38, 39 and 40.

A2 Emission Quenching

The emission from $W(CO)_5(4VP)$ is quenched by anthracene. The samples were excited at 420 nm and the emission spectrum was recorded from 500 to 800 nm. As baseline, we chose the 800 nm end of the spectrum. The intensity of the emission for various anthracene concentrations was considered to be proportional to the Emission Quantum yield. In two cases, after the Stern-Volmer plots for emission quenching had been obtained, the same tubes were irradiated at 490 nm and identical (within

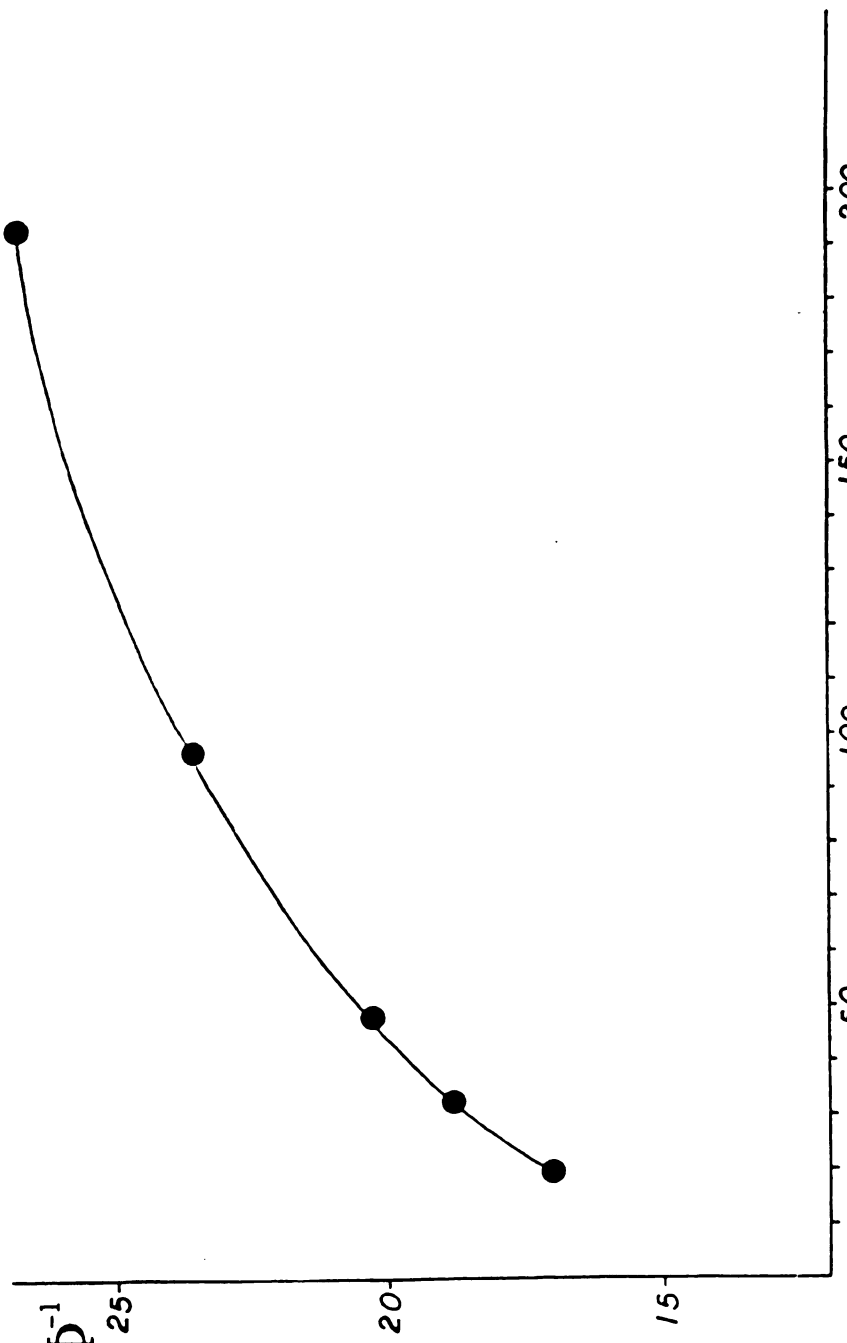

Figure 35. Effect of concentration of $W(CO)_5(4VP)$ on the cis-$W(CO)_4(4VP)_2$ formation quantum yield. Irradiation at 410 nm in benzene.

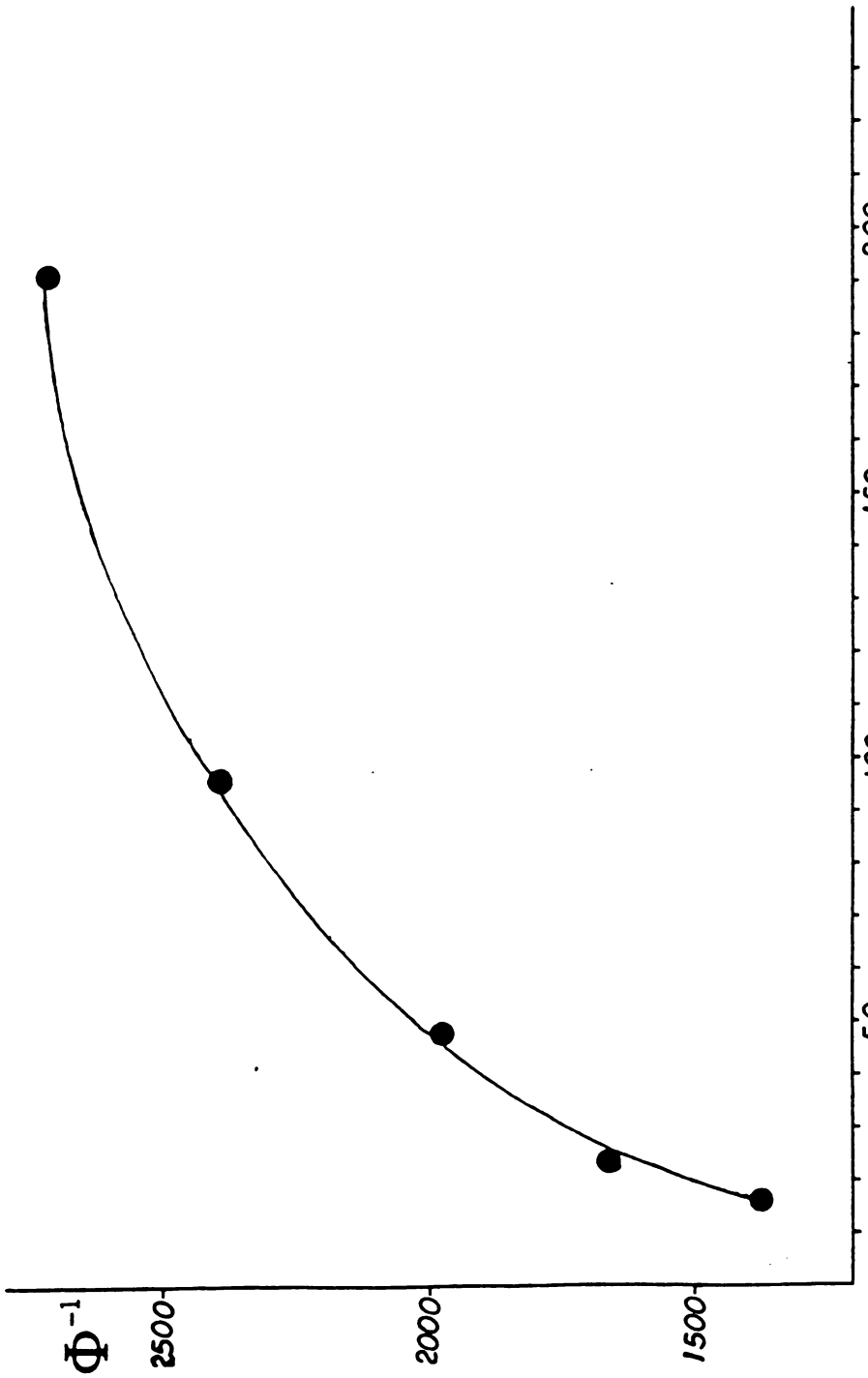

Figure 36. Effect of concentration of $W(CO)_5(4VP)$ on the cis-$W(CO)_4(4VP)_2$ formation quantum yield. Irradiation at 490 nm in benzene.

experimental error) Stern-Volmer slopes were obtained from the photoproduct quenching experiments. Figure 37 displays product quenching for irradiation at 410 nm of various $W(CO)_5(4VP)$ concentrations. Similarly, Figures 38, 39, 40 and 41 display the emission and the photochemistry at 490 nm irradiation quenching, in parallel when applicable, for various ground state complex concentrations. Finally, Table 17 summarizes the quenching results.

Table 17. Photoproduct and Emission Quenching from $W(CO)_5(4VP)$[a].

$[W(CO)_5(4VP)]$, (M)	$k_q\tau$, (M^{-1})
Irradiation at 410 nm	
0.0105	27.5[b]
0.00364	38.5[b]
0.00104	44.8[b]
Irradiation at 490 nm and emission quenching	
0.0105	372[b]
0.00508	164[b]
0.00508	156[b]
0.000897	564[b]
0.000897	530[c]
0.0000829	576[c]

[a] 4VP = 1-(4-pyridyl)pentanone

[b] product (cis-$W(CO)_4(4VP)_2$) quenching

[c] emission quenching, excitation at 420 nm.

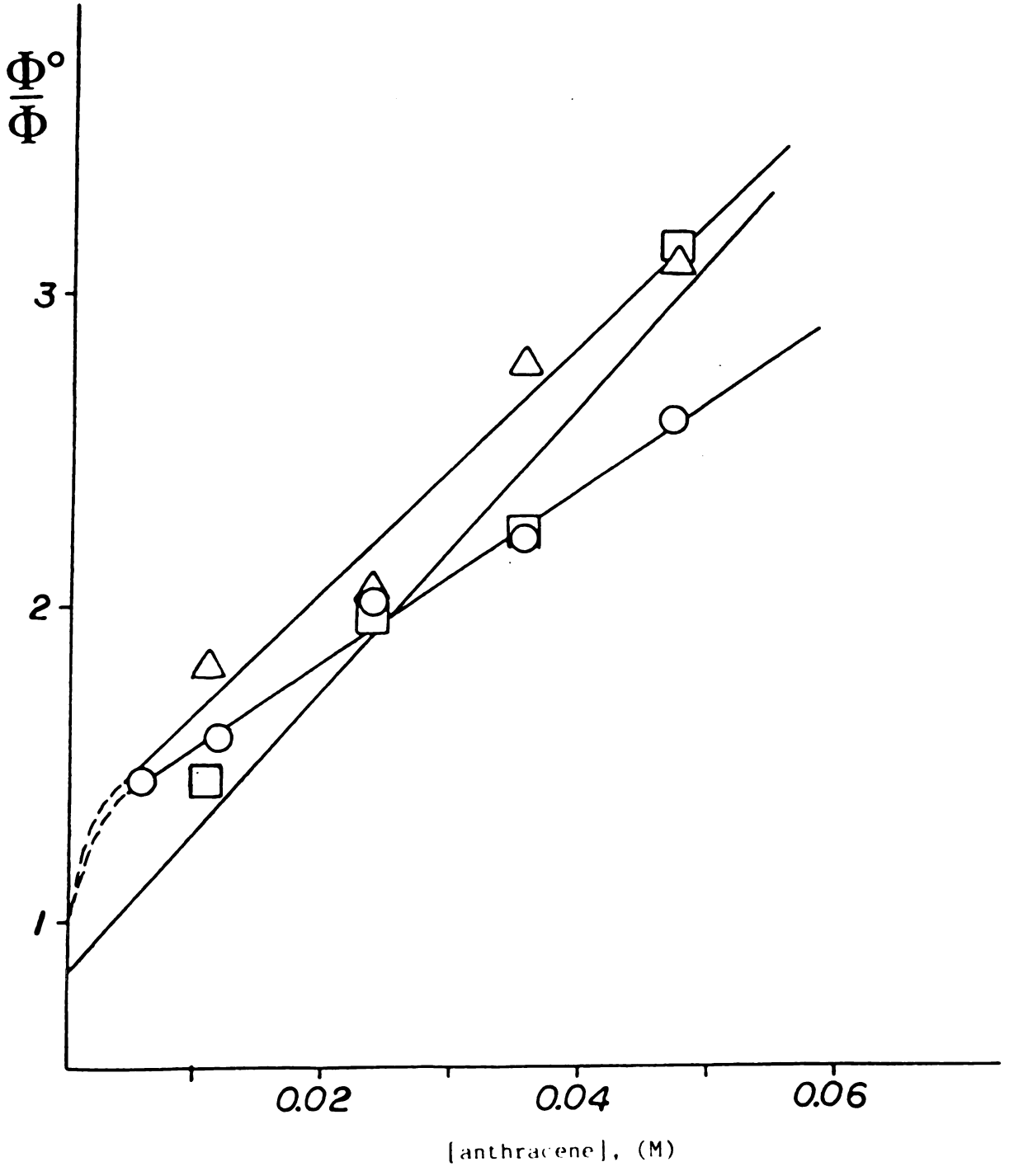

Figure 37. Stern Volmer plots for $W(CO)_5(4VP)$ irradiated at 410 nm in benzene. (○): [complex]=0.0105 M; (△): [complex]= 0.00364 M; (□): [complex]=0.00104 M.

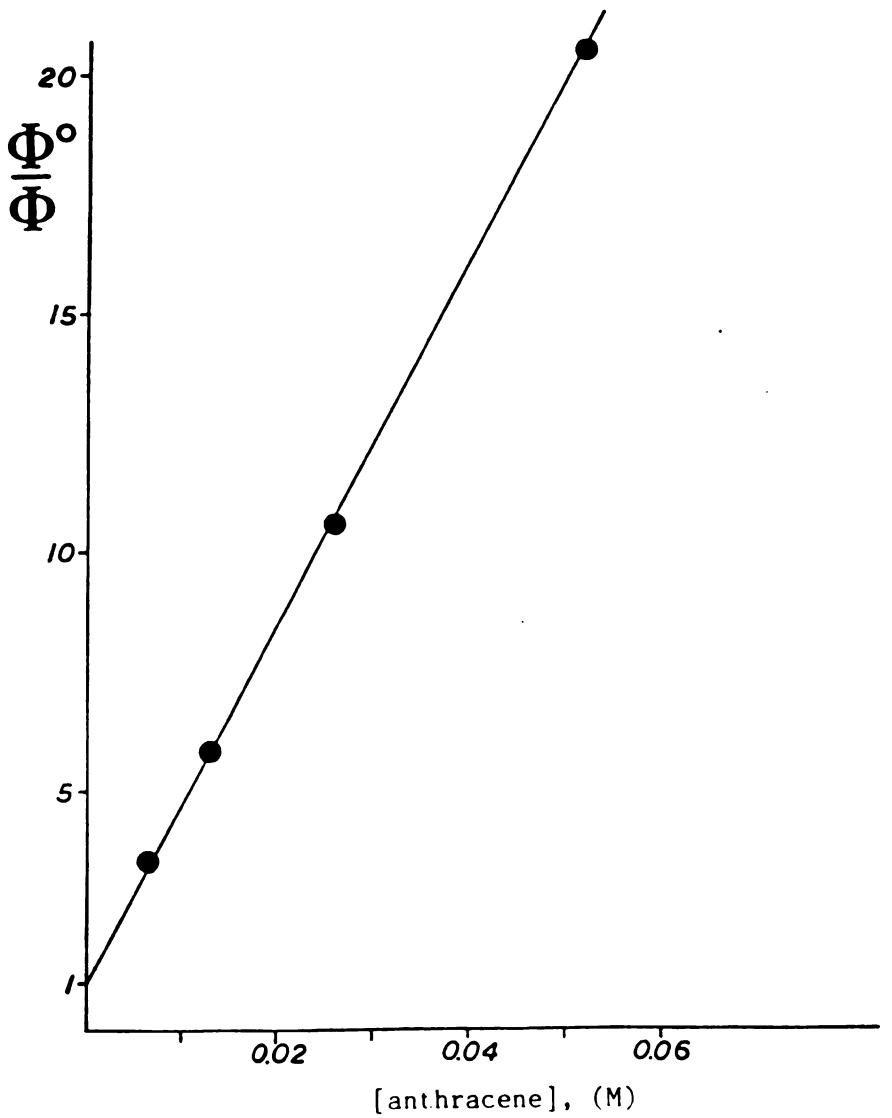

Figure 38. Stern Volmer plot for $W(CO)_5(4VP)$ irradiated at 490 nm in benzene. Cis-$W(CO)_4(4VP)_2$ formation quenching. $[W(CO)_5 4VP]$=0.0105 M.

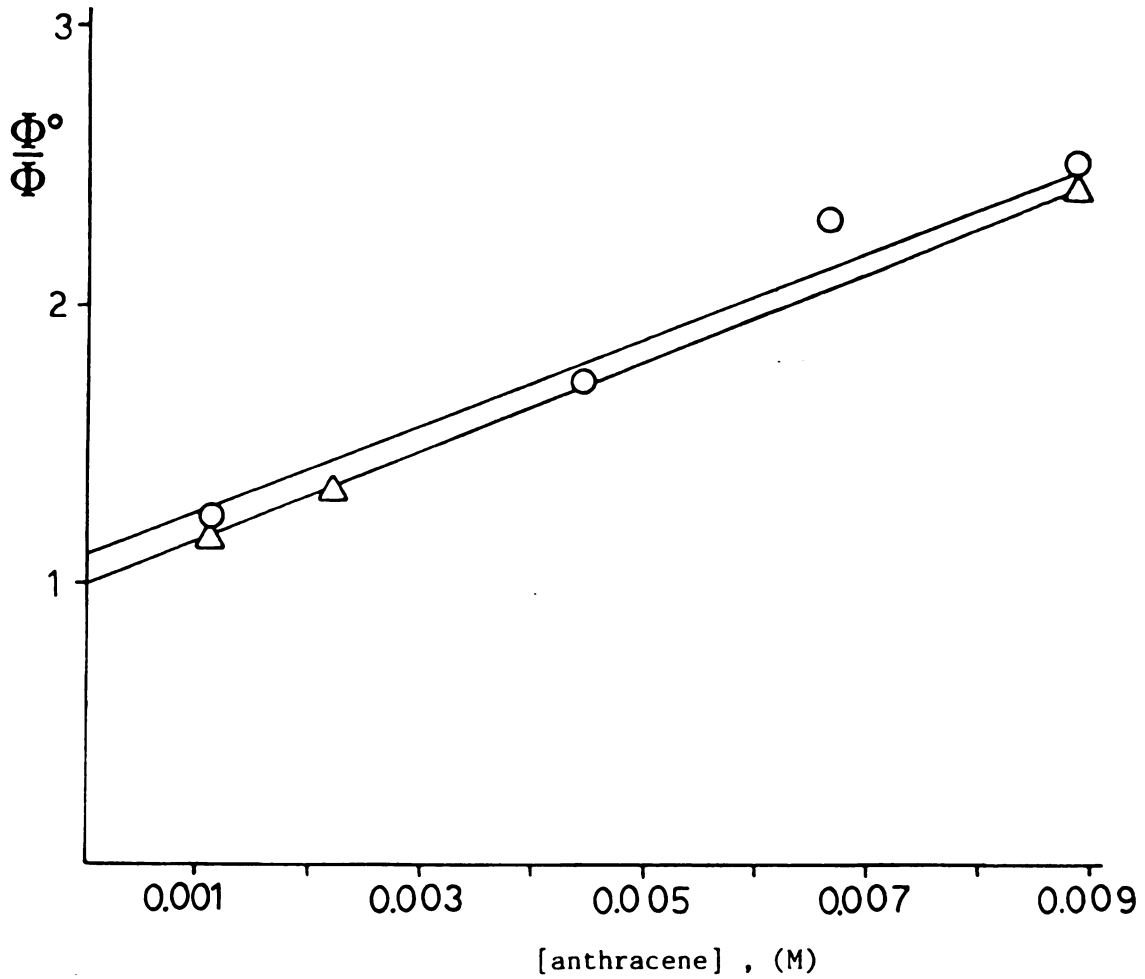

Figure 39. Stern Volmer plots for $W(CO)_5(4VP)$; $[W(CO)_5(4VP)]$= 0.00508 M. (△): cis-$W(CO)_4(4VP)_2$ formation quenching, irradiation at 490 nm in benzene. (○): Emission quenching, excitation at 420 nm.

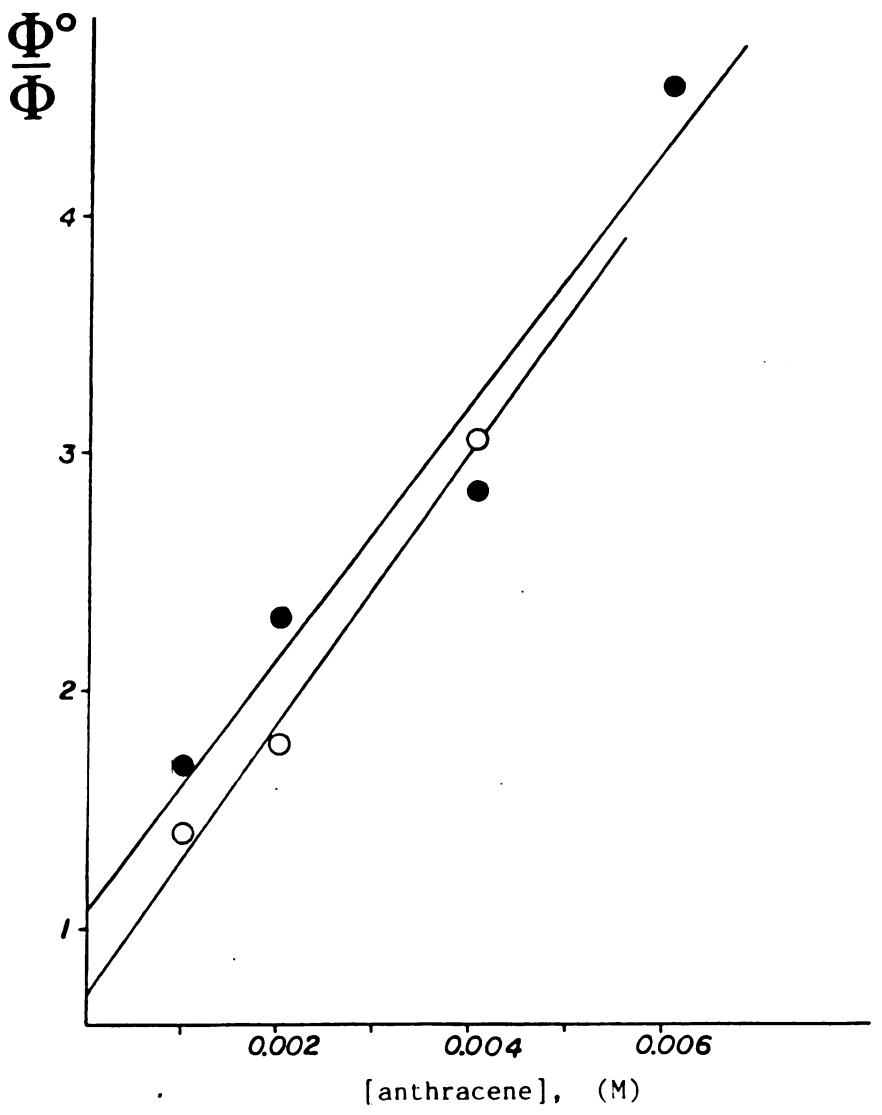

Figure 40. Stern Volmer plots for $W(CO)_5(4VP)$; $[W(CO)_5(4VP)]$= 0.000897 M. (○) : cis-$W(CO)_4(4VP)_2$ formation quenching, irradiation at 490 nm in benzene. (●) : Emission quenching, excitation at 420 nm.

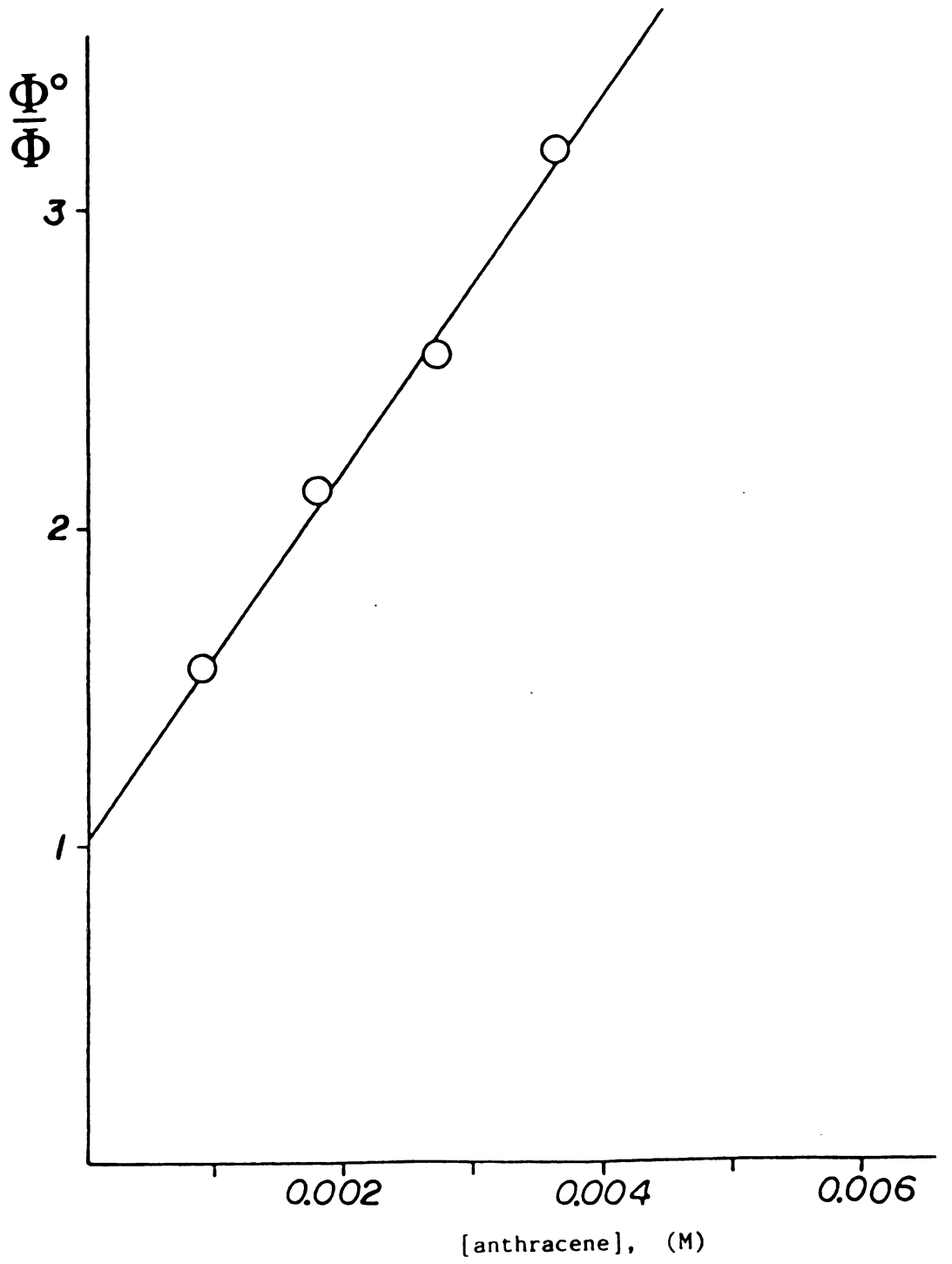

Figure 41. Stern Volmer for the emission quenching of $W(CO)_5(4VP)$ in benzene. $[W(CO)_5(4VP)]$=0.0000829 M. Excitation at 420 nm.

B Chemical Quenching

4-valerylpyridine (4VP) quenches both photochemistry and luminescense from $W(CO)_5(4VP)$.

B1 Reaction Quenching

At 4-valerylpyridine concentrations in the range of 0.001-0.007 M, we obtained the results displayed in Figure 42, for cis-$W(CO)_4(4VP)_2$ formation quenching at both long (λ_{irr}>475 nm) and short (λ_{irr}>400 nm) wavelengths of irradiation. Higher 4-valerylpyridine concentrations (0.1-0.8 M) were found to suppress the reaction completely; no tetracarbonyl product is produced. It is important to note that the quenching plots obtained at long and short wavelengths of irradiation have different slopes which are given in Table 18.

Table 18. cis-$W(CO)_4(4VP)_2$ formation Stern-Volmer Quenching by 4VP for λ_{irr} > 400 and λ_{irr} > 475 nm.[a]

	slope,(M^{-1})
λ_{irr} > 400 nm	282
λ_{irr} > 475 nm	732

[a] solvent benzene, $[W(CO)_5(4VP)]$ = 0.02 M.

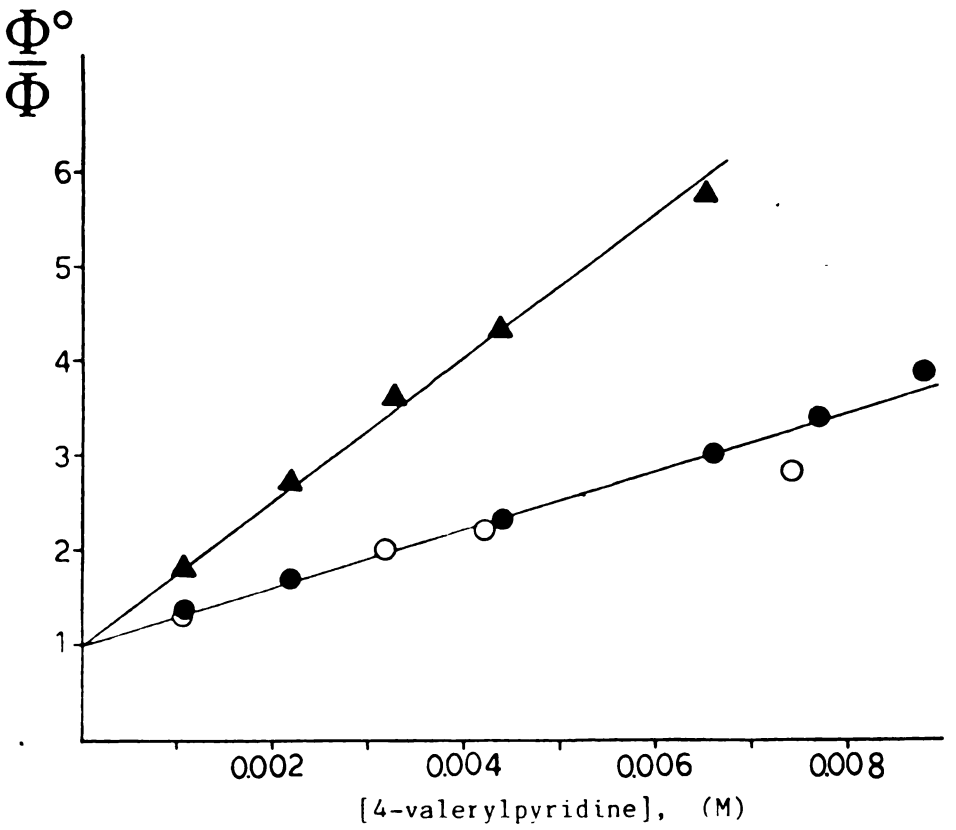

Figure 42. Stern Volmer plots for $W(CO)_5(4VP)$ in benzene. Cis-$W(CO)_4(4VP)_2$ formation quenching by free ligand (4VP).

(○): $[W(CO)_5(4VP)]=0.0201$ M, $\lambda_{irr}>400$ nm.

(●): $[W(CO)_5(4VP)]=0.0206$ M, $\lambda_{irr}>400$ nm.

(△): $[W(CO)_5(4VP)]=0.0204$ M, $\lambda_{irr}>475$ nm.

B2 Emission Quenching

Figure 43 displays the Stern-Volmer quenching by 4AP of the emission at 623 nm of $W(CO)_5(4VP)$ excited at 420 nm. The slope was calculated as 2 M^{-1}.

Figure 44 displays the emission quenching results for the same compound by 4VP. The excitation wavelength for the latter experiment was 410 nm. The area under each peak was taken as proportional to the emission intensity. The emission spectra were traced and the emission peaks were cut off and weighted. The slope was calculated as 1.2 M^{-1}.

Intermediate Trapping Experiments

The above experiments show that free ligand quenches the cis-$W(CO)_4(4VP)_2$ formation but they do not prove that this is because 4VP traps an intermediate, returning the starting material. As a matter of convenience (easily analyzed products by HPLC), 1-(4-pyridyl)butanone (4BP) was used to trap the intermediates coming from $W(CO)_5(4VP)$.

Short (λ_{irr}>400 nm) and long (λ_{irr}>475 nm) wavelength irradiation of $W(CO)_5(4VP)$ in the presence of 1-(4-pyridyl) butanone (4BP) yield $W(CO)_5(4BP)$ as the main product. Two additional peaks in the HPLC analysis appear where the peaks of cis-$W(CO)_4(4VP)(4BP)$ and cis-$W(CO)_4(4BP)_2$ appeared in the cross-coupling experiments. Control experiments proved that cis-$W(CO)_4(4VP)_2$ reacts thermally in a first-order reaction (Figure 45) with 1-(4-pyridyl)butanone to give the mixed

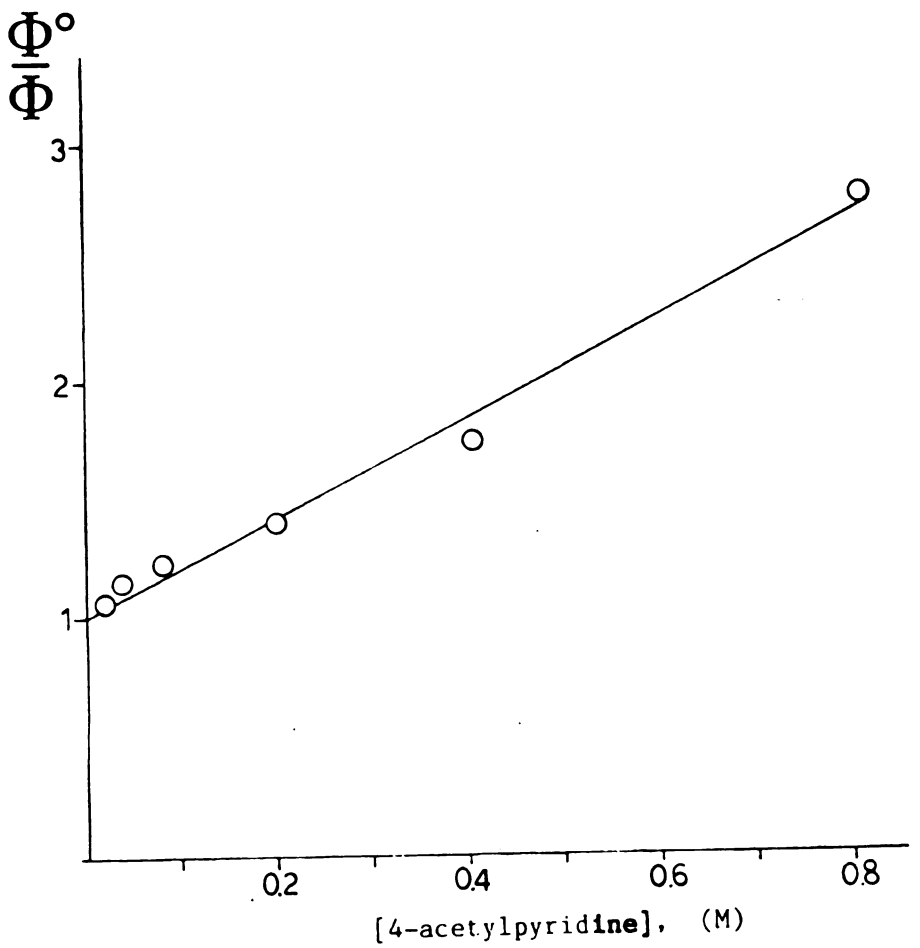

Figure 43. Stern Volmer emission quenching plot of $W(CO)_5(4VP)$ by 4AP in benzene. $[W(CO)_5(4VP)]=1.41\ 10^{-4}$ M. Excitation at 420 nm.

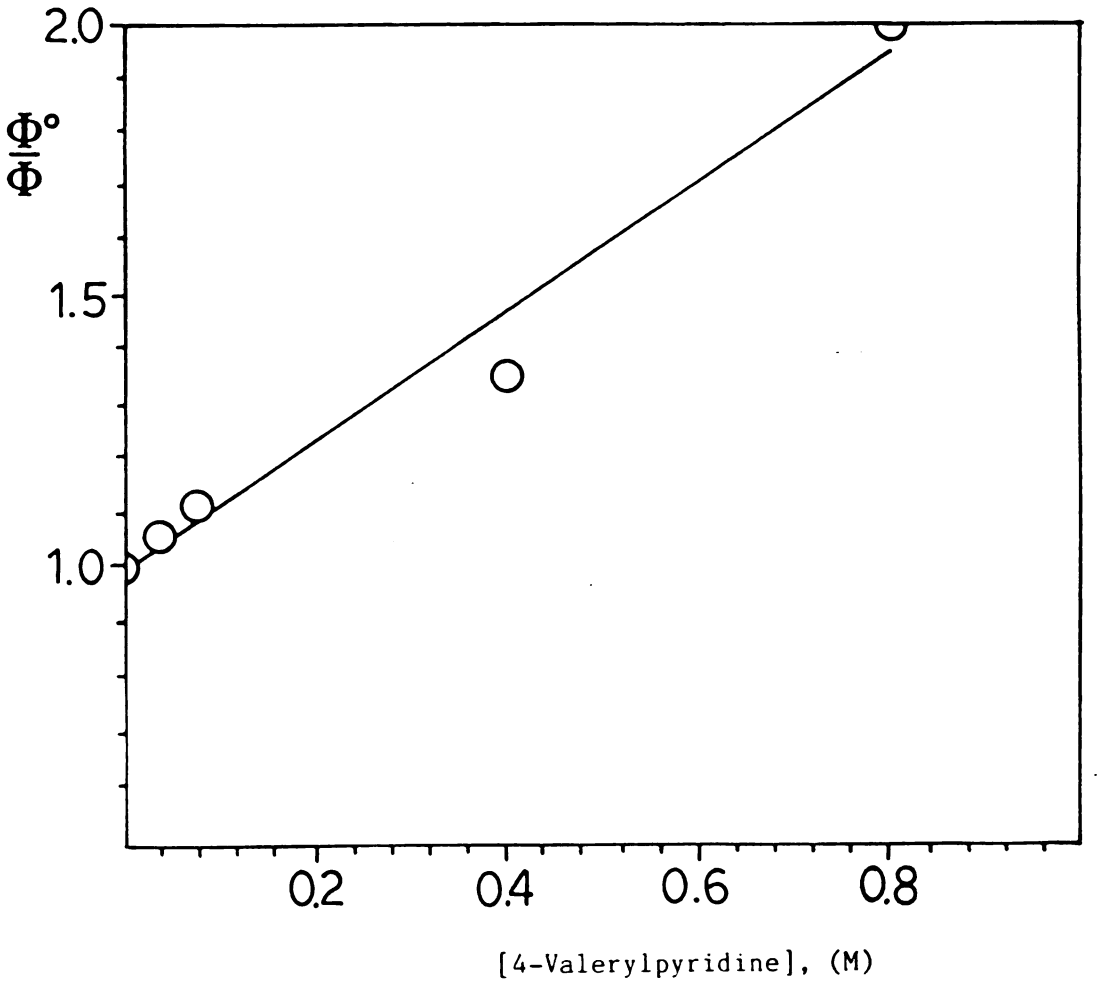

Figure 44. Stern Volmer emission quenching plot of $W(CO)_5(4VP)$ by 4VP in benzene. $[W(CO)_5(4VP)]=6.7\ 10^{-5}$ M. Excitation at 410 nm.

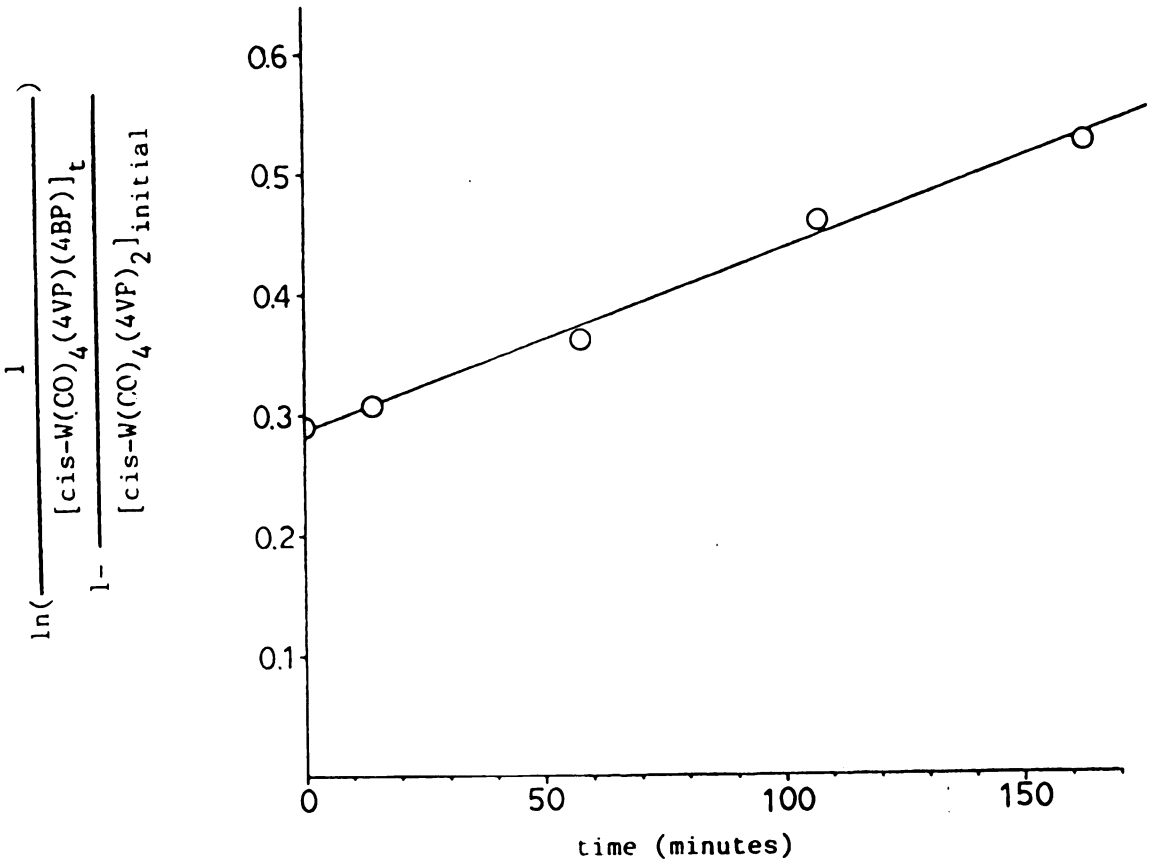

Figure 45. Thermal reaction kinetics of cis-$W(CO)_4(4VP)_2$ with 4BP in benzene. [cis-$W(CO)_4(4VP)_2$]=0.000589 M; [4BP]=0.00324 M. Temperature: 29 °C.

pyridyl ligand Tetracarbonyl complex. The rate constant of this first order reaction is calculated as the slope of Figure 45 and was found 1.65 10^{-3} min^{-1}. Table 19 displays the concentrations of cis-$W(CO)_4(4VP)(4BP)$, cis-$W(CO)_4(4VP)_2$ and cis-$W(CO)_4(4BP)_2$ which have been produced in parallel to the concentrations of $W(CO)_5(4BP)$.

Figures 46 and 47 display the variations in the concentration of $W(CO)_5(4BP)$, cis-$W(CO)_4(4VP)_2$ and cis-$W(CO)_4(4VP)(4BP)$ produced at various 4BP concentrations at $\lambda_{irr}>400$ and $\lambda_{irr}>475$ nm, respectively. Figure 48 displays the concentrations of cis-$W(CO)_4(4BP)_2$ produced at various 4BP concentrations at $\lambda_{irr}>400$ nm. Figure 49 displays the Stern-Volmer quenching plots of total tetracarbonyl formation by 4BP at both $\lambda_{irr}>400$ and $\lambda_{irr}>475$ nm. The slopes were calculated as 516 and 1378 M^{-1}, respectively.

Table 19. Effect of Added Butyrylpyridine on Photoproduct Formation with Visible Irradiation of $W(CO)_5(4VP)$.[a]

[4BP],M	[$W(CO)_5(4BP)$][b]		[cis-$W(CO)_4(4VP)_2$][b]		[cis-$W(CO)_4(4BP)(4VP)$][b]		[cis-$W(CO)_4(4BP)_2$][b]		[Total Tetracarbonyl][b]	
	>400	>475	>400	>475	>400	>475	>400	>475	>400	>475
0	0	0	37.7	12.0	0	0	0	0	37.7	12.0
0.00077	3.3	5.1	25.6	5.2	2.6	2.1	0[c]	0[c]	28.2	7.3
0.00154	7.5	9.1	18.4	2.1	3.7	2.4	0.08	0[c]	22.2	4.5
0.00231	11.7	12.6	13.5	1.1	4.4	2.5	0.17	0[c]	18.1	3.6
0.00308	15.4	15.2	11.0	0.2	4.7	2.2	0.19	0[c]	15.9	2.4
0.00462	19.3	18.9	7.2	0.0	5.2	1.7	0.47	0[c]	12.9	1.7
0.00616	25.2	21.3	5.2	0.0	5.2	0.77	0.60	0.2	11.0	0.97
0.0077	27.8	23.0	3.6	0.0	4.5	0.63	0.74	0.006	8.8	0.64

[a] Four freeze-pump-thaw degassed benzene solutions 0.020 M in $W(CO)_5(4VP)$ irradiated in parallel through the appropriate cutoff filters such that yields are proportional to quantum yields; 6 hrs. at >400 nm, 25.5 hrs. at >475 nm. A 450-W Hanovia mercury arc provided 10^{16}-10^{17} photons $L^{-1}s^{-1}$.

[b] Product concentrations in units of 10^{-4} M.

[c] Product detectable but not measurable.

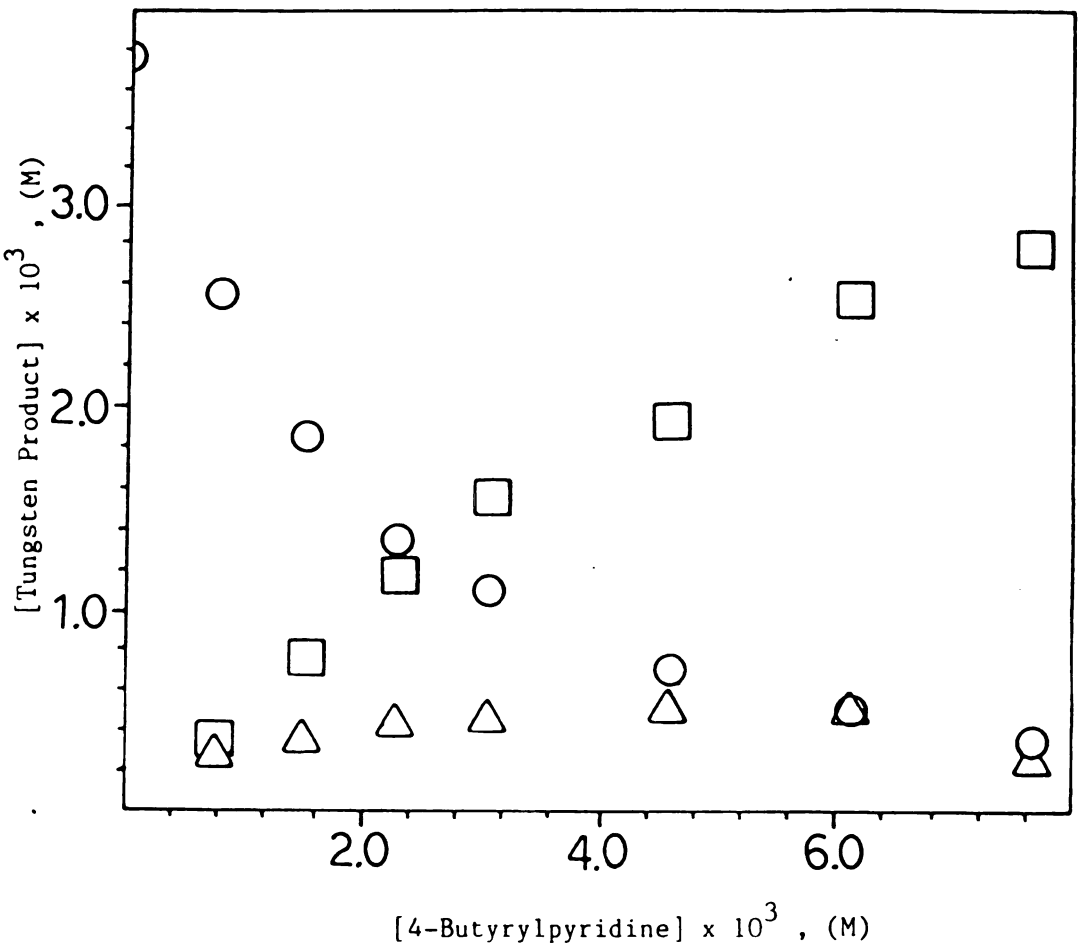

Figure 46. Product distribution after irradiation of $W(CO)_5(4VP)$ in the presence of 4BP in benzene. $[W(CO)_5(4VP)]=0.0202$ M.

Irradiation with $\lambda > 400$ nm.

(△): cis-$W(CO)_4(4VP)(4BP)$.

(□): $W(CO)_5(4BP)$.

(○): cis-$W(CO)_4(4VP)_2$.

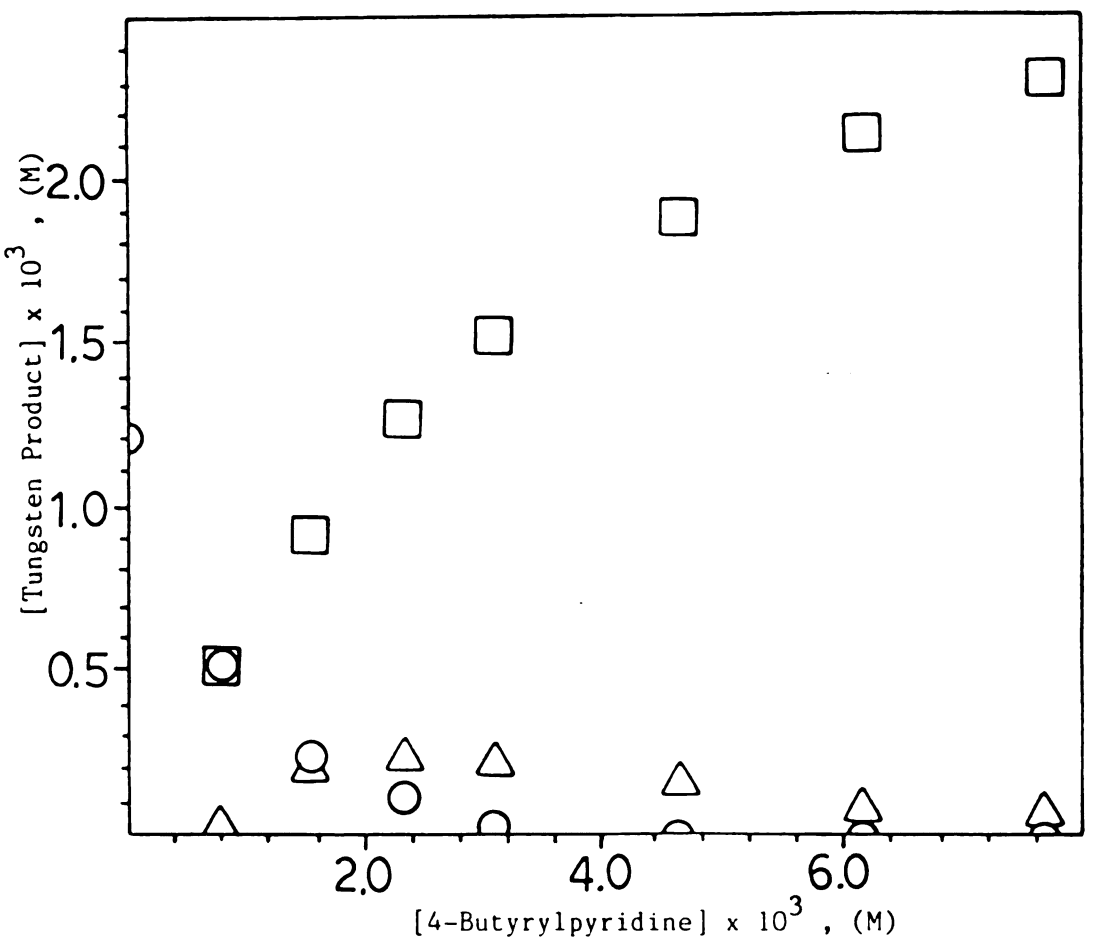

Figure 47. Product distribution after irradiation of $W(CO)_5(4VP)$ in the presence of 4BP in benzene. $[W(CO)_5(4VP)]$=0.0202 M. Irradiation with $\lambda > 475$ nm.

(△): cis-$W(CO)_4(4VP)(4BP)$.

(□): $W(CO)_5(4BP)$.

(○): cis-$W(CO)_4(4VP)_2$.

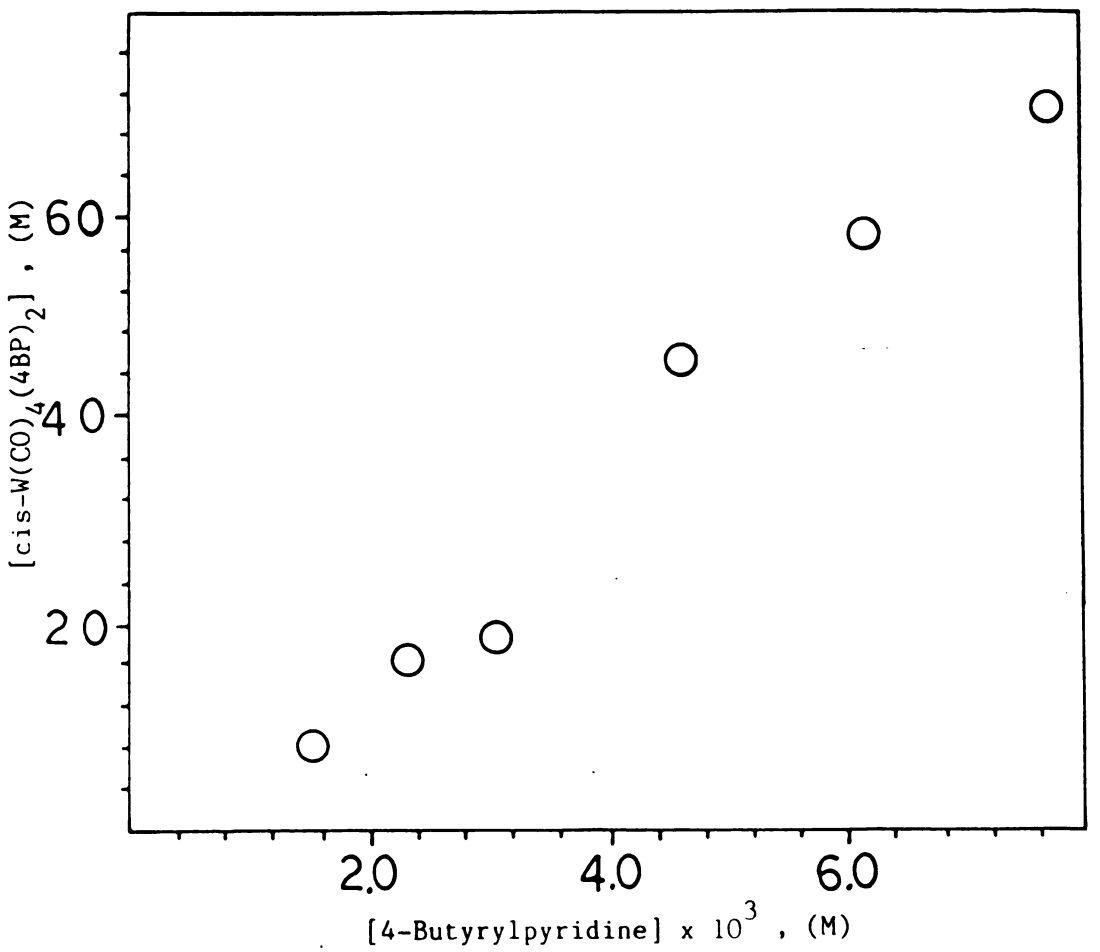

Figure 48. Variation of the concentration of cis-$W(CO)_4(4BP)_2$ produced upon irradiation of $W(CO)_5(4VP)$ in benzene with $\lambda > 400$ nm, in the presence of 4BP. $[W(CO)_5(4VP)]=0.0202$ M.

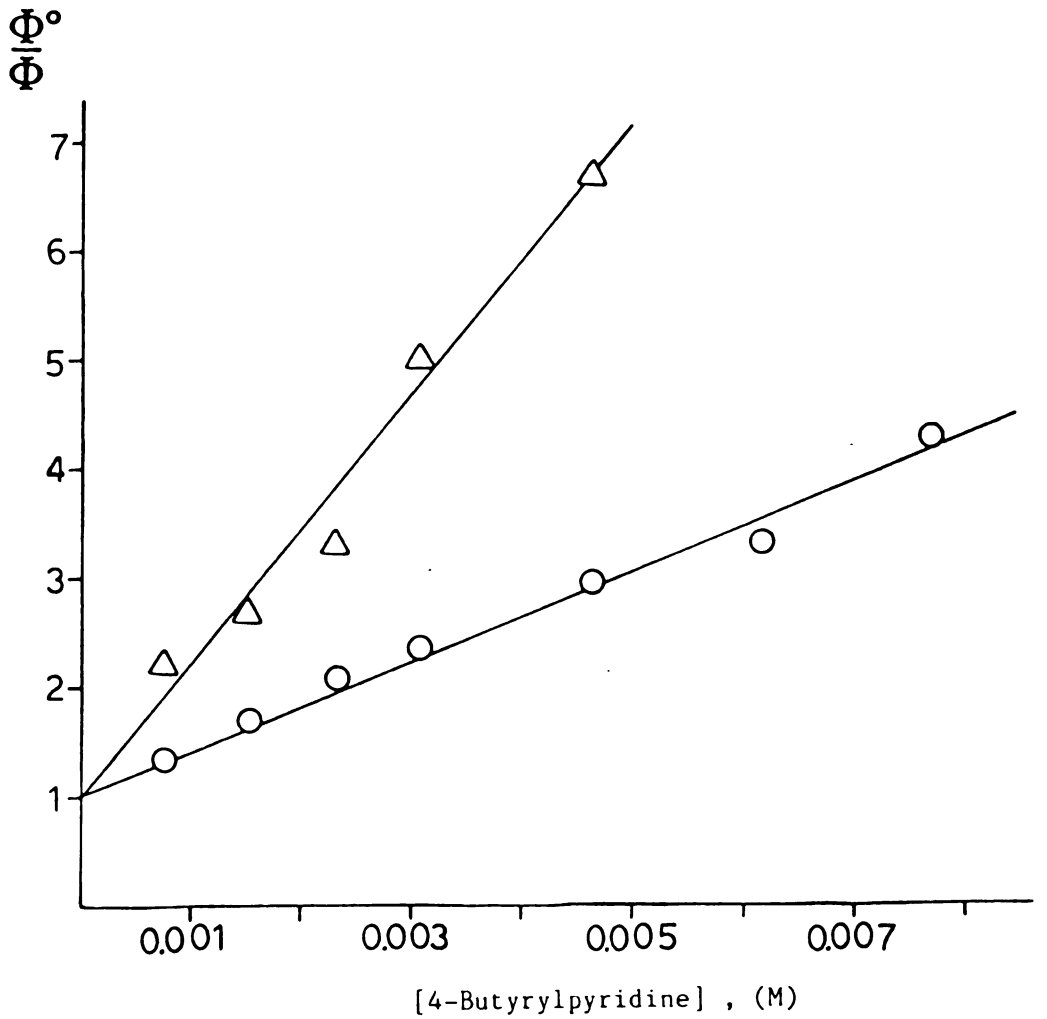

Figure 49. Stern Volmer plots for $W(CO)_5(4VP)$ in benzene. Total tetracarbonyl product (cis-$W(CO)_4(4VP)_2$, cis-$W(CO)_4(4BP)_2$ and cis-$W(CO)_4(4VP)(4BP)$) formation quenching by free ligand (4BP).
(△): $[W(CO)_5(4VP)]$=0.0202 M, $\lambda_{irr} > 475$ nm.
(○): $[W(CO)_5(4VP)]$=0.0202 M, $\lambda_{irr} > 400$ nm.

DISCUSSION

Photoreduction of Ketones by Tetrahydrofuran.[99]

Tetrahydrofuran proved to be an unsatisfactory hydrogen donor, giving maximum quantum yields for octahydro-2,2'bifuran (DTHF) well below 0.25, the statistical value expected if THF is involved only in a hydrogen abstraction process (Table 3). It is assumed that the lower quantum yield results from electron transfer quenching[100] by THF of the excited triplet ketone.

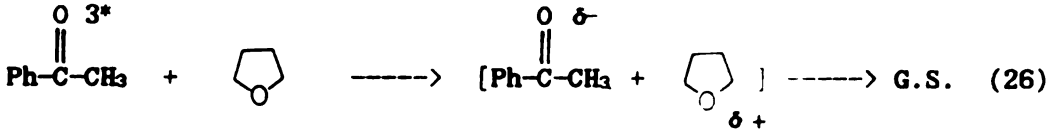

(26)

It is interesting though that 2-tetrahydrofuryl radical reacts with acetonitrile solvent to give 2-tetrahydrofuryl acetaldimine ($THFCH_3CN$). This product seems to be formed at the expense of DTHF in Scheme 12.

Scheme 12

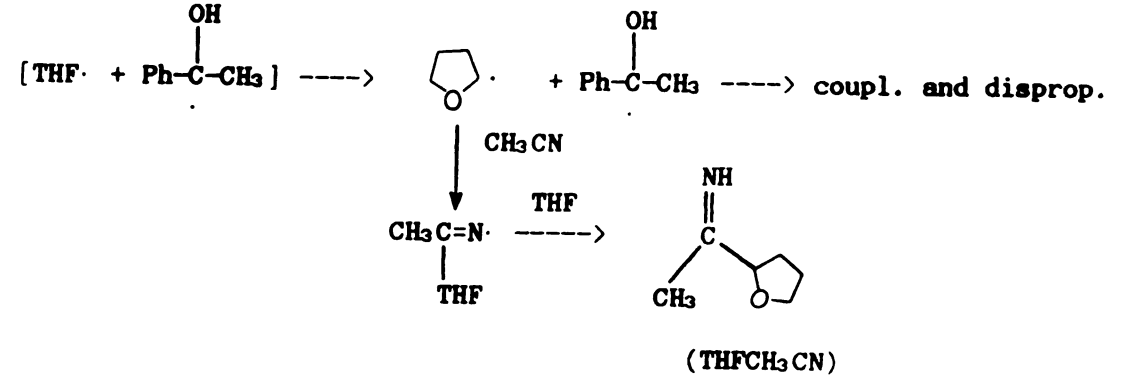

($THFCH_3CN$)

The fact that the quantum yields of DTHF are larger than the quantum yields of THFCH_3CN in phenyl ketones, while the opposite happens in the pyridyl ketones, has to do with the relative reactivity of the corresponding ketones (Table 3). The more reactive phenyl ketones yield higher steady-state concentration of 2-tetrahydrofuryl radicals, with the result that bimolecular coupling dominates over the reaction with solvent. In any case, it would be interesting to further investigate this unique example of CH_3CN reacting with radicals.

Further studies using THF as a hydrogen donor in the photoreduction of complexed pyridyl ketones were interrupted at this point after the irradiation of Pentaammine 4-acetylpyridine Ruthenium(II) complex in the presence of THF led to pyridyl ligand decomposition.

Pyridyl Ketone Pentaammine and bis(2,2'bipyridine) Ruthenium(II) Complexes. Absorption and Emission Studies.

$[Ru(NH_3)_5(4AP)]^{2+}$, $[Ru(NH_3)_5(4PhBP)]^{2+}$, $[Ru(NH_3)_5(4EsterBP)]^{2+}$, etc. complexes show a characteristic broad MLCT absorption at ~510 nm in acetonitrile.[101] The increased absorption at 313 nm compared to the free ligand hydrochloride salts is probably due to underlying LF transitions. Comparison of the extinction coefficients of $[Ru(NH_3)_5(4AP)]^{2+}$ and $[Ru(NH_3)_5(MeINic)]^{2+}$ at 313 nm gives a small difference (17 M^{-1} cm^{-1}) due to the pyridyl ketone $n\pi^*$

transition, since esters do not have low-lying $n\pi^*$ transitions.[102] This ε value is low compared with the extinction coefficient at 313 nm of 4PhBP.HCl which is 104 M^{-1} cm^{-1} (Table 4) and is due to $n\pi^*$ absorption. It proves though that a portion of the 313 nm irradiation populates the $n\pi^*$ excited state of the pyridyl ketone ligand. These complexes do not emit either at room temperature or at 77°K.[85a]

The corresponding bis(2,2'bipyridine) complexes cis-$[Ru(bipy)_2(4AP)_2)]^{2+}$, cis-$[Ru(bipy)_2(4PhBP)_2]^{2+}$ and cis-$[Ru(bipy)_2(4EsterBP)_2]^{2+}$ show intense CT absorption below 500 nm. The extremely high absorptions (ε~7.5 10^3 M^{-1} cm^{-1}) at 313 nm are due only partially to underlying LF transitions and mainly to the bipy ligand. 2,2'bipyridine coordinated to Ruthenium is forced to be planar. 4,5-Diazafluorene, because of its structure, forces the two pyridine rings into the same plane and it should be an adequate model for the planar 2,2'bipyridine. Its absorption spectrum[84] is red shifted compared to that of 2,2'bipyridine,[83] absorbing strongly at 313 nm (ε~6.4 10^3 M^{-1} cm^{-1} compared to free bipy: ε ~83 M^{-1} cm^{-1}, in acetonitrile). On the other hand, the emission spectra of the two compounds (bipy and 4,5-diazafluorene) are identical (Figure 12). This fact suggests a planar conformation for the 2,2'bipyridine in the excited state, in analogy to biphenyl.[103] The 0-0 emission band of 2,2'bipyridine is also 4-5 Kcal/mol red shifted compared to 4PhBP and 4EsterBP

(Table 5, Figures 10 and 11). This fact, combined with the emission spectra of cis-$[Ru(bipy)_2(4AP)_2]^{2+}$, cis-$[Ru(bipy)_2(4PhBP)_2]^{2+}$ and cis-$[Ru(bipy)_3]^{2+}$, allows the conclusion that the π^* orbital of coordinated 2,2'bipyridine lies lower energetically than that of the pyridyl ketone ligands.

Raman Studies.

$[Ru(NH_3)_5(4AP)]^{2+}$ gave excited state Raman spectrum while $[Ru(NH_3)_5(py)]^{2+}$ did not, consistent with Ford's model[101] for a MLCT lowest excited state for the first complex and a LF lowest excited state for the second one.[101] cis-$[Ru(bipy)_2(4AP)_2]^{2+}$ failed to show MLCT excited state scattering, probably due to short lifetimes of the excited states created by 355 nm excitation, while cis-$[Ru(bipy)_2(py)_2]^{2+}$ gave the expected Ru ---> bipy CT excited state scattering.[86] These results might be interpreted by Woodruff's model of a localized MLCT excited state or combined with the fact that $[Ru(phen)_3]^{2+}$ does not exhibit excited state Raman spectrum,[104] to suggest that the species observed by Raman are not the MLCT excited states but some intermediates (probably produced from the MLCT excited state and returning to it so no permanent change is observed) having monocoordinated 2,2'bipyridine. 1,10-Phenanthroline, due to its structural rigidity, recombines to the metal

center in the picosecond time scale, beyond the limits of the nanosecond instrumentation used.

Photochemical Studies.

As we stated in the Introduction, the Type II reaction can be used to monitor the rate of internal conversion of the IL upper excited states to the lower ones in coordination compounds.

It was found that in $[Ru(NH_3)_5(4VP)]^{2+}$ the internal conversion is slow to compete with Type II cleavage of the coordinated 4VP.[17] Two types of pyridyl ketone ligands were investigated: one with reactivity comparable to or higher than 4VP so it could be applied to the cis-$[Ru(bipy)_2L_2]^{2+}$ case where possible deactivation to the energetically lower-lying bipy might enhance k_{IC}, and one of lower reactivity, which possibly would compensate for the failure of the bimolecular photoreduction of coordinated 4AP. Table 20 compares the reactivities of some phenyl ketones with reference to valerophenone.

4PhBP and 4EsterBP were prepared and their τ^{-1}, and k_r values are also presented in Table 20. The values for the corresponding hydrochloride salts are also included in Table 20. τ values are calculated from $k_q\tau$ values assuming $k_q = 1\times10^{10}$ M^{-1} sec^{-1} for ethyl sorbate in acetonitrile.[85e] k_r values for the pyridyl ketones and their hydrochloride salts were calculated as $k_r = 1/\tau$ assuming $k_d << k_r$. This is a

Table 20. Relative Reactivities of Various Phenyl Ketones, Pyridyl Ketones and the Corresponding Pyridyl Ketone Hydrochloride Salts.

Ketone	$\tau^{-1}(sec^{-1})^a$	$k_r\ 10^7(sec^{-1})^a$	Ketone	$\tau^{-1}(sec^{-1})^b$	$k_r\ 10^7(sec^{-1})^b$	Ketone	$\tau^{-1}(sec^{-1})^b$	$k_r\ 10^8(sec^{-1})^b$
	8.3 10^8	0.83		4.90 10^7[c] 6.25 10^7[d]	4.90[c] 6.25[d]	4BP.HCl	4.29 10^8[c]	4.29[c]
	1.25 10^8	12.5	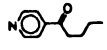	1.00 10^9[c] 6.85 10^8[e]	100.0[c] 68.5[c,e]	4VP.HCl	3.37 10^9[c]	33.7[c]
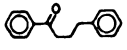	3.85 10^8	38.5	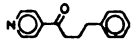	1.03 10^9	103.0[f]	4PhBP.HCl	4.88 10^9[f]	48.8
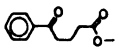	1.0 10^7	1.0	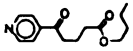	5.99 10^7[f]	6.0[f]	4EsterBP.HCl	3.17 10^8[f]	3.17

[a] Benzene solvent, ref. 105.

[b] Acetonitrile solvent, unless otherwise noted.

[c] Ref. 85f.

[d] Benzene solvent, ref. 91.

[e] Benzene solvent.

[f] This work, Table 8.

logical assumption since Φ_{II} for the two ketones as well as for the corresponding hydrochloride salts studied (4PhBP, 4EsterBP and 4PhBP.HCl, 4EsterBP.HCl) are mutually equal, so the term $k_r/(k_r + k_d)$ in equation 11 has to be one. According to Table 20, 4-butyrylpyridine would be a good candidate ligand for a slow Type II reaction, but photoproduced ethylene has not been possible to be analyzed reproducibly.[85g]

Despite the photochemical instability of $[Ru(NH_3)_5(4AP)]^{2+}$ in the presence of THF, $[Ru(NH_3)_5(4PhBP)]^{2+}$, $[Ru(NH_3)_5(4EsterBP)]^{2+}$, cis-$[Ru(bipy)_2(4PhBP)_2]^{2+}$ and cis-$[Ru(bipy)_2(4EsterBP)_2]^{2+}$ did not undergo photoinduced ligand dissociation in acetonitrile during the irradiation periods employed. Pentaammine complexes upon long irradiations tend to bleach, a fact which has to be attributed to oxidation rather than to dissociation[85h] since no free ligand is detected. No corresponding phenomenon was observed with the 2,2'bipyridine complexes. The Ruthenium porphyrines, $RuTPP(4PhBP)_2$ and $RuOEP(4PhBP)_2$, were also photostable since no free ligand was detectable after long irradiation. Quantitative ligand liberation from the 2,2'bipyridine complexes could not be achieved even after reflux with PPh_3 in n-butyronitrile as reported by Whitten.[32] Therefore, we concentrated on measurements of free olefin formation from the Internal Ligand Type II cleavage.

The Type II product quantum yields increase slightly with increasing concentration in the case of the free pyridyl ketones because of solvation of the biradical by the pyridyl nitrogen (Figure 14).[85d,91] The corresponding hydrochloride salts are insensitive to ketone concentration[85d] (Figure 14). With the Ruthenium complexes, the picture is quite different (Figures 15 and 16). At low complex concentrations, the olefin quantum yield progressively increases, reaches a maximum, and then decreases as the complex concentration increases further. This behavior correlates with the absorption of light at 313 nm by the corresponding complex. At the concentration point where all the 313 nm radiation is absorbed, a bimolecular quenching process starts lowering the quantum yield. Ruthenium complexes were proven to be good triplet excited ketone quenchers. They were found to quench Type II cleavage of butyrophenone (Figures 21, 22 and 23; Table 9). The lifetime of butyrophenone is $1.34\ 10^{-7}$ sec,[108] so k_q values for the Ruthenium complexes (Table 21) are calculated using the relation $k_q = k_q\tau/(1.34\times10^{-7})$.

Table 21. Rate Constants for Quenching of Triplet BP by Various Ruthenium Complexes in Acetonitrile.

Ruthenium Complex	k_q (M^{-1} sec^{-1})
$[Ru(NH_3)_5(4AP)](BF_4)_2$	$3x10^9$
cis-$[Ru(bipy)_2(4AP)_2](BF_4)_2$	$2x10^9$
cis-$[Ru(phen)_2(4AP)_2](BF_4)_2$	$2x10^9$

It is obvious from Table 21 that Ruthenium complexes quench the $n\pi^*$ excited ketones very efficiently. The diffusion control limit is about $2x10^{10}$ M^{-1} sec^{-1}.[73] This result is what is expected for a metal ion complexed to a ligand which has an equal or lower triplet excitation energy than the ketone donor.[107] On the other hand, it has been shown that bare rare earth chlorides quench the Type II reaction from phenyl ketones more slowly ($k_q \simeq 10^8$), probably due to solvation; the solvent molecules have high excitation energies.[108]

It has been assumed that hydrochloride salt formation has the same effect as metal coordination in the absence of orbital mixing. It is suggested here that the ^1H-nmr signal of the pyridyl protons is a useful method to compare the effect of metal coordination and protonation on the pyridyl ligand. Table 22 shows that metal coordination seems to have a similar effect on the pyridyl ketone ligand as

Table 22. Pyridyl Proton Chemical Shifts in Free Pyridyl Ketone Ligands, Their Hydrochloride Salts and Their Ruthenium Complexes.

Compound	Solvent	δ H's o- to Nitrogen	δ H's m- to Nitrogen
4PhBP	$CDCl_3$	8.76	7.65
4PhBP.HCl	$CDCl_3$	9.11	8.28
	D_2O	8.82	8.20
$[Ru(NH_3)_5(4PhBP)]^{2+}$	D_2O	8.35	7.28
$cis-[Ru(bipy)_2(4PhBP)_2]^{2+}$	D_2O	8.85	8.42
$RuTPP(4PhBP)_2$	C_6D_6	3.40	5.51
$RuOEP(4PhBP)_2$	C_6D_6	1.59	5.15
4EsterBP	$CDCl_3$	8.81	7.75
4EsterBP.HCl	$CDCl_3$	9.10	8.39
	D_2O	8.88	8.33
$[Ru(NH_3)_5(4EsterBP)]^{2+}$	D_2O	8.60	7.52
$cis-[Ru(bipy)_2(4EsterBP)_2]^{2+}$	D_2O	8.89	8.55-8.45
	$CDCl_3$	9.05	8.54

hydrochloride salt formation, in the cases of the 2,2'bipyridine complexes, while in the pentaammine complexes the pyridyl proton chemical shifts seem to correlate better to the free pyridyl ketones. No conclusion can be drawn for the Ruthenium porphyrines since the pyridyl protons are shifted upfield by the ring current of the porphyrine. In any case, since complexation does not cause any dramatic change in the chemical shifts of the pyridyl protons, we accept that pyridyl ketone ligand hydrochloride salts are reasonable models for the Ruthenium complexes. Multiplying the $\Phi_{(II)}$ of each Ruthenium complex by the ratio (R) of the extinction coefficients at 313 nm of the Ruthenium complex to the corresponding ligand hydrochloride salt, we obtain the corrected quantum yield of the Ruthenium complex for partial light absorption by the ketone chromophore. Table 23 compares the observed and the corrected quantum yields of all the complexes studied.

τ values for the Ruthenium complexes studied in this thesis (Table 8) have been calculated accepting $1x10^{10}$ M^{-1} sec^{-1} as the k_q value for ethyl sorbate in acetonitrile,[85e] using the relation $\tau = k_q \tau/(1.0x10^{10})$ and have been corrected for the bimolecular self-quenching effect of Ruthenium complexes mentioned above; in other words, (k_r+k_d) values represent the sum of the rate constants of chemical reaction and decay of the Ruthenium complexes if no bimolecular quenching was taking place and have been

Table 23. Type II Fragmentation Quantum Yields for the Hydrochloride Salts, Pentaammine, 2,2'Bipyridine and Porphyrine Ruthenium(II) Complexes of the Pyridyl Ketones.[a]

Pyridyl Ketone	HCl Salt		Pentaammine Ruthenium Complexes			bis 2,2'Bipyridine Ruthenium Complexes			TPP Ruthenium Complexes			OEP Ruthenium Complexes	
	$\Phi_{(II)}$	R	Φ_{obs}	Φ_{corr}	R	Φ_{obs}	Φ_{corr}	R	Φ_{obs}	Φ_{corr}	R	Φ_{obs}	Φ_{corr}
4PhBP	0.093	4.2	0.014	0.059	37	0.0072	0.27	59	0.00020	0.012	132	0.00022	0.029
4EsterBP	0.096	5.3	0.0051	0.027	48	0.0017	0.082						

[a] All the experimental quantum yields (Φ_{obs}) cited, correspond to 0.020 M solution of the corresponding compound in acetonitrile except the porphyrines which are for 0.010 M solutions in methylene chloride.

calculated from (28), which has been derived from (27). τ^{-1} and (k_r+k_d) values are cited in Table 24.

$$\tau^{-1} = k_r + k_d + k_q\,[\text{complex}] \qquad (27)$$

$$k_r + k_d = \tau^{-1} - k_q\,[\text{complex}] \qquad (28)$$

Table 24. Lifetime Data for Ruthenium Complexes.[a]

Ruthenium Complex	$1/\tau^b$,(sec^{-1})	$0.02xk_q$	($k_r + k_d$)[c],(sec^{-1})
$[Ru(NH_3)_5(4PhBP)]^{2+}$	$1.4x10^9$	$6.0x10^7$	$1.3x10^9$
cis-$[Ru(bipy)_2(4PhBP)_2]^{2+}$	$2.9x10^9$	$4.0x10^7$	$2.9x10^9$
$[Ru(NH_3)_5(4EsterBP)]^{2+}$	$1.5x10^8$	$6.0x10^7$	$9.0x10^7$
cis-$[Ru(bipy)_2(4EsterBP)_2]^{2+}$	$4.2x10^8$	$4.0x10^7$	$3.8x10^8$

[a] τ^{-1} values concern 0.02 M solutions of the corresponding complex in acetonitrile.

[b] From Table 8.

[c] From Equation 28.

As it is noted in Table 23, the corrected quantum yield of $[Ru(NH_3)_5(4PhBP)]^{2+}$ is approximately equal to the quantum yield of 4PhBP.HCl, while the corrected quantum yield of $[Ru(NH_3)_5(4EsterBP)]^{2+}$ is about 3.6 times lower than the quantum yield of 4EsterBP.HCl. What keeps the quantum yield low even after correction for partial light absorption by

the ketone chromophore are probably both concentration self-quenching and a competing Internal Conversion process.

Table 25 compares the quantum yields of $[Ru(NH_3)_5(4PhBP)]^{2+}$ and $[Ru(NH_3)_5(4EsterBP)]^{2+}$ with the quantum yields of $[Ru(NH_3)_5(4\text{-Valerylpyridine})]^{2+}$, $[Ru(NH_3)_5(\beta\text{-methyl-4-butyrylpyridine})]^{2+}$ and $[Ru(NH_3)_5\ \gamma\text{-methyl-4-butyrylpyridine})]^{2+}$, which are taken from reference 17.

Table 25. Comparison of the Quantum Yields of Type II Products of Various Pentaammine Ruthenium Complexes.

complex	$\Phi_{(II)}$	Φ_{corr}
$[Ru(NH_3)_5(4PhBP)]^{2+}$	0.014[a]	0.058
$[Ru(NH_3)_5(4EsterBP)]^{2+}$	0.0051[a]	0.027
$[Ru(NH_3)_5(\beta Me4BP)]^{2+}$	0.023[b]	0.099
$[Ru(NH_3)_5(4VP)]^{2+}$	0.019[b]	0.093
$[Ru(NH_3)_5(\gamma Me4VP)]^{2+}$	0.020[b]	0.096

[a] Acetonitrile solutions 0.02 M in Ru complex irradiated at 313 nm.

[b] Acetonitrile solutions 0.01 M in Ru complex irradiated at 313 nm.

The Type II products quantum yield is given by equation 11: $\Phi_{(II)} = \Phi_{(ISC)} x \alpha x [k_r/(k_r+k_d)]$; α is the probability that the 1,4-biradical (intermediate) will cleave to form enol and olefin. For para substitution, $\Phi_{(ISC)}$ and α are

constant. $\Phi_{(II)}$ for $[Ru(NH_3)_5(4PhBP)]^{2+}$ is within experimental error equal to the $\Phi_{(II)}$ of $[Ru(NH_3)_5(\beta Me4BP)]^{2+}$, $[Ru(NH_3)_5(4VP)]^{2+}$ and $[Ru(NH_3)_5(\gamma Me4BP)]^{2+}$. Therefore, for $\Phi_{(II)}$ to be constant, the term $k_r/(k_r+k_d)$ in equation 11 has to be one or $k_r >> k_d$. In other words, for $[Ru(NH_3)_5(4PhBP)]^{2+}$, $k_r = k_r+k_d = 1.3\ 10^9\ sec^{-1}$ (Table 24). Using this value as a calculation basis, the k_r and k_d values of $[Ru(NH_3)_5(4EsterBP)]^{2+}$ are calculated from (31) which is derived as follows:

$$\Phi_1 = \Phi([Ru(NH_3)_5(4PhBP)]^{2+}) = \Phi_{(ISC)} \times \alpha \times k_{r1}\tau_{1(experimental)} \quad (29)$$

$$\Phi_2 = \Phi(\text{Ru complex}) = \Phi_{(ISC)} \times \alpha \times k_{r2}\tau_{2(experimental)} \quad (30)$$

(31) is obtained by dividing (29) by (30):

$$k_{r2} = k_{r1} \times [\Phi_2/\Phi_1] \times \frac{(1/\tau_2)_{experimental}}{(1/\tau_1)_{experimental}} \quad (31)$$

This way, it has been calculated from (31) that $k_r = 5.1\ 10^7\ sec^{-1}$ for $[Ru(NH_3)_5(4EsterBP)]^{2+}$. The (k_r+k_d) value for this complex is $9.0 \times 10^7\ sec^{-1}$ (Table 24). Therefore, $k_d = 3.9 \times 10^7\ sec^{-1}$. Assuming the same k_d value for $[Ru(NH_3)_5(4PhBP)]^{2+}$, it is calculated from $k_r+k_d = 1.3 \times 10^9\ sec^{-1}$ that $k_r = 1.3 \times 10^9\ sec^{-1}$. We started this method of calculation by assuming that k_r for $[Ru(NH_3)_5(4PhBP)]^{2+}$ was $1.3 \times 10^9\ sec^{-1}$, and we verified this value after one cycle of calculations by obtaining the same value and a slow rate of

Internal Conversion (3.9×10^7 sec^{-1}). The calculated value of k_d ($k_d = 3.9 \times 10^7$ sec^{-1}) verifies the upper limit (10^8 sec^{-1}) that was set previously for the rate of the Internal Conversion of the Ruthenium Pentaammine complexes.[17] This value for the rate of the Internal Conversion has to be taken with caution, though, because it is about half the rate of self quenching ($0.02 \times k_q = 6.0 \times 10^7$ sec^{-1}; Table 24), which means that the main deactivation process is by self quenching and not by Internal Conversion. Subtraction of two large numbers (k_r and $0.02 \times k_q$) from a large number (experimental $1/\tau$ value) leaves a large uncertainty in the result. Therefore, it is suggested here that the calculated k_d value for the Ruthenium pentaammine complexes to be considered as an upper limit for the Internal Conversion rather than an absolute value.

For the bis(2,2'bipyridine) complexes, the picture is somewhat similar. Comparing the quantum yield of cis-$[Ru(bipy)_2(4PhBP)_2]^{2+}$ to the one of cis-$[Ru(bipy)_2(4EsterBP)_2]^{2+}$ (Table 23), it can be seen that the quantum yield of the second complex is 3 times lower than the one of the first complex. What lowers the quantum yield has to be an increased contribution of the internal conversion (k_d) in the ($k_r + k_d$) value. In order to find the exact k_r and k_d values for both bis(2,2'bipyridine) complexes, we assume for the moment that there is no internal conversion competing with the Type II chemical reaction from the ligand, in the case of cis-

$[Ru(bipy)_2(4PhBP)_2]^{2+}$, i.e. $k_r >> k_d$. That means that for cis-$[Ru(bipy)_2(4PhBP)_2]^{2+}$, $k_r = 2.9 \times 10^9$ sec^{-1}. Using (31) where Φ_1 is the quantum yield for cis-$[Ru(bipy)_2(4PhBP)_2]^{2+}$ and Φ_2 is the quantum yield for cis-$[Ru(bipy)_2(4EsterBP)_2]^{2+}$, for cis-$[Ru(bipy)_2(4EsterBP)_2]^{2+}$, $k_r = 9.9 \times 10^7$ sec^{-1}. Introducing this value in the equation $k_r + k_d = 3.8 \times 10^8$ sec^{-1}, $k_d = 2.8 \times 10^8$ sec^{-1}. This value of k_d has to be the same for cis-$[Ru(bipy)_2(4PhBP)_2]^{2+}$, so setting $k_d = 2.8\ 10^8$ sec^{-1} for cis-$[Ru(bipy)_2(4PhBP)_2]^{2+}$, produces $k_r = 2.6 \times 10^9$ sec^{-1}. We started this method of calculation by assuming that k_r for $[Ru(bipy)_2(4PhBP)_2]^{2+}$ was 2.9×10^9 sec^{-1}, and we obtained a better estimate ($k_r = 2.6 \times 10^9$ sec^{-1}). The cycles have to be repeated until two successive calculations of the k_r value are identical (self consistent). Introducing the new k_r value for cis-$[Ru(bipy)_2(4PhBP)_2]^{2+}$ into equation (31), we obtain for cis-$[Ru(bipy)_2(4EsterBP)_2]^{2+}$, $k_r = 8.9 \times 10^7$ sec^{-1} and $k_d = 2.9 \times 10^8$ sec^{-1}. k_d is the same for cis-$[Ru(bipy)_2(4PhBP)_2]^{2+}$ so k_r for the latter complex is found to be 2.6×10^9 sec^{-1} (self consistent).

k_r and k_d values for all four complexes are cited in Table 26. k_d's are given as k_{IC} (rate constant for internal conversion). If the Φ_{corr} values (Table 23) are used in equation 31, then the rates of the Internal Conversion are calculated as a $2.6\ 10^7$ sec^{-1} and $2.7\ 10^8$ sec^{-1} for the pentaammine and. bis(2,2'bipyridine) Ru(II) complexes, respectively.

Table 26. Rates of H-abstraction and Rates of Internal Conversion of Ruthenium Complexes.

Ru Complex	$\Phi_{(II)}$	$k_r + k_d (sec^{-1})$	$k_r (sec^{-1})$	$k_{ic} (sec^{-1})$
$[Ru(NH_3)_5(4PhBP)]^{2+}$	0.014	1.3×10^9	$1.3\ 10^9$	$\leq 3.9 \times 10^7$
$[Ru(NH_3)_5(4EsterBP)]^{2+}$	0.0051	9.0×10^7	5.1×10^7	$\leq 3.9 \times 10^7$
$cis-[Ru(bipy)_2(4PhBP)_2]^{2+}$	0.0072	2.9×10^9	2.6×10^9	2.9×10^9
$cis-[Ru(bipy)_2(4EsterBP)_2]^{2+}$	0.0017	3.8×10^9	8.9×10^7	2.9×10^9

In the case of the Pentaammine Ruthenium complexes, Internal conversion means deactivation from the upper IL excited state to lower-lying LF and MLCT states. In the case of the bis(2,2'bipyridine) complexes, an additional deactivation path seems reasonable; i.e. triplet energy transfer from the $n\pi^*$ excited pyridyl ketone to lower-lying planar bipy triplets. Comparing the k_{ic} values between the pentaammine and the bipy complexes cited in Table 26, the increased values for the bipy complexes might originate from this additional deactivation path.

A final point needing comment is that in the case of $cis-[Ru(bipy)_2(4PhBP)_2]^{2+}$, the corrected quantum yield is about 3 times higher than that of 4PhBP.HCl, while in the case of $cis-[Ru(bipy)_2(4EsterBP)_2]^{2+}$, the two quantum yields are approximately equal. In a possible explanation, the

elevated value of the Φ_{corr} of cis-$[Ru(bipy)_2(4PhBP)_2]^{2+}$ implies an intramolecular singlet energy transfer (sensitization); flat 2,2'bipyridines absorb strongly at 313 nm, operate as antennas, collecting the light and transferring some of the singlet energy to the reacting ligand 4PhBP, resulting in a higher quantum yield than the one expected due to only partial absorption of light by 4PhBP. Experiments using $[Ru(bipy)_3](BF_4)_2$ as a sensitizer failed to sensitize the Type II reaction from aliphatic ketones. The efficiency of singlet energy transfer depends on the lifetime of the singlet excited state[109] and $[Ru(bipy)_3](BF_4)_2$ has to intersystem cross fast due to heavy atom effect. Perhaps, if 4,5-diazafluorene is employed as a sensitizer, the results should be positive.

The case of cis-$[Ru(bipy)_2(4EsterBP)_2]^{2+}$ is different. The corrected quantum yield and the quantum yield of 4EsterBP.HCl are almost identical. This fact is rather coincidental and cannot be attributed to a slow rate of Internal Conversion. Rather, it has to be attributed to the fact that k_{IC} is about four times larger than k_r for this compound (Table 26). Intramolecular singlet sensitization is expected to give quantum yields higher than the expected ones but fast Internal Conversion, competing with k_r lowers the quantum yield again.

In order to obtain insight into the inter-ligand energy transfer, we consider Figure 50, which displays a three-dimensional structure of the Internal Ligand $n\pi^*$ excited

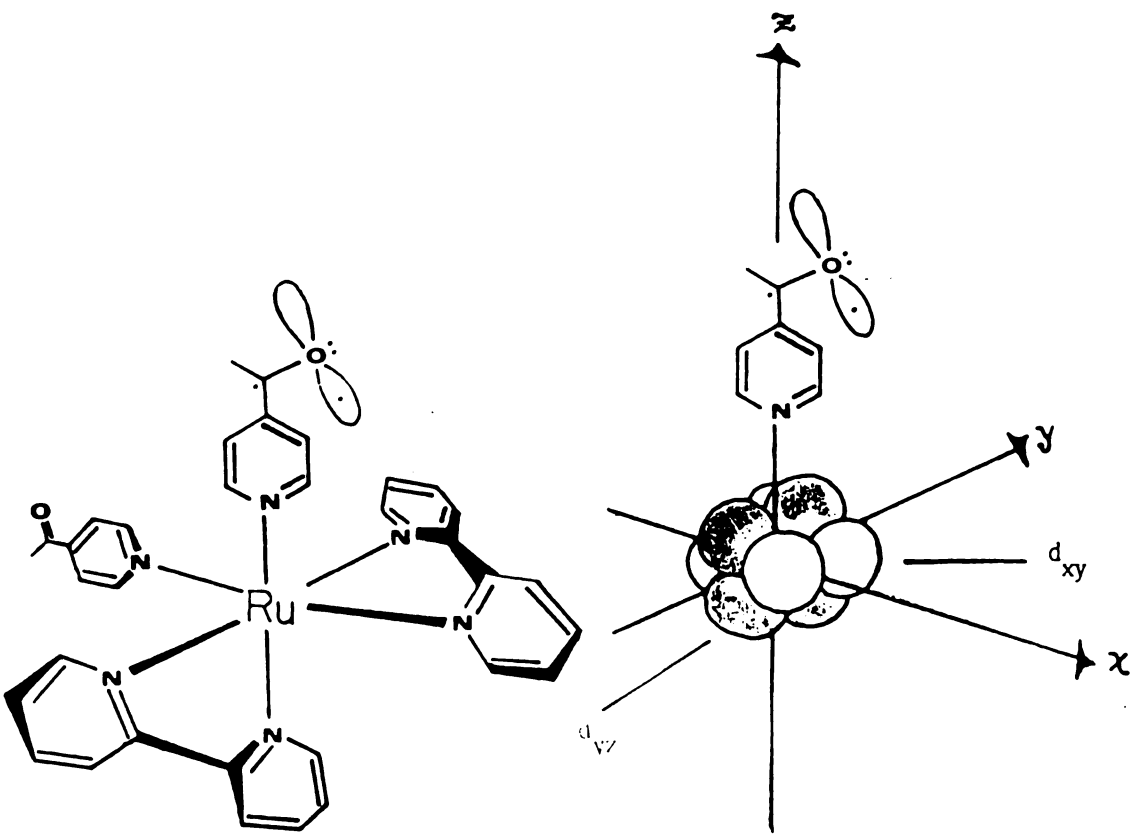

Figure 50. Internal Ligand ππ* excited state of cis-$[Ru(bipy)_2(4\text{-pyridyl ketone})_2]^{2+}$ complex.

state of a bis(2,2'bipyridine)-bis(4-pyridyl ketone) Ruthenium(II) complex. The plane of the pyridyl ring, in order to maximize π-back bonding, bisects the dihedral angle of the xz and yz planes. This arrangement places the n orbital of the carbonyl above the d_{xy} orbital, but the distance is too large to have efficient energy transfer. It seems reasonable to assume that energy transfer to the π-orbitals of 2,2'bipyridine has to be more efficient since these π-orbitals are directed upwards towards the n-orbital of the carbonyl. If we split the k_{IC} into two terms, one for energy transfer to the MLCT excited state and one for energy transfer to 2,2'bipyridine, and if we assume that the energy transfer to MLCT is equal in the pentaammine and the bis(2,2'bipyridine) complexes ($\leq 3.9 \times 10^7$ sec^{-1}, Table 26), we calculate that the energy transfer to 2,2'bipyridine is $\sim 2.5 \times 10^8$ sec^{-1}, 4 times higher than the energy transfer to MLCT, which reinforces the speculation based on Figure 50.

For the Ruthenium porphyrines, the corrected quantum yields are about 3 to 7 times lower than those of 4PhBP.HCl. The difference might be due to intermolecular quenching or most probably to fast internal conversion as well as intramolecular energy transfer (quenching) from the excited ketone to the porphyrine ring. Lack of lifetime data prevented further corrections based on intramolecular quenching, eventhough there is a clear dependence of Type II products quantum yield on ground state complex concentration (Figure 16). A rather crude model for the Ruthenium

porphyrine complexes is the cis-$[Ru(phen)_2(4AP)_2]^{2+}$ complex which is found to quench excited ketones rapidly (Table 21).

A proposed Jablonski diagram for the cis-$[Ru(bipy)_2$(4-pyridyl ketone)$_2]$ complexes is given in Figure 51.

There have been two cases in the literature where other workers have assumed slow internal conversion to explain their data, or they have given an estimate for the rate of the internal conversion. Wrighton has observed dual emission in systems like fac-$[(CH_3CN)Re(CO)_3(phen)]^+$[110] or fac-$[ClRe(CO)_3$(3-benzoylpyridine)$_2]$[111] at 77°K. The short-lived emission component (~10-20 us) is the structureless ReLCT transition, while the long-lived component (>50 us) has the same features of 1,10-phenanthroline or 3-benzoylpyridine emissions, and lifetimes 75 us and 1400 us, respectively. In order to explain the dual emission, Wrighton assumed slow and endothermic internal conversion from the IL excited state to the low ReLCT.

Finally, Whitten speculated,[32] without measuring rate constants, that $k_{IC} = 5x10^{12}$ sec^{-1} for cis-$[Ru(bipy)_2$(4-stilbazole)$_2]^{2+}$. Sensitized isomerization of complexed 4-stilbazole was inefficient, and he attributed the direct photoisomerization of complexed stilbazole to a singlet state reaction. He concluded the above value for k_{IC} by considering and arbitrarily correcting, for complexation, the values for fluorescence rate constant and quantum yield of trans-4-stilbazole.

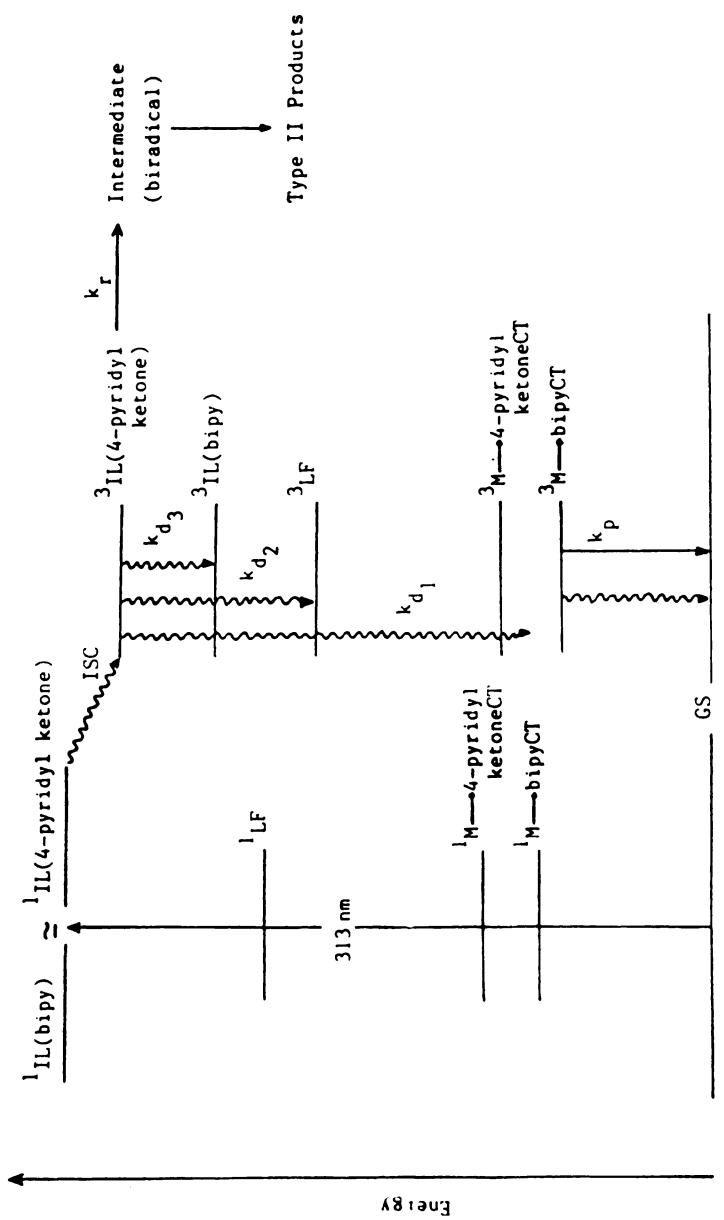

Figure 51. Jablonski diagram for cis-[Ru(bipy)$_2$ (pyridyl ketone)$_2$]$^{2+}$ complex.

Ruthenium 2,2'bipyrimidine and Ruthenium-Osmium 2,2'bipyrimidine Bridged Complexes.

All these complexes were synthesized in order to be used in resonance Raman spectroscopy. Resonance Raman Spectroscopy has proven to be a nice and relatively simple method to resolve the origin of the broad and structureless CT absorption bands of transition metal complexes. It was shown, for example, that $[Ru(bipym)_3]^{2+}$, under its peculiar absorption spectrum, hides two different MLCT transitions.[93] The same behavior is exhibited by the rest of the monometallic and bimetallic complexes cited in Tables 10 and 11.[104]

Tungsten Carbonyls.

Efforts to transfer the same technique used in Ruthenium complexes (i.e., estimation of Internal Conversion from IL to MLCT excited state by competition with fast internal ligand reaction) failed eventhough 14% of the light at 313 nm goes into the internal ligand $n\pi^*$ state, compared to only 5% in the case of $[Ru(NH_3)_5(4AP)]^{2+}$ complex. This lack of an internal ligand Type II reaction is probably due to a fast Internal Conversion to lower excited states, which seem to give photochemistry of their own. In the present study, the high concentration of $W(CO)_5(4VP)$ (0.02 M) needed for Type II products observation was helpful since the initially yellow solutions of $W(CO)_5(4VP)$, upon 313 nm irradiation, rapidly turned a deep red color, a fact missed

by earlier workers who used less than 10^{-4} M complex concentration. These low concentrations were essential since the photochemical reaction of $W(CO)_5L$ (L = substituted pyridine) was followed by measuring changes in the visible absorption spectra of $W(CO)_5L$. As noted in the introduction, the photochemical studies of $W(CO)_5$ (substituted pyridine), in the literature, always included an entering ligand in order to scavenge the $W(CO)_5$ and $W(CO)_4L$ intermediates. The photochemistry of this class of compounds in the absence of an entering ligand was never attempted, and it was considered complicated.[63] Our results led to the stoichiometric reaction (32).

$$2\ W(CO)_5(4VP) \xrightarrow{h\nu} W(CO)_6 + cis\text{-}W(CO)_4(4VP)_2 \qquad (32)$$

Electronic Absorption and Emission Spectra.

$W(CO)_5(4VP)$ absorption spectra both in benzene and in methylcyclohexane follow the same pattern as already reported for the $W(CO)_5(4AP)$ (4AP = 4-Acetylpyridine) complex.[69] The higher energy absorption band maximum at 402 nm in benzene is essentially unshifted by variations of the solvent medium (Figure 24). The lower energy band maximum is observed at 437 nm (methylcyclohexane) and is blue shifted in benzene, appearing as a shoulder to the red of the peak at 402 nm. The absorption bands at 402 nm and 430-437 nm have been assigned previously to a ligand field (LF)

$^1A_1(e^4b_2^2)$ ----> $^1E(e^3b_2^2a_1^1)$ symmetry allowed transition and a metal-to-ligand charge transfer (MLCT) transition, respectively.[60] The weak absorption maximum at ~330 nm does not shift at all when the solvent is varied. This absorption band has been previously assigned to LF transitions.[69]

Room temperature emission is observed (Table 13) in agreement with previous observations.[63,69] The emission maximum does not change drastically by varying the solvent, but it does by changing the ligand. In methylcyclohexane, a short wavelength shoulder appears, the origin of which is uncertain. Due to structural and spectral similarities, $W(CO)_5(4VP)$ is expected to behave like $W(CO)_5$4AP and the other complexes having an MLCT lowest excited state. The broad structureless emission is assigned to a MLCT emission.

Photochemistry of $W(CO)_5(4VP)$.

Most of the studies reported here were performed using $W(CO)_5(4VP)$ which has certain advantages over $W(CO)_5(4AP)$ or $W(CO)_5(4CNpy)$. $W(CO)_5(4VP)$ has higher solubility than both $W(CO)_5(4AP)$ and $W(CO)_5(4CNpy)$, so one can make much more concentrated solutions of the former complex in methylcyclohexane, as high as in benzene. It also proved to be ideal for HPLC analysis (short retention times of both $W(CO)_5(4VP)$ and cis-$W(CO)_4(4VP)_2$).

Irradiations were performed at both 410 nm, which presumably populates the LF transition exclusively, and at

490 nm, where $W(CO)_5(4VP)$ absorbs 10% as much as its maximum at 402 nm in benzene. According to Adamson,[69] assuming a gaussian shape for the LF absorptions, 490 nm irradiation populates primarily the MLCT excited state.

The quantum yields for direct LF population are 100 and 700 times higher than at 490 nm irradiation, in benzene and methylcyclohexane, respectively (Table 16). This fact can be interpreted either as a relatively inert, independently reacting MLCT state or as an unreactive MLCT state thermally populating the higher energy, reactive LF state. The latter is the standard interpretation.[63,65] On the other hand, the quantum yields in benzene and methylcyclohexane at 410 nm irradiation are comparable (0.066 vs. 0.026, respectively; Table 16), while at 490 nm irradiation, they differ substantially. In benzene, the 490 nm quantum yield is 16 times higher than in methylcyclohexane (Table 16). Taking into consideration the absorption spectra of $W(CO)_5(4VP)$, this variation of the quantum yields is consistent with the standard model for the photobehavior of $W(CO)_5$(substituted pyridine) complexes.[63,65] Irradiation at 490 nm populates some higher vibrational level of the MLCT lowest excited state which relaxes rapidly to the zero vibrational level of this excited state. The zero vibrational levels of the LF and MLCT excited states are closer in benzene than in methylcyclohexane, so thermal population of the LF state is more effective in benzene than in methylcyclohexane, with resulting higher quantum yields in the former solvent.

The small concentration dependence of the quantum yield at both short and long wavelengths of irradiation in benzene (Figures 35 and 36) probably represents two competing processes: a dissociative mechanism at all concentrations competing with an associative one at higher concentrations. According to Scheme 3, if an excited state reacts with a ground state substrate, it is expected that the reciprocal quantum yield of a product will be a linear function of the reciprocal concentration of the substrate (equation 19). At both 410 and 490 nm irradiation wavelengths, an identical dependence of the tetracarbonyl product quantum yield on ground state complex concentration was observed, which seems to be what is anticipated if both mechanisms displayed in Schemes 2 and 3 take place simultaneously.

Gray has suggested an associative mechanism as a possible reaction path of the MLCT excited states.[4] An associative process for $W(CO)_5(4VP)$ to produce $W(CO)_6$ and $cis\text{-}W(CO)_4(4VP)_2$ from an MLCT excited state requires the reaction of a long-lived MLCT state with a ground state molecule, which goes through a seven-coordinate transition state. Eventhough there are no seven-coordinate complexes of Tungsten in the +1 oxidation state it possesses in the MLCT state, there are several such Molybdenum complexes known, like $[\eta^5\text{-}C_5H_5Mo(CO)_3]_2$.[94b] Therefore, it seems reasonable for Tungsten to form a seven-coordinate transition state, and it is suggested here that the MLCT excited state of $W(CO)_5(4VP)$ reacts bimolecularly with the

ground state to give $W(CO)_6$ and cis-$W(CO)_4(4VP)_2$. As noted in the introduction, LF states are dissociative in nature and, therefore, are anticipated to react unimolecularly. In any case, the variation of the quantum yield with complex concentration is small, especially at 410 nm irradiation, a fact indicating that the main reaction path is through a unimolecular cleavage. The identical dependence of the tetracarbonyl product formation on ground state complex concentration at both 490 and 410 nm irradiations reinforces the hypothesis that the $W(CO)_5(4VP)$ complex reacts through interconverting excited states independent or where it is irradiated, a fact verified by quenching experiments described below.

Energy transfer quenching in benzene does not show a clear-cut concentration dependence of lifetime on ground state complex concentration (Table 17). Successive Stern-Volmer quenching though of emission and product formation at 490 nm irradiation gives identical lifetimes, within experimental error, at the same $W(CO)_5(4VP)$ concentration (Table 17, Figures 39 and 40). Linear Stern-Volmer plots yield $k_q\tau$ value of 547 ± 17 M^{-1} at 10^{-3} M, and 160 ± 4 M^{-1} at $5x10^{-3}$ M complex concentration in benzene. Therefore, the photoreactive state for long wavelengths of irradiation and the emitting state are kinetically identical. The fact that at 410 nm irradiations the quenching plots obtained have intercepts in general higher than unity (Figure 37) might be interpreted as two excited states being

quenched,[112] a short-lived one (presumably LF) and a long-lived one (presumably MLCT). The presentation so far implies that the two excited states interconvert but they do not equilibrate. If equilibration were taking place, the Stern-Volmer quenching plots would be identical, independently of where excitation was taking place. Lack of equilibration is most probably due to fast chemical reaction from the upper photolabile LF state. Our quenching plots of cis-$W(CO)_4(4VP)_2$ formation are similar to what Adamson obtained for the quenching of the photoexchange in $W(CO)_5(4CNpy)$ by ethanol in methylcyclohexane, implying that the same excited states are reponsible for the pyridyl ligand photoexchange reaction and the tetracarbonyl product formation.

In the preceding discussion, 490 and 410 nm irradiations imply monochromatic light, which was achieved by a monochromator, while in the discussion to follow $\lambda_{irr} >$ 400 nm means light including all the wavelengths above 400 nm. Correspondingly, $\lambda_{irr} >$ 475 nm means light which includes all the wavelengths above 475 nm. Since $\Phi_{(410)} >> \Phi_{(490)}$, we accept the common interpretation that irradiation with a 400 nm cutoff filter gives products coming primarily from the LF state, while irradiations with wavelengths longer than 475 nm give products originating from the initial population of the MLCT excited state.

As noted in the introduction, it has been speculated that excited $W(CO)_5L$ species (L is a nitrogen, oxygen or

phosphorous ligand) react by losing cis- or trans- CO or L,[55,56,65] and several models have been employed[3,61,65,113] to explain the reactivity patterns.

In our experiments, free ligand quenches cis-$W(CO)_4(4VP)_2$ formation with a good Stern-Volmer relation at both short (λ_{irr}>400 nm) and long (λ_{irr} > 475 nm) wavelengths of irradiation (Figure 42). At both wavelengths of irradiation most tetracarbonyl product seems to be formed through a unimolecular process giving a $W(CO)_5$ intermediate, which is effectively scavenged by the free ligand. Little, if any, CO photoliberation seems to be responsible for the tetracarbonyl product formation at least for visible light irradiation. No CO has been detected by gc/ms when $W(CO)_5(4VP)$ was irradiated in benzene in the absence of any entering ligand. If tetracarbonyl product was originating from loss of CO, addition of free ligand (4VP) would enhance the quantum yield, instead of quenching it. The fact though that at λ_{irr} > 400 nm we observe less efficient quenching than at λ_{irr} > 475 nm (Figure 42) implies that at shorter irradiation wavelengths, loss of CO becomes more significant, the main reaction path for tetracarbonyl product formation remaining the 4VP loss.

Further proof for the intermediacy of $W(CO)_5$, as a primary photoproduct,[61] came from trapping experiments. 4BP traps the intermediate $W(CO)_5$, quenching the formation of cis-$W(CO)_4(4VP)_2$ (Table 19), the main product being $W(CO)_5(4BP)$. Two other tetracarbonyl products are produced:

cis-$W(CO)_4(4VP)(4BP)$ and cis-$W(CO)_4(4BP)_2$. The total tetracarbonyl product formation is quenched with good Stern-Volmer relation both at $\lambda_{irr} > 400$ nm and $\lambda_{irr} > 475$ nm (Figure 49). The slopes are different, with the larger slope obtained at $\lambda_{irr} > 475$ nm, consistent with the product quenching by 4VP. Figures 46 and 47 display the product distribution, taken from Table 19, at $\lambda_{irr} > 400$ nm and $\lambda_{irr} > 475$ nm, respectively. Only at low concentrations of 4BP cis-$W(CO)_4(4VP)_2$ and cis-$W(CO)_4(4VP)(4BP)$ are producted as major products. If loss of CO was a competitive route, cis-$W(CO)_4(4VP)(4BP)$ should always be a major product. While the concentration of cis-$W(CO)_4(4VP)_2$ decreases monotonously with increasing concentration of 4BP, the concentration of cis-$W(CO)_4(4VP)(4BP)$, at $\lambda_{irr} > 475$ nm, increases then eventually decreases. At $\lambda_{irr} > 400$ nm, this behavior of the latter compound is less pronounced; the concentration of cis-$W(CO)_4(4VP)(4BP)$ is almost constant, a fact which allows the possibility that there is some CO loss and the $W(CO)_4(4VP)$ intermediate is trapped by the excess of 4BP. Another point which counts towards a minor CO loss hypothesis at $\lambda_{irr} > 400$ nm comes from Table 19. For comparable $W(CO)_5(4BP)$ formation at both $\lambda_{irr} > 400$ nm and $\lambda_{irr} > 475$ nm, the total tetracarbonyl product formation is always lower in the latter irradiation by a factor of 7-9. If we assume $W(CO)_5$ is the major intermediate responsible for photoproduct formation, then by increasing the concentration of 4BP, the intermediate is trapped more

efficiently, with resulting increase in the concentration of $W(CO)_5(4BP)$. The most probable route for this intermediate to give tetracarbonyl products is to react with the ground state $W(CO)_5(4VP)$, to give $W(CO)_6$ and $W(CO)_4(4VP)$. $W(CO)_4(4VP)$ finds itself in an environment of progressively increasing concentration of 4BP, so the concentration of cis-$W(CO)_4(4VP)(4BP)$ increases, while the concentration of cis-$W(CO)_4(4VP)_2$ decreases. Then it comes a point where the concentration of 4BP becomes high enough to trap more effectively the $W(CO)_5$ intermediate, so the concentration of cis-$W(CO)_4(4VP)(4BP)$ decreases.

Small amounts of cis-$W(CO)_4(4BP)_2$ produced have to come either from the photochemical reaction of photoproduced $W(CO)_5(4BP)$ or by thermal reaction of cis-$W(CO)_4(4VP)(4BP)$ with 4BP. Figure 48 shows that despite what happens to the concentrations of cis-$W(CO)_4(4VP)_2$ and cis-$W(CO)_4(4VP)(4BP)$, the concentration of cis-$W(CO)_4(4BP)_2$ increases by increasing the concentration of 4BP. The photochemical reaction seems reasonable since the concentration ratio of the photoproduced $W(CO)_5(4BP)$ to unreacted $W(CO)_5(4VP)$ at high 4BP concentrations is 1:3. But also the thermal formation of cis-$W(CO)_4(4BP)_2$ from cis-$W(CO)_4(4VP)(4BP)$ is consistent. Control experiments (Figure 45) prove that cis-$W(CO)_4(4VP)_2$ reacts in a first order thermal reaction with 4BP to give cis-$W(CO)_4(4VP)(4BP)$. This thermal reaction has been implied in the literature but the reports seem to contradict each other. Wrighton claims[67] that photolysis of

cis-$W(CO)_4X_2$ (X = py, 4CNpy, 4Bzpy, etc.) in the presence of PPh_3 gives cis-$W(CO)_4(PPh_3)X$. On the other hand, photolysis of cis-$W(CO)_4X_2$ with a bidentate ligand (L-L) like 1,10-Phenanthroline is believed to give cis-$W(CO)_4X(L\text{-}L)$ which thermally[67,68] gives cis-$W(CO)_4$. Our results suggest that the reaction is a first order thermal reaction (Figure 44) from the very beginning. On the other hand, cis-$Mo(CO)_4(C_5H_{10}NH)_2$ reacts smoothly[114] at 40°C with L to give cis-$Mo(CO)_4L(C_5H_{10}NH)$ and then cis-$Mo(CO)_4L_2$ which reinforces the thermal reaction hypothesis.

Wrighton[64] investigated the effects of entering group concentration on photosubstitution in $W(CO)_5$pip (pip = piperidine) and his results are displayed in Table 1. Eventhough he interpreted these results as there being no concentration effect on piperidine substitution, the trends he found parallel ours for short (λ_{irr} > 400 nm) wavelengths of irradiation (small variations in the quantum yields). Wrighton's complex has highly reactive LF as the lowest excited state, so it is expected to behave photochemically like $W(CO)_5$(4VP) when the latter complex is irradiated in its LF excited state. His data in Table 1 parallel ours cited in Table 19 and Figure 42.

A mechanism consistent with our results requires that the $W(CO)_5$ intermediate reacts not only with free ligand but also with ground state $W(CO)_5$(4VP) to yield $W(CO)_6$ and C_{4v}- or C_s-$W(CO)_4$(4VP). As has been proposed,[62] the C_{4v}-geometry

Scheme 13

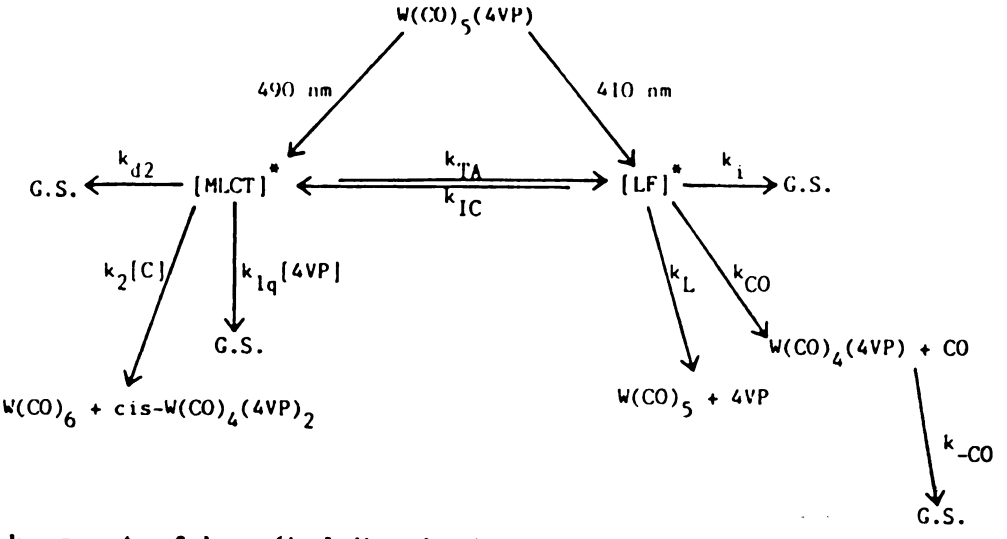

k_{d2} = rate of decay (including phosphorescence).

k_{1q} = rate of quenching of MLCT excited state by 4VP.

k_{TA} = rate of thermal activation.

k_{IC} = rate of internal conversion.

k_2 = bimolecular rate constant.

k_l = rate of decay of the LF excited state directly to ground state.

k_L = unimolecular rate constant for loss of 4VP.

k_{CO} = unimolecular rate constant for loss of CO.

k_{-CO} = rate constant for the coupling of the $W(CO)_4(4VP)$ intermediate with CO.

$k_1 = k_L + k_{CO}$.

$$W(CO)_5 + 4VP \xrightarrow{k_{BR}} W(CO)_5(4VP)$$

$$(W(CO)_5 + 4BP \xrightarrow{k_{BR}} W(CO)_5(4BP))$$

$$W(CO)_5 + W(CO)_5(4VP) \xrightarrow{k_{BM}} W(CO)_6 + Cs\text{-}W(CO)_4(4VP)$$

$$Cs\text{-}W(CO)_4(4VP) + 4VP \xrightarrow{k_{rast}} cis\text{-}W(CO)_4(4VP)_2$$

k_{BR} = rate constant for the Back Reaction.

k_{BM} = rate constant for the Bimolecular Reaction of $W(CO)_5$ with a ground state molecule.

k_{rast} = rate constant for coupling of $W(CO)_4(4VP)$ intermediate with 4VP.

can rearrange to the Cs, so the final product is the cis-disubstituted tetracarbonyl and not the trans.

Scheme 13 indicates a possible mechanism which explains the cis-$W(CO)_4(4VP)_2$ formation.

The mechanism suggests that the two excited states (MLCT and LF) interconvert, with the LF reacting dissociatively to give primarily $W(CO)_5$, which reacts with a ground state molecule to yield $W(CO)_6$ and Cs-$W(CO)_4$(4VP). The latter eventually finds a free 4VP to give cis-$W(CO)_4(4VP)_2$.

In an original attempt to explain why chemical quenching Stern-Volmer plots have different slopes at λ_{irr} > 400 and λ_{irr} > 475 nm (Figures 42 and 49), it was thought that a free ligand, besides trapping the $W(CO)_5$ intermediate, quenches some excited state. The most probable excited state to be quenched by 4VP is MLCT, which has been assumed to be involved in redox reactions but to be substitution inert.[10,115,116] Scheme 14 shows a degenerate electron transfer mechanism, which accounts for MLCT quenching by free ligand.

Scheme 14.

$$(CO)_5W(I)(py\text{-}x)^{\cdot(-)}\ (MLCT^*) + py\text{-}x \xrightarrow{k_{1q}} (CO)_5W(I)(py\text{-}x) + py\text{-}x^{\cdot(-)}$$

$$py\text{-}x^{\cdot(-)} \longrightarrow \text{G.S.}$$

Figures 43 and 44 prove that free ligand (4AP or 4VP) quenches the emission from the MLCT excited state but this quenching is too inefficient to explain the big difference (450 M^{-1}) in the Stern-Volmer slopes at $\lambda_{irr} > 400$ and $\lambda_{irr} > 475$ nm.

As mentioned above, less efficient quenching would be reasonable at $\lambda_{irr} > 400$ nm if some dissociation of CO was responsible for some $Cs-W(CO)_4(4VP)$ production, which in the presence of 4VP leads to the tetracarbonyl product.

If the mechanism proposed in Scheme 13 is correct, kinetic expressions derived from it should be consistent with experimentally measurable quantities.

It is reasonable to assume that thermal activation of MLCT populates lower ligand field states, responsible for loss of 4VP only, while higher energy wavelengths (around 400 nm) populate simultaneously higher ligand field states, responsible for loss of CO. Figure 52 shows this situation. Therefore, at $\lambda_{irr} > 475$ nm, $k_1 = k_L$.

According to Scheme 13, irradiation at $\lambda_{irr} > 475$ nm populates the MLCT state which gives products coming from the bimolecular reaction of this state with the ground state or from the LF state which is populated thermally from the MLCT state. Equation 33 describes this situation.

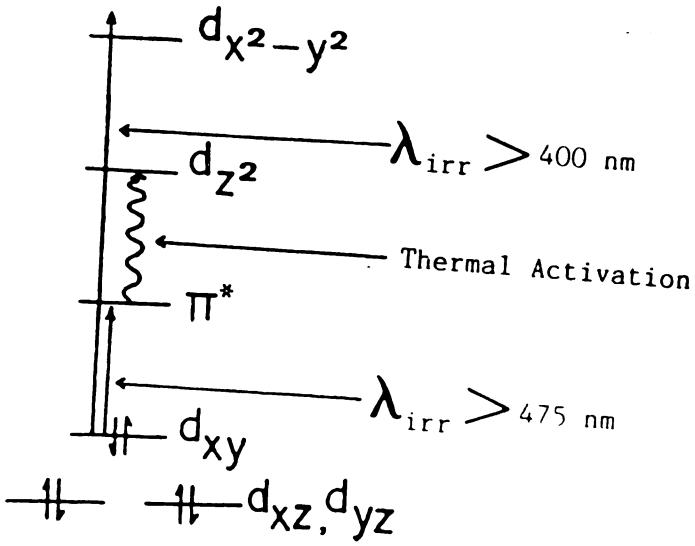

Figure 52. MLCT and LF transitions in $W(CO)_5(4VP)$.

$$\Phi_{\lambda>475} = \Phi_{(ISC)}\left[\frac{k_2[C]}{k_2[C]+k_{d2}+k_{1q}[4VP]+k_{TA}} + \frac{k_{TA}}{k_2[C]+k_{d2}+k_{1q}[4VP]+k_{TA}}(P + \right.$$

$$\frac{k_{IC}}{k_1+k_{IC}+k_i}\left(\frac{k_2[C]}{k_2[C]+k_{d2}+k_{1q}[4VP]+k_{TA}} + \frac{k_{TA}}{k_{TA}[C]+k_{d2}+k_{1q}[4VP]+k_{TA}}(P + \right.$$

$$\frac{k_{IC}}{k_1+k_{IC}+k_i}\left(\frac{k_2[C]}{k_2[C]+k_{d2}+k_{1q}[4VP]+k_{TA}} + \frac{k_{TA}}{k_2[C]+k_{d2}+k_{1q}[4VP]+k_{TA}}(P + \right.$$

$$\frac{k_{IC}}{k_1+k_{IC}+k_i}\left(\frac{k_2[C]}{k_2[C]+k_{d2}+k_{1q}[4VP]+k_{TA}} + \frac{k_{TA}}{k_2[C]+k_{d2}+k_{1q}[4VP]+k_{TA}}(P + \right.$$

$$\left.\frac{k_{IC}}{k_1+k_{IC}+k_i}\left(\frac{k_2[C]}{k_2[C]+k_{d2}+k_{1q}[4VP]+k_{TA}} + \ldots\ldots\ldots\ldots\ldots\right]\right. \qquad (33)$$

P is the probability the thermally populated LF state will give products and is best described according to Scheme 13 and Figure 52 as:

$$P = \frac{k_L}{k_2+k_{IC}+k_i} \times \frac{k_{BM}[C]}{k_{BM}[C] + k_{BR}[4VP]} \qquad (34)$$

Equation 33 describes the situation the directly populated MLCT state will react ($\Phi_{(ISC)}\frac{k_2[C]}{k_2[C]+k_{d2}+k_{1q}[4VP]+k_{TA}}$) or will thermally populate the LF state ($\Phi_{(ISC)}\frac{k_{TA}}{k_2[C]+k_{d2}+k_{1q}[4VP]+k_{TA}}$), which either reacts with probability P, or internally converts to MLCT with

probability $\frac{k_{IC}}{k_I+k_{IC}+k_i}$, which either reacts, or thermally populates the LF to react or repopulate the MLCT. This continuous interconversion between the two states is described by the infinite terms in 33.

To simplify equation 33, let:

$$\frac{k_2[C]}{k_2[C]+k_{d2}+k_{1q}[4VP]+k_{TA}} = A \quad (35):$$ Probability MLCT reacts.

$$\frac{k_{TA}}{k_2[C]+k_{d2}+k_{1q}[4VP]+k_{TA}} = B \quad (36):$$ Probability MLCT populates thermally the LF state.

$$\frac{k_{IC}}{k_I+k_{IC}+k_i} = D \quad (37):$$ Probability LF internally converts to MLCT state.

Substituting 35, 36 and 37 into 33, one obtains equation 38.

$$\Phi_{\lambda>475} = \Phi_{(ISC)}\,[A+B(P+D(A+B(P+D(A+B(P+D(A+B(P+...] \quad (38)$$

Equation 38 can be written as 39.

$$\Phi_{\lambda>475} = \Phi_{(ISC)}\,[(A+BP)(1+BD+B^2D^2+B^3D^3+B^4D^4+...)] \quad (39)$$

B and D are positive and less than unity, therefore, the sun of the infinite terms of the series $(1+BD+B^2D^2+B^3D^3+B^4D^4+.....)$ converges to $1/(1-BD)$; therefore, eq. 39 becomes 40.

$$\Phi_{\lambda>475} = \Phi_{(ISC)}\,(A+BP)\left(\frac{1}{1-BD}\right) \qquad (40)$$

Both B and D represent efficiencies; therefore, they are both less than unity. B is expected to be much less than unity since thermal activation is slow compared with other exoergonic processes like radiative or radiationless decay to ground state. Therefore, $BD \ll 1$ so 40 becomes 41.

$$\Phi_{\lambda>475} \simeq \Phi_{(ISC)}\,[A+BP] \qquad (41)$$

Substituting back into 41, the expressions from 35, 36 and 37 one obtains, after performing the multiplications, 42.

$$\Phi_{\lambda>475} \simeq \Phi_{(ISC)}\left[\frac{k_2[C]}{k_2[C]+k_{d2}+k_{1q}[4VP]+k_{TA}} + \frac{k_{TA}}{k_2[C]+k_{d2}+k_{1q}[4VP]+k_{TA}}P\right] \qquad (42)$$

Inverting 42, one obtains 43.

$$\Phi_{\lambda>475}^{-1} \simeq \Phi_{(ISC)}^{-1}\left[\frac{1}{\frac{k_2[C]}{k_2[C]+k_{d2}+k_{1q}[4VP]+k_{TA}} + \frac{k_{TA}P}{k_2[C]+k_{d2}+k_{1q}[4VP]+k_{TA}}}\right] \qquad (43)$$

Multiplying the numerator and denominator of 43 by $1/[C]$, we obtain 44.

$$\Phi_{\lambda>475}^{-1} \simeq \Phi_{(ISC)}^{-1} \left[\frac{1}{\frac{k_2}{k_2[C]+k_{d2}+k_{1q}[4VP]+k_{TA}} + \frac{k_{TA}P}{[C](k_2[C]+k_{d2}+k_{1q}[4VP]+k_{TA})}} \right] \frac{1}{[C]} \quad (44)$$

It is obvious from 44 that by increasing 1/[C], the slope decreases, as found experimentally (Figure 35).

Equation 42 can be approximated by considering that the bimolecular reaction plays only a minor role at low values of [C], the main reaction path being the unimolecular reaction from the thermally activated LF state. In other words, $k_{TA}P >> k_2[C]$. This hypothesis is valid if one considers the quantum yield difference at 490 nm irradiation in benzene and methylcyclohexane; if the bimolecular reaction was an important component of the $\Phi_{\lambda>475}$ the two quantum yields should not be substantially different. Under this point of view, 42 is modified to 45.

$$\Phi_{\lambda>475} = \Phi_{(ISC)} \left(\frac{k_{TA}P}{k_2[C]+k_{d2}+k_{1q}[4VP]+k_{TA}} \right) \quad (45)$$

Substituting 34 into 45, we obtain 46.

$$\Phi_{\lambda>475} = \Phi_{(ISC)} \left(\frac{k_{TA}}{k_2[C]+k_{d2}+k_{1q}[4VP]+k_{TA}} \right) \left(\frac{k_L}{k_L+k_{IC}+k_I} \times \frac{k_{BM}[C]}{k_{BM}[C]+k_{BR}[4VP]} \right) \quad (46)$$

Equation 46 in the absence of 4VP becomes:

$$\Phi_{\lambda>475} = \Phi_{(ISC)} \left(\frac{k_{TA}}{k_2[C]+k_{d2}+k_{TA}}\right)\left(\frac{k_L}{k_L+k_{1C}+k_1}\right) \qquad (47)$$

Considering that k_{1q} [4VP] is too low (Figures 43 and 44) and dividing 47 by 46, one obtains the Stern-Volmer equation for quenching by free ligand (4VP).

$$(\Phi^0/\Phi)_{\lambda>475} = 1 + \frac{k_{BR}}{k_{BM}[C]}[4VP] \qquad (48)$$

The slope of 48 at [complex] = 0.02 M is 732 M^{-1}, therefore, k_{BR}/k_{BM} = 15.

At λ_{irr}>400 nm, we have to take into consideration that two processes might give products; loss of CO (k_{CO}) and loss of 4VP (k_L). The quantum yield is given by 49.

$$\Phi_{\lambda>} = \Phi_{(ISC)}\left[P + \frac{k_{1C}}{k_1+k_{1C}+k_1}\left(\frac{k_2[C]}{k_2[C]+k_{d2}+k_{1q}[4VP]+k_{TA}} + \frac{k_{TA}}{k_2[C]+k_{d2}+k_{1q}[4VP]+k_{TA}}\left(P + \right.\right.\right.$$

$$\frac{k_{1C}}{k_1+k_{1C}+k_1}\left(\frac{k_2[C]}{k_2[C]+k_{d2}+k_{1q}[4VP]+k_{TA}} + \frac{k_{TA}}{k_2[C]+k_{d2}+k_{1q}[4VP]+k_{TA}}\left(P + \frac{k_{1C}}{k_1+k_{1C}+k_1}\right.\right.\right.$$

$$\left.\left.\left.\left(\frac{k_2[C]}{k_2[C]+k_{d2}+k_{1q}[4VP]+k_{TA}} + \frac{k_{TA}}{k_2[C]+k_{d2}+k_{1q}[4VP]+k_{TA}}\left(P + \frac{k_{1C}}{k_1+k_{1C}+k_1}\right.\right.\right.\right.\right.$$

$$\left.\left.\left.\left.\left.\left(\frac{k_2[C]}{k_2[C]+k_{d2}+k_{1q}[4VP]+k_{TA}} + \right.\right.\right.\right.\right.\right] \qquad (49)$$

P is the probability with which the Ligand Field state will give products and is best described according to Scheme 13 and Figure 52 as:

$$P = \frac{k_{co}}{k_1+k_{d1}} \times \frac{k_{rest}[4VP]}{k_{rest}[4VP]+k\text{-}co[CO]} + \frac{k_L}{k_1+k_{d1}} \times \frac{k_{BH}[C]}{k_{BH}[C]+k_{BR}[4VP]} \qquad (50)$$

k_{d1} includes both deactivation processes: internal conversion (k_{IC}) and direct deactivation of the LF excited state to ground state (k_1). The infinite terms in 49 are needed to describe the fact that LF partially deactivates to the lower MLCT which thermally repopulates the LF excited state and the cycle is repeated.

Substituting 35, 36 and 37 into 49, one obtains 51.

$$\Phi_{\lambda>400} = \Phi_{(ISC)}[P+ D(A+ B(P+ D(A+ B(P+ D(A+ B(P+ D(A+ B(P+.....] \qquad (51)$$

51 can be written as 52.

$$\Phi_{\lambda>400} = \Phi_{(ISC)}[P+ AD](1+DB+D^2B^2+D^3B^3+D^4B^4+.....] \qquad (52)$$

$(1+DB+D^2B^2+D^3B^3+D^4B^4+.....)$ converges to $1/(1-DB)$, therefore, 52 becomes 53.

$$\Phi_{\lambda>400} = \Phi_{(ISC)}[(P + DA)(\frac{1}{1-BD})] \quad (53)$$

DB<<1, so 53 becomes 54.

$$\Phi_{\lambda>400} \simeq \Phi_{(ISC)}[P + DA] \quad (54)$$

Substituting back into 54, the expressions for 35, 36 and 37, one obtains 55.

$$\Phi_{\lambda>400} \simeq \Phi_{(ISC)}[P + (\frac{k_2[C]}{k_2[C]+k_{d2}+k_{1q}[4VP]+k_{TA}} \times \frac{k_{IC}}{k_1+k_{IC}+k_i})] \quad (55)$$

Inverting 55 and multiplying the numerator and denominator by 1/[C], one obtains 56.

$$\Phi_{\lambda>400}^{-1} \simeq \Phi_{(ISC)}^{-1} \frac{[C]^{-1}}{\frac{P}{[C]} + \frac{k_2 k_{IC}}{(k_2[C]+k_{d2}+k_{1q}[4VP]+k_{TA})(k_1+k_{IC}+k_i)}} \quad (56)$$

It is obvious from 56 that increasing 1/[C] the slope decreases, as found experimentally (Figure 36).

Equation 55 can be approximated by considering the fact that $\Phi_{410} >> \Phi_{490}$. In other words, the reaction originating from direct population of the LF state is much faster than

the reaction taking place through the MLCT state, i.e., bimolecular reaction of MLCT and thermal activation to LF state.

$$P>>\left(\frac{k_2[C]}{k_2[C]+k_{d2}+k_{1q}[4VP]+k_{TA}} \times \frac{k_{IC}}{k_1+k_{IC}+k_i}\right)$$, so 55 becomes 57.

$$\Phi_{\lambda>400} \simeq \Phi_{(ISC)}P \qquad (57)$$

Substituting 50 into 57, one obtains 58.

$$\Phi_{\lambda>400} \simeq \Phi_{(ISC)}\left(\frac{k_{CO}}{k_1+k_{d1}} \times \frac{k_{fast}[4VP]}{k_{fast}[4VP]+k\text{-}co[CO]} + \frac{k_L}{k_1+k_{d1}} \times \frac{k_{BM}[C]}{k_{BM}[C]+k_{BR}[4VP]}\right) \qquad (58)$$

It is assumed that $k_{fast}[4VP]>>k\text{-}co[CO]$ at all 4VP concentrations. This is a logical assumption since CO is a gas and, after its generation, diffuses to the vacuum space above the degassed samples, until its chemical potential is equal in the two phases. 58 reduces to 59.

$$\Phi_{\lambda>400} \simeq \Phi_{(ISC)}\left(\frac{k_{CO}}{k_1+k_{d1}} + \frac{k_L}{k_1+k_{d1}} \times \frac{k_{BM}[C]}{k_{BM}[C]+k_{BR}[4VP]}\right) \qquad (59)$$

In the absence of 4VP, 59 becomes 60.

$$\Phi_{\lambda>400} \simeq \Phi_{(ISC)}\left(\frac{k_{CO}}{k_1+k_{d1}} + \frac{k_L}{k_1+k_{d1}}\right) \qquad (60)$$

The Stern-Volmer equation is obtained from 59 and 60 and is given by 61.

$$(\Phi^{0}/\Phi)_{\lambda>400} = 1 + \frac{k_L k_{BR}}{k_{CO}(k_{BM}[C]+k_{BR}[4VP])+k_L k_{BM}[C]}[4VP] \quad (61)$$

To obtain an estimate of k_L/k_{CO}, equation 61 was simulated for various k_L/k_{CO} values, considering that $k_{BR}/k_{BM}[C] = 732$, as was found from equation 48. Figure 53 displays the situation. For $k_{CO} = 0$ equation 61 reduces to equation 48 for irradiation with $\lambda_{irr}>475$ nm. As the ratio k_L/k_{CO} decreases, the simulated, through equation 61, lines fall between the lines obtained at $\lambda_{irr}>475$ and $\lambda_{irr}>400$ irradiations. At approximately k_L/k_{CO} 2.5, the theoretical line simulates the experimental points at $\lambda_{irr}>400$ nm well. The small discrepancy is due rather to experimental error.

We assumed that for $\lambda_{irr} > 400$ nm in the presence of 4VP, part of the tetracarbonyl product formation originates from loss of 4VP and part from loss of CO. This hypothesis explained the less efficient quenching of cis-$W(CO)_4(4VP)_2$ formation at $\lambda_{irr} > 400$ nm since the slope of 61 is obviously less than the slope of 49 and gave us an estimate of the relative ratio of the rate constants for CO and 4VP loss from the LF excited state.

Of course, the presence of an entering ligand like 4VP or 4BP complicates the situation. CO loss in the absence of any entering ligand produces $W(CO)_4(4VP)$ which recombines with either CO or 4VP to give starting material or

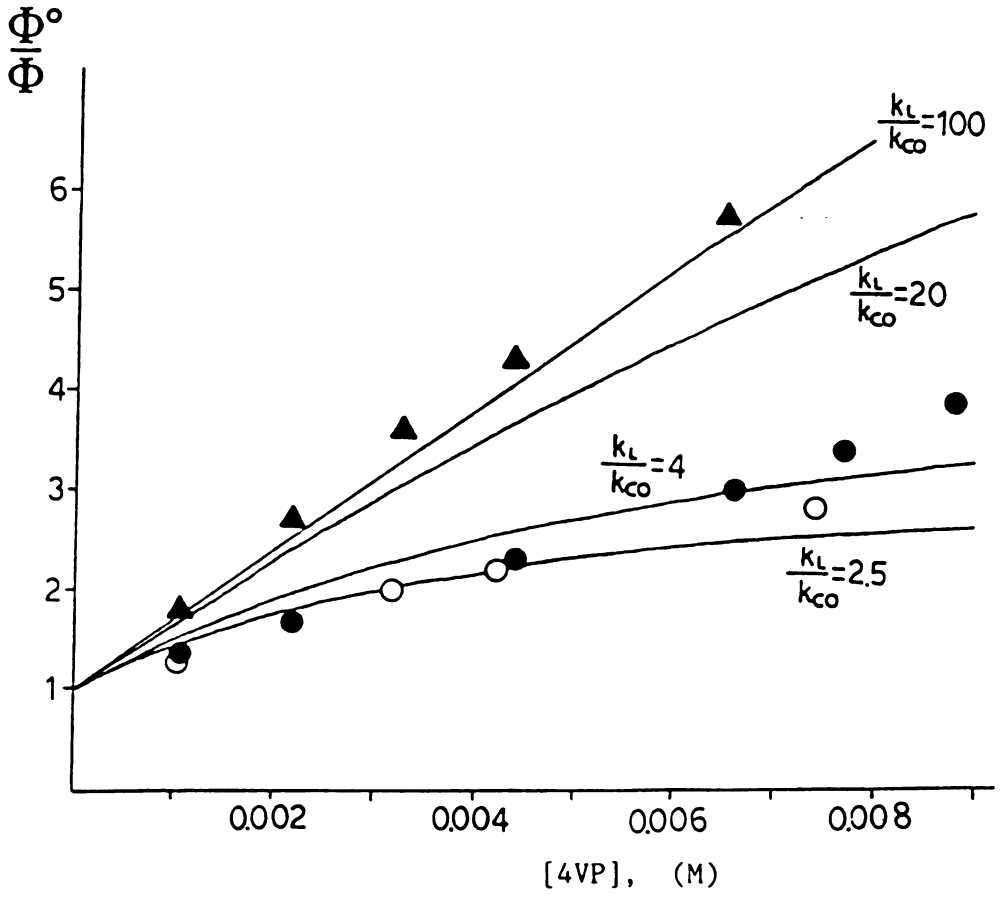

Figure 53. Simulation of equation 61 for the Stern Volmer quenching by 4VP of cis-$W(CO)_4(4VP)_2$ formation from $W(CO)_5(4VP)$ at various k_L/k_{CO} values.

The experimental points shown have the same meaning as in Figure 42.

tetracarbonyl product, respectively. One might argue that cis-$W(CO)_4(4VP)_2$, in the absence of 4VP originates from this very process which is illustrated by 62 and 63.

$$W(CO)_5(4VP) \xrightarrow{h\nu} W(CO)_5 + 4VP \qquad (62)$$

$$W(CO)_5(4VP) \xrightarrow{h\nu} W(CO)_4(4VP) + CO \qquad (63)$$

Cross recombination is expected to give $W(CO)_6$ and cis-$W(CO)_4(4VP)_2$. This process though seems inprobable since presence of free 4VP would not quench the tetracarbonyl product formation. Instead, it would enhance it.

The only precedent dispropotionation reaction 32 has in the literature is the reaction 64:

$$2\ W(CO)_5(PPh_3) \xrightarrow{h\nu} W(CO)_6 + \text{cis-}W(CO)_4(PPh_3)_2 \qquad (64)$$

suggested by not elaborated by Zink.[117]

In conclusion, the synthesis of cis-$W(CO)_4L_2$ by irradiation of $W(CO)_5L$ with UV light in the presence of L is still valid since, even if we assume that all tetracarbonyl products originate from a $W(CO)_5$ intermediate, the photoproduced $W(CO)_6$ reacts further to form $W(CO)_5L$ so that the yield of the final product is increased. In cases though where the ligand L is reactive under UV light irradiation (like 4VP which gives the Type II reaction), in order to make cis-$W(CO)_4L_2$, one has to irradiate $W(CO)_5L$

with visible light in the absence of L, limiting the chemical yield to 50% but avoiding ligand side photoreactions.

Summary.

The results described in this thesis indicate that for the Ester-pyridyl ketone ligand in pentaammine or bis(2,2'bipyridine) Ruthenium(II) complexes, internal conversion to lower excited state competes directly with the chemical reaction from the $n\pi^*$ Internal Ligand upper excited state. This competition allows an accurate estimation of the rate of the internal conversion. In the case of the bis(2,2'bipyridine) complexes, we obtained some evidence that an inter-ligand communication may exist. Possibly singlet energy transfer from 2,2'bipyridine to coordinated pyridyl ketones and triplet energy transfer from the coordinated pyridyl ketones to 2,2'bypyridine.

The case of Tungsten carbonyl complexes is different. Internal Conversion is much faster than chemical reaction. Lower excited states (LF and MLCT) give distinct photochemistry. Research towards this direction forced us to introduce a new mechanism for cis-$W(CO)_4L_2$ formation. This product comes from $W(CO)_5L$ primarily not by loss of CO (at least for irradiations at wavelengths longer than 400 nm), as was believed, but by loss of L and subsequent attack of the $W(CO)_5$ intermediate on a ground state molecule. It appears that the classical photoexchange reaction

$$W(CO)_5L + X \xrightarrow{h\nu} W(CO)_5X + L$$

and the Tungsten Tetracarbonyl formation

$$2\ W(CO)_5L \xrightarrow{h\nu} W(CO)_6 + cis\text{-}W(CO)_4L_2$$

follow the same mechanism.

Suggestions for Further Study.

The problem of the bimolecular photochemical reaction of the coordinated pyridyl ketone ligand remains. A reactive hydrogen donor-like sodium succinate should be a good candidate for intramolecular photoreduction of coordinated 4-Acetylpyridine. Another direction would be to move to complexes having LF lowest excited state, but because of geometric and bonding reasons, photodissociation would be avoided. A good candidate would be trans-$[Rh(cyclam)(4PhBP)_2](BF_4)_2$ (cyclam = 1,4,8,11-Tetraazacyclotetradecane).[118] Thus, a direct comparison between IL ----> MLCt and IL ----> LF Internal Conversion rates would be made.

The Tungsten carbonyls open a new chapter in the possible carbonyl exchange reactions between coordinatively unsaturated carbonyls and coordinatively saturated ones. It would be interesting to see in other systems like $Fe(CO)_5$, irradiated with PPh_3 and yielding $Fe(CO)_3L_2$,[119] if the mechanism followed is Mechanism I or Mechanism II, according to our model.

Mechanism I.

$$Fe(CO)_5 \xrightarrow{h\nu, L} Fe(CO)_4L + CO$$

$$Fe(CO)_4L \xrightarrow{h\nu} Fe(CO)_3L + CO$$

$$Fe(CO)_3L \xrightarrow{L} Fe(CO)_3L_2$$

Mechanism II.

$$Fe(CO)_5 \xrightarrow{h\nu, L} Fe(CO)_4L + CO$$

$$Fe(CO)_4L \xrightarrow{h\nu} Fe(CO)_4 + L$$

$$Fe(CO)_4 + Fe(CO)_4L \longrightarrow Fe(CO)_5 + Fe(CO)_3L$$

$$Fe(CO)_3L + L \longrightarrow Fe(CO)_3L_2$$

A more careful study at high entering ligand and $W(CO)_5L$ concentrations would elucidate any minor bimolecular mechanism taking place in parallel to the dominating unimolecular process. A nice experiment to prove any bimolecular process involving the MLCT excited state would be to find an efficient quencher with intermediate triplet energy between LF and MLCT excited states. High concentrations of this quencher would quench all reactions originating from the LF excited state. By varying the complex concentration, a plot of $1/\Phi$ vs. 1/[complex] for tetracarbonyl product formation at long wavelength irradiation would be linear. It would be easier to perform

this experiment in methylcyclohexane since the spacing between the two excited states is larger than in benzene and the thermal activation would be slower.

EXPERIMENTAL

EXPERIMENTAL

Instrumentation

All compounds were identified on the basis of their physical and spectroscopic properties using the instruments described below.

Nuclear magnetic resonance spectra (nmr: Proton and Carbon-13) at 250 MHz were obtained with a Bruker WM-250 MHz Fourier Transform Nuclear Magnetic Resonance Spectrophotometer. All chemical shifts (δ) are reported in parts per million (ppm) downfield from tetramethylsilane (TMS). All coupling constants (J) are reported in Hz.

Infrared absorption spectra (IR) were determined either on a Perkin Elmer model 283B or on a Perkin Elmer model 599 spectrophotometer. All absorptions are reported in wavenumbers (cm^{-1}) and are characterized as broad (b), strong (s), medium (m) and weak (w).

Low resolution mass spectra (ms) were determined on a Finnigan 4021 Gc-Ms at an ionization potential of 70 eV for electron impact ionization. Melting points (mp) were

determined with a Thomas Hoover capillary melting point apparatus. All melting points are uncorrected. Elemental analyses were performed by Spang Microanalytical Laboratory, Eagle Harbor, Michigan 49951. Absorption spectra were measured with a Varian Cary 21 spectrophotometer, courtesy of Dr. Chang (all ε are reported in units of M^{-1} cm^{-1}). Emission spectra were measured on a Perkin Elmer MPF-44A fluorescence spectrophotometer equipped with a differential corrected spectra unit and Hitachi phosphorescence accessory.

Preparative scale separations were done on a Varian Aerograph model 920 gas chromatograph fitted with a thermal conductivity detector. Analytical scale separations were done either on a model 1200 Varian Aerograph fitted with a flame ionization detector or on a High Pressure Liquid Chromatography system composed of two model 110A Beckman pumps, a DuPont Instruments column compartment fitted with an injection port, and a model LC-75 Perkin Elmer spectrophotometric detector. Relative peak areas were determined using an infotronics CRS 309 Computing Integrator for gas chromatographic analysis or a model 3380 Hewlett Packard recorder-integrator for HPLC analysis.

Chemicals

Solvents

Benzene: 3.5 liters of thiophene-free benzene (Fischer Scientific or Mallinckrodt Chemical Co.) was stirred over

several changes of concentrated sulfuric acid (300 nm) until the sulfuric acid remained colorless. The benzene was washed first with distilled water (2 x 300 ml), then with saturated sodium bicarbonate (3 x 300 ml) until a white precipitate no longer formed. It was then washed with distilled water (2 x 200 ml) and dried over anhydrous magnesium sulfate. It was refluxed over phosphorous pentoxide overnight and distilled through a one meter column packed with stainless steel helices; the first and last 300 ml being discarded: bp = 80.0°C.

Acetonitrile: Aldrich Gold Label acetonitrile was used as received. Acetonitrile (Fischer Scientific Co.) was purified according to the procedure of O'Donnell.[120] Analytical grade acetonitrile was distilled from 10 g anhydrous sodium carbonate and 15 g potassium permaganate, made slightly acidic with concentrated sulfuric acid, decanted from the precipitated ammonium sulfate and distilled through a half meter column packed with stainless steel helices: bp = 82°C.

Methylcyclohexane: Methylcyclohexane (Fischer Scientific, Eastman Chemical Co.) was purified according to the procedure of Foster.[121] Methylcyclohexane (500 ml) was stirred over several changes of concentrated sulfuric acid (100 ml) until the sulfuric acid remained colorless. It was washed with distilled water (3 x 200 ml), saturated potassium carbonate (3 x 100 ml), distilled water (2 x 100 ml) and dried over anhydrous potassium carbonate. It was

distilled through a 30 cm Vigreaux column over lithium aluminum hydride; the first and last 50 ml being discarded: bp = 101°C.

Tetrahydrofuran: Tetrahydrofuran (Fischer Scientific, EM Science or Mallinckrodt Chemical Co.) was purified according to a procedure cited in *Organic Syntheses.*[122] Tetrahydrofuran (1.5 l) was refluxed over 10 g cuprous chloride overnight and distilled through a 30 cm Vigreaux Column, then it was distilled three times over lithium aluminum hydride; the first and the last 10% being discarded: bp = 66°C.

Ethanol: Ethanol was refluxed overnight over sodium metal and distilled; the first and last 10% being discarded: bp = 78°C.

Methanol: Methanol (Mallinckrodt SpectAR and J. T. Baker Spectrophotometric grade) was used as received.

Dichloromethane: Dichloromethane (Fischer Scientific Co.) was distilled over lithium aluminum hydride; the first and the last 10% being discarded: bp = 39.5°C.

Hexane: UV grade Hexane (Burdick & Jackson Laboratories, Inc.) was used as received. Mixed Hexane (EM Science) was purified by washing with sulfuric acid in a manner similar to benzene, dried with anhydrous sodium sulfate, magnesium sulfate or potassium carbonate and distilled over calcium hydride; the first and the last 10-20% being discarded: bp = 69 $\pm$ 2.5°C.

Ethyl Acetate: UV grade Ethyl Acetate (Burdick & Jackson Laboratories, Inc.) was used as received.

Internal Standards

n-hexadecane (C16): was available from previous work.

n-tetradecane (C14): n-tetradecane, pure grade was obtained from Phillips Petroleum Co. and used as received.

n-tridecane (C13): was available from previous work.

p-dichlorobenzene (pDCB): was obtained from Matheson Coleman & Bell Chemical Co. and used as received.

Methyl benzoate: was obtained from Aldrich Chemical Co. and used as received.

External Standards

acetophenone: acetophenone (Fischer Scientific Co.) was passed through an alumina column and then fractionally distilled through a 30 cm Vigreaux column; the first and last 20% being discarded. Pure acetophenone (>99.9% by g.c.) was obtained by subsequent spinning band distillation.

n-heptadecane (C17): was obtained from Chemical Samples Co. and used as received.

pentacarbonyl-(4-acetylpyridine) Tungsten(0): See below.

Quenchers

Ethyl sorbate: ethyl sorbate was used as received from Aldrich Chemical Co.

Anthracene: Anthracene (blue-violet fluorescence) was used as received from Matheson Coleman & Bell Chemical Co.

4-Valerylpyridine: See below.

Actinometers

Valerophenone: was prepared by the Friedel Crafts acylation of benzene by valeryl chloride by Dr. B. P. Giri.

o-methylvalerophenone: was prepared earlier by Dr. C. P. Chen.[90]

o-methylbutyrophenone: was prepared earlier by Dr. C. P. Chen.[90]

Potassium Reineckate: was prepared from the ammonium Reinecke's salt ($[(NH_4Cr(NH_3)_2(SCN)_4].H_2O$ - Aldrich Chemical Co.) according to the procedure of Adamson.[98] The ammonium Reinecke's salt (10 g, 28.2 mmol) was dissolved in 50 ml of warm (40-50°C) water. Solid potassium nitrate (28.5 x 1.5 mmol) was added followed by cooling over ice and filtration. The product was recrystallized from a warm, 5% potassium nitrate solution in water, washed with 2 ml of cold water and dried over phosphorous pentoxide under vacuum. All the operations were carried out in dim red light. UV-Vis. λ_{max} 392 nm, broad absorption between 480 and 580 nm; IR (KBr): 3600-2800 (b.s), 3310 (s), 3200 (s), 2240-1800 (b.s), 1605

(s), 1395 (s), 825 (w), 710 (s), 520 (m), 480 (m), 352 (s) cm^{-1}.

Uranyl nitrate: uranyl nitrate ($UO_2(NO_3)_2.6H_2O$) - Analytical reagent was used as received from Mallinckrodt Chemical Company.

Ketones

Acetophenone: See above.

Benzophenone: received from Aldrich Chemical Co. and recrystallized twice from petroleum ether; mp., 49-50°C.

1-phenyl-1-butanone; butyrophenone:[123] n-butyl bromide (59 g, 0.43 mol) in 80 ml of ether was added to a well-stirred mixture of 11.7 g (0.48 mol) of magnesium turnings and 30 ml of anhydrous ether; when the reaction was completed, 25 g (0.24 mol) of benzonitrile in 100 ml of ether was added, and the reaction mixture was refluxed for 7 hrs. Then 200 ml of 10 M HCl was added and reflux continued for another 12 hrs. At the end of the period, the reaction mixture was cooled and transferred to a separatory funnel where the ether layer was collected. The water layer was washed three times with ether and the ether extracts were combined with the original ether layer which subsequently was washed with water followed by saturated potassium carbonate solution; dried with anhydrous potassium carbonate. Ether was removed under reduced pressure and the slightly yellow product was fractionally distilled twice to give 16.9 g (46%) product which was >99.9% pure by gc., bp =

117°C (9.3 Torr); UV (CH_3CN) λ_{max} 277 nm (ε 954), 317.5 nm (ε 56), ε_{313} = 54.50 M^{-1} cm^{-1}; H-nmr ($CDCl_3$): (δ) 1.0 (t,3H), 1.5-2.0 (qui,2H), 2.9 (t,2H), 7.4-7.6 (m,3H aromatic), 7.9-8.1 (m,2H aromatic); m/e (rel. int.): 148 (28), 106 (12), 105 (100), 77 (8), 55 (2); IR (CCl_4): 3090 (w), 3070 (w), 2965 (s), 2940 (m), 1694 (s), 1601 (m), 1451 (s), 1414 (w), 1370 (m), 1360 (m), 1214 (s), 1180 (m), 900 (w) cm^{-1}.

4-acetylpyridine; 4AP: was obtained from Aldrich Chemical Co. and vacuum distilled before use or was prepared by the method described by Rosemary Bartoszek, Ph.D. Thesis, Michigan State University, 1981.

4-benzoylpyridine; 4Bzpy: was obtained from Aldrich Chemical Co. and recrystallized three times from petroleum ether prior to use; mp., 72°C.

1-(4-pyridyl)butanone (4-butyrylpyridine); 4BP:[124,125] A solution containing 59 g (0.48 mol) of n-propyl bromide in 80 ml of anhydrous ether was added dropwise to a well-stirred mixture of 11.7 g (0.50 mol) of magnesium turnings and 30 ml of anhydrous ether. After the reactions subsided, a solution containing 25 g (0.24 mol) of 4-cyanopyridine in 60 ml of anhydrous ether and 40 ml of benzene was added to the stirred solution over 5 min. The resultant mixture was refluxed with stirring for 7 hrs. At the end of the period, 200 ml of a 10 M hydrochloric acid solution was added slowly with cooling, and reflux was continued for another 12 hrs. Then, upon cooling, the solution was made basic with solid

potassium carbonate and solid potassium hydroxide. Filtration removed the precipitated salts which were washed with ether. The aqueous solution was extracted with ether until the ether extracts were colorless. The ether extracts were combined, washed three times with 30 ml saturated potassium carbonate solutions, one time with 30 ml of a saturated salt solution, and dried with anhydrous potassium carbonate. Ether was removed under reduced pressure to leave a brown oil which was distilled three times under vacuum to give 6.4 g (18%) of product which was >99.9% pure by gc. UV (methylcyclohexane) λ_{max} 279 nm (ε 3390); H-nmr ($CDCl_3$): (δ) 1.01 (t,3H), 1.78 (hext,2H), 2.97 (t,2H), 7.74 (dd,2H aromatic), 8.80 (dd,2H aromatic); m/e (rel. int.) 149 (M,25), 121 (27), 106 (100), 78 (93), 51 (79); IR (CCl_4): 3075 (w), 3030 (w), 2970 (s), 2940 (w), 1700 (s), 1412 (s), 1271 (m), 1217 (m), 1206 (s), 1063 (w), 990 (w), 900 (w) cm^{-1}.

1-(4-pyridyl)pentanone (4-valerylpyridine); 4VP:[124,125] was synthesized by the method used for 1-(4-pyridyl)butanone using 79 g (0.58 mol) of n-butylbromide, 14 g (0.59 mol) of magnesium turnings and 30 g (0.29 mol) of 4-cyanopyridine. The synthesis gave a brown oil which was distilled four times under vacuum to give 15 g (32%) of the product which was >99.9% pure by gc. bp., 140-141°C (10 Torr); UV (methylcyclohexane) λ_{max} 279 nm (ε 2892); H-nmr (C_6D_6): (δ) 0.81 (t,3H), 1.20 (hex,2H), 1.52 (qui,2H), 2.44 (t,2H), 7.33 (dd,2H aromatic), 8.58 (dd,2H aromatic); ($CDCl_3$): (δ) 0.80

(t,3H), 1.25 (hex,2H), 1.55 (qui,2H), 2.85 (t,2H), 7.59 (dd,2H aromatic), 8.63 (dd,2H aromatic); C-nmr (C_6D_6; 2.5% $Cr(acac)_3$ added): (δ) 13.9, 22.5, 25.9, 38.4, 121, 142.9, 151.1, 199.1; IR (CCl_4): 3080 (w), 3030 (w), 2960 (s), 2935 (s), 1705 (s), 1595 (w), 1555 (w), 1410 (s), 2269 (m), 1222 (m), 1210 (m), 1070 (w) cm^{-1}; m/e (rel. int.): 164 (M+1,100), 121(62), 106(66), 78(18), 51(11).

4-phenyl-1-(4-pyridyl)butanone; 4PhBP: A solution containing 43.8 g (0.22 mol) of 1-bromo-3-phenyl propane (Aldrich Chemical Co.) in 80 ml of anhydrous ether was added dropwise to a well-stirred mixture of 5.35 g (0.22 mol) of magnesium turnings and 30 ml of anhydrous ether in a flame-dried, three-neck, round bottom flask equipped with a mechanical stirrer. The reaction was assisted to start by traces of iodine. After the vigorous reaction subsided, the reaction mixture was refluxed for 10 hrs. under argon until all the magnesium had been consumed. Then a solution containing 20.8 g of 4-cyanopyridine in 200 ml of 3:2 (v/v) anhydrous ether - benzene was added to the stirred solution upon cooling over 5 min. The resultant mixture was refluxed with stirring for 12 hrs. At the end of the period, 200 ml of a 10 M hydrochloric acid solution was poured slowly with cooling. Reflux was continued for another 24 hrs. Then, upon cooling, the solution was made basic by addition of solid potassium carbonate. Filtration removed the precipitated salts which were washed with ether. The aqueous solution was extracted with ether until the ether

extracts were colorless. All the ether solutions were combined, washed three times with 30 ml saturated potassium carbonate solution and dried with anhydrous potassium carbonate. Ether was removed under reduced pressure to leave a brown oil which was fractionally distilled under vacuum to give a yellow solid. This product was dissolved in benzene, decolorized with decolorizing carbon and precipitated by the addition of pentane and cooling in the refrigerator for 24 hrs. to give 22.4 g (45%) of white flakes. (Pure product was also obtained by a spinning-band distillation following the first fractional distillation). mp., 38-39°C; bp., 156-157°C (11.6 Torr); UV (CH_3CN) λ_{max} 280 nm (ε 2078), ε_{313} = 124 M^{-1} cm^{-1}; nmr ($CDCl_3$): (δ) 2.08 (qui,2H), 2.72 (t,2H), 2.96 (t,2H), 7.1-7.3 (m,5H aromatic), 7.65 (dd,2H aromatic), 8.76 (dd,2H aromatic); IR (CCl_4): 3040 (w), 3010 (m), 2920 (b,w), 2840 (w), 1690 (s) cm^{-1}; m/e (rel. int.): 225(M,16), 205(20), 104(100), 91(46), 78(32), 65(14), 51(32).

n-butyl-4-[(4-pyridyl)carbonyl] butyrate; 4EsterBP: was prepared from the enamine[125,127] derivative of 4-acetylpyridine which was added to n-butyl acrylate (Aldrich Chemical Co.).

4-Acetylpyridine (10 g, 0.0826 mol); pyrrolidine (30 g, 0.422 mol, 5 molar excess) and a catalytic amount of p-toluene sulfonic acid (0.2 g) were dissolved in 150 ml of purified (as described above) benzene and refluxed for 24 hrs. with continuous removal of water (dean stark). Benzene

and excess pyrrolidine were removed under reduced pressure and the resulting oil was diluted with 80 ml of acetonitrile. n-Butyl acrylate (16 g, 1.5 molar excess) was added and the solution was refluxed for 24 hrs. with a drying tube on the top of the condenser. Then 30 ml of an aqueous solution containing 14 g of sodium acetate and 14 g of an 80% acetic acid solution was added. The resulting solution was refluxed for another 2.5 hrs. At the end of the period, 100 ml of water was poured into the solution and addition of a large excess of solid potassium carbonate resulted in the separation of two phases. The lower water layer was washed several times with ether and the ether extracts were combined with the upper organic layer. The solution was dried with anhydrous potassium carbonate and the ether was removed under reduced pressure. Distillation under vacuum gave a slightly brown oil collected between 150 and 200°C. This oil was passed through an Alumina column (Alumina Activated 80-200 mesh: dimensions: 20 cm x 1 cm; solvents: eluent, 100 ml hexane followed by 85% hexane, 15% ethyl acetate) collecting 10 ml fractions. In the first 60 ml, there were only impurities. Between 100 and 150 ml, there was found only product. Analysis of the fractions was performed by gas chromatography (gc column C at 210°C). All solvents were removed and the product was distilled under vacuum once more to give 0.82 g (4%). bp., 163-164°C (11 Torr); UV (CH_3CN) λ_{max} 274.5 nm (ε 1884), ε_{313} = 112 M^{-1} cm^{-1}; H-nmr ($CDCl_3$): (δ) 0.92 (t,3H), 1.38 (hex,2H), 1.61

(qui,2H), 2.07 (qui,2H), 2.45 (t,2H), 3.09 (t,2H), 4.10 (t,2H), 7.75 (dd,2H aromatic), 8.81 (dd, 2H aromatic); IR (CCl_4): 2965 (s), 2938 (s), 2875 (m), 1718 (s), 1703 (s), 1405 (s), 1218 (s), 1202 (s), 1150 (m), 1065 (m), 1048 (m), 812 (m) cm^{-1}; m/e (rel. int.): 249 (M,4), 175 (23), 147 (25), 121 (12), 106 (100), 85 (21), 78 (61), 51 (37).

Pyridyl Ketone Hydrochloride Salts

Both hydrochloride salts were prepared by bubbling hydrogen chloride gas through an ether solution of the pyridyl ketone. The salts were purified by repeating recrystallizations from methylene chloride and n-pentane until a colorless product was received. The final product was washed with ether and dried under vacuum.

4-phenyl-1-(4-pyridyl)butanone hydrochloride; 4PhBP.HCl: mp., 130-131°C, decomposes; UV (CH_3CN) λ_{max} 275 nm (ε 1238), ε_{313} = 104 M^{-1} cm^{-1}; (CH_2Cl_2) λ_{max} 274 (ε 2734), ε_{313} = 166 M^{-1} cm^{-1}; H-nmr (D_2O): (δ) 8.82 (d,2H,J=6.1), 8.20 (d,2H,J=6.4), 7.23-7.12 (m,5H), 3.07 (t,2H,J=7.0), 2.61 (t,2H,J=7.6), 1.96 (qui,2H,J=7.0); IR (KBr): 3190 (w), 3090 (m), 3062 (s), 3029 (s), 1700 (s), 1593 (s), 1487 (s), 1223 (m), 1192 (m), 790 (s), 744 (s), 695 (s) cm^{-1}.

n-butyl-4-(4-pyridyl)carbonyl butyrate hydrochloride; 4EsterBP.HCl: mp., 137-138°C, decomposes; UV (CH_3CN) λ_{max} 271 nm (ε 2941), ε_{313} = 82 M^{-1} cm^{-1}; H-nmr (D_2O): (δ) 8.88 (d,2H,J=5.8), 8.33 (d,2H,J=5.8), 4.00 (t,2H,J=6.4), 2.41 (t,2H,J=7.3), 1.94 (qui,2H,J=7.0), 1.50 (qui,2H,J=7.0), 1.23

(hex,2H,J=7.3), 0.77 (t,3H,J=7.3); IR (KBr): 3050 (w), 2960 (w), 1725 (s), 1700 (s), 1593 (s), 1491 (s), 1381 (m), 1280 (s), 1228 (s), 1178 (s), 1078 (m), 800 (s), 745 (s) cm^{-1}.

Nitrogen Coordinating Ligands

Methyl-(4-pyridyl)formate (Methyl Isonicotinate); MeINic: was obtained from Aldrich Chemical Co. and was distilled under reduced pressure; the first and last 10% being discarded.

4-Cyanopyridine; 4CNpy: was used as received from Aldrich Chemical Co.

2,2'bipyridine; bipy: was used as received from Aldrich Chemical Co.

1,10-Phenanthroline, monohydrate; phen: was used as received from J. I. Baker Chemical Co.

2,2'bipyrimidine; bipym: was used as received from Alfa Products.

Tetraphenylporphyrine; TPP: was used as received from Aldrich Chemical Co.

Octaethylporphyrine; OEP: was obtained from Dr. Chang and was used without any further purification.

Pyrazine; pyz: was used as received from Aldrich Chemical Co.

4,5-Diazafluorene: was used as obtained from Dr. W. R. Cherry; University of Louisiana.

Photoreduction Products

In the photoreduction of acetophenone by THF[99], the following products were identified by gc/ms:

Octahydro-2,2'bifuran: m/e (rel. int.): 142 (0.7), 97 (0.5), 84 (2), 73 (0.9), 72 (4), 71 (100), 70 (39), 55 (3), 43 (30), 42 (5), 41 (12), 40 (3).

2-(2-tetrahydrofuryl) acetaldimine: One molar solution (2.8 ml) of acetophenone in 1:1 (v/v) THF/CH_3CN was degassed and irradiated for two days at 313 nm. The product was isolated by preparative gas chromatography using a U-shaped trap containing $CDCl_3$ and kept in a mixture of acetone/dry ice; nmr ($CDCl_3$): (δ) 2.00-1.88 (m,4H), 2.19 (s,3H), 2.62 (s,1H; the size of this peak descreases by addition of D_2O), 3.85-4.00 (m,3H); m/e (rel. int.): (by gc/ms) 71 (81), 44 (5), 43 (100), 42 (4), 41 (37), 40 (23).

1-phenyl 1-(2-tetrahydrofuryl) ethanol: m/e (rel. int.): 192 (M,1), 121 (100), 105 (8), 77 (4), 71 (26), 43 (30).

p-(2-tetrahydrofuryl) acetophenone: m/e (rel. int.): 147 (2), 122 (31), 121 (6), 107 (100), 103 (4), 80 (3), 79 (60), 78 (14), 77 (34), 53 (3), 51 (9), 45 (3), 43 (11), 40 (2).

Acetophenone pinacol: Identified by comparison of the g.c. retention time to an authentic sample which had been synthesized and purified by Dr. M. J. Thomas.

Type II Products

n-butyl acrylate: A 0.02 M solution (2.8 ml) of cis-$[Ru(bipy)_2(4EsterBP)_2](BF_4)_2$ in acetonitrile was degassed and irradiated for a week at 313 nm. The photoproduced n-butyl acrylate was identified by comparison of the g.c. retention time to an authentic sample (obtained from Aldrich). Its identity was also verified by gc/ms.

Photochemically Produced n-butylacrylate: m/e (rel. int.): 113 (0.23), 99 (1.32), 85 (6.39), 73 (35), 69 (1.44), 57 (4.5), 56 (44), 55 (100).

n-butyl acrylate obtained from Aldrich: m/e (rel. int.): 129 (M,0.38), 113 (0.34), 99 (1.38), 85 (6.5), 73 (41), 69 (1.58), 57 (5.9), 56 (56), 55 (100).

Ruthenium Complexes

Chloropentaammine Ruthenium(II) dichloride; $[Ru(NH_3)_5Cl]Cl_2$:[128,129] Hexaammine Ruthenium(III) trichloride (Strem Chemical, Inc.) (20 g, 6.5 mmol) was dissolved in 70 ml of 6 M hydrochloric acid solution with warming. The solution was refluxed for 4 hrs., during which a yellow precipitate formed. The mixture was cooled and filtered. The precipitate was washed first with 10 ml of 6 M hydrochloric acid solution then with 5 ml of methanol and was dried under vacuum to give 1.25 g (66%) of bright yellow crystals. IR (KBr): 3600-3000 (b,s), 1618 (m), 1300 (s), 800 (m) cm^{-1}.

Pentaamminepyridine Ruthenium(II) tetrafluoroborate and the pyridine substituted derivatives: These complexes were synthesized by a modification of Ford and Taube's methods.[15,75]

General synthetic procedure: Silver oxide (158 mg, 0.683 mmol) was dissolved in 4 ml of distilled water by the dropwise addition of trifluoroacetic acid with stirring. Chloropentaammine Ruthenium(III) dichloride (200 mg, 0.683 mmol) was added. The resultant mixture was stirred, then digested (heated to boiling to complete the precipitation of silver chloride). After 20 min., the precipitate was filtered then washed with two 5 ml portions of distilled water. The filtrate was diluted to 25 ml with distilled water and placed in an addition funnel. The pyridyl ketone ligand, in 3-10 molar excess, was flushed with argon in a 3-neck 100 ml round bottom flask covered with aluminum foil. Methanol (2 ml) was added to improve ligand solubility in the resultant aqueous solution.

Granular zinc (50 g) was washed with 50 ml of 1.2 M hydrochloric acid solution. The acid solution was decanted and 5 g of mercuric chloride was added to the zinc, which reacted immediately to give the amalgam. Water, 150 ml, and 5 ml of concentrated sulfuric acid were added on the top and the whole mixture was stirred for 10 min. The zinc mercury-amalgam was washed with distilled water until the washings were slightly acidic, then with acetone and finally with

ether. It was air dried and packed into a column which was fitted to the middle neck of a 3-neck round bottom flask containing the ligand. The other two necks were stoppered with rubber septums. On top of the zinc-mercury amalgam column (reduction column) was fitted a funnel containing the Ruthenium(III) solution, on top of which was attached another funnel containing 20 ml of distilled water. The entire system was flushed with argon for 10 min.

The light yellow Ruthenium(III) solution (25 ml) was passed through the reducing column over a period of 30 minutes, giving a deep yellow Ruthenium(II) solution which was added to the stirred ligand slowly. When the addition was completed, the reducing column was washed with two 10 ml portions of distilled water. Stirring was continued for 30 min. and then ammonium tetrafluoroborate (144 mg, 0.683 x 2 mmol) was added directly to the flask. The resultant solution was refrigerated for a minimum of 12 hrs. The water was then removed under reduced pressure. The resultant precipitate was dissolved in the minimum amount of dry acetone and added dropwise to 500 ml of argon bubbled ether. The precipitated complex was immediately filtered. The product was purified by reprecipitation from acetone/ether repeating the method of the original complex isolation. The precipitate was dried under vacuum for 12 hrs. and stored in the dark.

Pentaamminepyridine Ruthenium(II) tetrafluoroborate; $[Ru(NH_3)_5(py)](BF_4)_2$:[101] was synthesized using 200 mg (0.683

mmol) of $[Ru(NH_3)_5Cl]Cl_2$ and 2 ml of pyridine (1.97 g, 0.683 x 3.7 mmol). The complex was recrystallized once from acetone/ether to yield 180 mg (60%). UV-Vis. (water) λ_{max} 244 nm (ε 3798), 407 nm, (ε 4900); IR (KBr): 3700-3000, 1636, 1525-1350, 1290, 1225-925, 760, 700 cm^{-1}.

Pentaammine 4-acetylpyridine Ruthenium(II) tetrafluoroborate; $[Ru(NH_3)_5(4AP)](BF_4)_2$:[101] was synthesized using 200 mg (0.683 mmol) of $[Ru(NH_3)_5Cl]Cl_2$ and 580 mg of 4-acetylpyridine (0.683 x 7 mmol). The complex was recrystallized twice from acetone/ether to yield 230 mg (70%). UV-Vis. (CH_3CN) λ_{max} 268.5 nm (ε 3696), 509 nm (ε 11256), ε_{313} = 336 M^{-1} cm^{-1}; H-nmr (D_2O): (δ) 8.60 (d,J=6.8), 7.53 (d,J=6.2), 2.52 (s); IR (KBr): 3650-3050 (b,s), 1685 (s), 1639 (w), 1590 (m), 1420 (m), 1365 (w), 1282 (s), 1200 (s), 1170 (w), 1225-925 (b,s), 1005 (s), 962 (w), 835 (w), 796 (w), 754 (w), 729 (w) cm^{-1}.

Pentaammine methylisonicotinate Ruthenium(II) tetrafluoroborate; $[Ru(NH_3)_5(MeINic)](BF_4)_2$:[76,101] was synthesized using 200 mg (0.683 mmol) of $[Ru(NH_3)_5Cl]Cl_2$ and 936 mg (0.683 x 10 mmol) of methylisonicotinate. The complex was recrystallized twice from acetone/ether to yield 296 mg (87%). UV-Vis. (CH_3CN) λ_{max} 264 nm (ε 4044), 488.5 nm (ε 11865), ε_{313} = 319 M^{-1} cm^{-1}; IR (KBr): 3700-3000 (b,s), 3360 (s), 3290 (s), 1730 (s), 1634 (m), 1606 (s), 1342 (m), 1325 (m), 1234 (m), 1200 (s), 1107 (s), 1150-850 (b,s), 761 (w), 740 (w), 675 (m), 610 (m), 573 (w) cm^{-1}.

Pentaammine 4-phenyl-1-(4-pyridyl)butanone Ruthenium(II) tetrafluoroborate; $[Ru(NH_3)_5(4PhBP)](BF_4)_2$: was synthesized using 200 mg (0.683 mmol) of $[Ru(NH_3)_5Cl]Cl_2$ and 768 mg (0.683 x 5 mmol) of 4-phenyl-1-(4-pyridyl) butanone. The complex was recrystallized twice from acetone/ether to yield 316 mg (79%). UV-Vis. (CH_3CN) λ_{max} 268 nm (ε 3860), 505 nm (ε 10572), ε_{313} = 432 M^{-1} cm^{-1}; H-nmr (D_2O): (δ) 8.35 (d,2H), 7.28 (d,2H), 7.25-7.10 (m,5H), 2.95-2.80 (broad,2H), 2.7-2.5 (broad, 2H), 2.0-1.9 (broad,2H); IR (KBr): 3700-2900 (b,s), 1720-1557 (b,s), 1690 (s), 1680 (s), 1592 (s), 1405 (s), 1300 (m), 1200 (s), 1160-960 (b,s), 745 (w), 692 (w) cm^{-1}.

Pentaammine n-butyl-4-[(4-pyridyl) carbonyl] butyrate Ruthenium(II) tetrafluoroborate; $[Ru(NH_3)_5(4EsterBP)](BF_4)_2$: was synthesized using 200 mg (0.683 mmol) of $[Ru(NH_3)_5Cl]Cl_2$ and 850 mg (0.683 x 5 mmol) of n-butyl-4-[(4-pyridyl) carbonyl] butyrate. The complex was recrystallized twice from acetone/ether to yield 334 mg (80%). UV-Vis. (CH_3CN) λ_{max} 266.5 nm (ε 2989), 507 nm (ε 8853), ε-313 = 433 M^{-1} cm^{-1}; H-nmr (D_2O): (δ) 8.60 (d,2H), 7.52 (d,2H), 4.00 (t,2H,J=6.2), 3.00 (t,2H,J=5.5), 2.38 (t,2H,J=6.3), 1.91 (qui,2H,J=6.6), 1.49 (qui,2H,J=7.0), 1.23 (hex,2H,J=6.6), 0.76 (t,3H,J=6.9); IR (KBr): 3680-3020 (b,s), 2975 (m), 2870 (m), 1717 (s), 1685 (s), 1635 (s), 1592 (s), 1420 (m), 1290 (s), 1200 (s), 1230-900 (b,s), 835 (m), 750 (m), 540 (m) cm^{-1}.

Pentaammine 4-cyanopyridine Ruthenium(II) tetrafluoroborate; $[Ru(NH_3)_5(4CNpy)](BF_4)_2$:[130] was synthesized using 200 mg (0.683 mmol) of $[Ru(NH_3)_5Cl]Cl_2$ and 284 mg (0.683 x 4 mmol) of 4-cyanopyridine. The complex was recrystallized twice from acetone/ether to yield 161 mg (51%). UV-Vis. (water) λ_{max} 257.5 nm (ε 22680), 402 nm (ε 9536); IR (KBr): 3700-3000 (b,s), 2180 (s), 1691 (s), 1610 (s), 1429 (s), 1290 (s), 1200 (s), 1225-925 (b,s), 820 (w), 798 (w), 718 (w) cm^{-1}.

Diaquo cis-bis(2,2'bipyridine) Ruthenium(II) dichloride; cis-$[Ru(bipy)_2Cl_2].2H_2O$: was prepared by Dwyer's method.[78,79,131] Potassium hexachlororuthenate (Strem Chemicals, Inc.) (1.15 g, 2.67 mmol) was dissolved in 6.6 ml of 1.0 N hydrochloric acid solution. 2,2'bipyridine (1.114 g) was added and the resulting suspension was stirred for 10 days with a magnetic stirrer at room temperature in a stoppered flask covered with aluminum foil. The brownish-orange precipitate was collected, washed with water, and air dried to yield 1.46 g of $[bipyH][Ru(bipy)Cl_4].H_2O$. IR (KBr): 3650-3300 (b,s), 3200-2750 (b,s), 1618 (s), 1604 (s), 1583 (s), 1525 (s), 1470 (s), 1450 (s), 1431 (s), 1420 (s), 1320 (s), 1310 (s), 1268 (m), 1244 (m), 1230 (m), 1171 (s), 1160 (s), 1027 (m), 1010 (m), 990 (m), 980 (w), 919 (s), 868 (m), 774 (s), 768 (s), 725 (s), 638 (w), 622 (w), 602 (m) cm^{-1}.

$[bipyH][Ru(bipy)Cl_4].H_2O$ (1 g) was suspended in 20 ml of pure DMF and the mixture was refluxed for 3 hrs. The

initially formed brown solution soon turned to a deep brown-violet and finally to a deep violet color. During the last hour, most of the solvent was slowly distilled off, leaving a volume of about 5 ml. Then the solution was cooled and suspended in cold acetone (20 ml); 894 mg of dark, almost black crystals was collected. This product was recrystallized/ reduced by suspending it in 100 ml of 1:2 (v/v) water - ethanol and refluxing until all the solid had been dissolved to form the deep brown cis-$[Ru(bipy)_2(H_2O)Cl]^+$ complex. This solution was gravity-filtered, 10 g of LiCl was added into the filtrate solution and evaporated over a stream bath down to 45 ml. The solution remained at room temperature for 16 hrs. to complete crystallization. The crystals were washed with 20 ml of water then 10 ml of acetone and were dried under vacuum to give 593 mg (57%) of the deep purple cis-$[Ru(bipy)_2Cl_2].2H_2O$. UV-Vis. (CD_3CN) λ_{max} 244 nm (ε 31981), 297 nm (ε 53208) sh 288 nm, 378 nm (ε 8632), 553 nm (ε 9057); H-nmr ($CDCl_3$): (δ) 10.32 (d,J=5.9), 8.13 (d,J=8.1), 7.99 (d,J=8.1), 7.85 (t,J=7.9), 7.66-7.55 (m), 7.47 (t,J=8.0), 6.90 (t,J=6.8); IR (KBr): 3650-3150 (b,s), 3100 (w), 3070 (w), 1618 (m), 1600 (s), 1464 (s), 1444 (s), 1420 (s), 1310 (w), 1268 (w), 1120 (w), 1018 (m), 765 (s), 760 (s), 726 (m), 650 (w) cm^{-1}.

Aqueous cis-bis(1,10-Phenanthroline) Ruthenium(II) dichloride; cis-$[Ru(phen)_2Cl_2].2H_2O$:[78,79] was synthesized by the same method used for cis-$[Ru(bipy)_2Cl_2].2H_2O$ using 1.15

g (2.67 mmol) of potassium hexachlororuthenate (Strem Chemicals, Inc.) and 1.328 g (2.98 mmol) of 1,10-phenanthroline monohydrate. 487 mg (34%) of the deep purple - almost black - product was obtained. UV-Vis. (CD_3CN) λ_{max} 216 nm (ε 86159), 266.5 nm (ε 78476), 547 nm (ε 12012) sh 460 nm; IR (KBr): 3700-3100 (b,m), 3065 (w), 3042 (w), 1517 (m), 1421 (s), 1407 (s), 1283 (m), 1247 (m), 1195 (m), 1095 (m), 1088 (m), 840 (s), 765 (m), 714 (s) cm^{-1}.

Diaquo cis-bis(2,2'bipyridine) Ruthenium(II) dichloride and aqueous cis-bis(1,10-phenanthroline) Ruthenium(II) dichloride were transformed to the cis-bis(pyridine) or bis(substituted pyridine) bis(2,2'bipyridine) (or bis(1,10-Phenanthroline)) Ruthenium(II) tetrafluoroborate salts by refluxing them for 6 hrs. in 1:1 (v/v) water/methanol solution, containing 3-5 molar excess of the pyridyl ligand.[78,79] Addition of ammonium tetrafluoroborate and removal of all the solvents over a steam bath left the deep yellow-orange crude product which was dissolved in dry acetone, filtered, and precipitated by dropwise addition to 500 ml of ether. The product was recrystallized by dissolving it in dry acetone followed by the dropwise addition of ether until no more precipitation was observed; cooling in an ice bath completed the crystallization; the product was dried under vacuum.

<u>cis-bis(2,2'bipyridine)-bis(pyridine) Ruthenium(II) tetrafluoroborate; cis-$[Ru(bipy)_2(py)_2](BF_4)_2$</u>:[35,132] was synthesized using 100 mg (0.192 mmol) of cis-

$[Ru(bipy)_2Cl_2].2H_2O$ and 1 ml (0.98 g, 12.7 mmol) of pyridine. The complex was recrystallized twice from acetone/ether to yield 101 mg (70%). UV-Vis. (water) λ_{max} 243 (ε 29700) sh 254 nm, 289.5 nm (ε 67412), 338 nm (ε 20364), 463 nm (ε 14382) sh 428 nm; IR (KBr): 3420 (s), 3140 (s), 3049 (s), 2820 (w), 1600 (m), 1467 (s), 1445 (s), 1410 (s), 1160 (m), 1200-925 (b,s), 760 (s), 725 (s), 700 (s) cm^{-1}.

cis-bis(2,2'bipyridine)-bis(4-acetylpyridine) Ruthenium-(II) tetrafluoroborate; cis-$[Ru(bipy)_2(4AP)_2](BF_4)_2$:[132] was synthesized using 86.5 mg (0.166 mmol) of cis-$[Ru(bipy)_2Cl_2].2H_2O$ and 108 mg (0.166 x 2 mmol) of 4-acetylpyridine. Ammonium tetrafluoroborate (37.5 g, 0.166 x 2.2 mmol) was added. The complex was recrystallized twice from acetone/ether to yield 115 mg (78%) of the product. UV-Vis. (water) λ_{max} 243.5 nm (ε 20793) sh 254 nm, 288 nm (ε 67005), 445 nm (ε 14890) sh 392 nm; (CH_3CN) λ_{max} 244 nm (ε 18467) sh 252 nm, 286 nm (ε 49957), 422.5 nm (ε 11280) sh 364 nm, ε_{313} = 7588 M^{-1} cm^{-1}; H-nmr (CD_3CN): (δ) 2.54 (s,6H), 7.15-8.49 (m,16H), 8.9 (d,2H), 9.86 (d,2H); IR (KBr): 3650-3200 (b,s), 3070 (w), 1695 (s), 1604 (m), 1584 (w), 1465 (m), 1442 (m), 1425 (m), 1360 (m), 1260 (s), 1200-925 (b,s), 966 (m), 830 (s), 765 (m), 735 (m), 655 (w) cm^{-1}.

cis-bis(2,2'bipyridine)-bis(4-phenyl-1-(4-pyridyl) butanone) Ruthenium(II) tetrafluoroborate; cis-$[Ru(bipy)_2(4PhBP)_2](BF_4)_2$: was synthesized using 500 mg (0.961 mmol) of cis-$[Ru(bipy)_2Cl_2].2H_2O$ and 1.161 g (0.961 x

5.4 mmol) of 4-phenyl-1-(4-pyridyl)butanone. Ammonium tetrafluoroborate (216 mg, 0.961 x 5.4 mmol) was added. The complex was recrystallized twice from acetone/ether to yield 608 mg (61%) of the product. UV-Vis. (CH_3CN) λ_{max} 248 nm (ε 21557), 254 nm (ε 21972), 288 nm (ε 52180), 359 nm (ε 8997), 422 nm (ε 12768), 443 nm (ε 12353), ε_{313} = 7682 M^{-1} cm^{-1}; H-nmr (D_2O): (δ) 10.10 (d,J=1.10), 8.85 (d,J=5.5, Aromatic 4PhBP), 8.42 (d,J=6.2, Aromatic 4PhBP), 8.36 (d,J=8.4), 8.28 (d,J=8.4), 8.08 (t,J=7.7), 7.91-7.84 (m), 7.77-7.68 (m), 7.36-7.25 (m), 6.97-6.82 (m), 2.85 (t,J=6.7), 2.51 (t,J=7.7), 1.91 (qui,J=6.8); IR (KBr): 3700-2900 (b,m), 1687 (s), 1605 (m), 1468 (m), 1442 (m), 1412 (m), 1170-970 (b,s), 765 (s), 728 (m), 698 (m) cm^{-1}.

cis-bis(2,2'bipyridine)-bis(n-butyl-4-[(4-pyridyl) carbonyl] butanoate) Ruthenium(II) tetrafluoroborate; cis-$[Ru(bipy)_2(4EsterBP)_2](BF_4)_2$: was synthesized using 500 mg (0.961 mmol) of cis-$[Ru(bipy)_2Cl_2].2H_2O$ and 1.196 g (0.961 x 5 mmol) of n-butyl-4-[(4-pyridyl) carbonyl] butanoate which were refluxed in 20 ml of 1:1 (v/v) water/n-butanol for 6 hrs. Ammonium tetrafluoroborate (216 mg, 0.961 x 2.1 mmol) was added. . The product was recrystallized twice from acetone/ether to yield 916 mg (88%). UV-Vis. (CH_3CN) λ_{max} 293 nm (ε 64077) sh 255 nm, 365 nm (ε 10785), 403.5 nm (ε 12072), 456 nm (ε 13367) sh 483 nm, ε_{313} = 7895 M^{-1} cm^{-1}; H-nmr ($CDCl_3$): (δ) 10.02 (d,J=4.8), 9.05 (d,J=5.0, Aromatic 4EsterBP), 8.54 (d,J=5.1), 8.40 (d,J=8.4), 8.29 (t,J=9.4), 8.08-7.98 (m), 7.86-7.55 (m), (all the aromatic region

accounts for 24 H's), 4.05 (t,4H,J=6.6), 2.99 (t,4H,J=6.6), 2.38 (t,4H,J=7.1), 1.98 (broad m,4H,J=6.6), 1.58 (broad t,4H,J=6.6), 1.35 (broad m,4H,J=7.3), 0.90 (t,6H,J=7.3); (D_2O): (δ) 9.60 (d,J=5.1), 8.89 (d,J=5.9), 8.55-8.45 (m), 8.34-8.25 (m), 8.17-8.00 (m), 7.10 (broad t,J=6.6), (all the aromatic region accounts for 24 H's), 3.88 (t,4H,J=6.6), 2.98 (t,4H,J=6.6), 2.32 (t,4H,J=7.0), 1.87 (broad t,4H,J=7.3), 1.34 (broad t,4H,J=8.4), 1.08 (broad t,4H,J=7.7), 0.61 (t,6H,J=7.3); IR (KBr): 3700-3100 (b,s), 1725 (s), 1695 (s), 1635 (s), 1603 (s), 1461 (m), 1445 (m), 1418 (m), 1122 (s), 1082 (s) cm^{-1}.

cis-bis(1,10-Phenanthroline)-bis(pyridine) Ruthenium(II) tetrafluoroborate; $[Ru(phen)_2(py)_2](BF_4)_2$:[79] was synthesized using 50 mg (0.091 mmol) of cis-$[Ru(phen)_2Cl_2].H_2O$ and 1 ml (0.97 g, 12.6 mmol) of pyridine. Ammonium tetrafluoroborate (19 mg, 0.091 x 2 mmol) was added. The complex was recrystallized twice to yield 55 mg (76%) of the product. UV-Vis. (water)[133] λ_{max} 224 nm (ε 57916), 265 nm (ε 75707), 316 nm (ε 9337) sh 336 nm, 415 nm (ε 11375) sh 450 nm; IR (KBr): 3650-3125 (b,s), 3050 (s), 1632 (s), 1600 (s), 1580 (m), 1480 (m), 1443 (s), 1425 (s), 1410 (s), 1339 (m), 1298 (m), 1203 (m), 1200-900 (b,s), 840 (s), 763 (s), 719 (s), 700 (s) cm^{-1}.

cis-bis(1,10-Phenanthroline)-bis(4-acetylpyridine) Ruthenium(II) tetrafluoroborate; cis-$[Ru(phen)_2(4AP)_2](BF_4)_2$: was synthesized using 80 mg (0.150 mmol) of cis-$[Ru(phen)_2Cl_2].H_2O$ and 90.8 mg (0.150 x 5 mmol)

of 4-acetylpyridine. Ammonium tetrafluoroborate (32.8 mg, 0.150 x 2.1 mmol) was added. The complex was recrystallized twice from acetone/ether to yield 99.6 mg (76%). UV-Vis. (water) λ_{max} 222 nm (ε 66608), 263 nm (ε 70625), 415.5 nm (ε 19341) sh 434 nm; (CH_3CN) λ_{max} 221 nm (ε 61195), 264 nm (ε 66534), 409 nm (ε 16375) sh 440 nm, ε_{313} = 4813 M^{-1} cm^{-1}; nmr (CD_3CN): (δ) 8.9-7.6 (m,22H), 2.65 (s,6H); IR (KBr): 3650-3300 (b,s), 3240 (m), 3150 (m), 3045 (m), 1696 (s), 1429 (s), 1413 (s), 1268 (s), 1200-1000 (b,s), 840 (s), 718 (s) cm^{-1}.

bis(2,2'bipyridine)-1,10-Phenanthroline Ruthenium(II) tetrafluoroborate; $[Ru(bipy)_2(phen)](BF_4)_2$:[134,135] was synthesized using 101 mg (0.195 mmol) of cis-$[Ru(bipy)_2Cl_2].2H_2O$ and 97.6 mg (0.195 x 5 mmol) of 1,10-Phenanthroline monohydrate. Ammonium tetrafluoroborate (45 mg, 0.195 x 2.2 mmol) was added. The complex was recrystallized twice from acetone/ether to yield 116 mg (78%). UV-Vis. (water) λ_{max} 227 nm (ε 48284), 264 nm (ε 62426), 285.5 nm (ε 64260), 451 nm (ε 14426) sh 480 nm; IR (KBr): 3650-3000 (b,s), 1625 (w), 1600 (w), 1465 (m), 1444 (m), 1425 (m), 1200-925 (b,s), 840 (m), 765 (s), 725 (m), 715 (m) cm^{-1}.

2,2'bipyridine-bis(1,10-Phenanthroline) Ruthenium(II) tetrafluoroborate; $[Ru(bipy)(phen)_2](BF_4)_2$:[35] was synthesized using 200 mg (0.189 mmol) of cis-$[Ru(phen)_2Cl_2].H_2O$ and 73.8 mg (0.189 x 2.5 mmol) of 2,2'bipyridine. Ammonium tetrafluoroborate (39.5 mg, 0.189

x 2.1 mmol) was added. The complex was recrystallized twice from acetone/ether to yield 71 mg (47%). UV-Vis. (water) λ_{max} 223 nm (ε 57063), 263.5 nm (ε 85317), 450 nm (ε 14532); IR (KBr): 3650-3175 (b,s), 3050 (w), 1629 (m), 1600 (m), 1464 (m), 1445 (m), 1426 (s), 1410 (s), 1140 (s), 1200-925 (b,s), 842 (s), 765 (s), 718 (s) cm^{-1}.

Tris(1,10-Phenanthroline) Ruthenium(II) tetrafluoroborate; $[Ru(phen)_3](BF_4)_2$: was synthesized using 104 mg (0.194 mmol) of cis-$[Ru(phen)_2Cl_2].H_2O$ and 193 mg (0.195 x 5.0 mmol) of 1,10-Phenanthroline monohydrate. Ammonium tetrafluoroborate (40.8 mg, 0.195 x 2.0 mmol) was added. The complex was recrystallized twice from acetone/ether to yield 101 mg (64%). UV-Vis. (water) λ_{max} 222 nm (ε 73495), 262 nm (ε 97816) sh 288 nm, 421 nm (ε 15037) sh 388 nm, 447 nm (ε 15681); IR (KBr): 3660-3000 (b,s), 1628 (s), 1429 (s), 1413 (m), 1390 (w), 1209 (w), 1148 (m), 1190-900 (b,s), 849 (s), 780 (w), 726 (s) cm^{-1}.

Tris(2,2'bipyridine) Ruthenium(II) tetrafluoroborate; $[Ru(bipy)_3](BF_4)_2$:[18,136] was synthesized using 200 mg (0.384 mmol) of cis-$[Ru(bipy)_2Cl_2].2H_2O$ and 300 mg of 2,2'bipyridine (0.384 x 5.0 mmol). Ammonium tetrafluoroborate (100 mg, 0.384 x 2.5 mmol) was added. The volume of the solution was reduced over a steam bath until the first crystals appeared on its surface. Crystallization was induced by addition of saturated aqueous ammonium tetrafluoroborate solution. The product was recrystallized once from acetone/ether to yield 206 mg (72%) of orange

microcrystals. UV-Vis. (CH_3CN) λ_{max} 244 nm (ε 18513) sh 252 nm, 287 nm (ε 54895), 450 nm (ε 10273) sh's 420 nm and 390 nm; H-nmr (D_2O): (δ) 8.41 (d,6H,J=8.4), 7.92 (t,6H,J=8.1), 7.71 (d,6H,J=5.5), 7.24 (t,6H,J=7.3); IR (KBr): 3700-3000 (b,m), 1600 (m), 1461 (m), 1442 (m), 1421 (m), 1200-950 (b,s), 764 (s), 727 (m) cm^{-1}.

Tris(2,2'bipyrimidine) Ruthenium(II) chloride; $[Ru(bipym)_3]Cl_2$: was synthesized by a modification of Ludi and Hunziker's method.[36] Anhydrous Ruthenium trichloride (K & K Laboratories, Inc.) (100 mg, 0.482 mmol) was refluxed with 267 mg (0.482 x 3.5 mmol) of 2,2'bipyrimidine in 20 ml of pure DMF for 12 hrs. Then DMF was distilled off until only 3 ml was left; 20 ml of cold acetone was added in portions. The dark reddish-brown precipitate (presumably cis-$[Ru(bipym)_2Cl_2]$; IR (KBr): 3700-3200 (b,s), 3095 (w), 3070 (w), 3040 (w), 1570 (s), 1538 (s), 1400 (s), 1190 (m), 1070 (m), 1014 (s), 820 (s), 778 (m), 740 (s), 634 (m) cm^{-1}) was filtered, air dried and dissolved in 20 ml 1:1 (v/v) water/methanol. 2,2'bipyrimidine (76 mg, 0.481 mmol) was added and the resultant solution was refluxed for 10 hrs; then 10 ml of n-butanol was added and the solution was refluxed for another 14 hrs. LiCl (40 mg) was added and the solution was concentrated over a steam bath until the first crystals appeared on the surface of the solution; cooling completed the precipitation of the crude product which was recrystallized once from methanol/ether to yield 237 mg (76%) of the product. UV-Vis (water) λ_{max} 246.5 nm (ε

38463), 331 nm (ε 10398) sh's 360 nm, 412 nm and 452 nm; IR (KBr): 3650-2600 (b,s), 1625 (s), 1562 (s), 1543 (s), 1400 (s), 1098 (m), 1075 (m), 1020 (s), 810 (s), 762 (m), 744 (m) cm^{-1}.

bis(2,2'bipyridine) 2,2'bipyrimidine Ruthenium(II) tetrafluoroborate; $[Ru(bipy)_2(bipym)](BF_4)_2$:[36,37] was synthesized using 100 mg (0.192 mmol) of cis-$[Ru(bipy)_2Cl_2].2H_2O$ and 152 mg of 2,2'bipyrimidine (0.192 x 5.0 mmol). Ammonium tetrafluoroborate (43 mg, 0.192 x 2.2 mmol) was added. The orange product was recrystallized twice from acetone ether to yield 120 mg (84%). UV-Vis. (water) λ_{max} 243.5 nm (ε 28046), 283 nm (ε 44754), 417 nm (ε 9995); IR (KBr): 3650-3050 (b,s), 1629 (w), 1600 (m), 1571 (m), 1542 (w), 1467 (m), 1446 (m), 1402 (s), 1200-925 (b,s), 769 (s), 750 (m), 729 (w) cm^{-1}.

2,2'bipyrimidine-bis(1,10-Phenanthroline) Ruthenium(II) tetrafluoroborate; $[Ru(bipym)(phen)_2](BF_4)_2$: was synthesized using 200 mg (0.364 mmol) of cis-$[Ru(phen)_2Cl_2].H_2O$ and 297 mg (0.364 x 5 mmol) of 2,2'bipyridine. Ammonium tetrafluoroborate (79 mg, 0.364 x 2 mmol) was added. The complex was recrystallized twice from acetone/ether to yield 192 mg (66%). UV-Vis. (water) λ_{max} 222.5 nm (ε 25043), 262 nm (ε 36752) sh 290 nm, 392.5 nm (ε 6205) sh 424 nm; IR (KBr): 3650-3250 (b,s), 3140 (s), 3050 (s), 1630 (w), 1570 (m), 1542 (m), 1428 (s), 1405 (s), 1200-975 (b,s), 840 (s), 745 (m), 718 (s) cm^{-1}.

(bis(2,2'bipyridine)-2,2'bipyrimidine) Ruthenium(II)-bis(2,2'bipyridine) Ruthenium(II) tetrafluoroborate; $[Ru(bipy)_2(bipym)Ru(bipy)_2](BF_4)_4$:[36,37,39] was synthesized using 100 mg (0.192 mmol) of cis-$[Ru(bipy)_2Cl_2].2H_2O$ and 15.8 mg (0.192 x 2 mmol) of 2,2'bipyrimidine. The mixture was refluxed in 1:1 (v/v) water/methanol for 15 hrs. Ammonium tetrafluoroborate (43 mg, 0.192 x 2.5 mmol) was added at the end of the period. The green product was recrystallized twice from acetone/ether to yield 105 mg (41%). UV-Vis. (water) λ_{max} 245 nm (ε 34203), 278.5 nm (ε 67137), 411 nm (ε 21403) with broad sh 560 nm, 609 nm (ε 5444); IR (KBr): 3650-2600 (b,s), 1635 (m), 1604 (s), 1469 (s), 1445 (s), 1403 (s), 1310 (m), 1245 (m), 1189 (s), 1200-925 (b,s), 800 (s), 767 (s), 725 (m) cm^{-1}.

Synthesis of Monocarbonyl Tetraphenylporphyrinato Ruthenium(II); RuTPPCO(THF):[80-82]

In a typical synthesis, 500 mg (0.813 mmol) of Tetraphenylporphyrine and 500 mg (0.782 mmol) of Ruthenium dodecacarbonyl (Aldrich Chemical Co.) was dissolved in 50 ml of pure and dry toluene (purified in a manner similar to benzene by Dr. C. K. Chang's group) and refluxed under Argon for 3 days in a flask covered with aluminum foil. Toluene was removed under reduced pressure, the residue was extracted with benzene and passed through an alumina column (Fischer Scientific Co., Alumina Neutral, Brockman Activity I, 80-200 mesh; dimensions: 10 cm x 5 cm). Elution with

benzene removed some green impurities, followed by elution with 4:1 (v/v) benzene/THF which eluted the red band of the product. The product was recrystallized from methylene chloride/methanol to yield 271 mg (42%) of reddish-purple microcrystals. UV-Vis. (CH_2Cl_2) λ_{max} 299.5 nm (ε 9959) sh 312 nm, 411.5 nm (ε 130027), 528 nm (ε 11658) sh 560, ε_{313} = 9171 M^{-1} cm^{-1}; IR (KBr): 3050 (w), 3020 (w), 1955 (s), 1815 (w), 1593 (s), 1530 (m), 1485 (m), 1438 (s), 1350 (s), 1306 (m), 1205 (w), 1174 (s), 1068 (s), 1008 (s), 830 (s), 790 (s), 749 (s), 712 (s), 696 (s), 660 (m) cm^{-1}.

Synthesis of Bis(4-phenyl-1-(4-pyridyl) butanone) Tetraphenylporphyrinato Ruthenium(II); $RuTPP(PhBP)_2$:

RuTPP(4PhBP) was synthesized by a modification of the method reported for the preparation of bis(pyridine) tetraphenylporphyrinato Ruthenium(II).[80] RuTPPCO(THF) (271 mg, 332 mmol) was suspended in 200 ml of 3:1 (v/v) THF/benzene (both purified and dried) and irradiated in room temperature for 24 hrs. with the medium pressure Hg - lamp equipped with a pyrex filter, while Argon was bubbled through the solution. After the irradiation was stopped, 150 mg (0.332 x 2 mmol) of 4-phenyl-1-(4-pyridyl) butanone was added to the solution, and all solvents were removed under reduced pressure. The product was dissolved in the minimum amount of benzene and was passed through a Silica column (J. T. Baker Chemical Co. Silica Gel, 60-200 mesh; dimensions: 35 cm x 5 cm), eluting first with 9:1 (v/v) Hexane/Ethyl Acetate. A brown band moved fast, and when it

was completely eluted, there were added successively 300 ml each of 1:1 (v/v) benzene/hexane, 1:1 (v/v) benzene/methylene chloride, and pure methylene chloride. The last 900 ml were combined and the solvents were removed under reduced pressure. The product was recrystallized twice from methylene chloride/benzene to yield 292 mg (72%) of blue-purple fine microcrystals. UV-Vis. (CH_2Cl_2) λ_{max} 283 nm (ε 39909) sh's 250 nm and 308 nm, 418.5 nm (ε 144207) sh 404 nm, 507 nm (ε 25000) broad sh 532 nm, ε_{313} = 9756 M^{-1} cm^{-1}; H-nmr (C_6D_6): (δ) 8.12 (s,8H), 8.1-8.0 (m,8H), 7.7-7.6 (m,12H), 7.15-7.05 (m,6H), 6.9-6.8 (m,4H), 5.51 (d,4H), 3.40 (d,4H), 2.80 (t,4H), 2.00 (t,4H), 1.50 (qui,4H); IR (KBr): 3053 (w), 3024 (w), 2935 (w), 2860 (w), 1693 (s), 1599 (s), 1530 (m), 1495 (w), 1442 (m), 1350 (m), 1309 (w), 1230 (m), 1203 (m), 1178 (m), 1074 (m), 1005 (s), 794 (m), 755 (s), 718 (m), 704 (s), 672 (w) cm^{-1}.

Synthesis of bis(4-phenyl-1-(4-pyridyl) butanone) octaethylporphyrinato Ruthenium(II); $RuOEP(4PhBP)_2$:

It was synthesized by the same method as $RuTPP(4PhBP)_2$ using 500 mg (0.936 mmol) of Octaethylporphyrine and 500 mg (0.782 mmol) of Ruthenium dodecacarbonyl. The intermediate RuOEPCO(THF) could not be recrystallized quntitatively although enough crystals were obtained from trichloroethylene/heptane for spectroscopic identification: UV-Vis. (CH_2Cl_2) λ_{max} 254 nm (ε 23710), 303 nm (ε 19362), 321.5 nm (ε 19478), 392 nm (ε 249275), 514 nm (ε 16986), 547 nm (ε 41014), ε_{313} = 18957 M^{-1} cm^{-1}; H-nmr ($CDCl_3$): (δ) -

2.65 (s,3H; in our efforts to recrystallize the compound from methylene chloride/methanol, THF was propably substituted by methanol, the protons of which give this resonance), 1.94 (t,12H), 4.03 (q,8H), 9.95 (s,4H); IR (KBr): 2960, 2930, 2860, 1930, 1590, 1450, 1275, 1230, 1150, 1020, 990, 960, 845, 745 cm^{-1}. All the compound received from the first step was dissolved in 200 ml 1:1 (v/v) THF/benzene (both purified and dried) and irradiated in room temperature for 24 hrs. with the medium pressure Hg-lamp equipped with a pyrex filter, while Argon was bubbled through the solution. At the end of the period, 200 mg (0.888 mmol) of 4-phenyl-1-(4-pyridyl) butanone was added to the solution; and all solvents were removed under reduced pressure. The product was dissolved in the minimum amount of benzene and was passed through an alumina column (Fischer Scientific Co., Alumina Neutral, Brockman Activity I, 80-200 mesh; dimensions: 10 cm x 5 cm), eluting with benzene. A yellow band moved fast followed by the blue-purple band of the $RuOEP(4PhBP)_2$, leaving brownish impurities on the top of the column. There was obtained 129 mg (13%) of the product. UV-Vis. (CH_2Cl_2) λ_{max} 285 nm (ε 41095), 401.5 nm (ε 85085), 498 nm (ε 14558), 524.5 nm (ε 30098), 619 nm (ε 10545), ε_{313} = 21810 M^{-1} cm^{-1}; H-nmr ($CDCl_3$): (δ) 9.33 (s,4H), 7.1-6.95 (m,6H), 6.85-6.75 (m,4H), 5.15 (d,4H), 3.80 (qt,16H), 2.15 (t,4H), 1.9-1.7 (m,>20H), 1.59 (d,4H), 1.40 (qui,4H); IR (KBr): 2960 (s), 2930 (s), 2870 (m), 1695 (s), 1598 (s),

1545 (w), 1455 (m), 1277 (m), 1235 (m), 1206 (w), 1015 (s), 960 (w), 840 (w), 750 (w), 705 (w) cm^{-1}.

Synthesis of Carbonyl pyrazino tetraphenylporphyrinato Ruthenium(II); RuTPPCOpyz:

RuTPPCO(THF) (50 mg, 0.061 mmol) was refluxed overnight in 50 ml of benzene in the presence of 1 g (12.5 mmol) of pyrazine. Color changed from purple-red to orange-red; and at the end of the period, the solution was cooled and passed through an alumina column (Fischer Scientific Co., Alumina Neutral, Brockman Activity I, 80-200 mesh; Dimensions: 10 cm x 5 cm), eluting with benzene. The orange-red band moved slowly and required between 1 and 2 l of benzene to pass through the column. The product was recrystallized twice from benzene/pentane to yield 28 mg (56%) of orange-red microcrystals. UV-Vis. (C_6H_6) λ_{max} 409 nm (ε 241176) sh 490 nm, 530 nm (ε 13753), 564 nm (ε 2906); IR (KBr): 3105 (w), 3055 (w), 3025 (w), 2958 (w), 2930 (w), 1961 (s), 1600 (m), 1530 (m), 1490 (m), 1445 (m), 1420 (w), 1354 (m), 1310 (m), 1210 (w), 1180 (w), 1075 (m), 1010 (s), 839 (w), 799 (s), 756 (s), 720 (s), 704 (s) cm^{-1}.

Synthesis of Carbonyl (Carbonyl pyrazino tetraphenylporphyrinato Ruthenium(II)) tetraphenylporphyrinato Ruthenium(II); CORuTPPpyzTPPRuCO:

RuTPPCO(THF) (100 mg, 0.123 mmol) was refluxed in benzene overnight in the presence of 5 mg (0.063 mmol) of pyrazine. The product was dissolved in the minimum amount

of benzene and loaded on an alumina column (Fischer Scientific Co., Alumina Neutral, Brockman Activity I, 80-200 mesh; dimensions: 10 cm x 5 cm), eluting first with 2 lts of benzene, followed by 300 ml of 9:1 (v/v) benzene/methanol. The product was recrystallized once from benzene/pentane to yield 71 mg (37%) of deep red microcrystals. UV-Vis. (C_6H_6) λ_{max} 408 nm (ε 428198) sh 492 nm, 530 nm (ε 34987), 563 nm (ε 5574); H-nmr ($CDCl_3$): (δ) 8.30 (s,16H), 7.95, 7.70-7.45 (d,m,40H), -0.56 (s,4H); IR (KBr): 3055 (w), 3025 (w), 1958 (s), 1812 (w), 1526 (s), 1595 (s), 1440 (s), 1415 (w), 1350 (s), 1304 (m), 1206 (w), 1175 (m), 1155 (w), 1129 (w), 1070 (s), 1010 (s), 830 (w), 790 (s), 749 (s), 712 (s), 695 (s), 660 (w) cm^{-1}.

Osmium Complexes

Aqueous cis-bis(2,2'bipyridine) Osmium(II) chloride; cis-$[Os(bipy)_2Cl_2].H_2O$:[92]

Ammonium Hexachloroosmate (Aldrich Chemical Co.) (500 mg, 1.094 mmol) was suspended in 11 ml of DMF and refluxed for 1 h. with 346 mg (1.094 x 2 mmol) of 2,2'bipyridine. The solution darkened in color, was cooled, filtered and 10 ml of methanol was added. This solution was added to 500 ml of ether and the product precipitated as brown flakes. Recrystallization from methanol/ether gave 711 mg of the product, presumably cis-$[Os(bipy)_2Cl_2]xH_2O$. IR (KBr): 3600-2700 (b,s), 3350 (s), 3000 (s), 2780 (w), 1603 (s), 1465 (s), 1444 (s), 1420 (s), 1312 (s), 1242 (m), 1165 (m), 1158 (s), 1070 (w), 1023 (m), 891 (m), 768 (s), 720 (s) cm^{-1}.

All material obtained from the above synthesis was dissolved in 30 ml of 2:1 (v/v) DMF/methanol and cooled in an ice bath. Water (200 ml) was bubbled with Argon for 15 min.; sodium dithionite (0.5 g) was dissolved in it and this solution was added slowly to the DMF/methanolic solution upon cooling and stirring. The resultant solution remained in the ice bath for 15 min. while dark red-purple microcrystals precipitated. The product was washed with water, methanol, ether and air dried to yield 450 mg (70%). UV-Vis. (CH_3CN) λ_{max} 236.5 nm (ε 22426), 297 nm (ε 40059), 385 nm (ε 7278), 460 nm (ε 6391), 555 nm (ε 7929); IR (KBr):

3650-3100 (b,m), 3090 (w), 3070 (m), 3045 (m), 1600 (m), 1590 (m), 1465 (s), 1452 (s), 1413 (s), 1250 (s), 1010 (s), 990 (m), 795 (w), 754 (s), 719 (m), 711 (m), 654 (m) cm^{-1}.

Aqueous bis(1,10-phenanthroline) Osmium(II) chloride; cis-$[Os(phen)_2Cl_2].H_2O$;[92] was synthesized by the same method used for the synthesis of cis-$[Os(bipy)_2Cl_2].H_2O$ using 500 mg (1.094 mmol) of Ammonium Hexachloroosmate (Aldrich Chemical Co.) and 454 mg (1.094 x 2.1 mmol) of 1,10-Phenanthroline monohydrate. The first step produced 767 mg of product, presumably cis-$[Os(phen)_2Cl_2]xH_2O$. IR (KBr): 3650-2850 (b,s), 2760 (m), 1625 (m), 1600 (m), 1579 (m), 1510 (w), 1460 (m), 1430 (s), 1410 (s), 1221 (w), 1095 (w), 1020 (w), 845 (s), 711 (s) cm^{-1}. Treatement with 200 ml of an Argon-bubbled aqueous solution containing 0.5 g of sodium dithionite, produced 518 mg (74%) of the dark purple microcrystalline product. UV-Vis. (CH_3CN) λ_{max} 220.5 nm (ε 92556), 266.5 nm (ε 97256), 532.5 nm (ε 16053) sh's 460 and 640 nm; IR (KBr): 3700-3100 (b,m), 3080 (w), 3050 (w), 1645 (m), 1630 (m), 1605 (m), 1560 (m), 1498 (m), 1428 (s), 1409 (m), 1275 (s), 1194 (s), 1092 (s), 1053 (s), 911 (m), 835 (s), 730 (m), 710 (s) cm^{-1}.

Ruthenium-Osmium 2,2'bipyrimidine bridged, mixed ligand binuclear complexes; were synthesized essentially as described by Meyer.[39]

In a typical procedure $[Ru(biden)_2(bipym)](BF_4)_2$ (biden = bidentate ligand: 2,2'bipyridine or 1,10-Phenanthroline) was refluxed with 1.5 molar excess of cis-

$[Os(biden)_2Cl_2].H_2O$, in 25 ml of 2:2:1 (v/v/v) water/methanol/n-butanol for 2 days. Then all solvents were removed over a steam bath and the residue was dissolved in water, filtrated and passed through a cation exchange column (Sephadex C-25; dimensions: 35 cm x 1 cm). Elution with 100 ml of an aqueous ammonium tetrafluoroborate solution removed yellowish-brown impurities; then 100 ml of a 20% ammonium tetrafluoroborate aqueous solution eluted the green product. The eluent was evaporated to dryness, the product was extracted with dry acetone and precipitated by addition to ether. Purification was achieved by recrystallization (twice) from acetone/ether.

(bis(2,2'bipyridine)-bipyrimidine Ruthenium(II)) bis-(2,2'bipyrimidine) Osmium(II) tetrafluoroborate; $[Ru(bipy)_2(bipym)Os(bipy)_2](BF_4)_4$;[39] was synthesized using 50 mg (0.067 mmol) of $[Ru(bipy)_2(bipym)](BF_4)_2$ and 60 mg (0.067 x 1.5 mmol) of cis-$[Os(bipy)_2Cl_2].H_2O$ to yield 38 mg (40%) of the product. UV-Vis. (water) λ_{max} 243 nm (ε 13788) sh 250 nm, 283.5 nm (ε 23372), 417 nm (ε 5665) sh's 396 nm, 500 nm and 560 nm, 623 nm (ε 731); IR (KBr): 3700-3000 (b,s), 3320 (w), 3110 (w), 1608 (w), 1440 (s), 1295 (m), 1300-890 (b,s), 770 (m), 730 (w), 670 (w), 664 (w) cm^{-1}.

bis(2,2'bipyridine)-bipyrimidine Ruthenium(II)) bis-(1,10-Phenanthroline) Osmium(II) tetrafluoroborate; $[Ru(bipy)_2(bipym)Os(phen)_2](BF_4)_4$; was synthesized using 51 mg (0.068 mmol) of $[Ru(bipy)_2(bipym)](BF_4)_2$ and 66 mg (0.068 mmol) of cis-$[Os(phen)_2Cl_2].H_2O$ to yield 51 mg (51%) of the

green product. UV-Vis. (water) λ_{max} 264 nm (ε 18302) sh 280 nm, 410 nm (ε 5951), 631 nm (ε 1453); IR (KBr): 3075 (w), 1640 (w), 1605 (m), 1545 (w), 1469 (m), 1450 (m), 1433 (m), 1407 (s), 1200-900 (b,s), 845 (m), 769 (s), 752 (m), 732 (w), 720 (m) cm^{-1}.

bis(1,10-Phenanthroline)-2,2'bipyrimidine Ruthenium(II) bis(2,2'bypyridine) Osmium(II) tetrafluoroborate; $[Ru(phen)_2(bipym)Os(bipy)_2](BF_4)_4$; was synthesized using 53 mg (0.067 mmol) of $[Ru(phen)_2(bipym)](BF_4)_2$ and 44 mg (0.067 x 1.1 mmol) of cis-$[Os(bipy)_2Cl_2].H_2O$ to yield 42 mg (43%) of the green product. UV-Vis. (water) λ_{max} 261 nm (ε 43248) sh 280 nm, 407 nm (ε 12096) sh's 510 nm and 560 nm, 629 nm (ε 2799); IR (KBr): 3660-3000 (b,s), 1632 (w), 1608 (w), 1428 (s), 1184 (m), 1230-865 (b,s), 845 (m), 769 (m), 724 (m), 708 (w) cm^{-1}.

(bis(1,10-Phenanthroline)-2,2'bipyrimidine Ruthenium-(II)) bis(1,10-Phenanthroline) Osmium(II) tetrafluoroborate; $[Ru(phen)_2(bipym)Os(phen)_2](BF_4)_4$; was synthesized using 50 mg (0.063 mmol) of $[Ru(phen)_2(bipym)](BF_4)_2$ and 44 mg (0.063 x 1.1 mmol) of cis-$[Os(phen)_2Cl_2].H_2O$ to yield 30 mg of the product (29%). UV-Vis. (water) λ_{max} 222 nm (ε 102083), 262 nm (ε 126304), 392 nm (ε 22610) sh's 412 and 560 nm, 623 nm (ε 2280), 766 nm (ε 1259); IR (KBr): 3680-3150 (b,s), 3080 (m), 1630 (w), 1603 (w), 1579 (w), 1430 (s), 1415 (m), 1184 (w), 1200-900 (b,s), 845 (s), 720 (s) cm^{-1}.

Tungsten Complexes

Pentacarbonyl (4-substituted-pyridine) Tungsten(0) Complexes; were synthesized by the classical method of Strohmeier.[49] In a typical synthesis, 1.41 g (4 mmol) of Hexacarbonyl Tungsten(0) (Alfa Products) was dissolved in 150 ml of dry THF and under continuous Argon bubbling through the solution irradiated for 2 hrs. with a Hanovia 450 watt medium pressure Hg-lamp equipped with a Pyrex filter. The solution turned yellow and at the end of the irradiation period, 4.0 to 4.2 mmol of the ligand was added, dissolved in 5 ml of dry THF. The solution turned immediately to reddish-brown. Solvents were removed under reduced pressure and the residue was dissolved in the minimum amount of benzene or ethyl acetate and chromatographed on alumina (Look for the column specifications under each separate compound.). Solid products were recrystallized from petroleum ether.

Pentacarbonyl (4-acetylpyridine) Tungsten(0); $W(CO)_5(4AP)$;[60,69] was synthesized using 1.41 g (4 mmol) of Hexacarbonyl Tungsten(0) and 485 mg (4 mmol) of 4-acetylpyridine. The product was chromatographed once on alumina (Alumina Activated, Alcoa, Type F-20, mesh 80-200; dimensions: 35 cm x 5 cm) eluting with 4:1 (v/v) benzene/hexane. The yellow band was collected and the product was recrystallized once from petroleum ether to yield 908 mg (51%) of the yellow $W(CO)_5(4AP)$. mp., 114°C, decomposes; Vis. (C_6H_6) λ_{max} 402 nm (ε 9210) sh's 430 nm and

332 nm, ε_{313} = 2308 M^{-1} cm^{-1}; (methylcyclohexane) λ_{max} 404 nm (ε 8244) sh 332 nm, 441 nm (ε 8109); H-nmr (C_6H_6): (δ) 8.03 (dd,2H,J=5.2,1.7), 6.40 (dd,2H,J=4.9,1.5), 1.76 (s,3H); C-nmr (C_6H_6; 1% (w/v) $Cr(acac)_3$ added): (δ) 25.9, 122.8, 142.2, 156.8, 194, 199.2, 202.2; m/e (rel. int.): 444 (7), 417, 338 (10), 360 (4), 351 (15), 332 (18), 295 (11), 267 (32), 121 (73), 106 (85), 78 (93); IR (KBr): 2075 (s), 2200-1750 (b,s), 1695 (s), 1414 (s), 1360 (m), 1333 (w), 1265 (s), 1212 (m), 960 (w), 824 (m), 597 (s), 564 (m), 372 (s) cm^{-1}.

Pentacarbonyl Methyl-(4-pyridyl) formate Tungsten(0); $W(CO)_5$(MeINic); was synthesized using 1.41 g (4.0 mmol) of Hexacarbonyl Tungsten(0) and 596 mg (4.0 mmol) of methyl isonicotinate. The product was chromatographed on alumina (Alumina Activated, Alcoa, Type F-20, mesh 80-200; dimensions: 35 cm x 5 cm) eluting with 3:2 (v/v) benzene/petroleum ether. The yellow band was collected and used without any further purification. Received 102 mg of product (5.5%). mp., 110°C, decomposes; Vis. (C_6H_6) λ_{max} 402 nm (ε 8483) sh 332 nm, ε_{313} = 1983 M^{-1} cm^{-1}; (methylcyclohexane) λ_{max} 405 nm (ε 9549) sh's 430 nm and 332 nm; C-nmr: (C_6H_6; 1% (w/v) $Cr(acac)_3$ added): (δ) 52.6, 124.8, 156.7, 163.9, 199.1, 202.3; m/e (rel. int.): 461 (5), 352 (9), 295 (5), 266 (15), 240 (8), 212 (10), 184 (13), 137 (37), 106 (100), 78 (68); IR (KBr): 2970 (s), 2943 (s), 2065 (s), 2100-1775 (b,s), 1730 (s), 1430 (m), 1410 (s), 1285

(s), 1260 (s), 1224 (m), 1135 (s), 1110 (s), 855 (w), 795 (s), 764 (s), 700 (m) cm^{-1}.

Pentacarbonyl (4-benzoylpyridine) Tungsten(0); $W(CO)_5(4Bzpy)$;[69] was synthesized using 1.41 g (4 mmol) of Hexacarbonyl Tungsten(0) and 732 mg (4 mmol) of 4-benzoylpyridine. The product was chromatographed once on alumina (Alumina Activated, Alcoa, Type F-20, mesh 80-200; dimensions: 35 cm x 5 cm) eluting with 9:1 (v/v) benzene/hexane. The yellow band was collected and recrystallized once from petroleum ether to yield 863 mg (43%) of the $W(CO)_5(4Bzpy)$. mp., 127°C, decomposes; Vis. (C_6H_6) λ_{max} 403 nm (ε 9424) sh's 430 nm and 332 nm; (methylcyclohexane) λ_{max} 405 nm (ε 8082) sh 332 nm, 435 nm (ε 7106); H-nmr (C_6D_6): (δ) 8.00 (dt,2H,J=4.9,1.5), 6.49 (tt,2H,J=7.6,1.5), 6.00-5.95 (m,5H); C-nmr (C_6H_6; 1% (w/v) $Cr(acac)_3$ added): (δ) 124.9, 130.2, 134, 135.7, 144.3, 156, 192, 198.3, 202; m/e (rel. int.): 508 (4), 480 (4), 452, 425, 354 (30), 296 (16), 268 (52), 240 (30), 212 (43), 184 (60), 105 (100), 77 (48); IR (KBr): 2075 (s), 1990 (s), 1965 (s), 1865 (s), 2150-1750 (b,s), 1664 (s), 1460 (m), 1428 (m), 1284 (s), 950 (w), 945 (w), 845 (w), 700 (m), 650 (m) cm^{-1}.

Pentacarbonyl (4-cyanopyridine) Tungsten(0); $W(CO)_5(4CNpy)$;[63,69] was synthesized using 1.41 g (4 mmol) of Hexacarbonyl Tungsten(0) and 416 mg of 4-cyanopyridine. The product was chromatographed on alumina (Alumina Activated,

Alcoa, Type F-20, mesh 80-200; dimensions: 35 cm x 5 cm) eluting with 9:1 (v/v) benzene/petroleum ether. The yellow band was collected and the product was recrystallized once from petroleum ether to yield 508 mg (30%) of the yellow $W(CO)_5$(4CNpy). mp., 107.5-108.5°C; Vis. (C_6H_6) λ_{max} 404 nm (ε 7364) sh's 330 nm and 430 nm; H-nmr (C_6H_6): (δ) 7.67 (dd,J=5.2,1.8), 5.73 (dd,J=5.0,1.8); C-nmr ($CDCl_3$): (δ) 114.9, 121.2, 127.1, 157.1, 198.1; m/e (rel. int.): 428 (2), 372 (2), 344 (7), 316 (4), 288 (4), 261 (6), 104 (100), 77 (40); IR (KBr): 2065 (s), 2200-1750 (b,s), 1484 (w), 1445 (m), 1355 (w), 1220 (w), 1155 (w), 822 (w), 755 (s), 700 (m) cm^{-1}.

Pentacarbonyl 1-(4-pyridyl) butanone Tungsten(0); $W(CO)_5$(4BP); was synthesized using 1.41 g (4 mmol) of Hexacarbonyl Tungsten(0) and 597 mg (4 mmol) of 4-butyrylpyridine. The product was chromatographed once on alumina (Alumina Activated, Alcoa, Type F-20, mesh 80-200; dimensions: 35 cm x 5 cm) eluting with 3:2 (v/v) benzene/petroleum ether. The yellow band was collected and the product was recrystallized from petroleum ether to yield 930 mg (49%) of the $W(CO)_5$(4BP). mp., 81.2-82.2°C; Vis. (C_6H_6) λ_{max} 402 nm (ε 8967) sh's 430 nm and 332 nm; (methylcyclohexane) λ_{max} 405 nm (ε 7305) sh 332 nm, 438 nm (ε 7069); H-nmr (C_6H_6): (δ) 8.10 (dd,2H,J=5.0,1.4), 6.51 (dd,2H,J=4.0,1.5), 2.12 (t,2H,J=7.0), 1.51 (hex,2H,J=7.3), 0.81 (t,3H,J=7.3); C-nmr (C_6D_6; 1% (w/v) $Cr(acac)_3$ added): (δ) 14, 17, 40, 123, 143, 157, 196, 199, 202; m/e (rel.

int.): 473, 445, 417, 389, 352 (8), 268 (17), 240 (10), 212 (14), 184 (19), 149 (24), 121 (25), 106 (100), 78 (65); IR (KBr): 2970 (s), 2940 (s), 2888 (m), 2075 (s), 2200-1750 (b,s), 1696 (s), 1420 (s), 1405 (m), 1363 (s), 1272 (s), 1241 (s), 1220 (m), 1209 (s), 1000 (s), 903 (w), 818 (s) cm^{-1}.

Pentacarbonyl [1-(4-pyridyl) pentanone] Tungsten(0); $W(CO)_5(4VP)$; was synthesized using 1.41 g (4 mmol) of Hexacarbonyl Tungsten(0) and 685 mg (4.2 mmol) of 1-(4-pyridyl) pentanone. The product was chromatographed on alumina (Alumina Acid, Brockman Activity I, mesh 80-200; dimensions: 35 cm x 5 cm) twice; the first time, it was eluted with Hexane until a yellowish impurity had been completely removed, followed by 85:15 (v/v) Hexane/ethyl acetate which eluted the yellow-orange product. The second time it was passed through the column, it was eluted with 85:15 (v/v) Hexane/ethyl acetate until the yellow $W(CO)_5(4VP)$ had been completely eluted. All solvents were removed under reduced pressure to yield 660 mg (34%) of a thick oil which was identified as $W(CO)_5(4VP)$ based on its spectra data. Vis. (C_6H_6) λ_{max} 402 nm (ε 8534) sh's 430 nm and 332 nm, ε_{313} = 2220 M^{-1} cm^{-1}; (methylcyclohexane) λ_{max} 405 nm (ε 8353) sh 332 nm, 437 nm (ε 7664), ε_{313} = 2206 M^{-1} cm^{-1}; H-nmr (C_6D_6): (δ) 0.86 (t,3H), 1.23 (hex,2H), 1.52 (qui,2H), 2.23 (t,3H), 6.59 (dd,2H), 8.17 (dd,2H); ($CDCl_3$): (δ) 0.98 (t,3H), 1.44 (hex,2H), 1.74 (qui,2H), 2.98 (t,2H), 7.70 (dd,2H), 9.02 (dd,2H); C-nmr (C_6D_6; 2.5% (w/v)

$Cr(acac)_3$ added): (δ) 14, 23, 26, 38.4, 122.8, 142.9, 156.8, 196.7, 199.4, 202.5; ($CDCl_3$; 2.5% (w/v) $Cr(acac)_3$ added): (δ) 13.5, 22, 25.8, 38.4, 123, 143, 156.8, 197, 198, 202; IR (CCl_4): 2950 (s), 2915 (s), 2850 (m), 2060 (s), 1900 (s), 1700 (s) cm^{-1}.

Photoproduct Isolation and Identification

cis-Tetracarbonyl bis(1-(4-pyridyl)pentanone) Tungsten(0); cis-$W(CO)_4(4VP)_2$:

About 1 g of pentacarbonyl 1-(4-pyridyl)pentanone Tungsten(0) was dissolved in 25 ml of purified benzene, transferred to eight elongated test tubes and degassed with four freeze-pump-thaw cycles. The tubes were flame sealed and irradiated for four days with visible light above 400 nm (Look at the "methods and techniques" part of the experimental section of this thesis.). Then tubes were opened, benzene was removed under reduced pressure and the residue was dissolved in 3 ml of ethyl acetate and chromatographed on alumina (Alumina Acid, Brockman Activity I, mesh 80-200; dimensions: 35 cm x 1 cm) eluting first with 85:15 (v/v) hexane/ethyl acetate until all the unreacted $W(CO)_5(4VP)$ (yellow band), and all the $W(CO)_6$ (moving with the front of the solvent), having been produced in parallel to the product had been removed followed by 1:1 (v/v) hexane/ethyl acetate which eluted the red band of the product. All solvents were removed under reduced pressure and the product was isolated as dark red needles after

recrystallization from ethyl acetate-hexane. The product was dried under vacuum to give about 260 mg (about 20%). mp., sublimes above 260°C; Vis. (C_6H_6) λ_{max} 490.5 nm (ε 8798) sh 390 nm; ε_{600} = 2834 M^{-1} cm^{-1}; (methylcyclohexane): broad absorption in the visible region with maximum around 520 nm, broad sh around 620 nm; H-nmr (C_6D_6): (δ) 0.81 (t,3H), 1.17 (hex,2H), 1.48(qui,2H), 2.21 (t,2H), 6.72 (dd,2H), 8.44 (dd,2H); ($CDCl_3$): (δ) 0.95 (t,3H), 1.40 (hex,2H), 1.70 (qui,2H), 2.95 (t,2H), 7.65 (dd,2H), 8.90 (dd,2H); C-nmr (C_6D_6; 1% (w/v) $Cr(acac)_3$ added): (δ) 13.9, 22.5, 26, 38.4, 122.8, 142.9, 155.7, 197, 205.5, 213; ($CDCl_3$; 2% (w/v) $Cr(acac)_3$ added): (δ) 13.9, 22.5, 26, 39, 122.9, 142.9, 156, 198, 204.8, 213; IR (KBr): 2955 (m), 2930 (m), 2870 (m), 1990 (s), 1880 (s), 1855 (s), 1810 (s), 1695 (s), 1605 (s), 1410 (s), 1220 (w), 1200 (m), 980 (w), 840 (w), 790 (w) cm^{-1}; Elemental Analysis Data: Calculated for $WC_{24}N_2H_{26}O_6$: (%) C, 46.31; N, 4.50; H, 4.21; W, 29.55. Found: C, 45.93; N, 4.47; H, 4.14; W, 27.08.

Hexacarbonyl Tungsten(0):

Hexacarbonyl Tungsten(0) precipitated partially out of concentrated (~0.05 M) benzene or methylcyclohexane solutions of $W(CO)_5(4VP)$ after prolonged irradiation. In one case, it was collected and identified by its mass and Carbon-13 nmr spectra by comparison with an authentic sample obtained from Alfa Products.

Photoproduced $W(CO)_6$: C-nmr (C_6D_6): (δ) 191; m/e (rel. int.): 352 (36), 324 (7), 296 (32), 268 (100), 240 (50), 212 (60), 184 (66).

$W(CO)_6$ obtained from Alfa Products: C-nmr (C_6D_6): (δ) 191; m/e (rel. int.): 352 (97), 324 (18), 296 (19), 268 (61), 240 (31), 212 (54), 184 (100).

Methods and Techniques

Preparation of Samples

Photochemical Glassware: Class A pipets, Class A volumetric ware and Pyrex syringes with chrome-plated brass needles were used to prepare sample solutions for photolysis. All glassware was cleaned by rinsing with acetone, then distilled water, followed by boiling in a distilled water solution of Alconox Laboratory Glassware Detergent for one hour then pouring out the hot solution and changing for five times the distilled water in the container, followed again by boiling in fresh sample of distilled water for one hour with subsequent changes of the distilled water for another five times. All glassware was dried at 140°C in an oven used only for photochemical glassware.

Irradiation Tubes: Photolysis tubes (13 x 100 nm Pyrex culture tubes) were cleaned in a manner identical to the photochemical glassware. The necks were drawn out to the desired length by rotation in an oxygen flame.

Stock Solutions and Photolysis Solutions: A Sartorious Model 2403 balance (accurate to ± 0.001) was used to weight the desired amount of substrate into a volumetric flask which was then diluted to volume with the appropriate solvent. Solutions were used directly or by pipetting an appropriate aliquot into another volumetric flask and diluting to volume.

Degassing Procedures: A 5 ml syringe was used to fill the irradiation tubes with 2.8 ml of the appropriate solution. The tubes were attached to a vacuum line on a manifold fitted with 12 stopcocks using one-hole rubber stoppers (size 00). For room temperature emission studies, the test tubes were attached to the vacuum line on another manifold using ground joints, sealing being ensured by the use of high-vacuum silicon grease. All samples were degassed by four freeze-pump-thaw cycles (for emission studies the cycles were six): frozen by the cold vapor over the surface of liquid nitrogen followed by slow immersion into it, pumped for 10-20 minutes at 5 x 10 Torr. then allowed to thaw by standing in air. At the end of the final cycle, the tubes being frozen, were sealed with an oxygen torch under vacuum.

Irradiation Procedures: Photochemical studies involved the use of four different irradiation apparati. Three of these involved the use of Hanovia 450 watt medium-pressure mercury lamps cooled by quartz immersion wells which were placed inside a "merry-go-round" apparatus (7 mm slit

width). The entire apparatus was placed inside a large crock filled with distilled water. All tubes were irradiated in parallel to ensure that each received an equal amount of light. Three different filter solutions were employed.

Filter A. To isolate the 313 nm region, an aqueous filter solution of 0.001 M potassium chromate and 1% potassium carbonate was used.

Filter B. To cut all the light below 400 nm while equally transparent at all longer wavelengths, an aqueous filter solution of 1 M sodium nitrite was used.

Filter C. In order to cut all the light below 475 nm an aqueous filter solution of 0.05 M potassium chromate and 1% potassium carbonate was used.

The fourth apparatus was a 1000 watt Hg-Xe lamp in line with a Bausch & Lomb high-intensity grating monochromator (catalog No. 33-86-76) (Filter D) held 3 cm from the quartz window of a jar containing a merry-go-round apparatus with windows on the outside of sample holders.

Analysis of Samples

Identification of photoproducts: Photoreduction products using THF as a hydrogen donor were identified by their mass spectrometric data (gc/ms).

The alkene photoproducts of phenyl ketones, phenyl ketone hydrochloric salts and pentaammine or bis(2,2'bipyridine) Ruthenium complexes (styrene and n-butyl

acrylate) were identified by comparison with the gas chromatographic (gc) retention times of authentic samples. Styrene becomes apparent from its characteristic odor, while n-butyl acrylate was also identified by gc/ms.

Cis-tetracarbonyl bis(4-valerylpyridine) Tungsten(0) being produced by the irradiation of Pentacarbonyl (4-valerylpyridine) Tungsten(0) was isolated (see above) and identified based on its spectral and elemental analysis data.

Hexacarbonyl Tungsten(0) produced with Tetracarbonyl bis(4-valerylpyridine) Tungsten(0) upon irradiation of pentacarbonyl (4-valderylpyridine) Tungsten(0) was identified by its HPLC retention time, by its characteristic carbon-13 nmr resonance peak at 191 ppm, and its mass spectrum.

Cis-tetracarbonyl bis(4-acylpyridine) Tungsten(0) produced from $W(CO)_5$(4AP), $W(CO)_5$(4Bzpy) and $W(CO)_5$(4BP) were identified from the carbonyl peaks in the carbon-13 nmr spectrum by comparison of the spectrum before and after irradiation; the photochemical reactions in these cases were carried out in four freeze-pump-thaw cycle degassed and flame-sealed nmr tubes originally attached to ground glass joints.

Ligand Fragmentation: Samples after irradiation were checked for ligand fragmentation by the comparison of the gc or HPLC retention time with an authentic sample.

Gas Chromatography Procedures: On column, sample injections of 0.2 to 0.4 microliters were made into 1/8 inch diameter aluminum columns using nitrogen as the carrier gas. The hydrogen flow rate was 30 ml/min and the air flow rate 300 ml/min. The following columns were employed:

Column A: 19.4% FFAP, Chromosorb P 60:80 DMCS, 30 ml/min (Nitrogen flow rate); 8' x 1/8"; 140°C Column, 200°C injector, 280°C detector (styrene analysis); 120°C Column, 200°C injector, 280°C detector (n-butyl acrylate analysis); 180°C column, 200°C injector, 280°C detector (acetophenone analysis); 190°C column, 200°C injector, 280°C detector (o-methyl acetophenone analysis).

Column B: 5% QF-1, 1.25% Carbowax 20 M, Chromosorb G 60:80 DMCS acid washed, treated with $Me_3SiNHSiMe_3$; 25 ml/min (Nitrogen flow rate); 8' x 1/8"; 140°C column, 200°C injector, 280°C detector (acetophenone analysis); 130°C column, 200°C injector, 280°C detector (4-acetyl pyridine analysis); 98°C column, 230°C injector, 250°C detector (2-(2-tetrahydrofuryl) acetaldimine analysis); 105°C column, 230°C injector, 250°C detector (octahydro-2,2'bifuran analysis).

Column C: 5% SE-30, Chromosorb W 60:80 DMCS acid washed; 30 ml/min (Nitrogen flow rate); 5' x 1/8"; 210°C column, 250°C injector, 280°C detector (4-phenyl-1-(4-pyridyl) butanone and n-butyl-4-[(4-pyridyl) carbonyl] butanoate analysis).

Column D: 19% FFAP, Chromosorb G 60:80 DMCS; 30 ml/min (Nitrogen flow rate); 12' x 1/8"; 175°C column, 230°C injector, 290°C detector (2-(2-tetrahydrofuryl) acetaldimine analysis); 200°C column, 230°C injector, 290°C detector (octahydro-2,2'bifuran analysis).

High-Pressure Liquid Chromatography Procedures: Through an injector accessory, sample injections of 20 microliters were made into a 25 cm normal phase silica column using mixtures of UV-grade Hexane and Ethyl Acetate as mobile phase, pushed through the column by two high-pressure pumps; the ratio of the solvents was automatically set by a microprocessor. The following column was employed:

Column E: Ultrasphere Si 5um (Altex Scientific, Inc.); 25 cm x 4.6 mm; 1.5 ml/min (carrier solvent flow rate); 35°C column temperature; 85% Hexane, 15% Ethyl Acetate, detector at 270 nm (Pentacarbonyl(4-Butyrylpyridine) Tungsten(0) and Cis-Tetracarbonyl bis(4-valerylpyridine) Tungsten(0) analysis); 95% Hexane, 5% Ethyl Acetate, detector at 290 nm (Hexacarbonyl Tungsten(0) analysis).

Actinometry and Quantum Yield Determination

Internal standards were used for all analyses except the following cases in which external standards were employed:

a) Analysis of 4-acetylpyridine being produced from cis-bis (2,2'bipyridine)-bis (4-phenyl-1-(4-pyridyl) butanone) Ruthenium(II) tetrafluoroborate.

b) Analysis of Hexacarbonyl Tungsten(0) being produced from Pentacarbonyl (4-Valerylpyridine) Tungsten(0).

c) One Stern-Volmer experiment, quenching Pentacarbonyl (4-Valerylpyridine) Tungsten(0) with anthracene.

No particular standard was used for photochemical experiments in benzene analyzed by HPLC with the detector at 270 nm; the solvent (benzene) played the role of a standard.

No standard was necessary for experiments analyzed by visible light absorption at 600 nm.

For the experiments analyzed by gc or HPLC, the photoproduct concentration was determined using the ratio (area of product/area of internal (or external) standard). A detector response factor (RF) was determined to account for the difference in molar response for each compound. The response factor is the reciprocal slope of the plot of concentration ratio of compound to standard versus area ratio of compound to standard. Response factors are listed in Table 27. Product concentrations are determined from (65). When the solvent (benzene) was used as internal

$$[\text{product}] = RF \times [\text{Standard}] \times (\text{area of product/area of standard}) \quad (65)$$

standard, the response factor determined (RF_{obs}) is the product of the real. Response factor (RF) times the concentration of benzene. i.e., $RF_{obs} = RF \times [\text{benzene}]$; [benzene] is constant since benzene is the solvent.

Table 27.

Internal (external) standard:	Compound analyzed	RF
p-dichlorobenzene:	octahydro-2,2'bifuran	1.0[a]
p-dichlorobenzene:	2-(2-tetrahydrofuryl) acetaldimine	1.2[a]
methyl benzoate:	octahydro-2,2'bifuran	1.08[a]
methyl benzoate:	THFCH$_2$CN	1.3[a]
n-tridecane:	n-butyl acrylate	2.22
n-tetradecane:	styrene	1.57
n-hexadecane:	acetophenone	2.25
n-hexadecane:	o-methyl acetophenone	2.0[d]
n-hexadecane:	4-acetylpyridine	3.01
n-heptadecane:	4-acetylpyridine	3.06[a]
benzene:	cis-W(CO)$_4$(4VP)$_2$	0.0126
benzene:	cis-W(CO)$_4$(4VP)(4BP)	0.0126[b]
benzene:	cis-W(CO)$_4$(4BP)$_2$	0.00554
acetophenone:	W(CO)$_6$	0.0355
benzene:	4VP	0.0255
benzene:	4BP	0.0257

[a] The response factor was calculated by the formula RF = (No. of carbons of standard)/(No. of carbonds of compound); carbons single bonded to oxygen counted as one half; carbons double bonded to oxygen not counted at all.

[b] Compound not available. RF considered equal to the one measured for cis-W(CO)$_4$(4VP)$_2$.

Valerophenone Actinometry; was used for product quantum yield determinations at 313 nm irradiations. For extremely long 313 irradiations (one week or more; cases of cis-$[Ru(bipy)_2(4EsterBP)_2](BF_4)_2$, $RuTPP(4PhBP)_2$ and $RuOEP(4PhBP)_2$), o-methyl valerophenone and o-methyl butyrophenone were used as actinometers.[90] A 0.1 M solution of the actinometer in benzene containing a known concentration of Hexadecane (internal standard) was irradiated simultaneously with the desired compound in the merry-go-round apparatus and analyzed in Column A or B. Photoproduct quantum yields were determined from (66). The quantum yields for 0.1 M valerophenone, 0.1 M o-methyl valerophenone and 0.1 M butyrophenone are 0.33, 0.016 and 0.0014 mol/einstein, respectively.[90] In some experiments,

$$\Phi_{(product)} = \frac{[product]}{[product\ from\ actinometer]} \times Q.Y._{(of\ actinometer)} \qquad (66)$$

the quencher was absorbing part of the light; an absorbance correction was made by multiplying $\Phi_{product}$ by the following quantity based on Beer's Law:

$$\frac{([quencher]\ \varepsilon^{313}\ quencher + [ketone]\ \varepsilon^{313}\ ketone)}{([ketone]\ \varepsilon^{313}\ ketone)} \qquad (67)$$

When the reacting compound (ketone) concentration is low and therefore does not absorb all the incident irradiation, a correction has to be made again by multiplying the photoproduct quantum yield by the quantity (68) based also on Beer's Law.

$$[1-T_{(actinometer)}]/[1-T_{(ketone)}] \qquad (68)$$

Photoreduction Quantum Yields were determined by the irradiation of a constant aliquot of stock ketone solution in the presence of a hydrogen donor. The absolute quantum yields of photoproduct formation were determined by adding various aliquots of stock donor solution to a constant aliquot of stock ketone solution and diluting to volume. The tubes were prepared, irradiated and analyzed in the usual manner. A plot of $(\Phi_{product})^{-1}$ versus [hydrogen donor]$^{-1}$ yields a line in which the slope divided by the intercept equals k_d/k_r.

Type II quantum yields were determined by analyzing for the alkene or for the acetophenone.

Uranyl Oxalate Actinometry;[97] was used for cis-$W(CO)_4(4VP)_2$ quantum yield determination at 410 nm irradiation. An aqueous solution (2.8 ml) with precisely known concentrations of uranyl nitrate and oxalic acid (in the range of 0.01 M and 0.05 M, respectively) was irradiated in parallel to the Pentacarbonyl (1-(4-pyridyl) pentanone) Tungsten(0) samples, while another sample was kept in dark

as blank. Oxalic acid is consumed photochemically in the presence of Uranyl nitrate sensitizer according to the equation (69):

$$HOOC\text{-}COOH \xrightarrow{h\nu} CO + CO_2 + H_2O \qquad (69)$$

The oxalic acid consumed was determined by titration of both the blank sample and the irradiated sample with a standardized potassium permaganate solution (~6.0 x 10^{-3} M). Potassium permaganate reacting with $C_2O_4^{2-}$ decolorizes. Titration was completed when the pink color of potassium permaganate remains in the titrated solution.

The quantum yield for the oxalic acid consumption upon irradiation at 410 nm is 0.56 mol/einstein and photoproduct quantum yields were determined from (70):

$$\Phi_{product} = [product]/[oxalic\ acid\ consumed] \times 0.56 \qquad (70)$$

Potassium Reineckate Actinometry;[98] was used for the cis-tetracarbonyl (1-(4-pyridyl) pentanone) Tungsten(0) quantum yield determinations at 490 nm irradiations. An aqueous solution (2.8 ml) of the potassium Reinecke's salt (about 0.01 M) was irradiated in parallel to the pentacarbonyl (1-(4-pyridyl pentanone) Tungsten(0) samples while another sample was kept in dark as blank. Potassium Reinecke's salt photoreleases SCN^- according to the equation (71):

$$KCr(NH_3)_2(SCN)_4 \xrightarrow{h\nu} Cr(NH_3)_2(SCN)_3H_2O + KSCN \quad (71)$$

After the irradiation, 10 ml of an aqueous ferric nitrate solution (about 0.1 M) containing perchloric acid (0.5 M) was added to the actinometer solution (and to the blank). The totally released SCN^- forms a red 1:1 complex with Fe(III), the concentration of which was determined spectrophotometrically at 450 nm. (ε FeSCN complex at 450 nm = 4.3×10^3 M^{-1} cm^{-1}). The concentration of the photoreleased SCN^- is found as the difference between the irradiated and the blank sample.

The quantum yield for the SCN^- photoreleased upon irradiation at 490 nm is 0.305[98] and photoproduct quantum yields were determined from (72):

$$\Phi_{product} = [product]/[photoreleased\ SCN^-] \times 0.305 \quad (72)$$

Complex disappearance quantum yields were determined by comparing the complex with the internal (or external) standard area ratios of the solutions before and after irradiation. The factor R, given in (73), when multiplied by the original complex concentration and the result subtracted from the original complex concentration, gives the change in complex concentration (74) from which the disappearance quantum yield is calculated.

$$\frac{[(\text{area of complex})/(\text{area of standard})]_{\text{after irradiation}}}{[(\text{area of complex})/(\text{area of standard})]_{\text{before irradiation}}} = R \qquad (73)$$

$$[\text{complex}]_{\text{original}} - R \times [\text{complex}]_{\text{original}} = [\text{complex}] \qquad (74)$$

Concentration Dependence of quantum yields were determined by two methods. Either by using an actinometer in parallel to the tubes irradiated containing varying concentrations of the substrate or by normalization when the quantum yield at one point (concentration) was known from another experiment. The normalization factor (NF) is given in (75):

NF = (Quantum yield of the Photoproduct at the concentration of known Q.Y.)/(Physical property of the photoproduct at the concentration of known Q.Y.) (75)

The Quantum Yield at any other concentration is given by (76): Physical Property is either (photoproduct/standard)

Quantum yield of the photoproduct at any concentration = NFx(Physical property of the photoproduct at this concentration) (76)

area ratios for gc and HPLC analysis or Corrected Absorbance for visible light absorption analysis. The Corrected Absorbance of the photoproduct at 600 nm method was applied in cis-$W(CO)_4(4VP)_2$ analysis and is valid for low conversions: it is based on the equation (77):

$$A(600)_{corrected} = A(600)_{after\ irradiation} - A(600)_{before\ irradiation} \quad (77)$$

In the normalization method, the sample with the concentration of known quantum yield from an independent experiment plays the role of actinometer.

Stern Volmer Studies Photoproduct Quenching.

For the pyridyl ketone Norrish Type II fragmentation studies or for the pentacarbonyl (1-(4-pyridyl) pentanone) Tungsten(0) disproportionation studies, a constant aliquot of stock ketone (or Tungsten complex) solution was pipetted into several volumetric flasks. Varying aliquots of stock quencher solution were also pipetted into the flasks and diluted to volume. For the pyridyl ketone hydrochloride salts and for the pyridyl ketone Ruthenium complexes Norrish Type II fragmentation studies, solubility reasons prevented us from making stock solutions so the appropriate amount of the pyridyl ketone salts or the Ruthenium complexes were weighted directly into the volumetric flasks which, after the addition of the quencher solution and dillution to volume, gave the final solution for irradiation. Tubes were prepared, degassed, irradiated, and analyzed the way described before. The slope of Φ^o/Φ versus [Quencher] gave $k_q\tau$ for the reacting state.

Emission Quenching. Samples of known concentration of pentacarbonyl (1-(4-pyridyl) pentanone) Tungsten(0) in

benzene were prepared as described for emission studies; emission spectra were recorded for each sample and the peak intensity was taken to be proportional to the emission quantum yield (Φ_{em}). The slope of Φ_{em}^{o}/Φ_{em} versus [Quencher] gave $k_q \tau$ for the emitting state.

Absorption Spectra

Absorption Spectra were taken using 10 mm matched quartz cells. A Beckman recording quartz spectrophotometer with Gilford accessories was used to determine the extinction coefficients at 313 nm and to analyze runs with visible light absorption at 600 nm. Full spectra were recorded on a Varian Cary 21 UV-Vis. spectrophotometer.

Emission Spectra

Emission Spectra at room temperature were obtained using 13 x 100 mm Pyrex culture tubes degassed as described. Emission Spectra at 77°K were taken using a quartz dewar for liquid nitrogen. Sample solution concentrations were in the range of 10^{-4} to 10^{-5} M. A fast-turning chopper was used to cut short-lived emissions. Triplet energies in kcal/mol were calculated from the wavelength (λ) by the formula (78):

$$E(T) = 2860/\lambda \text{ (nm)} \qquad (78)$$

LIST OF REFERENCES

LIST OF REFERENCES

1. V. Balzani and V. Carassiti, "Photochemistry of Coordination Compounds", Academic Press, London, 1970, Chapter 5.

2. S. M. Fredericks, M. S. Wrighton *J. Am. Chem. Soc.* **1980**, *102*, 6166.

3. J. I. Zink *Mol. Photochem.* **1973**, *5*, 151.

4. H. B. Gray, K. R. Mann, N. S. Lewis, J. A. Thich, R. M. Richman *Adv. Chem. Ser.* **1978**, *168*, 44.

5. P. C. Ford, J. D. Petersen, R. E. Hintze *Coord. Chem. Rev.* **1974**, *14*, 67.

6. D. G. Whitten, P. J. Delaive, J. T. Lee, H. Abruna, H. W. Sprintschnik, T. J. Meyer *Adv. Chem. Ser.* **1978**, *168*, 28.

7. R. J. Watts, J. S. Harrington, J. Van Houten *Adv. Chem. Ser.* **1978**, *168*, 57.

8. N. Sutin, C. Greutz *Adv. Chem. Ser.* **1978**, *168*, 1.

9. J. N. Demas, A. W. Adamson *J. Am. Chem. Soc.* **1971**, *93*, 1800.

10. H. Gafney, A. W. Adamson *J. Am. Chem. Soc.* **1972**, *94*, 8238.

11. R. E. Hintze, P. C. Ford *Inorg. Chem.* **1975**, *14*, 1211.

12. P. C. Ford, G. Malouf, J. D. Petersen, V. A. Durante *Adv. Chem. Ser.* **1976**, *150*, 187.

13. P. C. Ford *Coord. Chem. Rev.* **1970**, *5*, 75.

14. P. C. Ford *Adv. Chem. Ser.* **1978**, *168*, 73.

15. D. A. Chaisson, R. E. Hintze, D. H. Steurmer, J. D. Petersen, D. P. McDonald, P. C. Ford *J. Am. Chem. Soc.* **1972**, *94*, 6665.

16. G. Malouf, P. C. Ford *J. Am. Chem. Soc.* **1974**, *96*, 601.

17. P. J. Wagner, R. Bartoszek-Loza *J. Am. Chem. Soc.* **1981**, *103*, 5587.

18. F. H. Burstall *J. Chem. Soc.* **1936**, 173.

19. J. P. Paris, W. W. Brandt *J. Am. Chem. Soc.* **1959**, *81*, 5001.

20. G. A. Crosby, W. G. Perkins, D. M. Klassen *J. Chem. Phys.* **1965**, *43*, 1498.

21. D. M. Klassen, G. A. Crosby *Chem. Phys. Lett.* **1967**, *1*, 127.

22. F. Zuloaga, M. Kasha *Photochem. Photobiol.* **1968**, *7*, 549.

23. D. M. Klassen, G. A. Crosby *J. Chem. Phys.* **1968**, *48*, 1853.

24. J. H. Baxendale, M. Fita *J. Chem. Soc., Dalton Trans.* **1972**, 1995.

25. J. N. Demas, G. A. Crosby *J. Mol. Spectrosc.* **1968**, *26*, 72.

26. J. Van Houten, R. J. Watts *J. Am. Chem. Soc.* **1975**, *97*, 3843.

27. J. Van Houten, R. J. Watts *Inorg. Chem.* **1978**, *17*, 3381.

28. B. Durham, J. V. Caspar, J. K. Nagle, T. J. Meyer *J. Am. Chem. Soc.* **1982**, *104*, 4803.

29. B. Durham, J. L. Walsh, C. L. Carter, T. J. Meyer *Inorg. Chem.* **1980**, *19*, 860.

30. B. Durham, S. R. Wilson, D. J. Hodgson, T. J. Meyer *J. Am. Chem. Soc.* **1980**, *102*, 600.

31. P. P. Zarnegar, D. G. Whitten *J. Am. Chem. Soc.* **1971**, *93*, 3776.

32. P. P. Zarnegar, C. R. Bick, D. G. Whitten *J. Am. Chem. Soc.* **1973**, *95*, 4367.

33. D. G. Whitten *Acc. Chem. Res.* **1980**, *13*, 83.

34. G. A. Crosby, W. H. Elfring, Jr. *J. Phys. Chem.* **1976**, *80*, 2206.

35. R. A. Krause *Inorg. Chim. Acta* **1977**, *22*, 209.

36. M. Hunziker, A. Ludi *J. Am. Chem. Soc.* **1977**, *99*, 7370.

37. E. V. Dose, L. J. Wilson *Inorg. Chem.* **1978**, *17*, 2660.

38. S. Tazuke, N. Kitamura *Pure & Appl. Chem.* **1984**, *56*, 1269.

39. K. A. Goldsby, T. J. Meyer *Inorg. Chem.* **1984**, *23*, 3002.

40. J. D. Petersen, W. R. Murphy, Jr., R. Sahai, K. J. Brewer, R. R. Ruminski *Coord. Chem. Rev.* **1985**, *64*, 261.

41. R. S. Drago, "Physical Methods in Chemistry", W. B. Saunders Co., Philadelphia, 1977, Chapter 6.

42. R. F. Dallinger, W. H. Woodruff *J. Am. Chem. Soc.* **1979**, *101*, 4391.

43. P. G. Bradley, N. Kress, B. A. Hornberger, R. F. Dallinger, W. H. Woodruff *J. Am. Chem. Soc.* **1981**, *103*, 7441.

44. W. K. Smothers, M. S. Wrighton *J. Am. Chem. Soc.* **1983**, *105*, 1067.

45. E. Krausz *Chem. Phys. Lett.* **1985**, *116*, 501.

46. H. W. Thompson, A. P. Garratt *J. Chem. Soc.* **1934**, *524*, 1817.

47. W. Strohmeier, K. Gerlach *Chem. Ber.* **1961**, *94*, 398.

48. W. Strohmeier, D. von Hobe *Chem. Ber.* **1961**, *94*, 164.

49. W. Strohmeier *Angew. Chem., Int. Ed. Engl.* **1964**, *3*, 730.

50. R. N. Perutz, J. J. Turner *J. Am. Chem. Soc.* **1975**, *97*, 4791.

51. J. K. Burdett, M. A. Graham, R. N. Perutz, M. Poliakoff, A. J. Rest, J. J. Turner, R. F. Turner *J. Am. Chem. Soc.* **1975**, *97*, 4805.

52. J. J. Turner, J. K. Burdett, R. N. Perutz, M. Poliakoff *Pure & Appl. Chem.* **1977**, *49*, 271.

53. D. R. Tyler, D. P. Petrylak *J. Organomet. Chem.* **1981**, *212*, 389.

54. R. Bonneau, J. M. Kelly *J. Am. Chem. Soc.* **1980**, *102*, 1220.

55. G. Boxhoorn, A. Oskam, T. M. McHugh, A. J. Rest *Inorg. Chim. Acta* **1980**, *44*, L1.

56. G. Boxhoorn, G. C. Schoemaker, D. J. Stufkens, A. Oskam, A. J. Rest, D. J. Darensbourg *Inorg. Chem.* **1980**, *19*, 3455.

57. J. M. Kelly, C. Long, R. Bonneau *J. Phys. Chem.* **1983**, *87*, 3344.

58. M. Wrighton, G. S. Hammond, H. B. Gray *J. Am. Chem. Soc.* **1971**, *93*, 4336.

59. M. Wrighton, G. S. Hammond, H. B. Gray *Inorg. Chem.* **1972**, *11*, 3122.

60. M. S. Wrighton, H. B. Abrahamson, D. L. Morse *J. Am. Chem. Soc.* **1976**, *98*, 4105.

61. A. J. Lees, A. W. Adamson *Inorg. Chem.* **1981**, *20*, 4381.

62. D. J. Darensbourg, M. A. Murphy *Inorg. Chem.* **1978**, *17*, 884.

63. A. J. Lees, A. W. Adamson *J. Am. Chem. Soc.* **1980**, *102*, 6874.

64. M. Wrighton *Inorg. Chem.* **1974**, *13*, 905.

65. M. Wrighton, G. S. Hammond, H. B. Gray *Mol. Photochem.* **1973**, *5*, 179.

66. M. Wrighton *Chemical Reviews* **1974**, *74*, 401.

67. H. B. Abrahamson, M. S. Wrighton *Inorg. Chem.* **1978**, *17*, 3385.

68. S. Chun, E. E. Getty, A. J. Lees *Inorg. Chem.* **1984**, *23*, 2155.

69. A. J. Lees, A. W. Adamson *J. Am. Chem. Soc.* **1982**, *104*, 3804.

70. P. J. Wagner, "Creation and Detection of the Excited State", Vol. 1A, A. A. Lamola, ed., Marcel Decker, New York, 1971, p. 173.

71. K. Sandros, H. J. L. Backstrom *Acta Chem. Scand.* **1962**, *16*, 956.

72. W. G. Herkstroeter, G. L. Hammond *J. Am. Chem. Soc.* **1966**, *88*, 6534.

73. P. J. Wagner, I. E. Kochevar *J. Am. Chem. Soc.* **1968**, *90*, 2232.

74. P. J. Wagner *Acc. Chem. Res.* **1971**, *4*, 168.

75. P. Ford, D. F. P. Rudd, R. Gaunder, H. Taube *J. Am. Chem. Soc.* **1968**, *90*, 1187.

76. R. G. Gaunder, H. Taube *Inorg. Chem.* **1970**, *9*, 2627.

77. N. N. Greenwood *J. Chem. Soc.* **1959**, 3811.

78. F. P. Dwyer, H. A. Goodwin, E. C. Gyarfas *Aust. J. Chem.* **1963**, *16*, 42.

79. B. Bosnich, F. P. Dwyer *Aust. J. Chem.* **1966**, *19*, 2229.

80. B. C. Chow, I. A. Cohen *Bioinorg. Chem.* **1971**, *1*, 57.

81. W. Sovocol, F. R. Hopf, D. G. Whitten *J. Am. Chem. Soc.* **1972**, *94*, 4350.

82. A. Antipas, J. W. Buchler, M. Gouterman, P. D. Smith *J. Am. Chem. Soc.* **1978**, *100*, 3015.

83. R. H. Linnell, A. Kaczmarzyk *J. Phys. Chem.* **1961**, *65*, 1196.

84. K. Kloc, J. Mlochowski, Z. Szulc *Heterocycles* **1977**, *9*, 849.

85. Rosemary Bartoszek, Ph.D. Thesis, Michigan State University, 1981; (a) page 111; (b) page 56; (c) page 65; (d) page 87; (e) page 93; (f) pages 30 and 90; (g) page 104; (h) page 104.

86. Y. C. Chung, N. Leventis, P. J. Wagner, G. E. Leroi *J. Am. Chem. Soc.* **1985**, *107*, 1416.

87. In EtOH-MeOH glass (4:1 v/v) at 77°K 9.79us: J. N. Demas, G. A. Crosby *J. Am. Chem. Soc.* **1971**, *93*, 2841; in methylene chloride at 298°K 0.19us: see ref. 125.

88. Y. C. Chung, N. Leventis, P. J. Wagner, G. E. Leroi *J. Am. Chem. Soc.* **1985**, *107*, 1414.

89. Y. C. Chung, Ph.D. Thesis, Michigan State University, 1985.

90. P. J. Wagner, C. P. Chen *J. Am. Chem. Soc.* **1976**, *98*, 239.

91. P. J. Wagner, G. Capen *Mol. Photochem.* **1969**, *1*, 173.

92. D. A. Buckingham, F. P. Dwyer, H. A. Goodwin, A. M. Sargeson *Aust. J. Chem.* **1964**, *17*, 325.

93. Y. C. Chung, N. Leventis, P. J. Wagner, G. E. Leroi *Inorg. Chem.* **1985**, *24*, 1966.

94. F. A. Cotton, G. Wilkinson, "Advanced Inorganic Chemistry"; Wiley, New York, 1980; (α): page 1073; (β): page 845.

95. M. H. Chisholm, S. Godleski *Prog. Inorg. Chem.* **1970**, *20*, 299.

96. O. A. Gansow, A. R. Burke *J. Chem. Soc. Chem. Comm.* **1972**, 456.

97. S. L. Murov, "Handbook of Photochemistry", Dekker, New York, 1973, p. 124; C. G. Hatchard, C. A. Parker *Proc. Roy. Soc.*, (London) **1956**, *A235*, 518; J. G. Calvet, J. N. Pitts, Jr., "Photochemistry", Wiley, New York, 1966, p. 783.

98. E. E. Wegner, A. W. Adamson *J. Am. Chem. Soc.* **1966**, *88*, 394.

99. M. Tokuda, M. Hasagawa, A. Suzuki, M. Itoh *Bull. Chem. Soc. Jpn.* **1974**, *47*, 2619.

100. J. A. Barltrop and J. D. Coyle, "Principles of Photochemistry", Wiley, Bristol, 1978, Chapter 4, p. 112.

101. G. Malouf, P. C. Ford *J. Am. Chem. Soc.* **1977**, *99*, 7213.

102. P. J. Wagner, D. A. Ersfeld *J. Am. Chem. Soc.* **1976**, *98*, 4515.

103. P. J. Wagner *J. Am. Chem. Soc.* **1967**, *89*, 2820.

104. Y. C. Chung, N. Leventis, P. J. Wagner, G. E. Leroi, unpublished results.

105. P. J. Wagner, A. E. Kemppainen *J. Am. Chem. Soc.* **1972**, *94*, 7495.

106. P. J. Wagner, A. E. Kemppainen *J. Am. Chem. Soc.* **1968**, *90*, 5896.

107. M. L. Bhanmik, M. A. El-Sayed *J. Phys. Chem.* **1965**, *69*, 275.

108. P. J. Wagner, H. N. Schott *J. Phys. Chem.* **1968**, *72*, 3702.

109. P. J. Wagner *Mol. Photochem.* **1971**, *3*, 169.

110. S. M. Fredericks, J. C. Luong, M. S. Wrighton *J. Am. Chem. Soc.* **1979**, *101*, 7415.

111. P. J. Giordano, S. M. Fredericks, M. S. Wrighton, D. L. Morse *J. Am. Chem. Soc.* **1978**, *100*, 2257.

112. P. J. Wagner *Mol. Photochem.* **1971**, *3*, 23.

113. A. W. Adamson *J. Phys. Chem.* **1967**, *71*, 798.

114. D. J. Darensbourg, R. L. Kump *Inorg. Chem.* **1978**, *17*, 2680.

115. V. A. Durante, P. C. Ford *J. Am. Chem. Soc.* **1975**, *97*, 6898.

116. C. Creutz, N. Sutin *Inorg. Chem.* **1976**, *15*, 496.

117. R. M. Dahlgren, J. I. Zink *Inorg. Chem.* **1977**, *16*, 3154; footnote 29.

118. D. B. Miller, P. K. Miller, N. A. P. Kane-Maguire *Inorg. Chem.* **1983**, *22*, 3831.

119. J. Lewis, R. S. Nyhalm, S. S. Sandhu, M. H. B. Stiddard *J. Chem. Soc.* **1964**, 2825.

120. J. F. O'Donnell, J. T. Ayers, C. K. Mann *Anal. Chem.* **1965**, *37*, 1161.

121. E. O. Foster *J. Chem. Phys.* **1962**, *37*, 1020.

122. *Organic Syntheses*, *46*, 105.

123. C. R. Hauser, W. J. Hamphlett, M. J. Weiss *J. Am. Chem. Soc.* **1948**, *70*, 426. For physical constants, see Irene E. Kochevar, Ph.D. Thesis, Michigan State University, 1970, page 56.

124. J. Gearien, E. Frank, M. Megany, C. Pohorny *J. Med. Chem.* **1971**, *14*, 552.

125. H. N. Al-Jallo, K. B. Prasad, K. S. Al-Dulami *J. Chem. Soc. (C)* **1969**, 2134.

126. H. O. House, M. Schellenbraum *J. Org. Chem.* **1963**, *28*, 34.

127. G. R. Pettit, D. C. Fessler, K. D. Paull, P. Hofer, J. C. Knight *J. Org. Chem.* **1970**, *35*, 1398.

128. A. Bino, F. Cotton *J. Am. Chem. Soc.* **1980**, *102*, 608.

129. L. H. Vogt, Jr., J. L. Katz, S. E. Wibberly *Inorg. Chem.* **1965**, *4*, 1157.

130. R. E. Clarke, P. C. Ford *Inorg. Chem.* **1970**, *9*, 495.

131. B. P. Sullivan, D. J. Salmon, T. J. Mayer *Inorg. Chem.* **1978**, *17*, 3334.

132. D. V. Pinnick, B. Durham *Inorg. Chem.* **1984**, *23*, 1440.

133. B. Bosnich, F. P. Dwyer *Aust. J. Chem.* **1966**, *19*, 2235.

134. J. V. Caspar, T. J. Mayer *Inorg. Chem.* **1983**, *22*, 2444.

135. G. A. Crosby, W. H. Elfring, Jr. *J. Phys. Chem.* **1976**, *80*, 2206.

136. J. Van Houten, R. J. Watts *J. Am. Chem. Soc.* **1976**, *98*, 4853.

APPENDIX

This section contains all the raw data obtained experimentally.

All concentrations are reported in mole/L(M).

Numbers in parentheses do not correlate well with the others And have not been considered in the calculations of the slopes of the corresponding double reciprocal or Stern-Volmer plots.

All bis(2,2'bipyridine) or bis(1,10-phenanthroline) complexes are of the cis- geometry.

Abbreviations

pDCB = p-dichlorobenzene

ArCOOMe = Methyl Benzoate

C13 = n-Tridecane

C14 = n-Tetradecane

C16 = n-Hexadecane

C17 = n-Heptadecane

EtOAc = ethyl acetate

Table 28. Mass Balance Experiment for the Photoreduction of Acetophenone by THF in acetonitrile.

	Before Irradiation Concentration	After Irradiation Concentration
Acetophenone	0.397	0.250
THF	2.00	not analyzed
DTHF[a]	---	0.00374
$THFCH_3CN$[b]	---	0.00313
pTHF-Acetophenone[c]	---	0.00407
1-Phenyl-1-(2-tetrahydrofuryl)-ethanol[d]	---	0.0119
Acetophenone Pinacol[e]	---	0.0263

[a] DTHF = octahydro 2,2'bifuran

[b] $THFCH_3CN$ = 2-(2-tetrahydrofuryl) acetaldimine

[c] pTHF-Acetophenone = 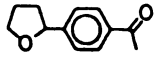

[d] 1-Phenyl-1-(2-tetrahydrofuryl)-ethanol = 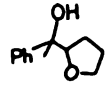

[e] Acetophenone Pinacol = 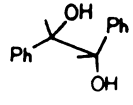

Table 29. Double Reciprocal for DTHF vs. $[THF]^{-1}$ in the Photoreduction of acetophenone by THF.

RUN 1.[a]

[THF]	$[THF]^{-1}$	area DTHF/area pDCB	[DTHF]	Φ_{DTHF}	Φ_{DTHF}^{-1}
0.80	1.250	0.264	0.00233	0.0121	82.4
1.20	0.833	0.338	0.00299	0.0156	64.1
1.60	0.625	0.365	0.00323	0.0168	59.5
2.00	0.500	0.416	0.00367	0.0191	52.3
2.40	0.417	0.478	0.00422	0.0220	45.5

[a]313 nm (Filter A), gc column B at 105°C acetonitrile solvent, [acetophenone] = 0.10 M, [pDCB] = 0.00833 M, I = 0.192 El^{-1} (Valerophenone actinometry).

RUN 2.[a]

[THF]	$[THF]^{-1}$	area DTHF/area pDCB	[DTHF]	Φ_{DTHF}	Φ_{DTHF}^{-1}
0.40	2.50	0.224	0.00197	0.00872	114.7
0.80	1.25	0.375	0.00332	0.0147	68.0
1.20	0.833	0.482	0.00426	0.0188	53.2
1.60	0.625	0.524	0.00462	0.0204	49.0
2.00	0.500	0.580	0.00512	0.0227	44.1
2.40	0.427	0.629	0.00555	0.0246	40.7

[a]313 nm (Filter A), gc Column B at 105°C, acetonitrile solvent, [acetophenone] = 0.10 M [pDCB] = 0.00883 M, I = 0.226 El^{-1} (Valerophenone actinometry).

RUN 3.[a]

[THF]	$[THF]^{-1}$	area DTHF/area pDCB	[DTHF]	Φ_{DTHF}	Φ_{DTHF}^{-1}
0.80	1.25	0.322	0.00319	0.0166	60.1
1.60	0.625	0.458	0.00453	0.0236	42.4
2.40	0.417	0.499	0.00494	0.0257	38.9
3.20	0.313	0.555	0.00549	0.0286	35.0

[a]313 nm (Filter A), gc column D at 175°C, benzene solvent, [acetophenone] = 0.10 M, [pDCB] = 0.00990 M, I = 0.192 El^{-1} (Valerophenone actinometry).

Run 4.[a]

[THF]	$[THF]^{-1}$	area DTHF/area pDCB	[DTHF]	Φ_{DTHF}	Φ_{DTHF}^{-1}
0.20	5.0	0.124	0.00123	0.00544	183.8
		0.130	0.00129	0.00571	175.1
1.57[b]	0.637	0.416	0.00404	0.0179	55.9
2.40	0.417	0.529	0.00524	0.0232	43.1
3.20[c]	0.313	0.232	0.00230	0.0359	27.9
		0.209	0.00207	0.0323	31.0

[a] 313 nm (Filter A), gc column D at 175°C, benzene solvent, [acetophenone] = 0.10 M, [pDCB] = 0.00990 M, I = 0.226 El^{-1} (Valerophenone actinometry).

[b] [pDCB] = 0.00970 M, [acetophenone] = 0.098 M.

[c] I = 0.064 El^{-1} (valerophenone actinometry).

Table 30. Double Reciprocal for $THFCH_3CN$ vs. $[THF]^{-1}$ in the Photoreduction of Acetophenone by THF[a].

[THF]	$[THF]^{-1}$	$\frac{\text{area } THFCH_3CN}{\text{area pDCB}}$	$[THFCH_3CN]$	$\Phi_{THFCH_3CN}^{-1}$
0.80	1.250	0.133	0.00141	136.2
1.20	0.833	0.149	0.00158	121.5
1.60	0.625	0.149	0.00158	121.5
2.00	0.500	0.176	0.00186	103.2
2.40	0.417	0.191	0.00202	95.2

[a] 313 nm (Filter A), gc column B at 98°C, acetonitrile solvent, [acetophenone] = 0.10 M, [pDCB] = 0.00883 M, I = 0.192 El^{-1} (Valerophenone actinometry).

Table 31. Double Reciprocal for DTHF vs. $[THF]^{-1}$ in the Photoreduction of 4-acetylpyridine by THF[a].

[THF]	$[THF]^{-1}$	area DTHF/area ArCOOMe	[DTHF]	Φ_{DTHF}^{-1}
1.00	1.00	0.0530	0.000121	1042
1.40	0.714	0.0684	0.000156	806
1.60	0.625	0.0806	0.000184	685
2.00	0.500	0.148	0.000282	(446)

[a] 313 nm (Filter A), gc column D at 200°C, acetonitrile solvent, [4-acetylpyridine] = 0.10 M, [ArCOOMe] = 0.00212 M, I = 0.126 El^{-1} (Valerophenone actinometry).

Table 32. Double Reciprocal for $THFCH_3CN$ vs. $[THF]^{-1}$ in the Photoreduction of 4-acetylpyridine by THF[a].

[THF]	$[THF]^{-1}$	area $THFCH_3CN$/area ArCOOMe	$[THFCH_3CN]$	$\Phi_{THFCH_3CN}^{-1}$
1.00	1.00	0.270	0.000742	169.8
1.40	0.714	0.368	0.00101	124.7
1.60	0.625	0.381	0.00105	120.0
2.00	0.500	0.969	0.00267	(47.2)

[a] 313 nm (Filter A), gc column D at 175°C, acetonitrile solvent, [4-acetylpyridine] = 0.10 M, [ArCOOMe] = 0.00212 M, I = 0.126 El^{-1} (Valerophenone actinometry).

Table 33. Double Reciprocal for DTHF vs. $[THF]^{-1}$ in the Photoreduction of Benzophenone by THF.[a]

[THF]	$[THF]^{-1}$	area DTHF/area ArCOOMe	[DTHF]	Φ_{DTHF}^{-1}
0.80	1.25	0.0605	0.00151	76.9
1.00	1.00	0.0638	0.00159	73.0
1.20	0.833	0.0672	0.00167	69.4
1.40	0.714	0.0706	0.00176	65.8
1.60	0.625	0.0725	0.00181	64.1
2.00	0.500	0.0741	0.00185	62.9

[a] 313 nm (Filter A), gc column D at 200°C, acetonitrile solvent, [benzophenone] = 0.10 M, [ArCOOMe] = 0.0231 M, I = 0.116 El^{-1} (Valerophenone actinometry).

Table 34. Double Reciprocal for $THFCH_3CN$ vs. $[THF]^{-1}$ in the Photoreduction of Benzophenone by THF.[a]

[THF]	$[THF]^{-1}$	area $THFCH_3CN$/area ArCOOMe	$[THFCH_3CN]$	$\Phi_{THFCH_3CN}^{-1}$
0.80	1.25	0.0509	0.00153	75.8
1.00	1.00	0.0512	0.00154	75.2
1.40	0.714	0.0520	0.00156	74.6
1.60	0.625	0.0637	0.00191	(60.6)
2.00	0.500	0.0612	0.00184	(62.9)

[a] 313 nm (Filter A), gc column D at 175°C, acetonitrile solvent, [benzophenone] = 0.10 M, [ArCOOMe] = 0.0231 M, I = 0.116 El^{-1} (Valerophenone actinometry).

Table 35. Double Reciprocal for DTHF vs $[THF]^{-1}$ in the Photoreduction of 4-benzoylpyridine by THF.[a]

[THF]	$[THF]^{-1}$	area DTHF/area ArCOOMe	[DTHF]	Φ_{DTHF}^{-1}
0.80	1.25	0.0125	0.000297	448.4
1.00	1.00	0.0129	0.000308	431.0
1.20	0.833	0.0137	0.000326	408.2
1.40	0.714	0.0127	0.000355	374.5
1.60	0.625	0.0166	0.000395	336.7
2.00	0.500	0.0230	0.000548	242.7

[a] 313 nm (Filter A), gc column D at 200°C, acetonitrile solvent, [4-benzoylpyridine] = 0.10 M, [ArCOOMe] = 0.0220 M, I = 0.133 El^{-1} (Valerophenone actinometry).

Table 36. Double Reciprocal for $THFCH_3CN$ vs. $[THF]^{-1}$ in the Photoreduction of 4-benzoylpyridine by THF.[a]

[THF]	$[THF]^{-1}$	area $THFCH_3CN$/area ArCOOMe	$[THFCH_3CN]$	$\Phi_{THFCH_3CN}^{-1}$
0.80	1.25	0.0145	0.000415	320.5
1.00	1.00	0.0178	0.000510	261.1
1.20	0.833	0.0205	0.000587	226.8
1.40	0.714	0.0215	0.000615	216.5
1.60	0.625	0.0224	0.000640	207.9
2.00	0.500	0.0216	0.000618	215.1

[a] 313 nm (Filter A), gc column D at 175°C, acetonitrile solvent, [4-benzoylpyridine] = 0.10 M, [ArCOOMe] = 0.0220 M, I = 0.133 El^{-1} (Valerophenone actinometry).

Table 37. Stern Volmer Data for 4-phenyl-1-(4-pyridyl) butanone.

RUN 1.[a]

[Q]	area styrene/area C14	[styrene]	Φ^o/Φ
0.0	0.384	0.00378	---
0.0	0.369	0.00363	---
0.0999	0.192	0.00189	1.96
0.200	0.130	0.00128	2.90
0.300	0.0992	0.000977	3.80
0.400	0.0633	0.000623	(5.96)
0.600	0.0526	0.000518	(7.16)
0.800	0.0402	0.000396	(9.37)

[a]Q = Ethyl sorbate, 313 nm (Filter A, 0.5 hrs.), gc column A at 120°C, acetonitrile solvent, [4PhBP] = 0.040 M, [C14] = 0.00627 M.

RUN 2.[a]

[Q]	area styrene/area C14	[styrene]	Φ^o/Φ
0.0	0.173	0.00161	---
0.0	0.159	0.00148	---
0.0503	0.115	0.00107	1.45
0.151	0.0723	0.000673	2.30
0.201	0.0577	0.000537	2.89
0.302	0.0358	0.000333	(4.65)
0.402	0.0332	0.000309	5.02

[a]Q = Ethyl sorbate, 313 nm (Filter A, 0.5 hrs.), gc column A at 120°C, acetonitrile solvent, [4PhBP] = 0.0401 M, [C14] = 0.00593 M.

Table 38. Stern Volmer data for 4-Phenyl-1-(4-pyridyl)butanone hydrochloride.[a]

[4PhBP.HCl]	[Q]	area styrene/area C14	[styrene]	Φ^{o}/Φ
0.0400	0.0	0.410	0.00392	---
0.0401	0.0	0.409	0.00391	---
0.0401	0.100	0.348	0.00333	1.18
0.0400	0.201	0.259	0.00248	(1.58)
0.0403	0.301	0.263	0.00251	1.56
0.0403	0.502	0.203	0.00194	2.02
0.0403	0.602	0.187	0.00179	2.19

[a]Q = Ethyl sorbate, 313 nm (Filter A, 4 hrs.), gc column A at 120°C, acetonitrile solvent, [C14] = 0.00609 M.

Table 39. Concentration Dependence of the Quantum Yield of the Type II cleavage of 4-Phenyl-1-(4-pyridyl)butanone.[a]

[4PhBP]	Abs.	area styrene/area C14	[styrene]	Φ	Φ_{corr}[d]
0.0042[b]	0.521	0.250	0.00144	0.27	0.39
0.0042[b]	1.042	0.239	0.00137	0.26	0.37
0.0084[c]	2.083	0.146	0.00168	0.32	0.35
0.0168[c]	4.17	0.190	0.00218	0.41	0.41
0.0336[c]		0.208	0.00239	0.45	0.45
0.0504[c]		0.226	0.00260	0.49	0.49
0.0672[c]		0.238	0.00274	0.52	0.52

[a] 313 nm (Filter A, 0.5 hrs.), gc column A at 120°C, acetonitrile solvent, I = 0.00529 El^{-1} (Valerophenone actinometry).

[b] [C14] = 0.00366 M.

[c] [C14] = 0.00732 M.

[d] The first four quantum yields were corrected for partial light absorption at 313 nm.

Table 40. Concentration Dependence of the Quantum Yield of the Type II reaction of 4-Phenyl-1-(4-pyridyl)butanone hydrochloride.[a]

[4PhBP.HCl]	Abs.	area styrene/area C14	[styrene]	Φ	Φ_{corr}[b]
0.00543	0.565	0.117	0.00135	0.073	0.10
0.0107	1.113	0.140	0.00161	0.088	0.095
0.0219	2.778	0.149	0.00171	0.093	0.093
0.0412		0.147	0.00169	0.092	0.092
0.0602		0.146	0.00168	0.091	0.091
0.0794		0.146	0.00168	0.091	0.091

[a]313 nm (Filter A, 4 hrs.), gc column A at 120°C, acetonitrile solvent, [C14] = 0.00732 M, I = 0.0184 El^{-1} (Valerophenone actinometry).

[b]The first two quantum yields were corrected for partial light absorption at 313 nm.

Table 41. Independent Quantum Yield Determination for the Type II Cleavage of Pentaammine 4-Phenyl-1-(4-pyridyl)butanone Ruthenium(II) Tetrafluoroborate.[a]

$[Ru(NH_3)_5(4PhBP)](BF_4)_2$	area styrene/area C14	[styrene]	Φ
0.0200	0.228	0.00255	0.015
0.0200	0.197	0.00220	0.013

[a] 313 nm (Filter A, ~ 20hrs.), gc column A at 120°C, acetonitrile solvent, [C14] = 0.00712 M, I = 0.166 El^{-1} (Valerophenone actinometry), Φ° = 0.014.

Table 42. Quantum Yield and Stern Volmer data for Penaammine 4-Phenyl-1-(4-pyridyl)butanone Ruthenium(II) Tetrafluoroborate.

RUN 1.[a]

$[Ru(NH_3)_5(4PhBP)](BF_4)_2$	[Q]	area styrene/area C14	[styrene]	Φ°/Φ
0.0200	0.0	0.254	0.00272	---
0.0200	0.0	0.260	0.00279	---
0.0193[b]	0.113	0.217	0.00210	1.31
0.0202	0.229	0.125	0.00134	2.06
0.0200	0.343	0.0931	0.000998	2.77
0.0200	0.458	0.0644	0.000691	3.99
0.0200	0.572	0.0594	0.000637	4.33
0.0201	0.686	0.0424	0.000455	(6.07)

[a]Q = Ethyl sorbate, 313 nm (Filter A, ~20 hrs.), gc column A at 120°C, acetonitrile solvent, [C14] = 0.00683 M, I = 0.214 El^{-1} (Valerophenone actinometry), Φ° = 0.013.

[b][C14] = 0.00615 M.

RUN 2.[a]

$[Ru(NH_3)_5(4PhBP)](BF_4)_2$	[Q]	area styrene/area C14	[styrene]	Φ°/Φ
0.0200	0.0	0.190	0.00174	---
0.0201	0.0	0.166	0.00152	---
0.0201	0.0	0.153	0.00140	---
0.0201	0.114	0.138	0.00126	1.23
0.0201	0.228	0.0911	0.000832	1.86
0.0200	0.343	0.0624	0.000570	2.72
0.0201	0.457	0.0451	0.000412	3.76
0.0200	0.571	0.0364	0.000333	4.65
0.0201	0.685	0.0301	0.000275	5.64

[a]Q = Ethyl sorbate, 313 nm (Filter A, ~15 hrs.), gc column A at 120°C, acetonitrile solvent, [C14] = 0.00582 M, I = 0.172 El^{-1} (Valerophenone actinometry), Φ° = 0.0090: rejected.

Table 43. Quantum Yield and Stern Volmer Data for cis-bis(2,2'bipyridine) bis(4-Phenyl-1-(4-pyridyl)butanone) Ruthenium(II) Tetrafluoroborate.

RUN 1.[a]

$[Ru(bipy)_2(4PhBP)_2](BF_4)_2$	[Q]	area styrene/area C14	[styrene]	Φ°/Φ
0.0200	0.0	0.123	0.00137	---
0.0200	0.0	0.121	0.00135	---
0.0200	0.114	0.0817	0.000913	1.49
0.0200	0.229	0.0692	0.000774	1.76
0.0200	0.458	0.0487	0.000544	2.50
0.0188[b]	0.754	0.0373	0.000392	3.47

[a]Q = Ethyl sorbate, 313 nm, (Filter A, ~25 hrs.), gc column A at 120°C, acetonitrile solvent [C14] = 0.00712 M, I = 0.191 El^{-1} (Valerophenone actinometry), Φ° = 0.0071.

[b][C14] = 0.00670 M.

RUN 2.[a]

$[Ru(bipy)_2(4PhBP)_2](BF_4)_2$	[Q]	area styrene/area C14	[styrene]	Φ°/Φ
0.0200	0.0	0.157	0.00168	---
0.0200	0.0	0.153	0.00164	---
0.0201	0.114	0.0954	0.00102	1.63
0.0200	0.229	0.0902	0.000967	1.72
0.0200	0.343	0.0707	0.000758	2.19
0.0200	0.457	0.0638	0.000684	2.43
0.0201	0.572	0.0491	0.000527	3.15
0.0201	0.686	0.0411	0.000441	3.76
0.0200	0.800	0.0393	0.000421	3.94

[a]Q = Ethyl sorbate, 313 nm, (Filter A, ~25 hrs.), gc column A at 120°C, acetonitrile solvent, [C14] = 0.00683 M, I = 0.231 El^{-1} (Valerophenone actinometry), Φ° = 0.0072.

Table 44. Concentration Dependence of the Quantum Yield of the Type II Cleavage of Pentaammine 4-Phenyl-1-(4-pyridyl)butanone Ruthenium(II) Tetrafluoroborate.[a]

$[Ru(NH_3)_5(4PhBP)](BF_4)_2$	area styrene/area C14	[styrene]	Φ [b]
0.00403	0.105	0.00109	0.0068
0.00506	0.127	0.00132	0.0082
0.00711	0.158	0.00165	0.010
0.00923	0.196	0.00204	0.013
0.0152	0.232	0.00242	0.015
0.0201	0.216	0.00225	0.014
0.0401	0.0984	0.00103	0.0064

[a] 313 nm, (Filter A, ~12 hrs.), gc column A at 120°C, acetonitrile solvent [C14] = 0.00664 M.

[b] Quantum Yields were calculated using as normalization base Φ = 0.014 for $[Ru(NH_3)_5(4PhBP)](BF_4)_2$ = 0.0201 M.

Table 45. Concentration Dependence of the Quantum Yield of the Type II cleavage of cis-bis(2,2'bipyridine)-bis(4-Phenyl-1-(4-pyridyl)butanone) Ruthenium(II) Tetrafluoroborate.[a]

$[Ru(bipy)_2(4PhBP)_2](BF_4)_2$	area styrene/area C14	[styrene]	Φ [c]
0.00418	0.172	0.00180	0.0112
0.00599	0.173	0.00181	0.0112
0.00802	0.163	0.00170	0.0106
0.0101	0.153	0.00160	0.0099
0.0200[b]	—	0.00116[b]	0.0072[b]
0.0301	0.0896	0.000935	0.0058
0.0401	0.0750	0.000783	0.0049

[a] 313 nm (Filter A, ~25 hrs.), gc column A at 120°C, acetonitrile solvent, [C14] = 0.00665 M.

[b] It is not a real point; calculated by plotting [styrene] vs. $[Ru(bipy)_2(4PhBP)_2](BF_4)_2$.

[c] Quantum Yields were calculated using as normalization base Φ = 0.0072 for $[Ru(bipy)_2(4PhBP)_2]$ = 0.0200 M (Table 8).

Table 46. Stern Volmer data for the cis-bis(2,2'bipyridine)- bis(4-Phenyl-1-(4-pyridyl)butanone) Ruthenium(II) Tetrafluoroborate Using Complex Concentration 0.010 M.[a]

$[Ru(bipy)_2(4PhBP)_2](BF_4)_2$	[Q]	area styrene/area C14	[styrene]	Φ^o/Φ
0.0100	0.0	0.101	0.00112	---
0.0100	0.0	0.0971	0.00108	---
0.0100	0.114	0.0720	0.000797	1.38
0.00998	0.229	0.0518	0.000573	1.92
0.0100	0.343	0.0447	0.000495	2.22
0.0100	0.458	0.0386	0.000427	2.58
0.00998	0.572	0.0330	0.000365	3.01

[a]Q = Ethyl sorbate, 313 nm, (Filter A, ~16 hrs.), gc column A at 120°C, acetonitrile solvent, [C14] = 0.00705 M.

Table 47. Mass Balance Styrene and 4-acetylpyridine Produced from the Type II Cleavage of cis-bis(2,2'bipyridine)-bis(4-Phenyl-1-(4-pyridyl)butanone) Ruthenium(II) Tetrafluoroborate.

EXPERIMENT 1.[a]

area styrene/area C14[b]	[styrene]	area 4AP/area C17[c]	[4AP][d]
0.153	0.00168	0.0125	0.000590

[a] 313 nm, (Filter A, ~25 hrs.), acetonitrile solvent, $[Ru(bipy)_2(4PhBP)_2](BF_4)_2$ = 0.0200 M.

[b] gc column A at 120°C, [C14] = 0.00683 M.

[c] Sample refluxed for 24 hrs. in acetonitrile in the presence of 147 mg PPh_3; then 0.0104 g C17 was added and diluted to 5.66 ml; [C17] = 0.00764 M; gc column B at 130°C.

[d] [4AP] = 0.000292 M as determined directly from the gc trace; reduced to 2.8 ml (original volume of the irradiated sample - to be directly comparable to [styrene]) [4AP] = 0.000590 M.

EXPERIMENT 2.[a]

area styrene/area C14[b]	[styrene]	area 4AP/area C16[c]	[4AP][d]
0.153	0.00164	0.00117	0.0000743

[a] 313 nm, (Filter A, ~25 hrs.), acetonitrile solvent, $[Ru(bipy)_2(4PhBP)_2](BF_4)_2$ = 0.0200 M.

[b] gc column A at 120°C, [C14] = 0.00683 M.

[c] Sample refluxed for 24 hrs. in n-butyronitrile in the presence of 147 mg PPh_3; then 0.0113 g C16 was added and the sample was diluted to 5 ml with n-butyronitrile; [C16] = 0.0118 M; gc column B at 130°C.

[d] [4AP] = 0.0000416 M as determined directly from the gc trace; reduced to 2.8 ml (original volume of the irradiated sample - to be directly comparable to [styrene]) [4AP] = 0.0000743 M.

Table 48. Quantum Yield and Stern-Volmer Data for the Type II Cleavage of n-butyl-4-[(4-pyridyl)carbonyl]butyrate.

RUN 1[a]

[Q]	area n-butyl acrylate/area C13	[n-butyl acrylate]	Φ°/Φ
0.0	0.122	0.00228	---
0.0	0.122	0.00228	---
0.00353	0.0812	0.00152	1.50
0.00706	0.0598	0.00112	2.04
0.0106	0.0452	0.000845	2.70
0.0141	0.0368	0.000688	3.31
0.0176	0.0323	0.000604	3.78
0.0212	0.0267	0.000499	4.57
0.0283[b]	0.0238	0.000441	5.17

[a]Q = Ethyl sorbate, 313 nm, (Filter A, 0.5 hrs.), gc column A at 108°C, acetonitrile solvent, [4EsterBP] = 0.0204 M, [C13] = 0.00842 M.

[b][4EsterBP] = 0.0202 M, [C13] = 0.00834 M.

RUN 2.[a]

[Q]	area n-butyl acrylate/area C13	[n-butyl acrylate]	Φ°/Φ
0.0	0.166	0.00242	---
0.0	0.164	0.00240	---
0.00337	0.108	0.00158	1.53
0.00673	0.0751	0.00110	2.19
0.0135	0.0522	0.000763	3.16
0.0168	0.0430	0.000628	3.84
0.0202	0.0353	0.000516	4.67
0.0270	0.0238	0.000348	(6.93)

[a]Q = Ethyl sorbate, 313 nm, (Filter A, 0.5 hrs.), gc column A at 108°C, acetonitrile solvent, [4EsterBP] = 0.0208 M, [C13] = 0.00658 M, I = 0.00543 El^{-1} (Valerophenone actinometry), Φ° = 0.44.

Table 49. Independent Quantum Yield Determination for the Type II Cleavage of the n-butyl-4-[(4-pyridyl)carbonyl]butyrate.[a]

area n-butyl acrylate/area C13	[n-butyl acrylate]	Φ
0.160	0.00308	0.37
0.158	0.00304	0.36

[a] 313 nm, (Filter A, ~40 min.), gc column A at 108°C, acetonitrile solvent, [4EsterBP] = 0.0200 M, [C13] = 0.00866 M, I = 0.00838 El^{-1} (Valerophenone actinometry), Φ = 0.37.

Table 50. Quantum Yield and Stern-Volmer Data for the Type II Cleavage of n-butyl-4-[(4-pyridyl)carbonyl]butyrate Hydrochloride.

RUN 1.[a]

[4EsterBP.HCl]	[Q]	$\frac{\text{area n-butyl acrylate}}{\text{area C13}}$	[n-but.acrylate]	Φ°/Φ
0.0305	0.0	0.132	0.00257	---
0.0296	0.0	0.117	0.00228	---
0.0301	0.0192	0.0801	0.00156	1.56
0.0304	0.0769	0.0422	0.000823	2.95
0.0287	0.115	0.0294	0.000573	4.24
0.0300	0.154	0.0221	0.000431	5.64

[a]Q = Ethyl sorbate, 313 nm, (Filter A, ~4 hrs.), gc column A at 108°C, acetonitrile solvent, [C13] = 0.00878 M, I = 0.0252 El^{-1} (Valerophenone actinometry), Φ° = 0.096.

RUN 2.[a]

[4EsterBP.HCl]	[Q]	$\frac{\text{area n-butyl acrylate}}{\text{area C13}}$	[n-but.acrylate]	Φ°/Φ
0.0300	0.0	0.171	0.00276	--
0.0227	0.0	0.164	0.00264	--
0.0295	0.0373	0.0722	0.00116	2.33
0.0294	0.112	0.0390	0.000629	4.29
0.0297	0.149	0.0275	0.000443	6.09

[a] Q = Ethyl sorbate, 313 nm, (Filter A, ~4 hrs.), gc column A at 108°C acetonitrile solvent, [C13] = 0.00726 M.

Table 51. Quantum Yield and Stern-Volmer Data for the Type II Cleavage of Pentaammine n-butyl-4-[(4-pyridyl)carbonyl]butyrate Ruthenium(II) Tetrafluoroborate.

$[Ru(NH_3)_5(4EsterBP)](BF_4)_2$	[Q]	$\frac{\text{area n-but.acrylate}}{\text{area C13}}$	[n-but.acrylate]	Φ^o/Φ
0.0200	0.0	0.102	0.00182	--
0.0201	0.0	0.0891	0.00159	--
0.0200	0.00789	0.0762	0.00136	1.26
0.0200	0.0158	0.0524	0.000933	1.83
0.0201	0.0316	0.0378	0.000673	2.54
0.0200	0.0473	0.0232	0.000413	4.14
0.0197	0.0624	0.0199	0.000350[b]	4.89

[a] Q = Ethyl sorbate, 313 nm, (Filter A, ~30 hrs.), gc column A at 108°C, acetonitrile solvent, [C13] = 0.00802 M, I = 0.290 El^{-1} (Valerophenone actinometry), Φ^o = 0.0059.

[b] [C13] = 0.00793 M.

Table 52. Independent Quantum Yield Determination for the Type II Cleavage of Pentaammine n-butyl-4-[(4-pyridyl)carbonyl]butyrate Ruthenium(II) Tetrafluoroborate.[a]

area n-butyl acrylate / area C13	[n-butyl acrylate]	Φ
0.0901	0.00146	0.0043
0.0906	0.00147	0.0043

[a] 313 nm, (Filter A, ~30 hrs.), gc column A at 108°C, acetonitrile solvent, $[Ru(NH_3)_5(4EsterBP)](BF_4)_2$ = 0.0200 M, [C13] = 0.00732 M, I = 342 El^{-1} (Valerophenone actinometry).

Table 53. Stern-Volmer Data for the Type II Cleavage of Cis-Bis (2,2'bipyridine) bis(n-butyl-4-[(4-pyridyl)carbonyl]butyrate) Ruthenium(II) Tetrafluoroborate.

RUN 1.[a]

$[Ru(bipy)_2(4EsterBP)_2](BF_4)_2$	[Q]	$\frac{\text{area n-but.acrylate}}{\text{area Cl3}}$	[n-but.acrylate]	Φ°/Φ
0.0200	0.0	0.0356	0.000620	--
0.0200	0.0	0.0360	0.000627	--
0.0200	0.00772	0.0323	0.000562	1.11
0.0200	0.0154	0.0282	0.000491	1.27
0.0200	0.0309	0.0219	0.000381	1.64
0.0200	0.0463	0.0175	0.000305	2.05
0.0200	0.0618	0.0153	0.000266	2.35

[a] Q = Ethyl sorbate, 313 nm, (Filter A, ~2 days), gc column A at 108°C, acetonitrile solvent, [Cl3] = 0.00784 M.

RUN 2.[a]

$[Ru(bipy)_2(4EsterBP)_2](BF_4)_2$	[Q]	$\frac{\text{area n-but.acrylate}}{\text{area Cl3}}$	[n-but.acrylate]	Φ°/Φ
0.0200	0.0	0.0761	0.00106	--
0.0200	0.0	0.0726	0.00101	--
0.0200	0.00799	0.0631	0.000880	1.18
0.0200	0.0160	0.0512	0.000714	1.45
0.0200	0.0320	0.0405	0.000565	1.84
0.0200	0.0559	0.0319	0.000445	2.33

[a] Q = Ethyl sorbate, 313 nm, (Filter A, ~4 days), gc column A at 108°C, acetonitrile solvent, [Cl3] = 0.00628 M.

Table 54. Determination and Concentration Dependence of the Quantum Yield of cis-bis(2,2'bipyridine)-bis(n-butyl-4-[(4-pyridyl)carbonyl]butyrate) Ruthenium(II) Tetrafluoroborate.[a]

$[Ru(bipy)_2(4EsterBP)_2](BF_4)_2$	area n-butyl acrylate / area C13	[n-butyl acrylate]	Φ
0.0200	0.159	0.00237	0.0016
0.0200	0.164	0.00244	0.0017
0.00995	0.263	0.00391	0.0027
0.00499	0.250	0.00372	0.0026
0.00249	0.131	0.00195	0.0013

Actinometry for the determination and concentration dependence of the Quantum Yield of the Type II cleavage of cis-bis(2,2'bipyridine)-bis(n-butyl-4-[(4-pyridyl)carbonyl]-butyrate) Ruthenium(II) tetrafluoroborate.[b]

There were used two sets of actinometers.

SET 1.[c]

Actinometer No.	area o-methyl acetophenone / C16	[o-methyl acetophenone]	I
1	0.217	0.00234	1.671
2a	0.201	0.00242	1.726
2b	0.180	0.00216	1.545

$I_{average}$ = 1.647 El^{-1}.

SET 2.[d]

Actinometer No.	area o-methyl acetophenone / C16	[o-methyl acetophenone]	I
1	0.464	0.0211	1.317
2a	0.405	0.0197	1.230
2b	0.419	0.0204	1.273

$I_{average}$ = 1.273 El^{-1}.

[a] 313 nm, (Filter A, ~7 days), gc column A at 108°C, acetonitrile solvent, [C13] = 0.00670 M, I = 1.46 El^{-1}.

[b] It was used o-methyl butyrophenone and o-methyl valerophenone actinometry.

[c] SET 1: Actinometer = o-methyl butyrophenone, gc column A at 190°C.
Actinometer No. 1: [o-methyl butyrophenone] = 0.104 M, [C16] = 0.00539 M.
Actinometer No. 2: [o-methyl butyrophenone] = 0.108 M, [C16] = 0.00601 M.

[d] SET 2: Actinometer = o-methyl valerophenone, gc column A at 190°C.
Actinometer No. 1: [o-methyl valerophenone] = 0.104 M, [C16] = 0.0227 M.
Actinometer No. 2: [o-methyl valerophenone] = 0.105 M, [C16] = 0.0243 M.

Table 55. Stern-Volmer Data for the Quenching of Butyrophenone by Pentaammine 4-acetylpyridine Ruthenium(II) Tetrafluoroborate.[a]

[Q]	area $PhCOCH_3$/area C16	$[PhCOCH_3]$	$[PhCOCH_3]_{corr.}$	Φ^o/Φ	$\Phi^o/\Phi_{corr.}$
0.0	0.380	0.0220	0.0220	--	--
0.0	0.371	0.0215	0.0215	--	--
0.00241	0.189	0.0109	0.0112	2.00	1.95
0.00516	0.118	0.00682	0.00725	3.20	3.01
0.00753	0.0770	0.00445	0.00486	(4.90)	(4.49)
0.00836	0.0788	0.00456	0.00503	4.78	4.33

[a] Q = Pentaammine 4-acetylpyridine Ruthenium(II) tetrafluoroborate, 313 nm, (Filter A), gc column A at 180°C, acetonitrile solvent, [butyrophenone] = 0.501 M, [C16] = 0.0257 M.

[b] Corrections were made for partial light absorption by the ketone.

Table 56. Stern-Volmer Data for the Quenching of Butyrophenone by cis-bis (2,2'bipyridine)bis(4-acetylpyridine) Ruthenium(II) Tetrafluoroborate.

RUN 1.[a]

[Q]	area $PhCOCH_3$/area C16	$[PhCOCH_3]$	$[PhCOCH_3]_{corr.}$[c]	Φ^o/Φ	$\Phi^o/\Phi_{corr.}$[c]
0.0	0.612	0.0340	0.0340	—	—
0.0	0.624	0.0347	0.0347	—	—
0.00106	0.237	0.0132	0.0171	2.61	2.01
0.00210	0.157	0.00873	0.0138	3.94	2.49
0.00311	0.109	0.00606	0.0113	5.68	3.04
0.00432	0.0759	0.00422	0.00926	8.15	3.71
0.00507	0.0518	0.00288	0.00691	(11.94)	(4.98)

RUN 2.[b]

[Q]	area $PhCOCH_3$/area C16	$[PhCOCH_3]$	$[PhCOCH_3]_{corr.}$[c]	Φ^o/Φ	$\Phi^o/\Phi_{corr.}$[c]
0.0	1.027	0.0550	0.0550	—	—
0.0	1.047	0.0561	0.0561	—	—
0.00106	0.448	0.0240	0.0311	2.32	1.79
0.00208	0.314	0.0168	0.0265	3.31	2.10
0.00323	0.206	0.0110	0.0209	5.06	2.66
0.00420	0.162	0.00868	0.0188	6.41	2.96
0.00514	0.132	0.00707	0.0172	7.86	3.23

[a] Q = $[Ru(bipy)_2(4AP)_2](BF_4)_2$, 313 nm, (Filter A), gc column A at 180°C, acetonitrile solvent, [butyrophenone] = 0.502 M, [C16] = 0.0247 M.

[b] Q = $[Ru(bipy)_2(4AP)_2](BF_4)_2$, 313 nm, (Filter A), gc column A at 180°C, acetonitrile solvent, [butyrophenone] = 0.502 M, [C16] = 0.0238 M, I = 0.144 El^{-1} (Valerophenone actinometry), Φ^o = 0.39.

[c] Corrections were made for partial light absorption by the ketone.

Table 57. Stern-Volmer Data for the Quenching of Butyrophenone by cis-bis(1,10-phenanthroline)bis(4-acetylpyridine) Ruthenium(II) Tetrafluoroborate.[a]

[Q]	area $PhCOCH_3$/area C16	$[PhCOCH_3]$	$[PhCOCH_3]_{corr.}$[b]	Φ^o/Φ	$\Phi^o/\Phi_{corr.}$[b]
0.0	0.303	0.0160	0.0160[c]	--	---
0.0	0.414	0.0218	0.0218	--	---
0.0	0.457	0.0241	0.0241	--	---
0.00105	0.391	0.0206	0.0244	1.12	0.99
0.00196	0.290	0.0153	0.0206	1.50	1.17
0.00296	0.212	0.0112	0.0170	2.05	1.42
0.00401	0.170	0.00895	0.0153	2.57	1.58
0.00342	0.196	0.0103	0.0165	2.23	1.47

[a] Q = $[Ru(phen)_2(4AP)_2](BF_4)_2$, 313 nm, (Filter A), gc column A at 180°C, acetonitrile solvent, [butyrophenone] = 0.502 M, [C16] = 0.0234 M, I = 0.0897 El^{-1} (Valerophenone actinometry), Φ^o = 0.27.

[b] Corrections were made for partial light absorption by the ketone.

[c] I = 0.0536 El^{-1} (Valerophenone actinometry).

Table 58. Determination and Concentration Dependence of the Quantum Yield of the Type II Cleavage of Ruthenium Tetraphenylporphyrinato bis(4-phenyl-1-(4-pyridyl) butanone).[a]

[RuTPP(4PhBP)$_2$]	area styrene/area C14	[styrene]	Φ
0.000475[b]	0.0524	0.000389	0.000263
0.00106[b]	0.110	0.000817	0.000552
0.00244[b]	0.139	0.00103	0.000694
0.00500[c]	0.0212	0.000182	0.000313
0.00758[c]	0.0139	0.000119	0.000205
0.0100[c]	0.0114	0.000177	0.000168
0.0183[d]	0.0368	0.000221	0.000157
0.0201[e]	0.0231	0.000304	0.000203

[a] 313 nm, (Filter A, 7-10 days), gc Column A at 120°C, methylene chloride solvent.

[b] [C14] = 0.00473 M, I = 1.48 El^{-1} (o-methylvalerophenone and o-methylbutyrophenone actinometry).

[c] [C14] = 0.00546 M; a solution of RuTPP(4PhBP)$_2$ in methylene chloride 0.00106 M was used as actinometer, irradiated in parallel to the other three samples. It was found for this sample: area styrene/area C14 = 0.0374.

[d] [C14] = 0.00383 M, I = 1.41 El^{-1} (o-methylbutyrophenone actinometry).

[e] [C14] = 0.00838 M, I = 1.50 El^{-1} (o-methylbutyrophenone actinometry).

Table 59. Determination of the Quantum Yield of the Type II Cleavage of Ruthenium Octaethylporphyrinato bis(4-phenyl-1-(4-pyridyl)butanone).[a]

$[RuOEP(4PhBP)_2]$	area styrene/area C14	[styrene]	Φ
0.0201	0.0251	0.00330	0.000220

[a] 313 nm, (Filter A, ~10 days), gc Column A at 120°C, methylene chloride solvent, [C14] = 0.00838 M, I = 1.50 El^{-1} (o-methylbutyrophenone actinometry).

Table 60. Data for the Calculation of the Response Factors of Various Compounds vs. Benzene for the HPLC Analysis.

Data for $W(CO)_5(4BP)$.[a]

Weight of $W(CO)_5(4BP)$	$[W(CO)_5(4BP)]$	$\frac{\text{area Benzene}}{\text{area 4VP}}$	RF
0.0096[b]	0.00203	2.749	0.00558
0.0107[b]	0.00226	2.431	0.00549

Data for 4VP.[a]

Weight of 4VP	[4VP]	$\frac{\text{area Benzene}}{\text{area 4VP}}$	RF
0.0138[c]	0.00339	7.281	0.0247
0.0126[b]	0.00773	3.384	0.0262

Data for 4BP.[a]

Weight of 4BP	[4BP]	$\frac{\text{area Benzene}}{\text{area 4BP}}$	RF
0.0155[c]	0.00416	6.078	0.0253
0.0108[b]	0.0113	2.311	0.0261

Data for $cis\text{-}W(CO)_4(4VP)_2$.[a]

Weight of $cis\text{-}W(CO)_4(4VP)_2$	$[cis\text{-}W(CO)_4(4VP)_2]$	$\frac{\text{area Benzene}}{\text{area } cis\text{-}W(CO)_4(4VP)_2}$	RF
0.0019[d]	0.00102	13.661	0.0139
0.0027[b]	0.000338	33.195	0.0112

Data for $W(CO)_6$.[a]

Weight of $W(CO)_6$	$[W(CO)_6]$	weight of acetophenone	[acetophenone]	area acetophenone / area $W(CO)_6$	SF
0.0111[b]	0.00315	0.1047[b]	0.0871	1.258	0.0455
0.0030[b]	0.00852	0.0810[b]	0.0674	2.192	0.0277

[a] HPLC analysis; detector at 270 nm, HPLC column D eluting with 85% hexane, 15% ethyl acetate at 1.5 ml/min. Detector attenuator at 64, recorder attenuator at 4.

[b] in 10 ml benzene.

[c] in 25 ml benzene.

[d] in 3 ml benzene.

[e] HPLC analysis; detector at 290 nm, HPLC column D eluting with 95% hexane, 5% ethyl acetate at 1.5 ml/min. Benzene does not show up in the HPLC trace. Detector attenuator at 64, recorder attenuator at 4.

Table 61. Mass Balance Experiment for the Irradiation of Pentacarbonyl 1-(4-pyridyl)pentanone Tungsten(0).[a]

	area $W(CO)_5$4VP / area acetophenone	$[W(CO)_5$4VP$]$[b,c]	area cis-$W(CO)_4(4VP)_2$ / area benzene	$[cis\text{-}W(CO)_4(4VP)_2]$[d]	area $W(CO)_6$ / area acetophenone	$[W(CO)_6]$[b,c]
Experiment 1.						
before irradiation	0.763	0.00958	---	---	---	---
after irradiation	0.137	0.00172	0.280	0.00353	0.590	0.00362
after irradiation	0.133	0.00167	0.278	0.00350	0.592	0.00364
Experiment 2.						
before irradiation	1.101	0.0129	---	---	---	---
after irradiation	0.727	0.00852	0.205	0.00258	0.461	0.00260
after irradiation	0.721	0.00845	0.222	0.00280	0.453	0.00256

[a] λ_{irr} > 400 nm, (Filter B, ~24 hrs.), benzene solvent.

[b] HPLC analysis, column B, eluting with 95% hexane, 5% EtOAc, Detector at 290 nm; 1.5 ml/min.

[c] Acetophenone solution was added as an external standard. 1 ml of sample was mixed with 1 ml of the acetophenone solution. In each sample, after dilution: [acetophenone] = 0.0840 M for the first experiment and [acetophenone] = 0.0770 M for the second experiment. Therefore, the actual concentrations of $W(CO)_5$ measured are half those reported on the table.

[d] HPLC analysis, column B, eluting with 85% hexane, 15% EtOAc, detector at 270 nm; 1.5 ml/min.

Table 62. Comperative Mass Balance Experiment for the Irradiation of Pentacarbonyl 1-(4-pyridyl)pentanone Tungsten(0), Degassed Normally and Under Carbon Monoxide.[a]

	area $W(CO)_5$4VP / area benzene	$[W(CO)_5(4VP)]$[b]	A_{600}	$[cis\text{-}W(CO)_4(4VP)_2]$[c]	area 4VP / area benzene	[4VP][b]
Before Irradiation	0.970	0.167	0.075	---	---	---
After Irradiation						
Sample Degassed	0.0650	0.0112	1.93	0.000681	---	---
Sample Under 2 atm CO	0.0663	0.0114	0.128	0.0000452	0.143	0.00429

[a] $\lambda_{irr} > 400$ nm, (Filter B, ~24 hrs.), benzene solvent (standard).

[b] HPLC analysis, column D elutind with 85% Hexane, 15% EtOAc, detector at 270 nm; 1.5 ml/min.

[c] Analyzed by the visible light absorption at 600 nm.

Table 63. Quantum Yield Data for Pentacarbonyl 1-(4-pyridyl)pentanone Tungsten(0) Photolysis at 490 nm.

Solvent Benzene.[a]

		[cis-$W(CO)_4(4VP)_2$]
area cis-$W(CO)_4(4VP)_2$/area benzene:	0.00117	$1.47\ 10^{-5}$
A_{∞}:	0.125	$4.41\ 10^{-5}$

$\Phi = 6.58\ 10^{-4} \pm 3.29\ 10^{-4}$

Solvent Methylcyclohexane.[b]

		[cis-$W(CO)_4(4VP)_2$]
area cis-$W(CO)_4(4VP)_2$/area benzene:	0.000234	$2.94\ 10^{-6}$
A_{∞}:	0.002	$7.06\ 10^{-7}$

$\Phi = 4.08\ 10^{-5} \pm 2.49\ 10^{-5}$

Actinometry (Potassium Reineckate).[c]

Act No.	[$KCr(NH_3)(NCS)_4$]	A_{450}, blank	A_{450}	$[SCN^-]_{measured}$	$[SCN^-]^d$,(M)
1	0.0103	1.016	2.522	$5.87\ 10^{-4}$	0.00160
2	0.0101	1.415	2.230	$5.19\ 10^{-4}$	0.000867
3	0.00946	0.784	2.054	$4.78\ 10^{-4}$	0.00135
4	0.0106	0.972	2.447	$5.69\ 10^{-4}$	0.00157
5	0.0113	1.113	2.684	$6.24\ 10^{-4}$	0.00167
6	0.0102	1.485	0.648[e]	$1.51\ 10^{-4}$	0.00187
7	0.0104	1.240	2.737	$6.37\ 10^{-4}$	0.00159
8	0.0100	1.338	0.623[e]	$1.45\ 10^{-4}$	0.00189
9	0.0109	1.238	2.391	$5.56\ 10^{-4}$	0.00123

$[SCN^-]_{total} = 0.0136$ M.

[a] $[W(CO)_5(4VP)] = 0.0504$ M, Filter D, ~42 hrs.

[b] $[W(CO)_5(4VP)] = 0.0501$ M, Filter D, ~42 hrs.

[c] Each actinometer was irradiated for about 6 hrs., $I = 0.0447\ El^{-1}$.

[d] These concentrations are the ones reduced to the original 2.8 ml solution of the actinometer, since in order to measure the SCN^- photoreleased, 10 ml of a solution of $Fe(NO_3)_3.9H_2O$, 0.1 M, containing $HClO_4$ (0.5 M) was added to the actinometer solution after irradiation.

[e] These solutions were too concentrated so they were diluted 1:5 before the absorption at 450 nm was measured.

Table 64. Quantum Yield Data for Pentacarbonyl 1-(4-pyridyl)pentanone Tungsten(0) Photolysis at 410 nm.

Solvent Benzene.[a]

		[cis-$W(CO)_4(4VP)_2$]
area cis-$W(CO)_4(4VP)_2$/area benzene:	0.0404	$5.09\ 10^{-4}$
A_{400}:	0.634	$2.24\ 10^{-4}$

$\Phi = 0.0657 \pm 0.0160$

Solvent Methylcyclohexane.[b]

		[cis-$W(CO)_4(4VP)_2$]
area cis-$W(CO)_4(4VP)_2$/area benzene:	0.0140	$1.76\ 10^{-4}$
A_{400}:	0.508	$1.79\ 10^{-4}$

$\Phi = 0.0285 \pm 0.0283$

Actinometry (Uranyl Oxalate).[c]

Solution 1.

[Uranyl Nitrate] = 0.0102 M.

[Oxalic Acid] = 0.0504 M.

Solution 2.

[$KMnO_4$] = 0.00651 M.

Actinometer Solution No.	Volume of $KMnO_4$ Solution (ml)
Blank	8.60
1	8.05
2	7.95

$[\text{Oxalic Acid}]_{reacted} = 3.49\ 10^{-3}$ M.

---

[a] $[W(CO)_5(4VP)] = 0.0504$ M, Filter D, ~24 hrs.

[b] $[W(CO)_5(4VP)] = 0.0501$ M, Filter D, ~24 hrs.

[c] $I = 0.00623\ El^{-1}$.

Table 65. Concentration Dependence of the Quantum Yield of $W(CO)_5(4VP)$ Photolysis at $\lambda = 490$ nm.[a]

$[W(CO)_5(4VP)]$	A_{600}	$[cis\text{-}W(CO)_4(4VP)_2]$	Φ [b]	Φ^{-1}
0.00520	0.152	$5.36\ 10^{-5}$	$3.67\ 10^{-4}$	$2.72\ 10^{3}$
0.00520	0.153	$5.40\ 10^{-5}$	$3.70\ 10^{-4}$	$2.70\ 10^{3}$
0.0104	0.173	$6.10\ 10^{-5}$	$4.18\ 10^{-4}$	$2.39\ 10^{3}$
0.0208	0.209	$7.37\ 10^{-5}$	$5.05\ 10^{-4}$	$1.98\ 10^{3}$
0.0208	0.210	$7.41\ 10^{-5}$	$5.08\ 10^{-4}$	$1.97\ 10^{3}$
0.0416	0.249	$8.79\ 10^{-5}$	$6.02\ 10^{-4}$	$1.66\ 10^{3}$
0.0504	---	$9.60\ 10^{-5}$[c]	$6.58\ 10^{-4}$	$1.52\ 10^{3}$
0.0623	0.299	$1.06\ 10^{-4}$	$7.27\ 10^{-4}$	$1.38\ 10^{3}$

[a] Filter D, ~3 days, Benzene solvent, analysis by the visible light absorption at 600 nm.

[b] Quantum yields calculated by normalization, using as a basis the quantum yield at $[W(CO)_5(4VP)] = 0.0504$ M.

[c] This is not a real point; calculated by plotting $[cis\text{-}W(CO)_4(4VP)_2]$ vs. $[W(CO)_5(4VP)]$.

Table 66. Concentration Dependence of the Quantum Yield of $W(CO)_5(4VP)$ Photolysis at λ = 410 nm.[a]

$[W(CO)_5(4VP)]$	A_{600}	$[cis\text{-}W(CO)_4(4VP)_2]$	Φ [b]	Φ^{-1}
0.00517	0.372	$1.31\ 10^{-4}$	$3.65\ 10^{-2}$	27.4
0.00517	0.387	$1.37\ 10^{-4}$	$3.82\ 10^{-2}$	26.2
0.0103	0.432	$1.52\ 10^{-4}$	$4.24\ 10^{-2}$	23.6
0.0207	0.502	$1.77\ 10^{-4}$	$4.93\ 10^{-2}$	20.3
0.0310	0.542	$1.91\ 10^{-4}$	$5.32\ 10^{-2}$	18.8
0.0413	0.579	$2.04\ 10^{-4}$	$5.68\ 10^{-2}$	17.6
0.0504	---	$2.11\ 10^{-4}$[c]	$5.88\ 10^{-2}$	17.0
0.0517	0.599	$2.11\ 10^{-4}$	$5.88\ 10^{-2}$	17.0

[a] Filter D, ~3 days, benzene solvent, analysis by the visible light absorption at 600 nm.

[b] Quantum yields calculated by normalization, using as a basis the quantum yield at $[W(CO)_5(4VP)]$ = 0.0504 M.

[c] This is not a real point; calculated by plotting $[cis\text{-}W(CO)_4(4VP)_2]$ vs. $[W(CO)_5(4VP)]$.

Table 67. Stern-Volmer Data for $W(CO)_5(4VP)$ irradiated at 490 nm.[a]

[Q]	area cis-$W(CO)_4(4VP)_2$/area standard[b]	Φ^0/Φ
0.0	0.0853	---
0.0	0.0866	---
0.00650	0.0243	3.53
0.0130	0.0148	5.81
0.0260	0.00817	10.55
0.0520	0.00421	20.43

[a] Filter D, 2 days, $[W(CO)_5(4VP)]$ = 0.0105 M, anthracene quencher, benzene solvent, HPLC analysis, column D eluting with 85% Hexane, 15% EtOAc; 1.5 ml/min.

[b] As standard was used a $W(CO)_5(4AP)$ solution in benzene (0.00294 M), 1 ml of which was added externally after irradiation in each sample.

Table 68. Stern-Volmer Data for $W(CO)_5(4VP)$ Irradiated at 490 nm.[a]

[Q]	A_{600}	[cis-$W(CO)_4(4VP)_2$]	Φ^0/Φ
0.0	0.067	$2.36\ 10^{-5}$	---
0.00101	0.048	$1.69\ 10^{-5}$	1.40
0.00203	0.038	$1.34\ 10^{-5}$	1.77
0.00406	0.022	$7.76\ 10^{-6}$	3.05

[a] Filter D, 2 days, [$W(CO)_5(4VP)$] = $8.97\ 10^{-4}$ M, benzene solvent, anthracene quencher, analysis by visible light absorption at 600 nm. A_{600} before irradiation = 0.

Table 69. Stern-Volmer Data for the $W(CO)_5(4VP)$ Emission Quenching.[a]

[Q]	Emission Peak Intensity[b]	Φ^o/Φ
0.0	42.50	---
0.00101	25.25	1.68
0.00203	18.50	2.30
0.00406	15.00	2.83
0.00608	9.38	4.53

[a] $[W(CO)_5(4VP)] = 8.97\ 10^{-4}$ M, benzene solvent anthracene quencher. Excitation at 420 nm. Emission scan from 500-800 nm, slits 12-12 nm, scan speed 60 nm/min.

[b] Indentations of the chart paper at maximum intensity.

Table 70. Stern-Volmer Quenching Data for the cis-$W(CO)_4(4VP)_2$ Formation from $W(CO)_5(4VP)$ at [complex] = 0.00508 M.[a]

[Q]	A_{500}	[cis-$W(CO)_4(4VP)_2$]	Φ^0/Φ
0.0	0.213	$8.13\ 10^{-5}$	---
0.00111	0.184	$7.02\ 10^{-5}$	1.16
0.00222	0.160	$6.11\ 10^{-5}$	1.33
0.00888	0.088	$3.36\ 10^{-5}$	2.42

[a] Quencher anthracene, solvent benzene, irradiation at 490 nm, Filter D. HPLC analysis, Column D, eluting with 85% hexane, 15% ethyl acetate.

Table 71. Stern-Volmer Quenching Data for the Emission from $W(CO)_5(4VP)$ at [Complex] = 0.00508 M.[a]

[Q]	Emission peak height[b]	Φ^o/Φ
0.0	27.8	---
0.00111	21.0	1.32
0.00444	16.0	1.73
0.00666	12.0	2.31
0.00888	11.0	2.52

[a] Quencher anthracene, solvent Benzene, excitation at 420 nm. Emission spectra were recorded from 500-800 nm. Slits at 10 nm.

[b] Indentations of the chart paper.

Table 72. Stern-Volmer Data for $W(CO)_5(4VP)$ Emission Quenching.[a]

[Q]	Emission Peak Intensity[b]	Φ°/Φ
0.0	67.00	---
0.000912	42.90	1.56
0.00182	31.7	2.11
0.00274	26.4	2.54
0.00365	21.5	3.17

[a] $[W(CO)_5(4VP)] = 8.29\ 10^{-5}$ M, benzene solvent, anthracene quencher. Excitation at 420 nm. Emission scan from 500-800 nm, slits 12-12 nm, scan speed 60 nm/min.

[b] Indentations of the chart paper at maximum intensity.

Table 73. Stern-Volmer Data for $W(CO)_5(4VP)$ Irradiated at 410 nm.[a]

[Q]	A_{500}	[cis-$W(CO)_4(4VP)_2$]	Φ^0/Φ
0.0	0.508	0.000179	---
0.0	0.481	0.000170	---
0.00591	0.343	0.000121	1.45
0.0118	0.313	0.000110	1.59
0.0237	0.245	0.0000865	2.02
0.0355	0.223	0.0000787	2.22
0.0473	0.191	0.0000674	2.60

[a] [$W(CO)_5(4VP)$] = 0.0105 M, benzene solvent, anthracene quencher, analysis by the visible light absorption at 600 nm.

Table 74. Stern-Volmer Data for $W(CO)_5(4VP)$ Irradiated at 410 nm.[a]

[Q]	A_{600}	[cis-$W(CO)_4(4VP)_2$]	Φ°/Φ
0.0	0.127	$4.48\ 10^{-5}$	---
0.0	0.127	$4.48\ 10^{-5}$	---
0.0119	0.070	$2.47\ 10^{-5}$	1.81
0.0237	0.062	$2.19\ 10^{-5}$	2.05
0.0356	0.046	$1.62\ 10^{-5}$	2.77
0.0474	0.041	$1.45\ 10^{-5}$	3.09

[a] Filter D, [$W(CO)_5(4VP)$] = 0.00364 M, benzene solvent, anthracene quencher, analysis by the visible light absorption at 600 nm.

Table 75. Stern-Volmer for $W(CO)_5(4VP)$ Irradiated at 410 nm.[a]

[Q]	A_{600}	[cis-$W(CO)_4(4VP)_2$]	Φ^0/Φ
0.0	0.077	$2.72\ 10^{-5}$	---
0.0	0.079	$2.79\ 10^{-5}$	---
0.0119	0.054	$1.91\ 10^{-5}$	1.45
0.0237	0.040	$1.41\ 10^{-5}$	1.96
0.0356	0.035	$1.24\ 10^{-5}$	2.23
0.0474	0.025	$8.82\ 10^{-6}$	3.13

[a] Filter D, [$W(CO)_5(4VP)$] = 0.00104 M, benzene solvent, anthracene quencher, analysis by the visible light absorption at 600 nm.

Table 76. Chemical Quenching Stern-Volmer Data for $W(CO)_5(4VP)$ Irradiated at $\lambda > 400$ nm.[a]

RUN 1.[b]

[4VP]	area cis-$W(CO)_4(4VP)_2$/area benzene	[cis-$W(CO)_4(4VP)_2$]	Φ°/Φ
0.0	0.174	0.00219	---
0.0	0.172	0.00217	---
0.00106	0.135	0.00170	1.28
0.00318	0.0867	0.00109	2.00
0.00424	0.0797	0.00100	2.18
0.00742	0.0617	0.000777	2.81

RUN 2.[c]

0.0	0.272	0.00343	---
0.0	0.291	0.00367	---
0.00110	0.206	0.00260	1.37
0.00220	0.167	0.00210	1.69
0.00440	0.122	0.00154	2.31
0.00660	0.0933	0.00118	3.02
0.00770	0.0830	0.00105	3.40
0.00880	0.0728	0.000917	3.87

[a] benzene solvent (standard), 1-(4-pyridyl)pentanone quencher, HPLC analysis column D, eluting with 85% Hexane, 15% Ethyl Acetate; 1.5 ml/min.

[b] $[W(CO)_5(4VP)] = 0.0201$ M, Filter B, ~6 hrs.

[c] $[W(CO)_5(4VP)] = 0.0206$ M, Filter B, ~9 hrs.

Table 77. Chemical Quenching Stern-Volmer Data for $W(CO)_5(4VP)$ Irradiated at $\lambda >$ 475 nm.[a]

[4VP]	area cis-$W(CO)_4(4VP)_2$/area benzene	[cis-$W(CO)_4(4VP)_2$]	Φ°/Φ
0.0	0.0847	0.00107	---
0.0	0.101	0.00127	---
0.00109	0.0520	0.00655	1.79
0.00218	0.0344	0.000433	2.70
0.00327	0.0258	0.000325	3.60
0.00436	0.0216	0.000272	4.30
0.00654	0.0162	0.000204	5.74
0.00763	0.0111	0.000140	(8.36)

[a] Filter C, ~24 hrs., [$W(CO)_5(4VP)$] = 0.0204 M, benzene solvent (standard), 1-(4-pyridyl)pentanone quencher, HPLC analysis column D, eluting with 85% Hexane, 15% Ethyl Acetate; 1.5 ml/min.

Table 78. Stern-Volmer Data for $W(CO)_5(4VP)$ Emission Quenching by 4AP.[a]

[Q]	Emission Peak Intensity[b]	Φ°/Φ
0.0	60.8	---
0.0204	57.2	1.06
0.0408	52.8	1.15
0.0816	49.4	1.23
0.203	43.4	1.40
0.407	35.0	1.74
0.814	22.0	2.76

[a] $[W(CO)_5(4VP)] = 1.41\ 10^{-4}$ M, benzene solvent, 4-Acetylpyridine quencher. Excitation at 420 nm. Emission scan from 500-800 nm, slits 10-10 nm, scan speed 60 nm/min.

[b] Indentations of the chart paper at maximum intensity.

Table 79. Stern-Volmer Data for $W(CO)_5(4VP)$ Emission Quenching by 4VP.[a]

[Q]	Weight of the Paper Under the Emission Peak[b]	Φ°/Φ
0.0	0.71	---
0.0	0.75	---
0.0	0.75	---
0.0402	0.70	1.06
0.0804	0.66	1.12
0.402	0.55	1.35
0.805	0.37	2.00

[a] $[W(CO)_5(4VP)] = 6.7\ 10^{-5}$ M, benzene solvent, 4-Valerylpyridine quencher. Excitation at 410 nm. Emission scan from 500-800 nm, slits 10-10 nm, scan speed 60 nm/min.

[b] In grams.

Table 80. Intermediate Trapping Data for $W(CO)_5(4VP)$ Irradiated at $\lambda > 400$ nm.[a]

RUN 1

[4BP]	area $W(CO)_5$4BP / area benzene	$[W(CO)_5$4BP$]$	area $W(CO)_4(4VP)_2$ / area benzene	$[W(CO)_4(4VP)_2]$	area $W(CO)_4(4VP)(4BP)$ / area benzene	$[W(CO)_4(4VP)(4BP)]^b$
0.0	0.0	0.0	0.173	2.18×10^{-3}	0.0	0.0
0.0	0.0	0.0	0.183	2.31×10^{-3}	0.0	0.0
0.00147	0.124	6.87×10^{-4}	0.0853	1.07×10^{-3}	0.0351	4.42×10^{-4}
0.00441	0.348	1.93×10^{-3}	0.00449	5.66×10^{-5}	0.0427	5.38×10^{-4}
0.00588	0.416	2.30×10^{-3}	0.0	0.0	0.0420	5.29×10^{-4}
0.00735	0.467	2.59×10^{-3}	0.0	0.0	0.0338	4.26×10^{-4}
0.0103	0.513	2.84×10^{-3}	0.0	0.0	0.0160	2.02×10^{-4}

RUN 2

[4BP]	area $W(CO)_5(4VP)$ / area benzene	$[W(CO)_5(4VP)]$	area $W(CO)_4(4BP)$ / area benzene	$[W(CO)_5(4BP)]$	area 4VP / area benzene	[4VP]	area 4BP / area benzene	[4BP]
0.0	0.885	0.0202	---	---	0.0	0.0	0.0	0.0
0.0	0.596	0.0136	---	0.0	0.0	0.0	0.0	0.0
0.0	0.575	0.0131	---	0.0	0.0	0.0	0.0	0.0
0.00077	0.647	0.0148	0.0597	0.00033	0.00725	0.00018	[c]	[c]
0.00154	0.668	0.0152	0.135	0.00075	0.0603	0.00154	0.00640	0.00016
0.00231	0.689	0.0157	0.212	0.00117	0.0830	0.00212	0.0104	0.00027
0.00308	0.687	0.0157	0.278	0.00154	0.0983	0.00251	0.0171	0.00044
0.00462	0.712	0.0163	0.349	0.00193	0.134	0.00342	0.0381	0.00098
0.00616	0.720	0.0164	0.455	0.00252	0.172	0.00439	0.0702	0.00180
0.0077	0.728	0.0166	0.501	0.00278	0.196	0.00500	0.107	0.00275

RUN 2, CONTINUED

[4BP]	$\frac{\text{area cis-W(CO)}_4\text{(4VP)}_2}{\text{area benzene}}$	[cis-W(CO)$_4$(4VP)$_2$]	$\frac{\text{area cis-W(CO)}_4\text{(4VP)(4BP)}}{\text{area benzene}}$	[cis-W(CO)$_4$(4VP)(4BP)][b]	$\frac{\text{area cis-W(CO)}_4\text{(4BP)}_2}{\text{area benzene}}$	[cis-W(CO)$_4$(4BP)$_2$][b]
0.0	0.300	0.00378	---	0.0	---	0.0
0.0	0.298	0.00375	---	0.0	---	0.0
0.00077	0.203	0.00256	0.0205	0.00026	[c]	0.0
0.00154	0.146	0.00184	0.0297	0.00037	0.000668	$8.4\ 10^{-6}$
0.00231	0.107	0.00135	0.0349	0.00044	0.00137	$1.7\ 10^{-5}$
0.00308	0.0875	0.00110	0.0372	0.00047	0.00147	$1.9\ 10^{-5}$
0.00462	0.0571	0.00072	0.0409	0.00052	0.00371	$4.7\ 10^{-5}$
0.00616	0.0411	0.00052	0.0410	0.00052	0.00474	$6.0\ 10^{-5}$
0.0077	0.0283	0.00036	0.0361	0.00045	0.00584	$7.4\ 10^{-5}$

[a] [W(CO)$_5$(4VP)] = 0.0202 M, Irradiated with the $NaNO_2$ filter solution, benzene solvent (standard), 1-(4-pyridyl)butanone trapper, HPLC analysis column D, eluting with 85% Hexane, 15% EtOAc; 1.5 ml/min.

[b] cis-W(CO)$_4$(4VP)(4BP) and cis-(W(CO)$_4$(4BP)$_2$ have not been isolated. Concentrations were calculated using as standarization factor 0.0126; the same standarization factor as for cis-W(CO)$_4$(4VP)$_2$.

[c] Detectable but not measurable.

Table 8]. Intermediate Trapping Data for $W(CO)_5(4VP)$ Irradiated at $\lambda > 475$ nm.[a]

RUN 1

[4BP]	$\frac{\text{area } W(CO)_5(4BP)}{\text{area benzene}}$	$[W(CO)_5 4BP]$	$\frac{\text{area cis-}W(CO)_4(4VP)_2}{\text{area benzene}}$	$cis\text{-}[W(CO)_4(4VP)_2]$	$\frac{\text{area cis-}W(CO)_4(4VP)(4BP)}{\text{area benzene}}$	$[cis\text{-}W(CO)_4(4VP)(4BP)]$[b]
0.0	0.0	0.0	0.0742	$9.35\ 10^{-4}$	0.0	0.0
0.0	0.0	0.0	0.0821	$1.03\ 10^{-3}$	0.0	0.0
0.00147	0.146	$8.09\ 10^{-4}$	0.00181	$2.28\ 10^{-5}$	0.0227	$2.86\ 10^{-4}$
0.00441	0.277	$1.53\ 10^{-3}$	[c]	---	[c]	---
0.00588	0.400	$2.22\ 10^{-3}$	0.0	0.0	0.0	0.0
0.0103	0.556	$3.08\ 10^{-3}$	0.0	0.0	0.0	0.0

RUN 2

[4BP]	$\frac{\text{area } W(CO)_5(4VP)}{\text{area benzene}}$	$[W(CO)_5(4VP)]$	$\frac{\text{area } W(CO)_5(4BP)}{\text{area benzene}}$	$[W(CO)_5(4BP)]$	$\frac{\text{area 4VP}}{\text{area benzene}}$	[4VP]	$\frac{\text{area 4BP}}{\text{area benzene}}$	[4BP]
0.0	0.885	0.0202	---	0.0	---	0.0	---	0.0
0.0	0.788	0.0180	---	0.0	---	0.0	---	0.0
0.0	0.795	0.0181	---	0.0	---	0.0	---	0.0
0.00077	0.819	0.0187	0.0918	0.00051	0.0197	0.00005	0.00243	0.00006
0.00154	0.827	0.0189	0.164	0.00091	0.0440	0.00112	0.0106	0.00027
0.00231	0.798	0.0182	0.227	0.00126	0.0575	0.00147	0.0221	0.00057
0.00308	0.835	0.0191	0.274	0.00152	0.0669	0.00171	0.0358	0.00092
0.00462	0.816	0.0186	0.341	0.00189	0.0830	0.00212	0.0669	0.00172
0.00616	0.834	0.0190	0.385	0.00213	0.0945	0.00241	0.105	0.00270
0.0077	0.822	0.0188	0.416	0.00230	0.103	0.00263	0.146	0.00376

RUN 2, CONTINUED

[4BP]	$\frac{\text{area cis-W(CO)}_5\text{(4VP)}}{\text{area benzene}}$ · [cis-W(CO)$_4$(4VP)$_2$]	$\frac{\text{area cis-W(CO)}_4\text{(4VP)(4BP)}}{\text{area benzene}}$	[cis-W(CO)$_4$(4VP)(4BP)]	$\frac{\text{area cis-W(CO)}_4\text{(4BP)}_2}{\text{area benzene}}$	[cis-W(CO)$_4$(4BP)$_2$]
0.0	0.0968	0.00122	---	0.0	---	0.0
0.0	0.0926	0.00117	---	0.0	---	0.0
0.00077	0.0415	0.00052	0.0167	0.000021	[d]	0.0
0.00154	0.0164	0.00021	0.0191	0.00024	[d]	0.0
0.00231	0.00839	0.00011	0.0198	0.00025	[d]	0.0
0.00308	0.00192	0.00002	0.0176	0.00022	[d]	0.0
0.00462	0.0	0.0	0.0133	0.00017	[d]	0.0
0.00616	0.0	0.0	0.00610	0.000077	0.00161	0.000020
0.0077	0.0	0.0	0.00502	0.000063	0.0000441	6×10^{-7}

[a] [W(CO)$_5$(4VP)] = 0.0202 M, Irradiated with the K_2GrO_4 filter solution, benzene solvent (standard), 1-(4-pyridyl)butanone trapper, HPLC analysis column D, eluting with 85% Hexane, 15% EtOAc; 1.5 ml/min.

[b] cis-W(CO)$_4$(4VP)(4BP) and cis-W(CO)$_4$(4BP)$_2$ have not been isolated. Concentrations were calculated using as standarization factor 0.0126; the same as for cis-W(CO)$_4$(4VP)$_2$.

[c] Not determined.

[d] Detectable but not measurable.

Table 82. Thermal and Photochemical Behavior of cis-$W(CO)_4(4VP)_2$ in the Absence and in the Presence of 4BP.[a]

[4BP]	$\frac{\text{area cis-W(CO)}_4\text{(4VP)}_2}{\text{area benzene}}$	[cis-$W(CO)_4(4VP)_2$]	$\frac{\text{area cis-W(CO)}_4\text{(4VP)(4BP)}}{\text{area benzene}}$	[cis-$W(CO)_4(4VP)(4BP)$]
0.0	0.0611[b]	$7.40\ 10^{-4}$	0.0	0.0
0.0	0.0594[c]	$7.48\ 10^{-4}$	0.0	0.0
$4.90\ 10^{-4}$	0.0323[b]	$4.07\ 10^{-4}$	0.0129	$1.58\ 10^{-4}$
$4.90\ 10^{-4}$	0.0374[c]	$4.71\ 10^{-4}$	0.0164	$2.02\ 10^{-4}$

[a] [cis-$W(CO)_4(4VP)_2$] = $7.61\ 10^{-4}$ M, benzene solvent (standard), HPLC analysis, 85% Hexane, 15% EtOAc; 1.5 ml/min.

[b] Sample not irradiated; remained in dark at room temperature.

[c] Sample irradiated for ~24 hrs. with Filter B (λ_{irr} > 400 nm).

Table 83. Data for the Thermal Reaction of cis-$W(CO)_4(4VP)_2$ with 4BP.[a]

RUN 1.

time sec.	time min.	area cis-$W(CO)_4(4VP)_2$	area cis-$W(CO)_4(4VP)(4BP)$	area x[b] / area a-x	[x][c] / [a-x]	[x][d] / [a]	$\ln \frac{1}{1 - \frac{[x]}{[a]}}$
0	0.0	63252	21801[e]	0.345	0.345	0.257	0.297
890	14.83	57117	21035	0.368	0.368	0.269	0.313
3483	58.05	53877	24132	0.448	0.448	0.309	0.370
6445	107.42	42547	25510	0.600	0.600	0.375	0.470
9808	163.47	40719	28839	0.708	0.708	0.415	0.536
RUN 2.							
5005	83.42	59100	24311	0.411	0.411	0.291	0.344
7397	123.28	48857	25403	0.520	0.520	0.342	0.419
11745	195.75	46678	33997	0.728	0.728	0.421	0.546

[a] [cis-$W(CO)_4(4VP)_2$] = 0.000589 M, [4BP] = 0.00324 M in benzene, HPLC analysis column D, eluting with 85% Hexane, 15% EtOAc; 1.5 ml/min. Samples were kept in the dark between injections in the HPLC.

[b] x represents cis-$W(CO)_4(4VP)(4BP)$ at a certain time. [a] represents the initial concentration of cis-$W(CO)_4(4VP)_2$.

[c] $$\frac{[x]}{[a-x]} = \frac{\text{area x}}{\text{area (a-x)}}$$

[d] if $$\frac{[x]}{[a-x]} = A = \frac{[x]}{[a]-[x]} \quad \text{then} \quad \frac{[x]}{[a]} = \frac{1}{1 + \frac{1}{A}}$$

[e] Reaction taken place during degassing of the initial solution resulted in a non-zero initial concentration of cis-$W(CO)_4(4VP)(4BP)$.

MICHIGAN STATE UNIVERSITY LIBRARIES
3 1293 03145 4139